Dual strategies to correct abnormal ion transports in cystic fibrosis using construct therapy

---

Anna Katharina Kolonko

– Münster 2019 –

Biologie

Dissertationsthema

Dual strategies to correct abnormal ion transports in cystic fibrosis using construct therapy

Inaugural-Dissertation
zur Erlangung des Doktorgrades
der Naturwissenschaften im Fachbereich Biologie
der Mathematisch-Naturwissenschaftlichen Fakultät
der Westfälischen Wilhelms-Universität Münster

vorgelegt von

Anna Katharina Kolonko

aus

Bremen, Deutschland

– Münster 2019 –

Dekanin: Prof. Dr. Susanne Fetzner

Erster Gutachter: Prof. Dr. Wolf-Michael Weber
Zweiter Gutachter: Prof. Dr. Francisco M. Goycoolea

Tag der mündlichen Prüfung: 29.11.2019
Tag der Promotion: 12.12.2019

The work presented in this Thesis was mainly completed in the working group of Prof. Dr. Wolf-Michael Weber at the Institute of Animal Physiology, University of Münster, Germany. A part of the research was developed in the working group of Prof. Dr. Francisco M. Goycoolea at the School of Food Science and Nutrition, University of Leeds, United Kingdom.

ABSTRACT

Cystic fibrosis (CF) is the most common lethal genetic disorder in the Caucasian population affecting approximately one in 2,500 newborns. It is caused by mutations in the gene encoding for the chloride and bicarbonate channel cystic fibrosis transmembrane conductance regulator (CFTR). The underlying problem of the disease is an imbalanced homeostasis of ion and water transports in secretory epithelia causing problems in multiple organs, especially in the lung. This imbalance is evoked by impaired chloride secretion through CFTR and associated sodium hyperabsorption via the epithelial sodium channel (ENaC). Gene therapy would be a promising approach of treatment for the monogenic disorder. However, until today no gene therapy achieved clinical efficacy until today mostly due to unwanted immune responses towards viral vectors and limitations of DNA delivery. Hence, efficient gene therapy requires the development of suitable vehicles for the optimal delivery of genes to specific target cells at the expense of minimal toxicity. The natural polysaccharide chitosan (CS) might provide remedy as a suitable non-viral vector for gene delivery purposes because of its biodegradability and low cytotoxicity.

Therefore, in the context of this Thesis several chitosan-based nanosystems were designed and explored in order to develop a possible double-tracked strategy to treat abnormal ion transports in CF. Altogether four different systems were evaluated targeting CFTR and ENaC, respectively or at the same time. First, characterization of CS nanoparticles complexing wtCFTR-mRNA and α-ENaC antisense oligonucleotides (ASO), respectively revealed monodisperse complexes with a high zeta potential and hydrodynamic diameter under 200 nm making the complexes ideal for transfection purposes. In fact, functional Ussing chamber measurements showed significantly increased CFTR function as well as significantly decreased ENaC activity in human respiratory epithelial cells after successful transfection with CS wtCFTR-mRNA complexes and CS α-ENaC ASO complexes, respectively. Furthermore, CS was used to complex wtCFTR-mRNA and α-ENaC ASO simultaneously producing a co-transfection system. Even though the complexes displayed a small size under 200 nm and an appropriate zeta potential the relatively high polydispersity index made them unsuitable for transfection. In a last approach, the pungent ingredient of the chili pepper, namely capsaicin, was tested to reduce ENaC activity. Functional Ussing chamber experiments revealed a slightly decreasing effect on

the amiloride-sensitive current in primary human nasal epithelial (HNE) cells. Finally, CS nanocapsules incorporating capsaicin and adsorbing wtCFTR-mRNA to the surface were harnessed and characterized. The capsules displayed next to their small size many advantages over the complexes such as an increased stability making them more promising for transfection purposes. However, successful proof-of-principle of transfection of primary HNE cells with the capsules could not be achieved yet. Nevertheless, the results presented and discussed in this Thesis demonstrate that a promising start for the development of a double-tracked strategy to treat abnormal ion transports in CF has been made.

TABLE OF CONTENTS

LIST OF FIGURES

LIST OF TABLES

ABBREVIATIONS

%	percent
*	significance level of $p \leq 0.05$
µ	micro
16HBE14o-	human bronchial epithelial cells
A	Ampere
ABC	ATP-binding cassette
ADP	adenosine diphosphate
AF4	asymmetric flow field flow fractionation
Ag	silver
ALI	air liquid interface
ASL	airway surface liquid
ASO	antisense oligonucleotides
ATP	adenosine triphosphate
BCA	bicinchoninic acid
bp	base pairs
BSA	bovine serum albumin
C	Celsius
Ca^{2+}	calcium ion
$CaCl_2$	calcium chloride
cAMP	cyclic adenosine monophosphate
CAP	capsaicin
CD	circular dichroism
cDNA	complementary deoxyribonucleic acid
CF	cystic fibrosis
CFBE41o-	cystic fibrosis bronchial epithelial cells
CFTR	cystic fibrosis transmembrane conductance regulator
Cl^-	chloride ion
CMV	cytomegalovirus
CO_2	carbon dioxide
CS	chitosan
C_t	transepithelial capacitance
Cu^{2+}	copper ion
Da	Dalton
DA	degree of acetylation
DEPC	diethylpyrocarbonate
Dex	dexamethasone
DLS	dynamic light scattering
DMF	dimethylformamide
DMSO	dimethyl sulfoxide
DNA	deoxyribonucleic acid

DTT	dithiothreitol
E. coli	*Escherichia coli*
ECGS	epidermal cell growth supplement
ECL	enhanced chemiluminescence
EDTA	ethylenediaminetetraacetic acid
EDTA	Ethylenediaminetetraacetic acid
EGF	epidermal growth factor
ENaC	epithelial sodium channel
F	Farad
FBS	fetal bovine serum
FD	fast digest
FDA	United States Food and Drug Administration
FEV	forced expiratory volume
g	gram
g	gravitational acceleration
GAPDH	glyceraldehyde 3-phosphate dehydrogenase
G_t	transepithelial conductance
h	hour
h	human
H^+	proton
H_2O	water
H441	NCI-H441 (human lung adenocarcinoma cell line)
HCl	hydrochloric acid
HEPES	4-(2-hydroxyethyl)-1-piperazineethanesulfonic acid
HNE	primary human nasal epithelium
HRP	horseradish peroxidase
Hz	Hertz
IBMX	3-isobutyl-1-methylxanthine
I_{sc}	short-circuit current
IVT	*In vitro* transcription
k	kilo
K^+	potassium ion
kb	kilo bases
KCl	potassium chloride
KH_2PO_4	dipotassium phosphate
L	liter
LB	lysogeny broth
LCC	liquid covered culture
Li^+	lithium ion
m	meter
m	milli
M	molar
MALS	multi-angle light scattering

MEM	minimal essential medium
$MgCl_2$	magnesium chloride
min	minute
miRNA	micro ribonucleic acid
MOPS	3-(*N*-morpholino)propanesulfonic acid
mRNA	messenger ribonucleic acid
MSD	membrane spanning domain
MTT	3-(4,5-dimethylthiazol-2-yl)-2,5-diphenyltetrazolium bromide
Mw	molecular weight
n	amount of substance
n	nano
n	number of experiments
N	number of cells
N/P	negative/positive
Na^+	sodium ion
Na_2HPO_4	disodium hydrogen phosphate
NaCl	sodium chloride
NBD	nucleotide binding domain
NC	nanocapsules
NCI-H441	human lung adenocarcinoma cell line
NHERF1	Na^+/H^+-exchanger regulatory factor isoform-1
NIBS	non-invasive back scattering
NKCC1	$Na^+/K^+/2Cl^-$-cotransporter
ori	origin of replication
p	probability value
P. aeruginosa	*Pseudomonas aeruginosa*
P. pyralis	*Photinus pyralis*
PBS	phosphate buffered saline
PCR	polymerase chain reaction
PDI	polydispersity index
pEGFP	vector carrying enhanced green fluorescent protein
pH	*potentia hydrogenii*
PIC	protease inhibitor cocktail
PKA	protein kinase A
poly(A)	polyadenylation
PVDF	polyvinylidene fluoride
R domain	regulatory domain
R_g	radius of gyration
RGB	red, green, blue
R_h	radius of hydrodynamic diameter
rH	relative humidity
RI	refractive index
RLU	relative light units

RNA	ribonucleic acid
RT	room temperature
R_t	transepithelial resistance
RT-PCR	reverse transcriptase polymerase chain reaction
s	second
S	Siemens
S. aureus	*Staphylococcus aureus*
SD	standard deviation
SDS-PAGE	sodium dodecyl sulfate polyacrylamide gel electrophoresis
SEM	standard error of the mean
siRNA	small interfering ribonucleic acid
SPLUNC1	short palate lung and nasal epithelial clone 1
SV40	simian virus 40
TBE	tris/borate/EDTA
TBS	tris buffered saline
TEER	transepithelial electrical resistance
TEM	transmission electron microscopy
TMA	tetramethylammonium chloride
TPP	tripolyphosphate
TRPV1	transient receptor potential vanilloid 1
UG	Ultroser G
UV	ultraviolet
V	volt
vs.	versus
v/v	volume/volume
V_t	transepithelial potential
w/v	weight/volume
wt	wild type
wtCFTR	wild type CFTR
X-Gal	5-bromo-4-chloro-3-indolyl-β-D-galactopyranoside
α	alpha
β	beta
γ	gamma
δ	delta
Δ	Delta
ΔF508	most common mutation in cystic fibrosis
ζ	zeta; zeta potential
λ	lambda; wavelength
Ω	Ohm

1 INTRODUCTION

Nanotechnology was first introduced by Nobel laureate Richard P. Feynman during his lecture “There’s plenty of room at the bottom” in 1959 (Feynman, 1960). It is defined by the manipulation of matter at an extremely small scale, namely the nano-scale (1-100 nm). Since the early beginnings, many innovative developments in physics, chemistry and biology have demonstrated the promising and broad field of application of this unique technology. Especially in pharmaceutical nanotechnology and nanomedicine it was shown that the handling of materials, systems and devices on the nano-scale can offer solutions and benefits in many areas (Demetzos and Pippa, 2014). For example nanobiotechnology has been reported to benefit early diagnosis of cancer (Liu et al., 2007), detection of neurologic diseases with targeted contrast agents (Suffredini et al., 2014), enhancement of the pharmaceutical activity of herbal drugs (Ansari et al., 2012) or alternative routes of insulin delivery (Reis and Damgé, 2012), to name a few. Life cycle functions in cells operate as interconnected networks under tight genetic regulation and signalling control that respond to, are controlled by and can be disrupted by varying length scale processes (e.g., electrical, molecular, macromolecular and supramolecular) that take place at the domains of the nano-scale. Nanomedicine has emerged as a multidisciplinary field, in which the manipulation of matter at the nano-scale is harnessed for the purpose of diagnostic and therapy to face the prevailing challenges in health such as cancer, rare diseases and antimicrobial resistance.

A very promising field of application of nanomedicine is gene therapy. Conventional gene therapy aims at the therapeutic delivery of DNA to the cell with viral vectors, such as adenoviruses, adeno-associated viruses, lentiviruses or retroviruses, in order to treat a disease on a cellular level. In recent years a lot of research has been done in the field of gene therapy leading to many clinical trials for various widespread diseases including Alzheimer’s disease and cancer as well as for rare diseases such as cystic fibrosis, Huntington’s chorea or Duchenne muscular dystrophy, among other (Ginn et al., 2018). However, due to many limitations only very few gene therapies have been approved until now. Restrictions of conventional gene therapy using viral vectors are, amongst others, high immunogenicity and potential reversion of the virus to pathogenicity (Lundstrom and

Boulikas, 2003). Nanobiotechnology bottom-up approaches harnessing macromolecular self-assembly have further expanded the possibilities for deployment of non-viral vectors for a safer delivery of genes to their target such as cationic lipids, cell penetrating peptides or cationic polymers, such as chitosan (Santos-Carballal et al., 2018).

The development of non-viral vectors aims to reach at least the same level of gene expression and specificity obtained when using viral vectors. The advantages of the use of non-viral vectors are related to their low cost and ease of production, their reduced immunogenicity and immunotoxicity and, therefore, greater bio-safety, in comparison to viral-mediated gene therapy. Non-viral vectors offer important advantages such as the possibility of being produced in a large scale, greater flexibility for optimization and control of the formulation, the possibility to deliver large DNA sequences and also to develop dual therapy formulations, as the major focus of this Thesis.

The overarching goal of this Thesis is to contribute towards the eventual development of a novel dual construct therapy based on both gene (mRNA and antisense oligonucleotides) and drug (capsaicin) co-delivery as a cellular approach to restore the abnormal ion transports in cystic fibrosis. The work offers unprecedented *in vitro* proof of concept of the biological performance of chitosan-based nanomaterials using various epithelial cell models as the major investigative tools to evaluate the biological function. This chapter focuses on reviewing the fundamental aspects and state of the art of the major topics and techniques relevant to the Thesis and describes in detail the aim of the work.

1.1 Chitosan

Chitosan refers to a family of pseudonatural linear polysaccharides composed of randomly distributed β-(1-4)-linked D-glucosamine and *N*-acetyl-D-glucosamine units. It is the principal derivate of chitin, the second most abundant polysaccharide in nature after cellulose. Chitin is the supporting material in the exoskeleton of crustaceans such as crabs or shrimps, and insects and can also be found in fungal mycelia (Ravi Kumar, 2000). By partial deacetylation under thermoalkaline conditions (Figure 1), chitosan is derived from chitin at commercial scale. This chemical deacetylation yields a broad and heterogeneous range of chitosans (Chang et al., 1997). However, this process is environmentally

hazardous and makes it difficult to control the degree of polymerization and acetylation. A safer and more accurate alternative to process chitin is enzymatic treatment of chitosan by chitinases, chitosanases and chitin deacetylases (Schmitz et al., 2019; Tsigos et al., 2000).

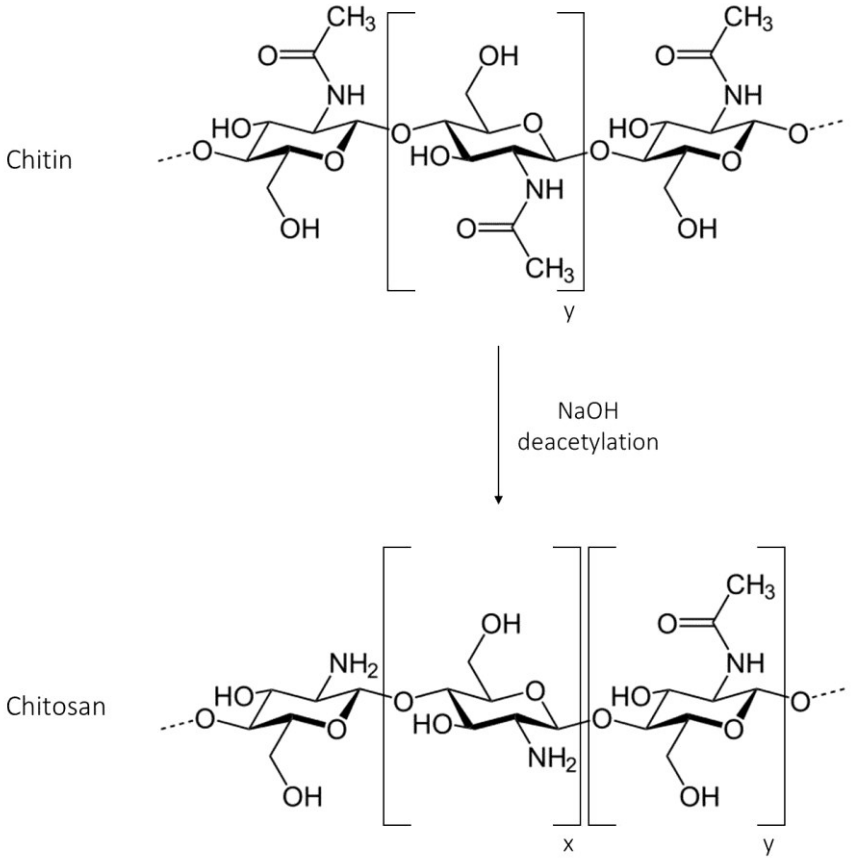

Figure 1: Chemical deacetylation of chitin to chitosan. (x) Deacetylated D-glucosamine and **(y)** acetylated *N*-acetyl-D-glucosamine units.

After processing, chitosan polymers vary in molecular weight (Mw), which is given by the degree of polymerization, degree of acetylation (DA) and pattern of acetylation. Thus, the rigorous characterization of chitosan for a given specific purpose is crucial as the structural features define the polymer's physicochemical properties and biological activity. During the deacetylation of chitin to synthesize chitosan, when the degree of deacetylation of the polycationic polymer reaches ~70% it becomes soluble in aqueous acidic solution (pH < 6.1), making it more functional than chitin in the formulation of a wide range of soft nanostructured materials such as gels, nanoparticles, nanofibers, films, etc. (Rinaudo, 2006). Additionally, chitosan displays many advantages. To name a few, the polymer is

biocompatible, biodegradable, mucoadhesive, non-toxic and exhibits adsorption properties making it a suitable agent for various applications (Cheung et al., 2015). Furthermore, chitosan has been reported to have anti-microbial (Martins et al., 2014), anti-fungal (Younes et al., 2014), anti-tumor (Karagozlu, 2014) and anti-oxidant (Ngo, 2014) activities extending its range of application to medicine. Altogether, these properties have gained traction to the use of chitosan in a broad range of industrial applications in agriculture (e.g. antifungal plant protection agent, fertilizer), biomedicine (e.g. wound dressing, tissue regeneration scaffolds), food industry (e.g. dietary supplement, food preservative and packaging additive) and cosmetics (e.g. skin and mouth protection), among other sectors (Schmitz et al., 2019).

The polycationic character of chitosan enables it to interact with and bind to negatively charged nucleic acids, mucins and sulphated glycosylaminoglycans in the glycocalyx and other drugs. This property, along with its biocompatibility, mucoadhesiveness and low cytotoxicity (Borchard, 2001; Grenha et al., 2010) as well as biodegradability in humans by lysozyme and several chitinases (Kean and Thanou, 2010), makes chitosan a very promising candidate for non-viral gene delivery. The first attempt at non-viral gene delivery using chitosan was already made over 25 years ago (Mumper et al., 1995). Since then research has been gaining ground in this field with delivery of nucleic acids spanning from plasmid DNA over siRNA to miRNA, to name a few (Mao et al., 2010; Santos-Carballal et al., 2018). Herein, the form of chitosan, in which the drug is administered, differs between many systems on a nano-scale.

1.2 Nanosystems

Nanoparticles are the essential building blocks of nanotechnology. Their ultrafine structure provides improved properties due to variations in specific characteristics such as size, distribution or surface area to volume ratio (Mir et al., 2017). Especially in pharmaceutical nanotechnology and drug delivery these features open a broad field of possibilities with a wide-ranging variety of nanosystems (Figure 2). Since the first report of a polymer-drug conjugate in 1955 (Jatzkewitz, 1955) tremendous progress in the development of drug delivery systems has been made. Here, the focus lies on tailoring size, physicochemical properties or surface functionalities of the systems to reach optimal conditions for a

specific purpose and increase the drug availability at tissue and cell level. Extensive research led to the approval of several nano-scale drug delivery systems by the United States Food and Drug Administration (FDA) including liposomes for eradication of fungal infections, micelles for treatment of vasomotor symptoms, nanocrystals against hypercholesterolemia or nanoemulsions for treatment of cancer, to mention a few (Ganta et al., 2014).

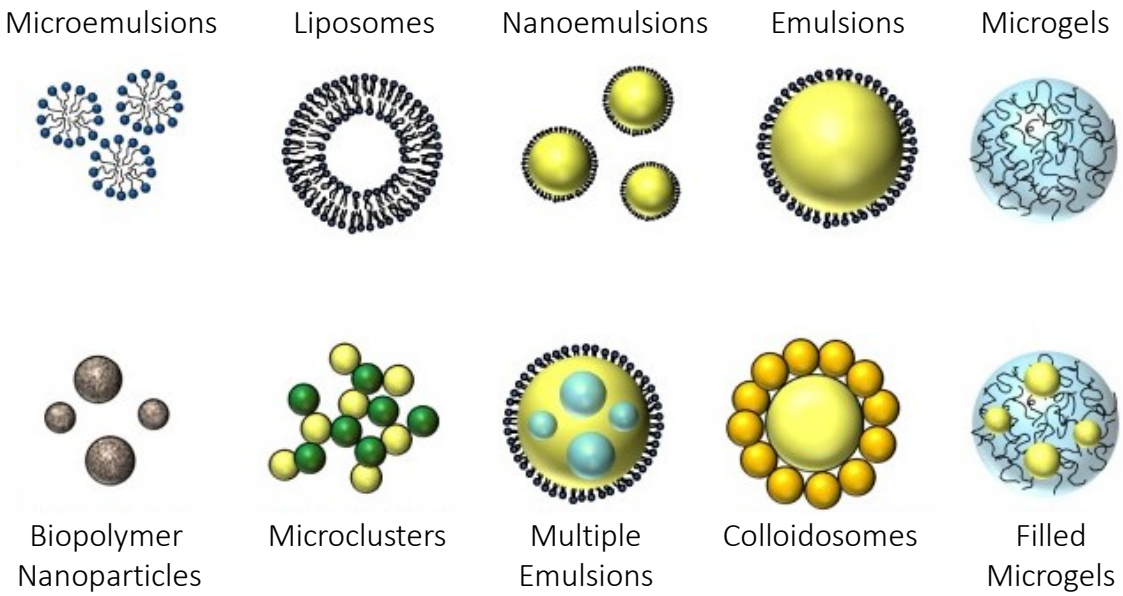

Figure 2: Nano-scale delivery systems. Adapted from McClements, 2015

The choice of vector for a specific drug is dependent on the characteristics of the cargo and the target, which is desired to be reached. For example negatively charged nucleic acids are able to form interpolyelectrolyte complexes with positively charged polymers such as chitosan (Figure 3a). For intracellular delivery, the positively charged nanocomplexes are then able to interact with the negatively charged cell membrane facilitating endocytotic uptake. Hydrophobic drugs such as capsaicin can be encapsulated in the oil-core of nanocapsules (Figure 3b). The superior stability of the nanocapsules could increase the possibility of the delivery system to reach its target. Coating of the capsules with chitosan provides a positive surface charge yet again assisting endocytotic uptake. Nanocomplexes and nanocapsules are discussed in further detail below.

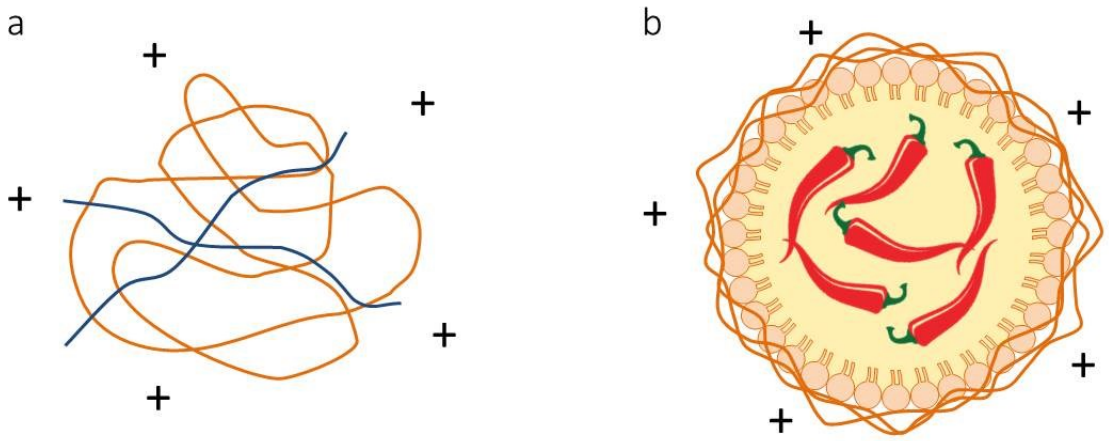

Figure 3: Representation of chitosan-based nanosystems. (a) Matrix-type nanocomplex consisting of chitosan and nucleic acids formed by electrostatic self-assembly; **(b)** Chitosan-coated nanocapsule loaded with capsaicin in the oil-core (orange: chitosan; blue: nucleic acid).

1.2.1 Nanocomplexes

The simplest method to prepare a chitosan-based system is by polyelectrolyte complexation. It is achieved by direct mixing of the oppositely charged polymer and nucleic acids in aqueous solution. Due to their electric charges, the two components form nanocomplexes via electrostatic self-assembly. This phenomenon is defined as electrostatic self-assembly and involves macromolecules that are connected by non-covalent interactions and form via association of small building blocks (Gröhn, 2008; Willerich and Gröhn, 2011). The characterization of chitosan plays an important role for this method as the polymer's features greatly affect its biological performance. For instance the Mw of chitosan defines the average number of monomers per chain as well as the distribution of the average chain length both affecting amongst others size and stability of the complexes (Sato et al., 2001). Furthermore, the DA determines the number of amine groups present in the polymer and strongly influences its degradability, inflammation, immune modulation and most importantly its ability to interact with nucleic acids (Buschmann et al., 2013).

When forming nanocomplexes it is crucial to characterize them regarding their negative/positive (N/P) charge ratio. The N/P charge ratio is defined as the molar ratio of positively charged amine groups of chitosan to negatively charged phosphate groups of nucleic acids. It greatly affects the condensation of nucleic acids by chitosan as well as the

net surface charge (i.e. zeta potential) and stability of the complexes (Mao et al., 2010). For example it was reported that particle size decreases with increasing N/P charge ratio indicating that an excess of chitosan condensates the nucleic acids resulting in a densely packed and smaller structure (Mao et al., 2001; Puras et al., 2013). Moreover, reports described increasing zeta potential of nanocomplexes with increasing N/P charge ratio showing that an excess of amino groups leads to an increased surface charge (Puras et al., 2013; Santos-Carballal et al., 2015). Also, it is known that the morphology of nanocomplexes of plasmid DNA and chitosan, determined by atomic force microscopy and assessed as the toroid to rod ratio, is sensitive to the N/P charge ratio (Danielsen et al., 2004). However, the influence of this on the biological performance of the nanocomplexes is not fully understood.

One of the great advantages of chitosan-based nanocomplexes is the possibility of complexation of any desired nucleic acid such as messenger RNA or antisense oligonucleotides.

1.2.1.1 mRNA

Messenger RNA (mRNA) is a single-stranded nucleic acid, which transfers genetic information from the DNA to the ribosome where protein synthesis takes place. Briefly, a DNA template is transcribed by the RNA polymerase into mRNA in the nucleus. Before the mature mRNA is transported into the cytoplasm it is processed by splicing of the introns and addition of a 5'cap for recognition at the ribosome and protection from RNases as well as a polyadenylation (poly(A)) tail for protection from exonucleases. At the ribosome, mRNA is translated into its encoding amino acid sequence resulting in the synthesis of the encoding protein.

Using mRNA for therapeutic purposes as the so called *transcript therapy* has been tested since the early 1990's and underwent tremendous developments since then (Weissman, 2015). In fact, mRNA displays many advantages for gene delivery compared to DNA. For example there is no need for nuclear localization facilitating the delivery to the target, namely the cytosol, and the risk of insertional mutagenesis, followed by oncogenic effects, is being avoided. Furthermore, mRNA is smaller than DNA providing easier transport into

the cell, exhibits reduced immunogenicity and is efficient at any point of the cell cycle (Bangel-Ruland et al., 2013; Sahin et al., 2014).

In order to reduce the susceptibility to degradation of *in vitro* transcribed RNA chemical modifications can be deployed. For instance addition of a 5'cap and a poly(A) tail either in the encoding vector or during *in vitro* transcription can improve stability of the nucleic acid (Yamamoto et al., 2009). Additionally, it was shown that the untranslated regions of mRNA also play a role in increasing the mRNA's turnover and therefore improve stabilization of the nucleic acid (Ferizi et al., 2015).

Currently three clinical trials are testing the efficiency of mRNA-based therapies targeting the proteins OX40L for intratumoral treatment of solid tumor or lymphoma, CFTR via lipid nanoparticle inhalation for treatment of cystic fibrosis and VEGF-A as intracardiac injection to treat heart failure (Kowalski et al., 2019). Even though no mRNA-mediated therapy was approved by the FDA yet these clinical trials show the importance of the topic and the promising prospects of *transcript therapy*.

1.2.1.2 Antisense oligonucleotides

Antisense oligonucleotides (ASO) are short, single-stranded DNA nucleotides, which are able to specifically bind to complementary nucleic acids by hydrogen bonding and thereby alter gene expression. Here, the bonding is based on the Watson-Crick base pairing. Statistically a 17-mer oligonucleotide occurs just once in the sequence of the human genome enabling extremely selective intervention with ASO of this length (Uhlmann and Peyman, 1990).

ASO display several functional mechanisms. The nucleotides can modify gene expression by sterically blocking of the ribosomal machinery (Figure 4a; Baker et al., 1997). Moreover, ASO can form RNA-DNA hybrids that become substrate for RNase H, a RNA hydrolyzing enzyme, resulting in mRNA degradation (Figure 4b; Wu et al., 2004). Further mechanisms include inhibition of RNA-binding proteins, splicing modulation and increasing the translational activity (Rinaldi and Wood, 2018).

ASO are usually chemically modified in order to increase their stability in biological fluids and protect them from degradation by nucleases. Modifications of ASO include analogues

with unnatural bases, modified sugars especially at the 2' position of ribose and altered phosphate backbones (Kurreck, 2003). The most common ASO with altered phosphate backbones are phosphorothioates. Here one non-bridging oxygen atom in the phosphodiester bond is replaced by sulfur (Kurreck, 2003).

The first application of ASO for a therapeutic purpose was reported in 1978 (Stephenson and Zamecnik, 1978). Since then advances in research led to the approval of six ASO-based drugs including Eteplirsen® for treatment of Duchenne muscular dystrophy and Nusinersen® for treatment of spinal muscular atrophy (Bennett, 2019) giving hope for the development of new drugs for these and other rare diseases.

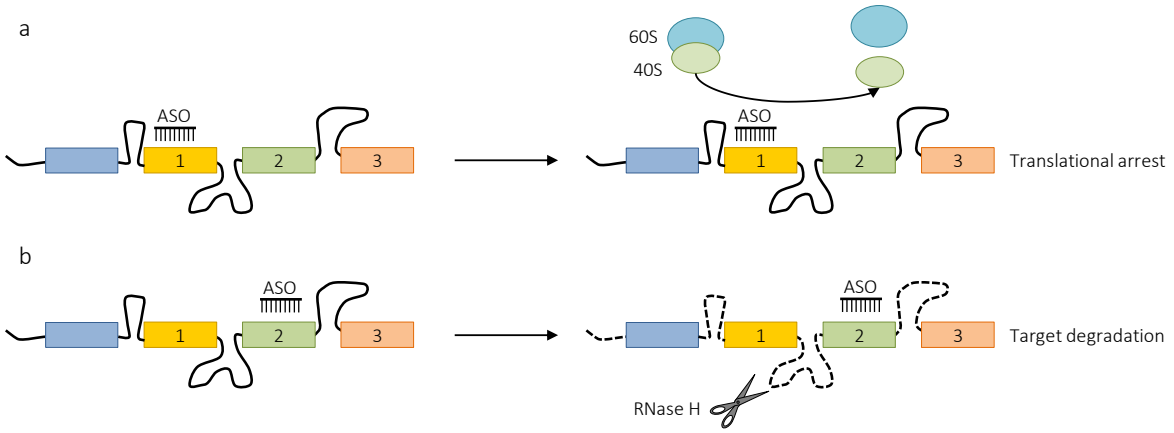

Figure 4: Mechanisms of action of antisense oligonucleotides. (a) Antisense oligonucleotides (ASO) targeting the AUG start site (1) can block the binding of RNA binding protein complexes leading to translational arrest; **(b)** ASO can form RNA-DNA hybrids with mRNA that become substrate for RNase H and resulting in mRNA degradation. Adapted from Rinaldi and Wood, 2018.

1.2.2 Nanocapsules

Nanocapsules are generally defined as nano-vesicular systems that exhibit a typical core-shell structure, in which the drug is confined to a reservoir or within a cavity surrounded by a polymer membrane or coating (Letchford, 2007). The active substance can be contained in the cavity either in liquid or solid form or as a molecular dispersion. Depending on the preparation method nanocapsules can also carry the active substance on their surfaces or absorbed to the polymeric membrane (Mora-Huertas et al., 2010).

In general six classical methods for the preparation of nanocapsules are known: nanoprecipitation, emulsion–diffusion, double emulsification, emulsion-coacervation, polymer-coating and layer-by-layer (Mora-Huertas et al., 2010). Numbered among

emulsion diffusion is the solvent displacement technique according to the principle of spontaneous emulsification. During this process acetone and ethanol migrate from the organic phase to the aqueous phase yielding an oil and water nanoemulsion. This nanoemulsion is stabilized by the surfactant, for example lecithin, which is adsorbed at the oil and water interface (Goycoolea et al., 2012; López-Montilla et al., 2002). With this technique chitosan-lecithin oil-core nanocapsules can be prepared (Figure 3b). Briefly, these nanocapsules consist of an oil-core lined with lecithin. The hydrophilic head groups of the surfactant face to the outside enabling the phospholipids to interact with chitosan forming a core-shell colloidal nanocapsule.

Nanocapsules display many advantages compared to other nano-scale delivery systems. Encapsulation of drugs can reduce systemic toxicity, protect vulnerable molecules from degradation and provide controlled-release properties (Whelan, 2001). Furthermore, their increased stability compared to nanocomplexes could enhance the likelihood of the capsules to reach their target and increase transfection efficiency. Most importantly, by encapsulation in the oil-core the bioavailability of hydrophobic substances such as capsaicin can be improved substantially.

1.2.2.1 Capsaicin

The vanilloid capsaicin (Figure 5) is the main pungent ingredient found in members of the *Capsicum* family, for example the chili pepper. The low polar compound (log P 3.66) is the agonist to the transient receptor potential vanilloid 1 (TRPV1), a ligand-gated, calcium permeable cation channel mainly expressed in cells of the nervous system (Caterina et al., 1997; Davies et al., 2010). TRPV1 is believed to transduce the sensations of noxious heat and pain (Immke and Gavva, 2006) hinting at the cause for the pungency of the vanilloid.

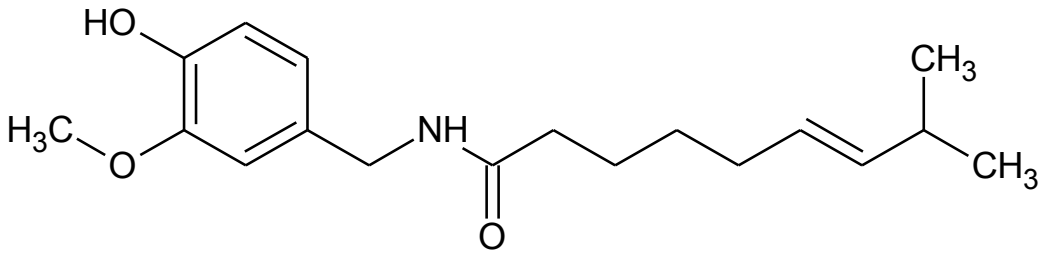

Figure 5: Structure of capsaicin

Capsaicin has been known for its wide range of therapeutic properties since ancient times (Maji and Banerji, 2016). The main therapeutic application of the lipophilic compound is as an analgesic in topical creams and dermal patches for pain relieve (Blair, 2018; Fattori et al., 2016). However, many other therapeutic benefits were described until today. Amongst others it has been reported to have anti-inflammatory (Kim et al., 2003), anti-obesity (Leung, 2014), hypolipidemic and anti-oxidant (Manjunatha and Srinivasan, 2007) effects. It was used to treat cancer (Clark and Lee, 2016), urologic diseases (Foster and Lake, 2014) and for protection of the gastrointestinal mucosa (Holzer and Lippe, 1988). Furthermore, it has also been found to reversibly open tight junctions (Shiobara et al., 2013), an effect that is modulated by its encapsulation in chitosan-coated nanocapsules and nanoemulsions (Kaiser et al., 2015b). Recent studies have documented that capsaicin has a direct effect on urinary sodium excretion by inhibiting epithelial sodium channel (ENaC) function and thereby affecting renal sodium reabsorption (Li et al., 2014). The versatile and broad range of application as well as the natural origin and uncritical degradation makes capsaicin a promising therapeutic agent for several medical conditions and diseases.

1.2.3 Characterization of nanosystems

In order to understand nano-scale delivery systems on a molecular level and to increase their biological performance it is important to characterize them regarding their physicochemical properties. Their properties are amongst others size, size distribution, zeta potential, morphology, binding efficiency, stability and cytotoxicity.

The size and size distribution of nanoparticles can be determined with dynamic light scattering (DLS). DLS monitors the time fluctuation in the intensity of light scattered by the particles in solution. Briefly, a laser beam hits a sample of particles in solution and is being scattered by the particles in a certain angle. Due to the Brownian motion, particles are moving constantly with speed depending on the particle's size. As their position fluctuates so does the intensity of back-scattered light. These fluctuations occur on a time scale measuring the time it takes a particle to move a significant fraction of the wavelength of light. With progressing time, the correlation of scattered intensity of the initial and final states decays. For spherical nanoparticles the decay rate of the time autocorrelation function of these intensity fluctuations is used to directly measure the diffusion coefficient,

which in turn can be used to calculate the hydrodynamic radius of a particle (Pecora, 2000).

An additional method to determine the size and shape of particles is asymmetric flow field-flow fractionation (AF4). AF4 is a versatile technique to separate and characterize macromolecules or particles and was first described in 1987 (Wahlund and Giddings, 1987). Heterogenic samples are separated by a cross-flow vertical to the laminar flow of the sample in a narrow channel. The particles are being pushed towards the bottom and due to their Brownian motion diffuse back into the center of the channel. Having a higher Brownian motion, smaller particles move further into the channel than larger particles. The parabolic laminar flow carries particles in the center with a higher velocity than particles in the marginal area of the channel. Therefore, samples are being separated by size with smallest particles eluting first. Furthermore, the system is connected to several detectors including a multi-angle light scattering (MALS) detector, a refractive index (RI) detector or a dual wavelength ultraviolet (UV) detector allowing detailed characterization of the separated particles (Wagner et al., 2014).

Another important parameter of nanoparticles is the zeta potential (ζ). The zeta potential is the electric potential measured at the slipping plane of a particle in suspension. The slipping plane is the border between the ionic double layer surrounding the particle, consisting of the firm Stern layer of ions attached to the particle and the diffuse layer of ions still attracted to the particle, and the ions in equilibrium in the suspension (Bhattacharjee, 2016). The zeta potential can give indication about the stability of particles. Particles with high zeta potential will likely repel each other avoiding precipitation while the repulsive forces of particles with low zeta potential are not strong enough to do so. Determination of the zeta potential can ensue from their electrophoretic mobility. When applying an electric field the particles will move towards the oppositely charged electrode at a certain speed. Zeta potential can then be calculated from the electrophoretic mobility using Henry's equation (Delgado et al., 2007).

Transmission electron microscopy (TEM) offers unique opportunities to observe and characterize the structure of nanoparticles with a resolution much higher than achieved with a light microscope. Briefly, imaging ensues by passage of an electron beam through the sample so that the beam is absorbed and scattered, producing contrast and an image.

Because the wavelength of the electron beam is 100,000-fold shorter than photons in visible light TEM can reach subnanometer resolutions (Winey et al., 2014). This way, properties such as size, shape or density of nanoparticles can be determined.

Other methods to characterize nanoparticles include gel electrophoresis (Scott et al., 1994), circular dichroism (Ranjbar and Gill, 2009) or several cytotoxicity assays (Lewinski et al., 2008) amongst others. An accurate and precise characterization of nano-scale delivery systems can considerably increase their ability to overcome biological barriers such as the blood-brain barrier or the mucus lining of internal organs such as the gastrointestinal tract or the lung.

1.3 Lung and airway epithelium

The lung is the principle organ in the respiratory system. Its key role is to permit efficient exchange of respiratory gases between the bloodstream and the environment. During this process air is inhaled through the nose and mouth passing from the larynx and trachea and onward into a rapidly dividing series of conductive bronchi and bronchioles (Effros, 2006). The bronchial airways terminate in alveolar ducts and sacs, which are lined with alveoli, small cavities responsible for the gas exchange. Around 300 million alveoli within the lung provide an estimated surface area of 90 m^2 (Effros, 2006). This structure allows efficient bidirectional transfer of approximately six liters of air per minute between the external environment and the alveoli (Rackley and Stripp, 2012). As the lung is constantly exposed to inhaled pathogens and particles, the airway epithelium acts as a physical barrier separating the external environment and the internal milieu. Hence, the main functions of the airway epithelium are maintaining a physical barrier to prevent particles and pathogens from entering the bloodstream, regulation of innate immune responses towards invading pathogens and finally controlling ion transport to keep the airways hydrated and sustain the mucociliary escalator (De Rose et al., 2018).

The physical barrier of the proximal airway epithelium is composed of a variety of cell types (Figure 6; Tam et al., 2011). Pulmonary neuroendocrine cells are stem cell-like and play a role in the regeneration of the airway epithelium (Cutz et al., 2007). Also stem cell-like, basal progenitor cells give rise to secretory and ciliated epithelial cells (Hong et al.,

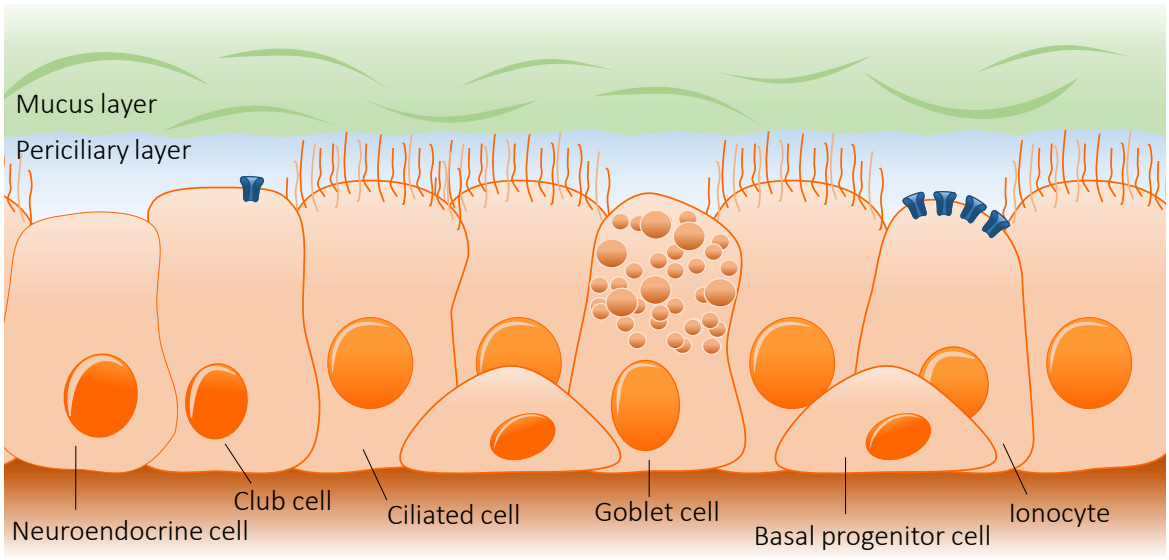

Figure 6: The proximal conducting airway epithelium. The proximal conducting airway epithelium is composed of a variety of cell types such as pulmonary neuroendocrine cells, club cells, ciliated cells, mucus producing goblet cells, basal progenitor cells and highly cystic fibrosis transmembrane conductance regulator (CFTR; blue) expressing ionocytes. The epithelium is lined with the airway surface liquid consisting of the periciliary layer and the mucus layer. The upper mucus layer is very proteinaceous and traps particles and pathogens. The lower periciliary layer is aqueous and has low viscosity for easier ciliary beating.

2004). Ciliated cells contain approximately 300 cilia per cell, which are responsible for mucus clearance via ciliary beating (Tam et al., 2011). Goblet cells have been reported to have electron-lucent acidic-mucin granules and secrete mucus into the airways (Jeffery, 1983). Club cells, formerly known as Clara cells, regulate bronchiolar epithelial integrity and immunity by producing bronchiolar surfactants and antiproteases (De Water et al., 1986). Two recent studies revealed a novel type of airway epithelial cells named pulmonary ionocytes (Montoro et al., 2018; Plasschaert et al., 2018). These cells have been shown to express higher levels of the cystic fibrosis transmembrane conductance regulator (CFTR), a chloride and bicarbonate channel important for ion transport and homeostasis in the airway epithelium. Together these polarized epithelial cells build a pseudostratified monolayer and maintain their integrity by apical junction complexes consisting of occluding tight junctions and anchoring adherens junctions (De Rose et al., 2018). While tight junctions regulate the paracellular transport of ions and certain molecules, adherens junctions are important for initiation and maintenance of cell-cell adhesion (Rezaee and Georas, 2014).

The innate immune response of the airway epithelium consists of two phases: the recognition of pathogens and the increased release of cytokines and antimicrobial

peptides as response to the recognition (Martin, 2005). The recognition of pathogens is mainly achieved by pattern recognition receptors such as toll-like receptors. In the airways ten different toll-like receptors as well as the cluster of differentiation protein 14 and CFTR are able to bind to conserved molecular patterns present on microbes and thereby recognize the pathogen (Bals and Hiemstra, 2004). Upon pathogen recognition airway epithelial cells release chemokines and cytokines to the basolateral side recruiting macrophages and neutrophils to kill the intruders (Bals and Hiemstra, 2004; Tam et al., 2011). Antimicrobial peptides such as lactoferrin, elafin or calprotectin are released to the apical side into the airway surface liquid (ASL) to eliminate the pathogens there (Bals and Hiemstra, 2004; De Rose et al., 2018).

The ASL plays an important role in the mucociliary escalator. It consists of two layers: the aqueous periciliary layer and the highly proteinatious mucus layer (Figure 6; Tarran, 2004). The mucus layer represents an unrestrained and tangled gel generated by high-molecular-weight mucins (Button and Boucher, 2008). Human respiratory tract mucus is reported to be a mixture of the mucin proteins MUC5AC produced in goblet cells in the surface epithelium, MUC5B produced mainly in mucus cells of the submucosal glands and to lesser extend MUC2 (Thornton et al., 2008). The main function of the mucus layer is to entrap essentially all of the particles and pathogens deposited on the airway surface during normal breathing (Button and Boucher, 2008). The low-viscosity and lubricant periciliary layer extends as high as the cilia and separates the mucus layer from the cell surface (Tarran, 2004). Its viscoelastic properties allow the airway cilia to beat rapidly (~5-15 Hz) and drive mucus clearance resulting in vectorial mucus transport ending in swallowing or expectoration in the oropharynx (Lee and Foskett, 2014; Randell and Boucher, 2006).

Critical for the mucociliary escalator is an appropriate homeostasis of the ASL dependent on transepithelial ion and water transports (Blouquit-Laye and Chinet, 2007). A fine balance between Na^+ absorption through the epithelial sodium channel (ENaC) and Cl^- secretion via CFTR on the apical epithelial membrane generates osmotic gradients promoting water flow in and out of the cell thereby regulating the hydration state of the ASL (Figure 7; Hollenhorst et al., 2011). Briefly, an electrochemical gradient generated by the Na^+/K^+-ATPase located on the basolateral side of epithelial cells promotes Na^+ absorption via ENaC. This gradient also promotes Cl^- influx on the basolateral side through

Na^+-coupled Cl^- transporters such as the $Na^+/K^+/2Cl^-$-cotransporter (NKCC1), which in turn leads to Cl^- secretion on the apical side of the cell by CFTR and to the lesser extent by Ca^{2+}-dependent Cl^- channels (Hollenhorst et al., 2011; Lee and Foskett, 2014). Failure to maintain adequate mucus hydration leads to impairment of mucociliary clearance and is a prominent feature of chronic airway diseases such as chronic obstructive pulmonary disease and cystic fibrosis (De Rose et al., 2018).

1.4 Cystic fibrosis

Cystic fibrosis (CF) is a chronic, life-shortening and rare hereditary disease causing severe damage to the respiratory tract and other organs. One affected newborn in 2,500 births makes the disease the most common autosomal recessive inherited disorder in the Caucasian population with a total of approximately 70,000 patients worldwide (Cutting, 2015; Ratjen and Döring, 2003). The classical clinical picture of CF is mainly characterized by fat maldigestion due to pancreatic insufficiency and chronic obstructive lung disease with bacterial colonization by microorganisms such as *Pseudomonas aeruginosa* and *Staphylococcus aureus* (Castellani and Assael, 2017). CF was first defined as a separate disease entity in 1938 (Andersen, 1938). About 50 years later in 1989 the gene of the defect protein responsible for the disease, the chloride and bicarbonate channel CFTR, was identified (Kerem et al., 1989; Riordan et al., 1989). Since the 1940s the average life expectancy of patients severely improved from about 6 months to approximately 40 years today (Davis, 2006; Keogh et al., 2018). Thanks to improved treatment and early diagnosis the median survival for those born in 2000 is expected to be in excess of 50 years (Hurley et al., 2014). Three main tests are used for the diagnosis of the disease. During newborn screening, the blood is tested for higher levels of immunoreactive trypsinogen released by the pancreas. A sweat test checks for increased concentrations of sodium and chloride in the sweat (CF: > 60 mmol/L; normal: < 40 mmol/L). Finally, a genetic test verifies DNA defects in the CFTR gene (Klimova et al., 2017).

CF is caused by mutations in the gene encoding for CFTR, a chloride and bicarbonate channel mainly expressed in the apical membrane of epithelial cells (O'Sullivan and Freedman, 2009). The loss of function leads to pathological changes in organs that express the chloride channel such as lung, pancreas, intestine, liver and reproductive tract evoking

a wide range of symptoms (Naehrig et al., 2017). The earliest disease complication of CF is *meconium ileus* represented by severe bowel obstruction caused by inspissated mucus and meconium occluding the mid or distal small bowel in newborns (Dupuis et al., 2016). Around 85% of patients suffer from pancreatic insufficiency caused by thickened secretions of intrapancreatic ducts leading to fat-soluble-vitamin deficiency, steatorrhea and malnutrition (Strandvik, 2010). Furthermore, the destruction of the pancreas can lead to an insulin deficiency causing both type I and type II diabetes (Marshall et al., 2005). One third of patients suffer from liver disease resulting from impaired secretory function of the biliary epithelium and ductal cholestasis (Colombo, 2007). Additionally, CF causes infertility in 98% of male patients due to obstructive azoospermia caused by congenital bilateral absence of the vas deference and concomitant absence of the seminal vesicles while 50% of female patients are able to conceive (Ahmad et al., 2013).

However, the prevailing symptom of the multiorgan disorder is CF lung disease defined by chronic airway infection, progressing to bronchiectasis, gas trapping, hypoxemia and hypercarbia. The resulting pulmonary insufficiency is responsible for approximately 80% of CF related deaths (O'Sullivan and Freedman, 2009). Figure 7 displays the suggested underlying mechanisms of CF lung disease. Next to its function as an ion channel CFTR has been reported to regulate other membrane proteins such as ENaC (Guggino and Stanton, 2006; Kunzelmann, 2003). The loss of function of CFTR is associated with sodium hyperabsorption mediated by the amiloride-sensitive sodium channel. The dysregulation of these proteins leads to an imbalance of ion and water transports in epithelial cells causing severe problems, especially in the lung. The excess of Na^+ absorption entails an increased influx of H_2O leading to dehydration and depletion of the ASL. The loss of Cl^- secretion and H_2O efflux prevents the correction of the low ASL volume. Hence, the reduced height of the periciliary layer leads to the thickened mucus weighing down the cilia impairing ciliary beating and hence mucociliary clearance (Boucher, 2002). The loss of the mucociliary escalator promotes chronic infections of the CF lung with bacteria. The prevailing microorganisms include *P. aeruginosa*, *S. aureus*, *Haemophilus influenzae* and *Burkholderia cepacia* (Harrison, 2007). It has been reported that the loss of bicarbonate secretion by CFTR leads to acidification of the ASL, which in turn impairs bacterial killing of the antimicrobial substances present in the fluid (Stoltz et al., 2015). A self-perpetuating cycle

of chronic bacterial infection, vigorous inflammation and airway obstruction arises causing progressive obstructive lung disease and finally lung failure (Sagel et al., 2007).

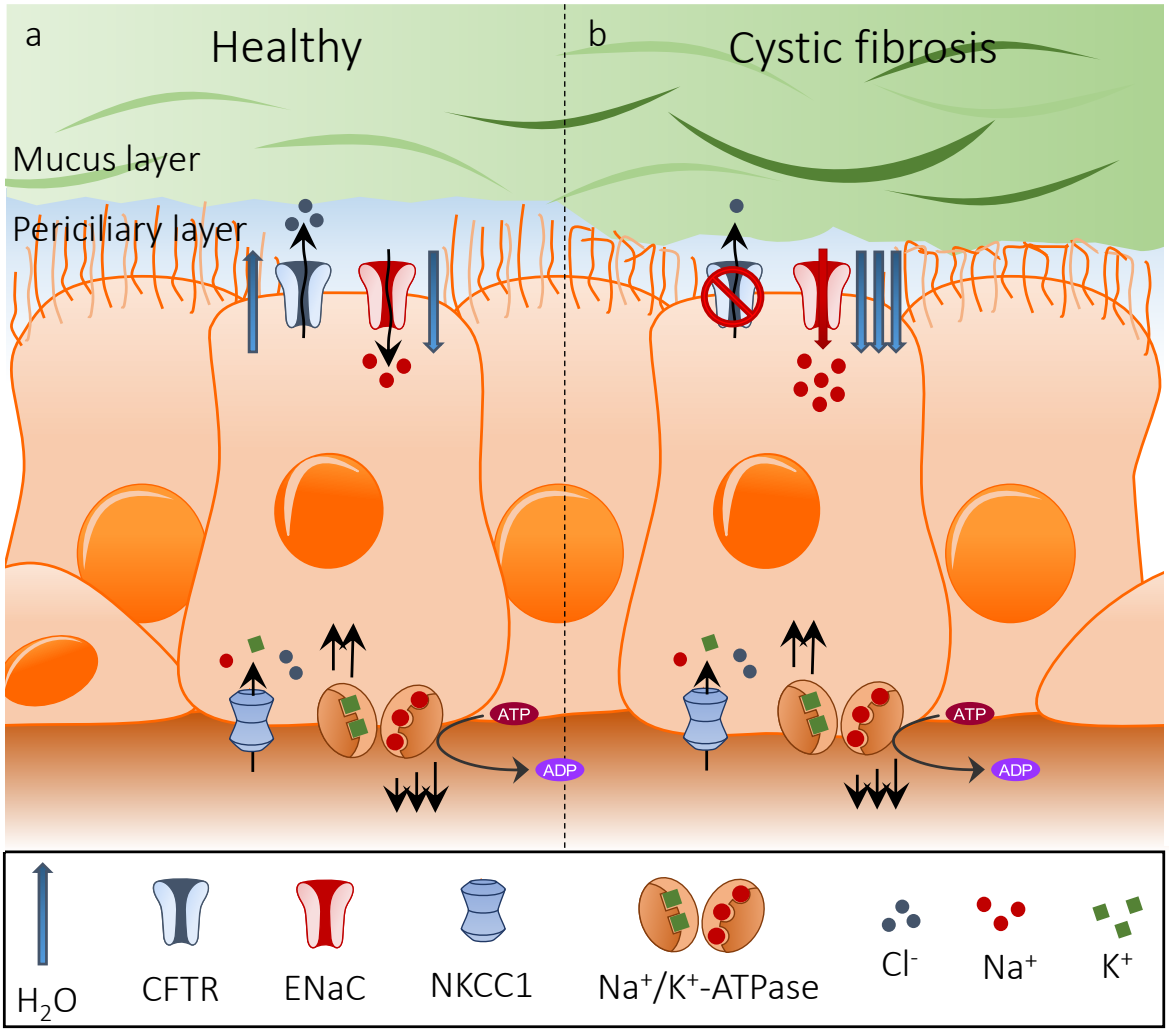

Figure 7: Ion transport in healthy and cystic fibrosis bronchial epithelial cells. (a) In the healthy bronchial epithelium the Na^+/K^+-ATPase on the basolateral side generates an electrochemical gradient by transporting Na^+ out of the cell thereby promoting Na^+ influx on the apical side via the epithelial sodium channel (ENaC). Furthermore, the $Na^+/K^+/2Cl^-$-cotransporter (NKCC1) transports Cl^- into the cell enabled by the electrochemical gradient. The accumulated Cl^- is secreted on the apical side of the cell by the cystic fibrosis transmembrane conductance regulator (CFTR). The ion flow across the apical membrane generates an osmotic gradient promoting H_2O to follow passively in and out of the cell. This homeostasis of ion and water transport keeps the periciliary layer of the airway surface liquid (ASL) adequately hydrated upholding ciliary beating. **(b)** However, in the cystic fibrosis bronchial epithelium no Cl^- is secreted due to defective CFTR accompanied by a Na^+ hyperabsorption via ENaC. The imbalance of ion transports leads to high H_2O influx dehydrating the ASL. The decrease in height of the periciliary layer and the increased viscosity of the mucus weigh down the cilia impairing ciliary beating and hence mucociliary clearance.

1.4.1 Cystic fibrosis transmembrane conductance regulator

CFTR is a cyclic adenosine monophosphate (cAMP)-dependent chloride and bicarbonate channel primarily expressed in the apical membrane of secretory epithelia in exocrine tissues. In 1989 the gene was discovered on the long arm of chromosome 7 (band q31) spanning approximately 250 kb of genomic DNA (Rommens et al., 1989). Altogether 24 exons were identified producing a protein consisting of 1,480 amino acids with an estimated Mw of 168 kDa (Riordan et al., 1989). CFTR is a member of the adenosine triphosphate (ATP)-binding cassette (ABC) membrane transporter gene superfamily. All ABC transporters share the same architecture consisting of two membrane spanning domains (MSD) and two cytosolic nucleotide binding domains (NBD) building two "half transporters", respectively. The transporters carry a variety of substrates in and out of the cell at the expense of ATP hydrolysis. Interestingly, CFTR is the only protein in the family to form a transmembrane ion channel pore (Csanády et al., 2019). Like all ABC transporters, the ion channel is constituted of two homologous halves each half containing one NBD and one MSD with six transmembrane α-helices. The two halves are linked by a cytoplasmic regulatory (R) domain (Figure 8; Sheppard and Welsh, 1999). Among the ABC transporters the unique R domain is only present in CFTR and plays a role in the gating of the ion channel (Chen et al., 2000). Two separate processes control the gating of CFTR. The R domain contains 18 potential phosphorylation sites (Moran, 2017). Hence, activation of the ion channel is achieved by phosphorylation of the R domain by the cAMP-dependent protein kinase (PKA), protein kinase C or casein kinase 2 (Venerando et al., 2013). The gating of the phosphorylated CFTR channels is then promoted by the binding of ATP at the NBDs. It was reported that intracellular concentration of approximately 2 mM ATP is high enough to ensure that most CFTR remain activated (Moran, 2017). Finally, hydrolysis of ATP closes the gate and stops Cl^- transport (Akabas, 2000; Gadsby et al., 2006). The fact that ATP is consumed during the gating cycle to mediate channel closure is unique to CFTR and reflects its revolution from classical ABC transporter to ion channel (Hwang and Kirk, 2013).

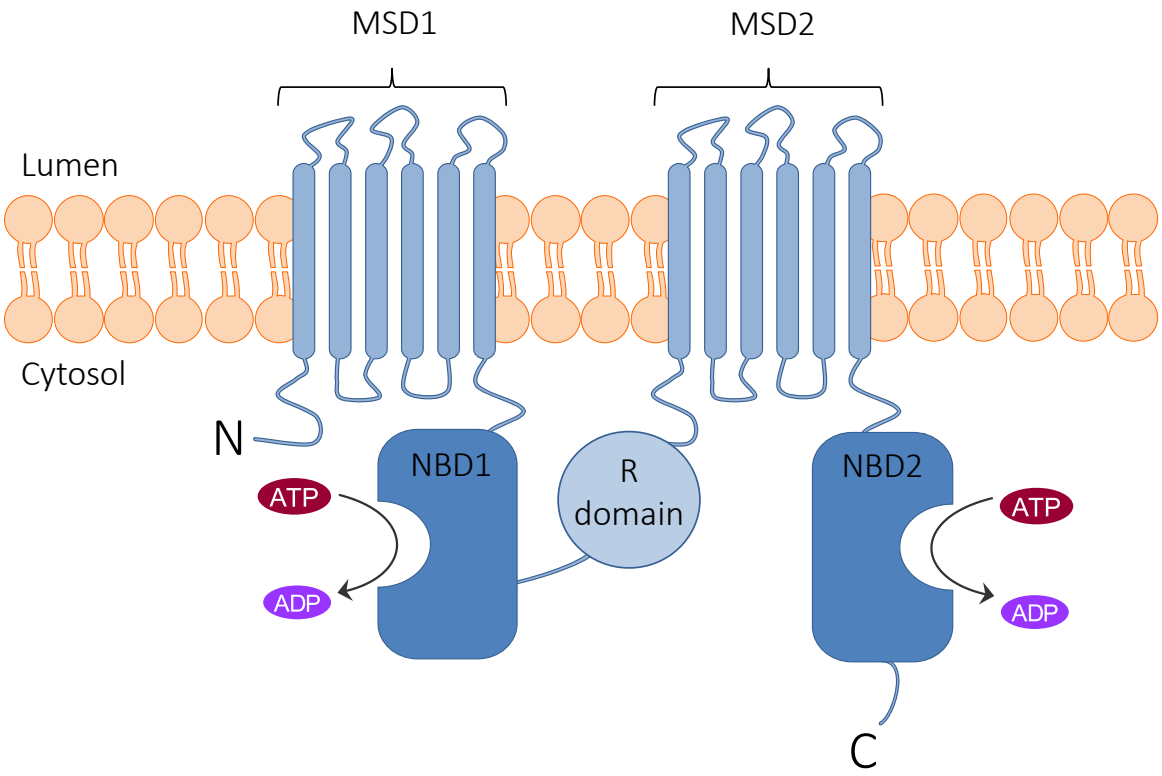

Figure 8: Structure of the cystic fibrosis transmembrane conductance regulator (CFTR). The chloride and bicarbonate channel consists of two homologous halves each containing two membrane spanning domains (MSD) and one nucleotide binding domain (NBD). The two halves are linked by a regulatory (R) domain. The gating of the phosphorylated CFTR channels is promoted by phosphorylation of the R domain and the binding of adenosine triphosphate (ATP) at the NBDs. Hydrolysis of ATP to adenosine diphosphate (ADP) closes the gate and stops Cl^- transport. Adapted from Sheppard and Welsh, 1999.

Next to its role as an ion channel CFTR has been reported to have many other regulatory functions. For example it was shown that CFTR is involved in the regulation of ENaC (Lu et al., 2007; Rubenstein et al., 2011) as represented in the disease pattern of CF. Further CFTR functions include regulation of outwardly rectifying chloride channels (Schwiebert et al., 1995), sensitizing of potassium channels to sulfonylurea compounds, inhibition of volume regulated ion channels or regulations of intracellular vesicle transport (Vankeerberghen et al., 2002).

To the present day more than 2,000 mutations in the encoding region of the gene were identified, of which around 200 have been characterized in terms of disease liability (Csanády et al., 2019; De Boeck and Amaral, 2016). Generally, the mutations are categorized in six different functional classes (Marson et al., 2016). Briefly, class I mutations lead to defective synthesis of CFTR due to nonsense or frameshift mutations. Class II-IV mutations are caused by missense mutations leading to impaired processing and

maturation (II), faulty regulation (III) and defective conductance (IV). Class V mutations are characterized by reduced function or synthesis of CFTR due to splicing defects or missense mutations while class VI mutations lead to reduced stability and increased turnover of the protein at the cell surface (Castellani et al., 2008; Ikpa et al., 2014). The most common mutation termed ΔF508 and is present in approximately 70% of defective CFTR alleles and is categorized as a class II mutation (Rowe et al., 2005). In Europe ΔF508 accounts for 70% of CF cases (Mirtajani et al., 2017) and worldwide approximately 90% of patients carry at least one ΔF508 allele (Guggino and Stanton, 2006). The ΔF508 protein is missing an amino acid on the surface of NBD1 due to a deletion of phenylalanine at the position 508. This defect leads to wrong folding of the protein, which is therefore retained in the endoplasmic reticulum and finally degraded by the ubiquitin-proteasome pathway (Gadsby et al., 2006; O'Sullivan and Freedman, 2009). Loss of function of CFTR caused by mutations in the gene coding for the ion channel leads to severe health impairments as discussed in 1.4 amongst others due to the missing regulation of ENaC.

1.4.2 Epithelial sodium channel

ENaC is primarily expressed in the apical membrane of many epithelial tissues including the lung, colon, kidney, salivary ducts and sweat ducts (Butterworth, 2010). The sodium channel belongs to the ENaC/Degenerin superfamily also including acid-sensing ion channels and Degenerin subunits involved in sensory transduction in nematodes such as *Caenorhabditis elegans* (Hanukoglu and Hanukoglu, 2016). ENaC is highly selective for Na^+ and Li^+ ions and can be specifically blocked by the diuretic amiloride (Alvarez de la Rosa et al., 2000). Its main function is the rate limiting step for transepithelial Na^+ absorption (Garty and Palmer, 1997). Hence, ENaC is involved in the regulation of blood pressure, the control of sodium balance and the regulation of the ASL and mucociliary clearance (Olivença et al., 2019; Rossier, 2014; Schild, 2010).

ENaC is a heterotrimer composed of three structurally related subunits termed α-, β- and γ-ENaC each displaying a Mw of 85-95 kDa in their unmodified state (Figure 9; Bhalla and Hallows, 2008). Each subunit is encoded by a different gene namely *SCNN1A* (α), *SCNN1B* (β) and *SCNN1C* (γ) (Moore and Tarran, 2018). The subunits, sharing 34-37% identity, are composed of two transmembrane segments (M1 and M2), a large hydrophilic

extracellular loop and intracellular N- and C-termini (Canessa et al., 1994). The transmembrane segments are postulated to form the channel pore (Kashlan and Kleyman, 2011). It was reported that some residues called HG motif within the M2 domain of α-ENaC contribute to the channel's conduction pore and bind amiloride (Kellenberger et al., 2002; Sheng et al., 2001). Current is only produced when α-ENaC is expressed while β- and γ-ENaC alone do not display production of current suggesting α-ENaC to be essential for the formation of the channel pore (Jain et al., 1999; Loffing and Schild, 2005). A fourth subunit termed δ-ENaC has been reported to assemble with β and γ-ENaC in human respiratory epithelial cells (Ji et al., 2006) and contribute to amiloride-sensitive current across primary human nasal epithelial cells (Bangel-Ruland et al., 2010). However, its relevance to lower airways transepithelial Na^+ absorption is not fully understood (Moore and Tarran, 2018).

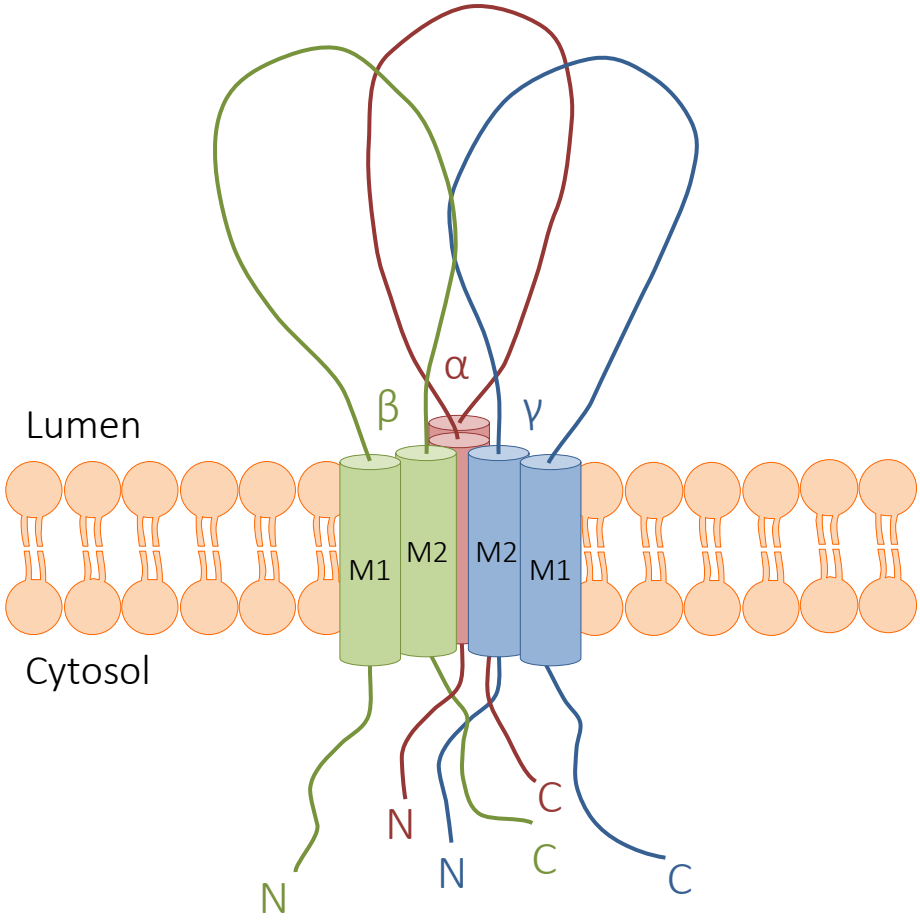

Figure 9: Structure of the epithelial sodium channel (ENaC). ENaC is a heterotrimer consisting of a single α, β, and γ subunit. Each subunit has two membrane-spanning domains (M1 and M2) with intracellular N- and C-termini and a large extracellular loop, respectively. Adapted from Bhalla and Hallows, 2008.

The regulation of ENaC is very versatilely operated by several intrinsic and extrinsic factors. Amongst others the sodium channel can be regulated by hormones, mechanical and cytoskeletal activity, proteolytic cleavage, ubiquitination, phosphorylation, self- and feedback-inhibition and pH (Bhalla and Hallows, 2008). Hormones involved in the regulation of ENaC are aldosterone, insulin or vasopressin to name a few (Bubien, 2010; Ecelbarger et al., 2001). Proteolytic cleavage plays an important role in regulating the activity of the sodium channels by increasing its open probability. Specific proteases have been shown to activate ENaC by cleaving channel subunits at their extracellular domains (Kleyman et al., 2009). Furthermore, ENaC is regulated by changes in both extracellular and intracellular sodium concentration. A change in channel activity as a result of changes in extracellular sodium concentration is known as sodium self-inhibition (Fuchs et al., 1977). Feedback-inhibition on the other hand is caused by increased intracellular sodium concentration (MacRobbie and Ussing, 1961). In the lung ENaC appears to be regulated by CFTR as in CF patients ENaC activity is upregulated suggesting a relationship of CFTR and ENaC (Berdiev et al., 2009).

1.4.1 Interaction of CFTR and ENaC

In the literature, many reports discuss the mechanisms of interaction of CFTR and ENaC demonstrating the importance of the issue. Several groups hint to a direct interaction of the two proteins. Using the yeast two-hybrid system a direct interaction between a CFTR polypeptide and the carboxyterminal part of the α-subunit of ENaC has been detected (Kunzelmann et al., 1997). Ji *et al.* pointed out that the amino termini of α- and β-ENaC were able to immunoprecipitate CFTR demonstrating direct interaction of the proteins (Ji et al., 2000). Other reports proposed it to be more likely that the ion channels interact non-directly mediated by other proteins. A popular model suggest that the Na^+/H^+-exchanger regulatory factor isoform-1 (NHERF1) might assemble CFTR and ENaC into a signaling complex including the non-receptor tyrosine kinase c-YES (Guggino and Stanton, 2006). This kinase, a member of the c-Src kinase family (Gilmore et al., 2001), is a potent inhibitor of ENaC and might regulate CFTR inhibition of ENaC activity. Furthermore, a regulatory protein called short palate lung and nasal epithelial clone 1 (SPLUNC1) has been shown to be a pH-sensitive regulator of ENaC that is unable to inhibit ENaC in the acidic CF

airway environment suggesting CFTR to control ENaC by regulating local acid–base balance (Garland et al., 2013). Gentzsch *et al.* suggested that CFTR inhibits the proteolytic cleavage of ENaC leading to increased channel activity (Gentzsch et al., 2010). Another model from Stutts *et al.* suggests that PKA is not able to effectively phosphorylate ENaC when CFTR is present (Stutts et al., 1997). However, other reports indicate that inhibition of ENaC is not specific to CFTR and seems to be mediated by Cl^- (König et al., 2001). Yet another study even reported that CFTR fails to inhibit ENaC altogether when expressed simultaneously in *Xenopus laevis* oocytes (Nagel et al., 2005).

Evidently, the interaction of CFTR and ENaC is still a matter of discussion and so far, no definite answer has been found. Understanding the biological mechanisms involved in the relationship of the two proteins could be extremely helpful in order to develop a therapy to treat the abnormal ion transports in CF.

1.4.2 Treatment of cystic fibrosis lung disease

Management of CF disease has traditionally relied on symptom-based treatments to slow the progression of the disease (Pittman and Ferkol, 2015). Conventional pulmonary treatment has targeted the downstream consequences of the disease such as mucus plugging and infection (Edmondson and Davies, 2016). Generally, the four basic approaches include mobilization of mucus secretion, rehydration of the airway surface and the application of anti-microbial as well as anti-inflammatory agents. In order to mobilize mucus secretion mucolytic agents such as Dornase alpha and N-acetylcysteine are used frequently. Dornase alpha is a recombinant human DNase. It is supposed to cleave the extracellular DNA present in the mucus thereby decreasing the viscosity of the sputum and subsequently aid airway clearance (Yang et al., 2016). Another mucolytic drug is N-acetylcysteine, which induces the hydrolysis of disulfide bonds in mucins also reducing viscosity (Duijvestijn and Brand, 2007). Furthermore, patients can perform chest physiotherapy in order to mobilize mucus secretion. This respiratory autogenic drainage moves mucus to the proximal airways where it can be coughed out (Bradley et al., 2006). Rehydration of the airway surface ensues with drugs such as hypertonic saline, mannitol or denufosol. Mannitol provides an osmotic gradient on the airway surface leading to rehydration and an increase in volume of the ASL (Nevitt et al., 2018). Hypertonic saline

has the same effect on the ASL resulting in improved mucociliary clearance (Wark and McDonald, 2018). Denufosol stimulates chloride secretion and ciliary beat frequency independent of CFTR (Ratjen et al., 2012). Antimicrobial treatment is a cornerstone in CF lung disease therapy since most patients suffer from recurring airway infection with bacteria such as *P. aeruginosa* or *S. aureus*. In this context antibiotics are used in four different ways: prophylaxis, eradication of early infection, suppression of chronic infection and in the treatment of exacerbations (Edmondson and Davies, 2016). Depending on the species of the pathogens, different antibiotics are being administered regularly orally, intravenously or via inhalation. Most common antibiotics in CF therapy are tobramycin, aztreonam and flucloxacillin, to name a few (Döring et al., 2012; Pittman and Ferkol, 2015). Since chronic inflammation of the airway tissue plays an important role in destruction of the lung, another important step in treating CF lung disease is the application of anti-inflammatory agents. Amongst others anti-inflammatory drugs applied in CF therapy include corticosteroids like prednisone, non-steroidal anti-inflammatory drugs such as ibuprofen, modifiers of intracellular signaling as well as anti-inflammatory cytokines or immunomodulators (Roesch et al., 2018).

In recent years a class of drugs termed CFTR modulators has been developed. “Personalized medicine” considers the individual genetic background of patients in order to find the most suitable drug for efficient therapy. There are several modes of action of CFTR modulators but they differ fundamentally from other CF therapies as they aim to improve or even restore the function of defective CFTR protein (Clancy et al., 2019). Potentiators restore CFTR activity and function by increasing the time that CFTR remains active at the cell surface (Clancy, 2014) while correctors act as chaperones that prevent misfolded CFTR from being degraded and allow trafficking to the cell surface (Pedemonte et al., 2005). The potentiator ivacaftor (Kalydeco®) was the first modulator approved by the FDA (Boyle and De Boeck, 2013; Ren et al., 2018). In 2017 the approval was extended for people with at least one of 23 residual function mutations based on *in vitro* and clinical data (Haq et al., 2019). As monotherapy of both potentiators and correctors only showed modest effects on patients combinational therapy was developed (Solomon et al., 2015). A promising therapy for patients with ΔF508 is a combination of ivacaftor and the corrector lumacaftor called Orkambi®. It was approved by the FDA in 2015 and has been reported to

improve the quality of life of patients (Gohil, 2015; Wainwright et al., 2015). However, the combinational therapy only reached modest improvement in lung function (approximately 3% statistically significant improvement of forced expiratory volume (FEV)) (Deeks, 2016). *In vitro* studies of ΔF508 homozygous bronchial epithelial cells revealed that chronic exposure to ivacaftor reduces the efficacy of lumacaftor by destabilizing rescued ΔF508 protein at the cell surface (Cholon et al., 2014). Complicating drug interactions further lumacaftor is a strong inducer of CYP3A, a monooxygenase responsible for the degradation of ivacaftor in the liver, limiting the efficacy of the drug (Connett, 2019). Hence, the search for new modulators with improved effect on CFTR activity does not stand still. Tezacaftor is a second generation CFTR corrector similar to lumacaftor. A combinational therapy of ivacaftor and tezacaftor called Symdeko® was approved by the FDA in 2018 (de la Torre and Albericio, 2019). The drug has been reported to significantly improve the predicted FEV in patients with two copies of ΔF508 (Haq et al., 2019).

Although these strategies of treatment have improved the quality of life as well as the life expectancy of patients significantly, a causative treatment for CF still needs to be found in order to treat all patients regardless of their genotype. An answer to this problem could be conventional gene therapy. This form of therapy implies the relocation of the correct copies of a gene to the affected cells with the aim of replacing the mutated gene and express functional protein. To date there have been almost 2600 gene therapy trials worldwide including 36 for CF (Ginn et al., 2018). Nowadays gene therapy is a therapeutic reality for some genetic diseases but the challenge in the CF field is to convert the extensive preclinical developments into an effective and safe treatment option (Donnelley and Parsons, 2018). For CF lung disease genetic therapies require repeated administration as the airway epithelium is constantly renewing. Therefore, the selection of the appropriate delivery method is essential (Pranke et al., 2019). The delivery platforms for CF gene therapy that received the most attention until today are viral vectors including adenoviruses, adeno-associated viruses, retroviruses and lentiviruses (Cooney et al., 2018). However, even though clinical trials have demonstrated evidence of CFTR expression no gene therapy using viral vectors achieved clinical efficacy until today (Pranke et al., 2019). One of the obstacles are the high immune responses of the patients after repeated application of viral vectors (Conese et al., 2011). Furthermore, the majority of viral

technologies has been reported to be unable to penetrate mucosal secretions leading to poor efficacy in the CF lung (Schuster et al., 2014). Altogether the uncertainty of triggering immunogenic responses, insertional mutagenesis, problems with large-scale production as well as the difficulty of packaging large nucleic acids are issues that make viral vectors unsuitable for CF gene therapy purposes (Foldvari et al., 2016). Therefore, efforts are being made in order to find a suitable non-viral vector for efficient gene therapy.

Non-viral vectors have the potential to overcome many of the limitations of viral vectors. They can be produced on a larger scale, they are relatively stable for storage purposes, can be administered repeatedly with minimal immune response and the dimension of the genetic material they can carry is practically unlimited (Villate-Beitia et al., 2017). In 2015 the UK Cystic Fibrosis Gene Therapy Consortium published the results of the first clinical trial of a non-viral gene therapy for CF using a cationic liposome-based vector (Alton et al., 2015). Inhaling the liposomal vector GL67A carrying plasmid DNA was safe over one year. Even though the therapy only showed marginal beneficial effect on lung function, the trial demonstrated that repeated administration of non-viral vectors for CF lung gene therapy is a promising approach. A favorable natural candidate for non-viral gene delivery is the biopolymer chitosan as stated before. The mucoadhesiveness of chitosan could be an advantage specifically for delivery of genetic material such as mRNA in the CF lung. Due to the interaction of chitosan and mucins chitosan complexes could enhance the retention time of the drug in the lung mucosa and thereby increase the chance of being uptaken by the airway epithelium (Menchicchi et al., 2015). Taking this into consideration this study aimed at a new approach for potential gene delivery using chitosan as a non-viral vector to target abnormal ion transports in CF.

1.5 Aim

A causative treatment to cure CF on a cellular level is yet to be developed. Gene therapy could be a promising approach to treat the single-gene based disease. However, problems arise from the delivery of DNA to the cell as well as from the commonly deployed viral vectors. The use of alternative nucleic acids such as mRNA or ASO could circumvent the hurdles generated by nuclear delivery of DNA. Furthermore, remedy could be provided by using non-viral vectors such as chitosan.

Therefore, the aim of this study was to design and explore several chitosan-based nanosystems in order to develop a possible double-tracked strategy to treat abnormal ion transports in CF. Altogether four different systems were evaluated targeting CFTR and ENaC, respectively or both at the same time. First, as a proof-of-principle chitosan-wtCFTR-mRNA complexes (Figure 10a) and chitosan-ENaC-ASO complexes (Figure 10b) were prepared, characterized and investigated for their ability to restore CFTR function and to reduce ENaC activity, respectively. Subsequently, after successful transfection of the complexed mRNA and ASO into human airway epithelial cells a co-transfection system consisting of chitosan, wtCFTR-mRNA and ENaC-ASO was designed and characterized in terms of its physicochemical properties (Figure 10c). Furthermore, chitosan-based nanocapsules loaded with capsaicin and coated with wtCFTR-mRNA were designed and physicochemically characterized as a combinatorial therapy system (Figure 10d). The promising results of the characterization led to *in vitro* and *ex vivo* cell culture experiments in order to evaluate the impact of the nanocapsules on human airway epithelial cells. Additionally, in the course of the work with the nanocapsules the effect of capsaicin on primary human nasal epithelial cells was evaluated.

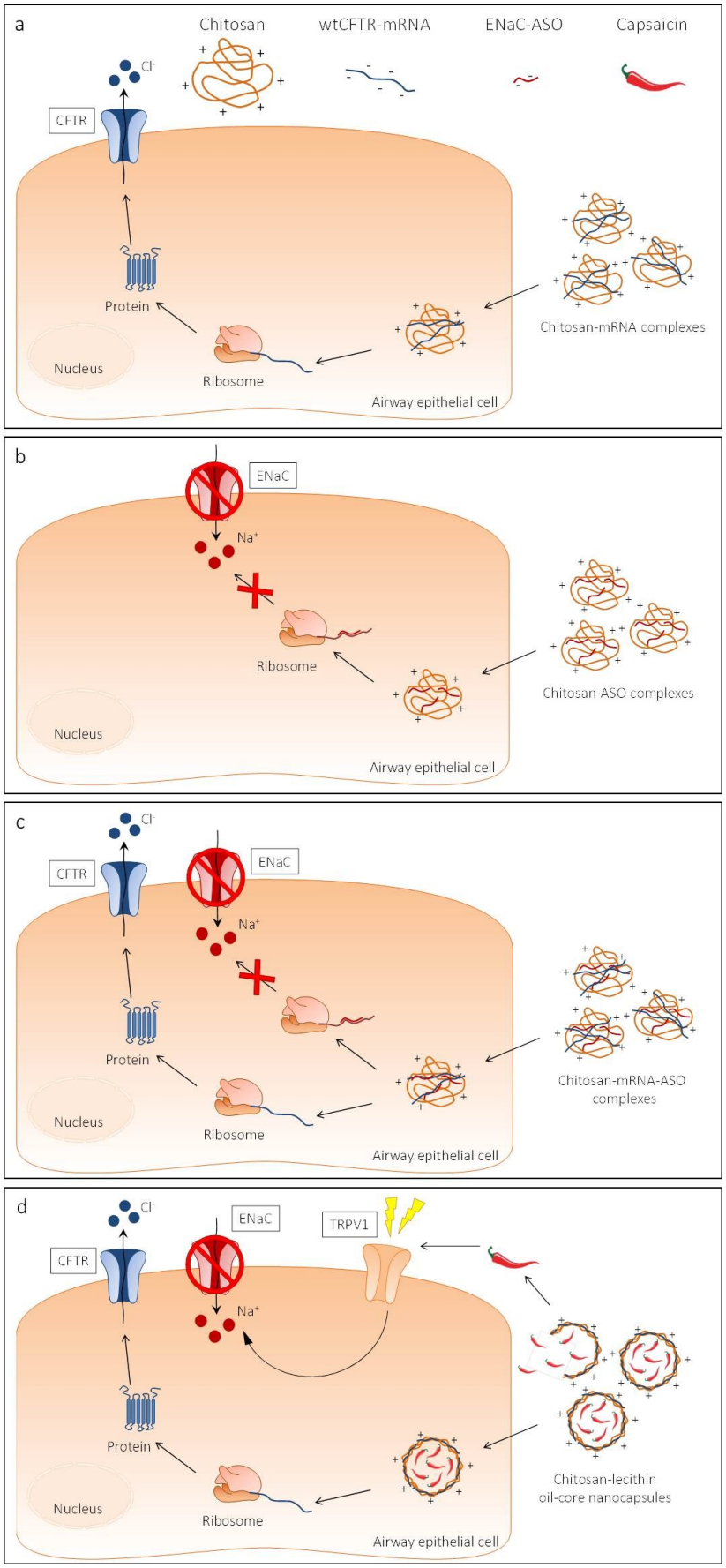

Figure 10: Graphical abstract and aim of this Thesis. Four different approaches to correct abnormal ion transports in human airway epithelial cells were testes. **(a)** Chitosan-mRNA complexes, **(b)** chitosan-ASO complexes, **(c)** chitosan-mRNA-ASO complexes and **(d)** chitosan-lecithin oil-core nanocapsules.

2 MATERIALS & METHODS

2.1 Materials

Lists of all chemicals, kits and other equipment used in this study can be found in the appendix. All experiments were performed with Millipore H_2O, if not stated otherwise.

2.2 Microbiological methods

2.2.1 Plasmid isolation from *CopyCutter™ EPI400™ Escherichia coli*

The bacterial strain *CopyCutter™ EPI400™ Escherichia coli* (Biozym Scientific GmbH, Hessisch Oldendorf, D) transformed with the plasmid pSTI-A120/hCFTR-cDNA (Figure 11) was cultivated in order to amplify the vector for further experiments. Amongst others the plasmid contains the human wild type (wt) CFTR gene (accession number: NP_000483.3) and a polyadenylation sequence of 120 adenines. The construct is a kind gift of Dr. C. Rudolph (Ludwig Maximilian University of Munich, Munich, D).

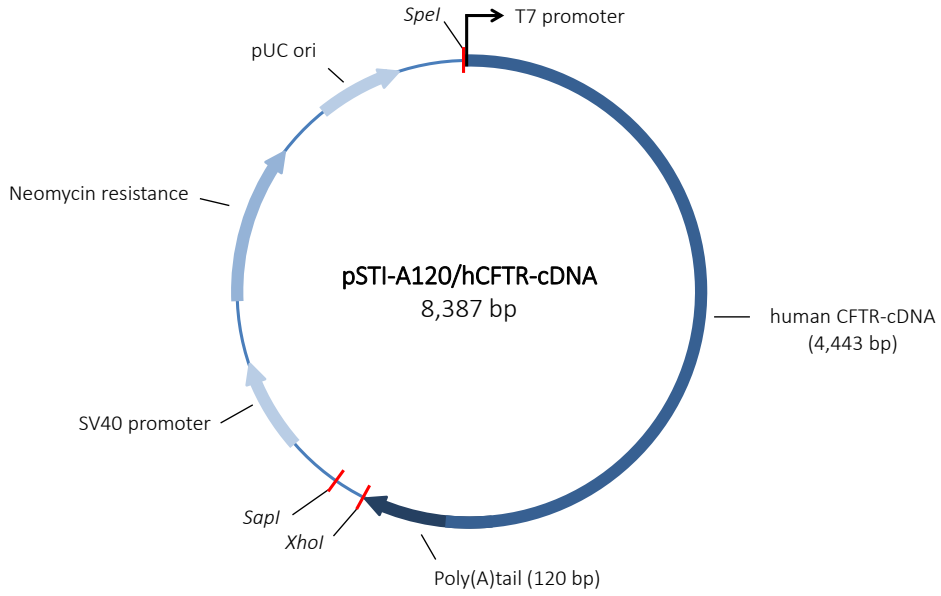

Figure 11: pSTI-A120/hCFTR-cDNA. The plasmid consists of 8,387 bp and carries the hCFTR-cDNA, to which a poly(A) tail of 120 adenines is attached. Upstream of the cDNA is a T7 promoter, which allows its transcription. Furthermore, the plasmid contains *SapI (LguI), XhoI and SpeI* restriction sites, a SV40 promotor, a neomycin (kanamycin) resistance and a pUC origin for controlled amplification of the vector.

2.2.1.1 Cultivation of *CopyCutter™ EPI400™ Escherichia coli*

In order to cultivate the transformed *CopyCutter™ EPI400™ E. coli* agar plates were prepared. For this lysogeny broth (LB) medium (Table 1) was supplemented with 2% (w/v) agar and autoclaved. After cooling of the medium to 55°C, 0.05 mg/mL kanamycin was added as selective antibiotic. For a blue-white selection, 0.05 µg/mL 5-bromo-4-chloro-3-indolyl-β-D-galactopyranoside (X-Gal; dissolved in dimethylformamide (DMF)) was added. Finally, the medium was filled into petri dishes. The hardened agar plates were incubated at 37°C for 30 min before 5 µL of the *CopyCutter™ EPI400™ E. coli* glycerol culture (700 µL fresh liquid culture in 300 µL glycerol) were plated onto them. The bacteria were cultivated overnight at 37°C.

Table 1: LB medium

Component	*Amount*
NaCl	170 mM
Tryptone	1% (w/v)
Yeast extract	0.5% (w/v)
H_2O	
pH 7.0	

2.2.1.2 Mini preparation of plasmid DNA

The mini preparation of plasmid DNA was prepared with an overnight culture of the cultivated *CopyCutter™ EPI400™ E. coli*. For this 4 mL of LB medium (Table 1) supplemented with 0.05 mg/mL kanamycin were inoculated with a single colony of the cultivated *CopyCutter™ EPI400™ E. coli* plates. The sample was incubated overnight at 37°C and 180 rpm to obtain a saturated culture. The plasmid DNA was then isolated with the *QIA®prep Spin Miniprep Kit* (Qiagen, Hilden, D) according to the manufacturer's instructions using 2 mL of the overnight culture. The plasmid DNA was eluted in 50 µL H_2O.

In order to confirm the amplification of the correct plasmid a restriction fast digest (FD) was carried out. Eluted plasmid DNA was mixed with *FD Green Buffer* (Thermo Fisher Scientific, Waltham, USA), the restriction enzymes *SpeI* and *XhoI* (Thermo Fisher Scientific)

as well as H_2O according to Table 2 and incubated for 5 min at 37°C in a water bath. Finally, the results were analyzed by agarose (0.8%) gel electrophoresis.

Table 2: Restriction digest of pSTI-A120/hCFTR following mini preparation

Component	*Amount*
Plasmid DNA	2 µL
FD Green Buffer (10 x)	2 µL
SpeI (FD)	1 µL
XhoI (FD)	1 µL
H_2O	ad 20 µL

2.2.1.3 Maxi preparation of plasmid DNA

In order to isolate a larger scale of plasmid DNA a maxi preparation was performed after confirmation of the correct plasmid by a mini preparation. Briefly, 100 mL LB medium (Table 1) were supplemented with 100 µL *CopyCutter™ Inducer* (Biozym Scientific GmbH), 0.05 mg/mL kanamycin and 100 µL of the cultivated *CopyCutter™ EPI400™ E. coli* from the overnight culture prepared for the mini preparation. The cultures were incubated overnight at 37°C and 180 rpm to obtain a saturated culture. The maxi preparation was performed using the *mi-Plasmid Maxiprep Kit* (metabion international AG, Planegg, D) following the manufacturer's instructions. The plasmid DNA was eluted in 250 µL H_2O. Finally, the concentration of the DNA was determined with a microvolume spectrophotometer.

2.3 Molecular biological methods

2.3.1 Linearization of pSTI-A120/hCFTR-cDNA

For preparation of wtCFTR-mRNA, the plasmid pSTI-A120/hCFTR (Figure 11) containing human wtCFTR-cDNA was linearized. In order to restrict the plasmid it was mixed with *Buffer Tango* (Thermo Fisher Scientific), the restriction enzyme *LguI* (Thermo Fisher Scientific) and nuclease-free H_2O according to Table 3 following incubation at 37°C

overnight in a heating block. To determine a positive outcome of the restriction and to check the right size and reactivity of the plasmid a DNA gel electrophoresis (1%) was performed using 1 µL of the linearized plasmid.

Table 3: Sample mix for the restriction of pSTI-A120/hCFTR

Component	*Amount*
pSTI-A120/hCFTR	10 µg
Buffer Tango (10 x)	10 µL
LguI	4 µL
Nuclease free H_2O	ad 100 µL

To purify the linearized plasmid a phenol extraction was performed. 100 µL linearized plasmid were mixed with 100 µL nuclease free H_2O and 200 µL phenol-chloroform. The solution was centrifuged for 15 min at 15,500 x *g* yielding two phases (lower organic phase and upper aqueous phase). Afterwards, the superior aqueous phase containing the nucleic acid was mixed with 200 µL phenol-chloroform and centrifuged for 15 min at 15,500 x *g*. The aqueous phase was separated and mixed with 200 µL chloroform and centrifuged under previous conditions. The volume of the aqueous phase was determined and mixed with 0.1 x volume sodium acetate (3 M; pH 5.2) and 2.5 x volumes ethanol (99%) in order to precipitate the DNA. The sample was incubated at -20°C overnight.

Finally, the sample was centrifuged at 4°C at 13,000 x *g* for 1 h. The supernatant was discarded and the pellet was resuspended in 500 µL ethanol (70%). Centrifugation was repeated under previous conditions and the supernatant was discarded. The pellet was then dried in a vacuum centrifuge for 10 min at 45°C. The pellet was resuspended in 10 µL nuclease free H_2O and the concentration of the linearized cDNA was determined with a microvolume spectrophotometer. The cDNA was stored at -20°C until further experiments were conducted.

2.3.2 DNA gel electrophoresis

In order to analyze the size and reactivity of DNA samples a DNA agarose gel electrophoresis was carried out. The principle of this method is the separation of DNA by

size through the pores of the agarose gel. Briefly, the negatively charged nucleic acid migrates through the gel by applying an electric field. During this process, larger molecules move slower than smaller molecules. The gel was cast in a horizontal gel chamber according to Table 4. For sample preparation, the desired amount of DNA was mixed with *6 x DNA loading dye* (Thermo Fisher Scientific) and loaded to the gel. 0.5 x TBE (Table 5) buffer was used as running buffer. For determination of size, *O'GeneRuler™ 1 kb Plus DNA Ladder* or *O'GeneRuler™ 100 bp Plus DNA Ladder* (Appendix Figure 59; Thermo Fisher Scientific) were used as marker. The gel was run at 128 V and then analyzed in a *BioDocAnalyze System* (Analytik Jena, Jena, D).

Table 4: Agarose gel (1%) for DNA gel electrophoresis

Component	*Amount*
Agarose	500 mg
0.5 x TBE	50 mL
Midori Green Advance	3 µL

Table 5: 0.5 x TBE

Component	*Amount*
Tris	45 mM
Boric acid	45 mM
EDTA	1 mM
pH 8.3	

2.3.3 *In vitro* transcription

An *in vitro* transcription (IVT) was carried out to transcribe the linearized plasmid cDNA and produce wtCFTR-mRNA using the *mMESSAGE mMACHINE™ T7 Transcription Kit* (Invitrogen, Carlsbad, USA). The samples were mixed according to Table 6 and incubated in a water bath at 37°C for 2 h. Afterwards, 1 µL Turbo DNAse was added to digest the DNA template following incubation in a water bath at 37°C for 15 min.

Table 6: Sample mix for the *in vitro* transcription. According to the *mMESSAGE mMACHINE™ T7 Transcription Kit* (Invitrogen)

Component	*Amount*
2 x NTP/CAP	10 µL
10 x Buffer	2 µL
T7-Polymerase (2 U/µL)	2 µL
Plasmid DNA	1 µg
Nuclease free H_2O	ad 20 µL

Subsequently, the mRNA was purified using the *RNeasy® Plus Mini Kit (50)* (Qiagen). In the process, 350 µL *RLT buffer* were mixed with 1% β-mercaptoethanol. After the solution was mixed with the IVT sample and transferred into a *gDNA eliminator spin column,* it was centrifuged at 9,300 x *g* for 1 min. The column was then discarded and the flow-through was mixed with 370 µL ethanol (70%). The mixture was transferred to an *RNeasy spin column* and centrifuged at 9,300 x *g* for 1 min. The flow-through was discarded and 700 µL *RW1 buffer* were given onto the spin column. After another centrifugation at 9,300 x *g* for 1 min and discard of the flow-through, 500 µL *RPE buffer* were added to the spin column. The sample was centrifuged again at 9,300 x *g* for 1 min and the flow-through was discarded. The last step was repeated once and the flow-through was discarded again after centrifugation at 9,300 x *g* for 2 min.

For elution of the mRNA, 50 µL nuclease free H_2O were pipetted onto the membrane in the spin column and incubated for 1 min before centrifugation at 9,300 x *g* for 1 min. This step was repeated once. The eluate was mixed with 0.1 x volume ammonium acetate stop solution (ammonium acetate 5 M, EDTA 100 mM) and 2.5 x volumes ethanol (70%) and stored at -20°C overnight in order to precipitate the nucleic acid.

Subsequently, the sample was pelleted at 4°C at 14,000 x *g* for 1 h. The supernatant was discarded and the pellet was resuspended in 500 µL ethanol (70%). Centrifugation was repeated under previous conditions and the supernatant was discarded. The pellet was then dried in a vacuum centrifuge for 10 min at 45°C. Finally, the pellet was resuspended in 10 µL nuclease free H_2O and the concentration of the mRNA was determined with a microvolume spectrophotometer. A satisfactory outcome of the IVT was determined with

a RNA gel electrophoresis (1%) using 0.5 µg of mRNA. The mRNA was stored at -20°C until further experiments were conducted.

2.3.4 RNA gel electrophoresis

To determine the size and reactivity of RNA samples a RNA gel electrophoresis was carried out. For this a denaturing agarose gel was prepared according to Table 7. Denaturation of the RNA is achieved through cleavage of the hydrogen bridge bonds by formaldehyde. The gel was cast in a horizontal gel chamber. Before adding the RNA running buffer and the formaldehyde, the diethylpyrocarbonate (DEPC) H_2O and agarose were heated until the agarose was completely dissolved and then cooled to approximately 60°C to avoid destruction of the formaldehyde. For preparation of the samples the desired amount of mRNA was mixed with *2 x RNA loading dye* (Thermo Fisher Scientific) and nuclease free H_2O to a final volume of 10 µL. Before loading the samples to the gel, they were incubated at 70°C for 10 min in order to avoid hairpin structures. 5 x RNA running buffer (Table 8) diluted 1:5 with DEPC H_2O (0.05%) was used as running buffer. For determination of size, *RiboRuler™ High Range RNA Ladder* (Appendix Figure 60; Thermo Fisher Scientific) was used as marker. The gel was run at 128 V and then analyzed in a *BioDocAnalyze System* (Analytik Jena).

Table 7: Agarose gel (1%) for RNA gel electrophoresis

Component	*Amount*
Agarose	500 mg
DEPC H_2O (0.05%)	37.5 mL
5 x RNA running buffer	10 mL
Formaldehyde (37%)	2.5 mL

Table 8: 5 x RNA running buffer. Protect from light. Dilute 1:5 in DEPC H_2O (0.05%) to use as running buffer.

Component	*Amount*
MOPS (3-(*N*-morpholino) propanesulfonic acid)	0.1 M
Sodium acetic	50 mM
EDTA (pH 8.0)	5 mM
DEPC H_2O (0.05%)	ad 1 L
pH 7.0	

2.3.5 RNA isolation from cells

Total RNA was isolated from cells using the *RNeasy® Plus Mini Kit (50)* (Qiagen). Before isolation of RNA from cells grown on T25 flasks or 6-well plates, cells were washed with PBS (Table 23; 37°C). Afterwards, *RLT buffer* supplemented with 1% β-mercaptoethanol (T25 flask 600 µL; 6-well plate 350 µL) was given onto the dish and cells were scraped off with a cell scraper. Cells grown on *Costar Transwell®permeable* filters were trypsinized following the protocol *Trypsinization Procedure for Corning® Transwell® Inserts* (Corning Inc., Lowell, USA). The cell pellet was then resuspended in 350 µL *RLT buffer* supplemented with 1% β-mercaptoethanol.

The cell lysate was homogenized by passing it through a needle (0.9 mm diameter) fitted to a syringe at least 5 times. Subsequently, the manufacturer's instructions were followed in order to isolate the total RNA from the cell lysate. The RNA was eluted in 30 µL nuclease-free H_2O and the concentration was determined with a microvolume spectrophotometer. The isolate was stored at -20°C.

2.3.6 Reverse transcriptase polymerase chain reaction

The reverse transcriptase polymerase chain reaction (RT-PCR) is a technique to amplify complementary DNA (cDNA) from RNA using reverse transcription. For the reaction, the *SuperScript® III Reverse Transcriptase* (Invitrogen) was used. Samples were prepared according to Table 9. In the first step, the RNA template was mixed with the Oligo$(dT)_{18}$ primers (Thermo Fisher Scientific), the dNTP mix (Thermo Fisher Scientific) and H_2O and incubated at 65°C for 5 min in order to avoid hairpin structures. Afterwards, the sample

was kept on ice for 1 min before the *5 x First Strand buffer*, dithiothreitol (DTT), *RiboLock RNase Inhibitor* (Thermo Fisher Scientific) and the reverse transcriptase were added. The sample was then incubated at 50°C for 60 min to allow the reverse transcription. Finally, the reaction was stopped by incubation of the sample at 70°C for 15 min. The obtained cDNA was assumed to have a concentration of 50 ng/µL and was stored at 4°C.

Table 9: RT-PCR reaction

Component	*Amount*
RNA	1 µg
Oligo(dT)$_{18}$ primer (10 pmol/µL)	1 µL
dNTP mix (10 mM each)	1 µL
5 x First Strand buffer	4 µL
DTT (0.1 M)	1 µL
RiboLock RNase Inhibitor (40 U/µL)	1 µL
SuperScript® III Reverse Transcriptase (200 U/µL)	1 µL
H_2O	ad 20 µL

2.3.7 Polymerase chain reaction

The polymerase chain reaction (PCR) is a sensitive technique that allows rapid amplification of a specific DNA fragment and was first described by Kary Banks Mullis (Mullis, 1990). Briefly, the PCR proceeds in three steps: denaturation, annealing and elongation. During the denaturation, the temperature is raised above the melting point of the DNA in order to separate the two strands. In the second step, the annealing, the sample is cooled down to allow specific primers to bind to the template DNA. Primers are short single-stranded DNA fragments complementary to a specific sequence of the template DNA, which is to be detected and amplified. In the third and last step, the elongation, the temperature is raised again to a point, at which the DNA polymerase is able to extend the primers by adding nucleotides thereby producing two complete double strands. These steps are repeated multiple times allowing the DNA to be multiplied exponentially (Garibyan and Avashia, 2013).

For the reaction, the *TopTaq™ DNA Polymerase Kit* (Qiagen) containing the thermostable *TopTaq™* DNA polymerase was used. Samples were prepared according to Table 10 and the PCR program was run according to Table 11. A satisfactory outcome of the PCR was determined with a DNA gel electrophoresis (1.5%) using 12 µL of the PCR product. Further information about the primers can be found in the appendix in chapter 6.4.

Table 10: PCR reaction

Component	*Amount*
DNA template (50 ng/µL)	2 µL
10 x TopTaq PCR buffer	5 µL
10 x CoralLoad	5 µL
dNTP mix (10 mM each)	1 µL
Primer Mix (10 µM each)	1 µL
TopTaq DNA Polymerase	0.25 µL
H_2O	ad 50 µL

Table 11: Cycling program for PCR. Steps 2.-4. were repeated in 27-33 cycles.

PCR step	*Temperature*	*Time*
1. Initial denaturation	94°C	3 min
2. Denaturation	94°C	30 s
3. Annealing	60°C	30 s
4. Elongation	72°C	1 min
5. Final elongation	72°C	10 min
6. End of reaction	4°C	∞

2.3.8 Sequencing

Before the amplified TRPV1 fragment could be sequenced it was cloned into the vector pSC-A-amp/kan using the *StrataClone PCR Cloning Kit* (Agilent, Santa Clara, USA) according to the manufacturers' instructions. The plasmid was then transformed into competent bacteria and finally isolated and purified as described in 2.2.1. For restriction of the

plasmid, the enzyme *EcoRI* (Thermo Fisher Scientific) was used. Finally, 6 µL of the plasmid DNA were mixed with 1 µL T3 or T7 promotors (10 pmol/mL) and sequenced by the company *StarSEQ* (Mainz, D). The determined sequence was compared to a sequence of human TRPV1 from the NCBI database (NM_080706.3; https://www.ncbi.nlm.nih.gov/). For this the sequences were aligned using the program *GeneDoc 2.7*.

2.4 Preparation of nanoformulations

2.4.1 Chitosan

The chitosan used was an ultrapure biomedical grade Heppe 70/5 (Batch-No. 212-170614-01) purchased from HMC+ GmbH (Halle/Saale, Germany, D). The Mw of this chitosan is 29.3 kDa and it has a DA of 17%. It was dissolved in H_2O with or without 85 mM NaCl with 5% stoichiometric excess of 5 M HCl.

2.4.2 Chitosan-mRNA complexes

The chitosan (CS) stock solution was diluted to reach the desired concentration for a working solution with a N/P charge ratio of 37, based on the results of the characterization of the CS-wtCFTR-mRNA complexes (Kolonko, 2016). The N/P charge ratio is defined as the molar ratio of amine to phosphate groups of chitosan and nucleic acids, respectively. The equivalent concentrations of charge were calculated using Equation 1:

$$n_{\text{nucleic acid}}\,(\text{mol}) = [c_{\text{nucleic acid}}\,(\text{g/L}) \times V_{\text{nucleic acid}}\,(\text{L})] \,/\, Mw_{\text{nucleic acid}}\,(\text{g/mol})$$

$$n_{\text{negative charges nucleic acid}}\,(\text{mol}) = n_{\text{nucleic acid}}\,(\text{mol}) \times \text{number of negative charges per mol}$$

$$n_{\text{positive charges chitosan}}\,(\text{mol}) = n_{\text{negative charges nucleic acid}}\,(\text{mol}) \times \text{charge ratio (N/P)} \quad (1)$$

The CS-wtCFTR-mRNA complexes were prepared by mixing the chitosan working solution with an equal volume of wtCFTR-mRNA (Table 12). The mixtures were incubated for 30 min at room temperature (RT) to allow self-assembly of the complexes.

Table 12: Composition of the CS-wtCFTR-mRNA complexes at N/P charge ratio 37. Charge ratio (N/P): molar ratio of equivalent charges of NH_3^+/PO_4^-; **wtCFTR-mRNA (nmol)**: equivalent concentration of PO_4^- from wtCFTR-mRNA; **chitosan (nmol)**: equivalent concentration of NH_3^+ from chitosan.

Charge ratio	*wtCFTR-mRNA*		*Chitosan*	
N/P	*(nmol)*	*(µg/µL)*	*(nmol)*	*(µg/µL)*
37	9.3	0.3	343.8	7.0

2.4.3 Chitosan-ASO complexes

The chitosan stock solutions were diluted to reach the desired concentrations for varying N/P charge ratio working solutions. The equivalent concentrations of charge of the amine and phosphate groups were calculated using Equation 1.

Three different ASO against the α-subunit of ENaC (accession number: NM_001038) were used in this study, including a sense control and an ASO labelled with a fluorescent 6-Fam tag (Table 13). The ASO sequence termed "ASOgreen" was designed by Segal *et al.* in 2002 and corresponds to the human α-ENaC mRNA at position 290 (Segal et al., 2002; Sobczak et al., 2009). The nucleotides were synthesized as phosphorothioates by metabion international AG.

The CS-ASO complexes of different N/P charge ratios were prepared by mixing a constant amount of ASO with 2 x volumes of the chitosan working solutions (Table 14, Table 15, Table 16). Briefly, 20 µL chitosan working solution with or without 85 mM NaCl were mixed with 10 µL ASO and 20 µL H_2O and incubated for 30 min at RT to allow self-assembly of the complexes.

Table 13: Sequences and application of antisense oligonucleotides against α-ENaC

Oligo Name	*Sequence 5'-3'*	*Application*
ASOgreen	TGG ATG GTG GTG TTG T	antisense
ASOgreen_sense	ACA ACA CCA CCA TCC A	sense (negative control)
5'Fam-ASOgreen	6-Fam-TGG ATG GTG GTG TTG T	antisense (fluorescent)

Table 14: Composition of CS-ASOgreen complexes at varying N/P charge ratios. Charge ratio (N/P): molar ratio of equivalent charges of NH_3^+/PO_4^-; **ASOgreen (nmol)**: equivalent concentration of PO_4^- from ASOgreen; **chitosan (nmol)**: equivalent concentration of NH_3^+ from chitosan.

Charge ratio	*ASOgreen*		*Chitosan*	
N/P	*(nmol)*	*(µg/µL)*	*(nmol)*	*(µg/µL)*
30	4.6	0.3	137.0	2.8
50	4.6	0.3	228.4	4.6
70	4.6	0.3	319.7	6.5
90	4.6	0.3	411.0	8.3
100	4.6	0.3	456.7	9.3

Table 15: Composition of CS-ASOgreen_sense complexes at varying N/P charge ratios. Charge ratio (N/P): molar ratio of equivalent charges of NH_3^+/PO_4^-; **ASOgreen_sense (nmol)**: equivalent concentration of PO_4^- from ASOgreen; **chitosan (nmol)**: equivalent concentration of NH_3^+ from chitosan.

Charge ratio	*ASOgreen_sense*		*Chitosan*	
N/P	*(nmol)*	*(µg/µL)*	*(nmol)*	*(µg/µL)*
30	4.8	0.3	144.3	2.9
50	4.8	0.3	240.5	4.9
70	4.8	0.3	336.7	6.8
90	4.8	0.3	433.0	8.8
100	4.8	0.3	481.1	9.8

Table 16: Composition of CS-5'Fam-ASOgreen complexes at varying N/P charge ratios. Charge ratio (N/P): molar ratio of equivalent charges of NH_3^+/PO_4^-; **5'Fam-ASOgreen (nmol)**: equivalent concentration of PO_4^- from ASOgreen; **chitosan (nmol)**: equivalent concentration of NH_3^+ from chitosan.

Charge ratio	*5'Fam-ASOgreen*		*Chitosan*	
N/P	*(nmol)*	*(µg/µL)*	*(nmol)*	*(µg/µL)*
30	4.7	0.3	140.0	2.8
50	4.7	0.3	233.1	4.7
70	4.7	0.3	326.4	6.6
90	4.7	0.3	419.6	8.5
100	4.7	0.3	466.2	9.5

2.4.4 Chitosan-mRNA-ASO complexes

The chitosan stock solution containing 85 mM NaCl was diluted to reach the desired concentrations for varying N/P charge ratio working solutions. The equivalent concentrations of charge of the amine and phosphate groups were calculated using Equation 1.

The CS-mRNA-ASO complexes of different N/P charge ratios were prepared by mixing a constant amount of mRNA and ASO with the chitosan working solutions (Table 17, Table 18 and Table 19). Briefly, 20 µL chitosan working solution were mixed with 15 µL ASO and 15 µL wtCFTR-mRNA and incubated for 30 min at RT to allow self-assembly of the complexes.

Table 17: Composition of CS-mRNA-ASOgreen complexes at varying N/P charge ratios. Charge ratio (N/P): molar ratio of equivalent charges of NH_3^+/PO_4^-; **wtCFTR-mRNA/ASOgreen (nmol):** equivalent concentration of PO_4^- from wtCFTR-mRNA/ASOgreen; **chitosan (nmol):** equivalent concentration of NH_3^+ from chitosan.

Charge ratio	*wtCFTR-mRNA*		*ASOgreen*		*Chitosan*	
N/P	*(nmol)*	*(µg/µL)*	*(nmol)*	*(µg/µL)*	*(nmol)*	*(µg/µL)*
10	2.47	0.053	0.46	0.01	29.3	0.30
30	2.47	0.053	0.46	0.01	87.8	0.89
50	2.47	0.053	0.46	0.01	146.4	1.48
70	2.47	0.053	0.46	0.01	205.0	2.08
90	2.47	0.053	0.46	0.01	263.5	2.67

Table 18: Composition of CS-mRNA-ASOgreen_sense complexes at varying N/P charge ratios. Charge ratio (N/P): molar ratio of equivalent charges of NH_3^+/PO_4^-; **wtCFTR-mRNA/ASOgreen_sense (nmol):** equivalent concentration of PO_4^- from wtCFTR-mRNA/ASOgreen_sense; **chitosan (nmol):** equivalent concentration of NH_3^+ from chitosan.

Charge ratio	*wtCFTR-mRNA*		*ASOgreen_sense*		*Chitosan*	
N/P	*(nmol)*	*(µg/µL)*	*(nmol)*	*(µg/µL)*	*(nmol)*	*(µg/µL)*
10	2.47	0.053	0.48	0.01	29.5	0.30
30	2.47	0.053	0.48	0.01	88.6	0.90
50	2.47	0.053	0.48	0.01	147.6	1.50
70	2.47	0.053	0.48	0.01	206.7	2.09
90	2.47	0.053	0.46	0.01	265.7	2.69

Table 19: Composition of CS-mRNA-5'Fam-ASOgreen complexes at varying N/P charge ratios. Charge ratio (N/P): molar ratio of equivalent charges of NH_3^+/PO_4^-; **wtCFTR-mRNA/5'Fam-ASOgreen (nmol):** equivalent concentration of PO_4^- from wtCFTR-mRNA/5'Fam-ASOgreen; **chitosan (nmol):** equivalent concentration of NH_3^+ from chitosan.

Charge ratio	*wtCFTR-mRNA*		*5'Fam-ASOgreen*		*Chitosan*	
N/P	*(nmol)*	*(µg/µL)*	*(nmol)*	*(µg/µL)*	*(nmol)*	*(µg/µL)*
10	2.47	0.053	0.47	0.01	29.4	0.30
30	2.47	0.053	0.47	0.01	88.1	0.89
50	2.47	0.053	0.47	0.01	146.9	1.49
70	2.47	0.053	0.47	0.01	205.6	2.08
90	2.47	0.053	0.46	0.01	264.4	2.68

2.4.5 Chitosan-lecithin oil-core nanocapsules

The chitosan-coated nanocapsules (NC) were prepared with slight modifications as previously described (Kaiser et al., 2015b). Briefly, 400 µL of an ethanolic lecithin solution (100 mg/mL) were mixed with 530 µL of a capsaicin (CAP) stock solution (24 mg/mL in ethanol). This was supplemented with 125 µL Miglyol® 812 N and 9.5 mL ethanol. The organic solution was immediately poured into 20 mL aqueous chitosan (0.5 mg/mL) under stirring. The milky mixture was concentrated in a rotavapor (Büchi R-210, Büchi Labortechnik GmbH, Essen, D) at 40°C while the pressure was slowly decreased to 0 mbar until 3.5-4.0 mL remained. The volume was topped up to 4.0 mL with H_2O if necessary to yield a final capsaicin concentration of 10 mM and a final chitosan concentration of 2.5 mg/mL. Unloaded nanocapsules were prepared by replacing the capsaicin solution with ethanol.

To coat the capsules with mRNA 15 µL of capsules were carefully mixed with different volumes of wtCFTR-mRNA (0.053 µg/µL) to reach varying charge ratios (Table 20). Samples were incubated at RT for 30 min to allow the mRNA to adsorb to the chitosan.

Table 20: Composition of the CS-capsules coated with wtCFTR-mRNA at varying N/P charge ratios. **Charge ratio (N/P)**: molar ratio of equivalent charges of NH_3^+/PO_4^-; **wtCFTR-mRNA (nmol)**: equivalent concentration of PO_4^- from wtCFTR-mRNA; **chitosan (nmol)**: equivalent concentration of NH_3^+ from chitosan.

Charge ratio	*wtCFTR-mRNA*		*Chitosan*	
N/P	*(nmol)*	*(µg/µL)*	*(nmol)*	*(µg/µL)*
5	33.8	0.053	185.1	2.5
10	17.8	0.053	185.1	2.5
50	3.7	0.053	185.1	2.5
75	2.5	0.053	185.1	2.5
100	1.9	0.053	185.1	2.5

2.5 Characterization of nanoformulations

2.5.1 Determination of hydrodynamic diameter and polydispersity index

The hydrodynamic diameter, or Z-average size, is the size of a particle in solution including a hydration layer surrounding the particle. The polydispersity index (PDI) is a dimensionless measure and gives an indication of the size distribution width. Both parameters of the nanosystems were measured by dynamic light scattering with non-invasive back scattering (DLS-NIBS) with a measurement angle of 173° using a *Zetasizer Nano ZS 6300* (Malvern Panalytical Ltd, Worcestershire, UK). Measurements were conducted using a folded capillary zeta cell (Model DTS1070; Malvern Panalytical Ltd) at 25°C. Samples were diluted in a range of 1:10-1:65 in H_2O before the measurement in order to achieve an acceptable count rate.

2.5.2 Determination of zeta potential

Zeta potential of the nanosystems was determined from their electrophoretic mobility with a *Zetasizer Nano ZS 6300* (Malvern Panalytical Ltd). Zeta potential was acquired by applying the Henry equation using the Smolouchowski approximation after exerting Laser Doppler Micro-electrophoresis and Phase analysis Light Scattering (Delgado et al., 2007). Measurements were conducted using a folded capillary zeta cell (Model DTS1070; Malvern Panalytical Ltd) at 25°C. Complexes were diluted in a range of 1:30-1:65 in KCl (1 mM); capsules were diluted 1:65 in H_2O.

2.5.3 Stability measurements

Stability of the nanosystems in transfection medium was determined by measuring their hydrodynamic diameter and PDI at different time points by DLS-NIBS with a measurement angle of 173° using a *Zetasizer Nano ZS 6300* (Malvern Panalytical Ltd). Measurements were conducted at 37°C using a low volume disposable cuvette (Sarstedt AG & Co, Hemer, D). The nanosystems were diluted in a range of 1:10-1:65 in *Opti-MEM™* (Thermo Fisher Scientific) or *Opti-MEM™* supplemented with HEPES (20 mM) and mannitol (270 mM) instead of water and incubated at 37°C in between measurements.

2.5.4 Gel retardation assay

In order to test the binding efficiency of nucleic acids to CS a gel retardation assay was carried out. This method is based on the principle of a gel electrophoresis. Briefly, nanosystems are loaded to an agarose gel and an electric field is applied. Negatively charged nucleic acids, which should migrate towards the anode, are expected to be retained in the pockets by the positively charged polymer.

For the CS-ASO complexes, an agarose gel (1.5%, Table 4) was cast. To prepare the samples, 6.6 µL CS was mixed with 3.3 µL ASO (0.3 µg/µL) and incubated at RT for 30 min before addition of *6 x DNA loading dye* (Thermo Fisher Scientific). The gel was run at 128 V for 40 min in 0.5 x TBE buffer (Table 5).

For the CS-coated nanocapsules, an agarose-formaldehyde gel (1%; Table 7) was cast. For preparation of the samples 5 µL wtCFTR-mRNA (0.053 µg/µL) were mixed with 5 µL CS-coated nanocapsules (blank and loaded) and incubated for 30 min at RT before addition of *2 x RNA loading dye* (Thermo Fisher Scientific). The gel was run at 128 V for 45 min in RNA running buffer (Table 8). Finally, the nucleic acid bands were visualized in a *BioDocAnalyze System* (Analytik Jena).

2.5.5 Asymmetric flow field-flow fractionation

Measurements were performed on an AF2000 Multiflow system from Postnova Analytics GmbH (Landsberg am Lech, D), which was set to be operated in AF4 mode. The system was coupled with an online 21 angle, multi-angle light scattering detector MALS (PN3621), a refractive index detector RI (PN3150) and a dual wavelength UV detector (PN3211), which was set for these experiments at 280 and 220 nm. Additionally, a DLS detector (Zetasizer Nano ZS, Malvern Panalytical Ltd.) was also fitted online using a light path quartz flow cell (ZEN0023) and 173° backscattered angle for R_h determination.

The AF4 system was equipped with an analytical asymmetric AF4 channel (Postnova Z-AF4-CHA-611) using a 350 µm spacer. The temperature of the channel was controlled by a thermostat (PN4020) set at 30°C for all experiments. A membrane made of regenerated cellulose with 10 kDa cut-off was used (Z-AF4-MEM-612-10KD, Postnova Analytics). Due to the presumed structure of the evaluated nanocapsules having as an outer layer the

adsorbed chitosan, the nanocapsules have then a positive net surface charge evidenced by zeta potential measurements. Therefore, in order to minimize the interactions between the nanocapsules and the residual negatively charged groups likely to be present in the membrane, an acetate buffer solution (0.18 M acetic acid, 0.02 M sodium acetate, pH=3.7) was used as a carrier liquid to carry out the elution. At the pH of the carrier liquid (pH=3.7) the surface of the membrane should be charged positively ($\zeta \sim 10$ mV). This will favor the polymer elution as repulsion forces will be generated between the cationic nanocapsules and the positively charged membrane (González-Espinosa et al., 2019).

The sample for analysis by AF4 was prepared by diluting the nanocapsules sample in the carrier liquid (0.18 M acetic acid, 0.02 M sodium acetate, pH 3.7) used to run the experiments in a ratio 4:1 (nanocapsules : carrier liquid), respectively. For each run, a volume of 2 µL was injected into the system. At this sample dilution and injection volume, good signal to noise was obtained.

A cross-flow programmed with a time delay exponential decay was used to carry out the elution. After injection at 0.2 mL/min, sample was focused for 3 min at a rate of 1.3 mL/min and with cross-flow set at 1 mL/min. At the end of the focusing period and a transition period of 0.2 min the profile of the cross-flow was gradually decreased over 60 min through a series of consecutive steps. These were as follows: a) For 0.2 min cross-flow was kept constant at 1 mL/min, b) cross-flow was then decreased at an exponent of decay of 0.2 to 0.1 mL/min over 40 min period and finally, c) the cross-flow was kept constant to 0.1 mL/min for 20 min. During this entire process, including the focus step, the detector flow was maintained at 0.5 mL/min, which ensures detector baseline stability.

Data collection and analysis were performed using NovaFFF software version 2.0.9.9. (Postnova Analytics GmbH). Measurements were repeated three times per sample and a blank sample (the solution used as a liquid carrier for measurement) was run as well. Before performing the evaluation of data, performed runs were always verified to ensure reproducibility of the elution profiles. Data collected for all runs were best fitted to random coil model. A series of preliminary experiments was carried out to optimize the method, sample concentration and injection volume.

2.5.6 Transmission electron microscopy

The ultrastructure of the chitosan-lecithin oil-core nanocapsules was investigated using TEM. Equal amounts of samples were mixed with uranyl acetate solution (negative staining, 1% w/v). Samples (8 µL) were placed onto a copper grid covered with *Formvar®* film and the excess of liquid was removed with the aid of a filter paper. The analyses were performed using JEM-1400 TEM (JEOL, Peabody, MA, USA) operated at 100 kV and captured on AMT 1K CCD using the software AMTV602.

2.6 Cell culture

2.6.1 CFBE41o- cells

The cell line CFBE41o- (provided by Dr. Dieter Gruenert, Department of Otolaryngology – head and neck surgery, University of California, San Francisco, USA) is often being used in CF research (Gruenert et al., 2004). In the early 1990s, it was generated from bronchial epithelial cells of a CF patient (Gruenert et al., 1988). This was achieved by transformation of the simian virus 40 (SV40) large T-antigen using the origin-of-replication defective plasmid pSVori-. The cells are homozygous for ΔF508, the most common mutation in CF. Even though CFBE41o- cells do not produce mucus (Murgia et al., 2017), it has been shown that under liquid covered culture (LCC) conditions the cells are able to form a confluent cell monolayer with functioning cell-cell-contacts and have a transepithelial resistance of 100-500 Ω (Ehrhardt et al., 2006; Gruenert et al., 2004). The cell line is a suitable preclinical model for the study of CF and is often used in current research (Faraj et al., 2019; Kamei et al., 2019; Puglia et al., 2018; Reece et al., 2018; Sharma et al., 2018).

CFBE41o- cells were cultivated on fibronectin in an incubator at 37°C with 5% CO_2 and 95% rH. The medium was replaced every 2-3 days with fresh cell culture medium (37°C; Table 22). Cell culture flaks and other culture vessels were wet with a fibronectin coating solution (Table 21) and then dried for 2-4 h at 37°C before seeding of the cells.

Table 21: Fibronectin coating solution (1%)

Component	*Amount*
BSA (7.5%)	0.13% (v/v)
Bovine collagen A (1 mg/mL)	3% (v/v)
Human Fibronectin (1 mg/mL)	1% (v/v)
H_2O	7.87% (v/v)
LHC Basal Medium	

Table 22: CFBE41o- cell culture medium

Component	*Amount*
FBS	10% (v/v)
L-Glutamine	2 mM
Penicillin/Streptomycin	100 U/mL
MEM Earle's Medium	

Table 23: Phosphate buffered saline (PBS)

Component	*Amount*
NaCl	137 mM
KCl	2.7 mM
Na_2HPO_4	10.2 mM
KH_2PO_4	1.8 mM
pH 7.4	

When CFBE41o- cells reached confluence, they were passaged in order to prevent morphological changes. Cells were washed with PBS (Table 23; 37°C) and then incubated with trypsin/EDTA (0.25%/ 0.02%; 37°C) for 7 min at 37°C in order to release the adherent cells from the flask. The reaction was then stopped with cell culture medium and the suspension was centrifuged at 500 x *g* for 5 min. The cell pellet was resuspended in fresh cell culture medium (37°C) and the desired amount of cells was transferred to a new fibronectin coated flask. For Ussing chamber experiments, 1.15 x 10^5 cells were seeded on

1% fibronectin coated *Costar Transwell®permeable* filters (Ø = 6.5 mm; REF 3470; Corning Inc.). The number of cells was determined using a *Neubauer* improved haemocytometer (Figure 12). The medium was changed every 2-3 days and experiments were conducted after approximately 10 days.

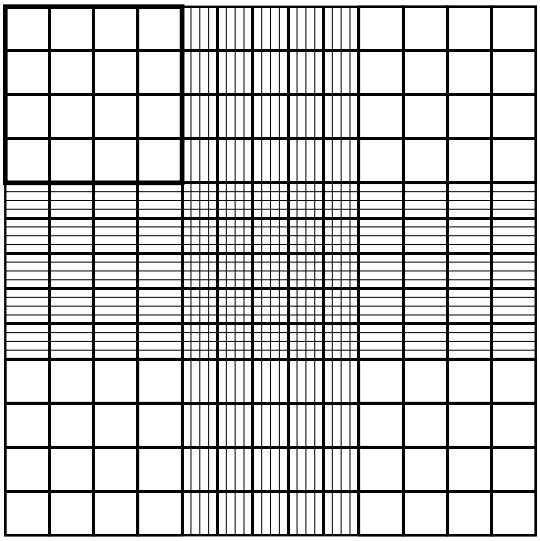

Figure 12: *Neubauer* improved haemocytometer. The Neubauer improved haemocytometer is used to determine the density of a cell suspension. The number of cells (N) counted in one large square (marked black) corresponds to the concentration of the cell suspension given in N x 10^4 cells/mL.

2.6.2 H441 cells

The cell line NCI-H441 (H441) was generated in 1982 by Brower *et al.* from the pericardial fluid of a male patient with papillary adenocarcinoma of the lung (Brower et al., 1986). The cells show characteristics of club cell-like bronchiolar lung epithelium and do not develop cilia. They express the surfactant proteins SP-A, SP-B, SP-C and SP-D and are therefore well suited for cultivation under air liquid interface (ALI) conditions. In addition, they are able to generate an acceptable transepithelial electrical resistance (TEER) both under LCC conditions (1,010 Ω x cm^2) and under ALI conditions (300 Ω x cm^2) (Salomon et al., 2014). Being an excellent *in vitro* model of the human distal lung epithelium, H441 cells are used in a broad spectrum in contemporary research (Castellani et al., 2018; De Leo et al., 2018; Kawami et al., 2019; Mies et al., 2019; Montesanto et al., 2019; Sumi et al., 2018).

The cells were cultured in uncoated T25 or T75 flasks in RPMI 1640 medium with supplements (Table 24). The medium of the cells was changed every 2-3 days and they were cultured at 37°C, 5% CO_2 and 95% rH.

Table 24: Standard H441 cell culture medium

Component	*Amount*
Antibiotic/Antimycotic solution (100 x)	100 U/mL (Penicillin) 100 µg/mL (Streptomycin) 250 ng/mL (Amphotericin)
Sodium pyruvate	1 mM
ITS media supplement	5 µg/mL (Insulin) 5 µg/mL (Transferrin) 5 ng/mL (Sodium Selenite)
Fetal bovine serum	10% (v/v)
RPMI 1640	

When the cells reached approximately 80% confluence they were passaged. Briefly, cells were washed with PBS (Table 23; 37°C) and then detached from the flask with trypsin/EDTA (0.25%/0.02%; 37°C) by incubation for 10 min at RT. The trypsin reaction was stopped with H441 cell culture medium. After centrifugation of the cell suspension for 5 min at 200 x *g*, the cell pellet was resuspended in fresh H441 cell culture medium and the desired amount of cells was transferred to a new flask.

For Ussing chamber experiments, cells were seeded onto uncoated *Costar Transwell®permeable* filters (Ø = 6.5 mm) with a density of 1×10^6 cells/cm^2. The number of cells was determined using a *Neubauer* improved haemocytometer (Figure 12). One day after seeding the H441 cell culture medium was replaced by H441 medium supplemented with dexamethasone (Table 25). This medium for the cultivation of H441 cells on filters contains dexamethasone in order to promote development of tight junctions and expression of ENaC (Ramminger et al., 2004). For cultivation of the cells under ALI conditions, the medium on the apical side of the filters was removed one day after seeding and cells were only supplied with medium on the basolateral side. The filters were cultured at least 7 days at 37°C, 5% CO_2 and 95% rH before experiments were conducted. For transfection experiments with H441 cells grown on filters, the medium was replaced by antibiotic-free H441 medium without dexamethasone 24 h before transfection.

Table 25: H441 Dex cell culture medium for cultivation on filters

Component	*Amount*
Dexamethasone	200 nM
Antibiotic/Antimycotic solution (100 x)	100 U/mL (Penicillin) 100 µg/mL (Streptomycin) 250 ng/mL (Amphotericin)
Sodium pyruvate	1 mM
ITS media supplement	5 µg/mL (Insulin) 5 µg/mL (Transferrin) 5 ng/mL (Sodium Selenite)
Fetal bovine serum	10% (v/v)
RPMI 1640	

2.6.3 Primary human nasal epithelial cells

In order to give more physiological relevance to this study primary cells of human nasal epithelium (HNE) were used. Until now no suitable animal model for CF research has been developed (Semaniakou et al., 2018). Therefore, primary cells are very attractive for drug delivery studies since they approximate the actual function of the tissue and therefore simulate an *in vivo* situation (Schmidt et al., 1998). Even though culturing of primary cells is very promising, it has several disadvantages such as limited amount of tissue and use of passage number, fastidious culturing method or donor-to-donor variability (Cho et al., 2010). However, this variability is contributing to simulating an *in vivo* situation since not all donors have the same level of CFTR or ENaC expression.

Nasal specimens were provided by patients undergoing nasal surgery from Maria and Josef Hospital (Greven, D). The samples were typically nasal polyps or nasal turbinates of patients suffering chronic sinusitis. Further samples were given voluntarily by healthy individuals through nasal brushings. The study was approved by the committees for human studies of the University of Münster (Ethik Kommission Münster; Aktenzeichen: 4IV Kusche). Declarations of Helsinki protocols were followed and all patients provided their written informed consent.

2.6.3.1 Processing of nasal specimens

After surgical removal of the nasal polyps or turbinates, the tissue was transferred into Ham's F12 Medium with supplements (Table 26). Samples were kept on ice until further processing. Subsequently, the cells were separated by enzymatic digestion. The tissue was kept under shaking at 4°C for 1-4 days in MEM *Jokliks Modification Medium* containing protease (Table 27).

After enzymatic digestion of the samples, the tissue was disposed and the supernatant was filtered through a cell strainer (pore size 40 µm). The suspension was then mixed with 1 mL of fetal bovine serum (FBS) to stop the protease reaction and centrifuged at 200 x *g* for 10 min. The supernatant was removed and the pellet was resuspended in 1 mL FBS and 9 mL MEM *Jokliks Modification Medium*. The suspension was again centrifuged at 200 x *g* for 10 min. After removal of the supernatant, the pellet was resuspended in 5 mL Ham's F-12 Nutrient Mixture and centrifuged at 200 x *g* for 10 min. The supernatant was discarded again and the pellet was resuspended in Ultroser G (UG) medium (37°C; Table 30).

Table 26: Medium for storage of human nasal epithelial tissue samples

Component	*Amount*
L-Glutamine	2 mM
Penicillin/Streptomycin	100 U/mL
Gentamycin	21 µM
Ham's F12 Nutrient Mixture	

Table 27: Medium for protease digestion of nasal specimens

Component	*Amount*
L-Glutamine	2 mM
Penicillin/Streptomycin	100 U/mL
Gentamycin	21 µM
Protease type XIV	0.035 U/mL
MEM *Jokliks Modification Medium*	

2.6.3.2 Nasal brushing procedure

Before use, the collecting brush was wet with sterile isotonic saline solution. After the patient cleared his nose, the brush was rubbed a few times rapidly against the medial and superior side of the inferior nasal meatus with rotatory and linear movements. The brush was immediately transferred into the collecting tube containing the collecting medium (37°C; Table 28) and shaken vigorously within the tube so that the cells detached from the brush into the medium. Subsequently, cells were centrifuged for 10 min at 200 x *g* and the cell pellet was resuspended in UG medium (37°C; Table 30). Cells were seeded on rat tail collagen according to the manufacturer's instructions (Gibco, Karlsruhe, D) in T25 or T75 flasks depending on the amount of cells. After 24 h, the medium was replaced carefully with fresh UG medium (37°C).

Table 28: Collecting medium for nasal brushings

Component	*Amount*
Antibiotic/Antimycotic solution (100 x)	100 U/mL (Penicillin) 100 µg/mL (Streptomycin) 250 ng/mL (Amphotericin)
RPMI 1640	

2.6.3.3 Liquid covered cultured filters

In case of the experiments with CS-wtCFTR-mRNA complexes, primary HNE cells were cultured under LCC conditions in primary cell culture medium (Table 29) on collagen (0.15 mg/mL bovine collagen A (Biochrom AG, Berlin, D)) at 37°C, 5% CO_2 and 95% rH. For this after the last centrifugation step of the processing of nasal specimens, the pellet was resuspended in 300 µL of primary cell culture medium and a drop of the cell suspension was added to a 4-well plate prior filled with 300 µL of primary cell culture medium. Number and viability of the cells were estimated under the microscope for further experiments. For transepithelial measurements cells were seeded on *Costar Transwell®permeable* filters (Ø = 6.5 mm) coated with collagen. The medium was changed every 2 days and cells were grown for 7-10 days before use.

Table 29: Primary cell culture medium

Component	*Amount*
L-Glutamine	2 mM
Penicillin/Streptomycin	100 U/mL
Gentamycin	21 µM
Epidermal growth factor	3.33 nM
Endothelial cell growth supplement	7.5 µg/mL
Hydrocortisone	100 nM
Transferrin	50 nM
Insulin	345 nM
Triido-Thyronine	3 nM
Ham's F12 Nutrient Mixture	

2.6.3.4 Submerged culture

Cells from nasal polyps or nasal brushings were cultured in UG medium (Table 30) on rat tail collagen (Gibco) at 37°C, 5% CO_2 and 95% rH. Cells were washed with PBS (Table 23; 37°C) every 2-3 days. Afterwards, PBS was replaced with fresh UG medium (37°C).

Table 30: UG medium

Component	*Amount*
Antibiotic/Antimycotic solution (100 x)	100 U/mL (Penicillin) 100 µg/mL (Streptomycin) 250 ng/mL (Amphotericin)
Ultroser G	2% (v/v)
DMEM/Ham's F12 1:1	

When cells reached approximately 80% confluence they were passaged and seeded on *Costar Transwell®permeable* filters (Ø = 6.5 mm) coated with rat tail collagen. Cells obtained from nasal polyps were passaged after 7 days, even if not confluent, to avoid growth of fibroblasts. To passage the cells they were washed with PBS (37°C) and

incubated with 2 mL trypsin/EDTA (0.25%/0.02%; 37°C) for 10 min. The trypsin reaction was stopped with 8 mL UG medium (37°C) and the cell suspension was centrifuged at 200 x *g* for 5 min. The cell pellet was resuspended in the according volume of fresh ALI-Ex Medium (300 µL per filter; RT; Table 31) and seeded onto the apical side of the filters. A full T75 flask yielded 12 filters; a full T25 yielded 6 filters. The number of filters was approximated according the confluence of the flask. The basolateral side of the filters was filled with 700 µL ALI-Ex Medium.

2.6.3.5 Expansion Phase

Cells on filters were cultivated 2-4 days under LCC conditions with ALI-Ex Medium (STEMCELL Technologies, Vancouver, CA; Table 31) in an incubator at 37°C, 5% CO_2 and 95% rH.

Table 31: PneumaCult™-Ex (ALI-Ex) Medium. Protect from light.

Component	*Amount*
PneumaCult™-Ex 50 x Supplement	2% (v/v)
Hydrocortisone	0.2 µM
PneumaCult™-Ex Basal Medium	

The medium of the cells was replaced every day with fresh ALI-Ex medium (RT). Cells were air-lifted after approximately 2-4 days. For this the medium of the basolateral side was replaced with fresh ALI-M medium (RT; Table 33). The apical side was left empty.

2.6.3.6 Maintenance Phase

Cells were cultivated on filters for about 21 days under ALI conditions with ALI-M medium (STEMCELL Technologies; Table 33) in an incubator at 37°C, 5% CO_2 and 95% rH.

Table 32: PneumaCult™-ALI Complete Base Medium. Protect from light.

Component	*Amount*
PneumaCult™-ALI 10 x Supplement	10% (v/v)
PneumaCult™-ALI Basal Medium	90% (v/v)

Table 33: PneumaCult™-ALI Maintenance (ALI-M) Medium. Protect from light.

Component	*Amount*
PneumaCult™-ALI Maintenance Supplement	1% (v/v)
Heparin	0.26 µM
Hydrocortisone	1 µM
PneumaCult™-ALI complete Base Medium (Table 32)	

The medium was replaced every 2-3 days with fresh ALI-M medium (RT). After 14 days, the cells were washed on the apical side with PBS (RT) to remove excess mucus. After approximately 21 days, cells were used for experiments.

2.6.4 Freezing and thawing of cells

For long-term storage of the immortalized cell lines, they were stored at -80°C in cell culture medium containing dimethyl sulfoxide (DMSO). The solvent serves as a cryoprotectant as it inhibits the formation of ice crystals and thereby prevents cell death during the freezing process. To freeze the cells a confluently covered T75 flask was washed with PBS (Table 23; 37°C) and then incubated with trypsin/EDTA (0.25%/ 0.02%; 37°C) for 7 min at 37°C in order to release the adherent cells from the flask. The reaction was then stopped with cell culture medium and the suspension was centrifuged at 500 x *g* for 5 min. The pellet was resuspended in 5.4 mL of ice cold freezing medium (CFBE41o-: Cell culture medium 50%, FBS 40%, DMSO 10%; H441: Standard H441 cell culture medium 95%, DMSO 5%) and 1.8 mL of the cell suspension was given into an ice cold cryopreservation tube, respectively. Cells were incubated on ice for 15 min and then at -20°C for 2 h or overnight. Finally, cells were stored permanently at -80°C.

To take cells back into culture they were thawed rapidly in order to protect them from DMSO as it displays cell toxic properties at RT. Cells were thawed in a water bath at 37°C and then immediately transferred into antibiotic free cell culture medium and centrifuged. The cell pellet was then resuspended in antibiotic free cell culture medium in order to avoid further cell stress and seeded onto a T25 flask. After 24 h, the medium was replaced carefully with fresh cell culture medium containing antibiotics.

2.6.5 MTT assay

The cytotoxicity of the nanoformulations and components was tested using a 3-(4,5-dimethylthiazol-2-yl)-2,5-diphenyltetrazolium bromide (MTT) assay. This colorimetric assay was first conducted by Mosmann in 1983 and is based on the reduction of MTT by NADH- and NADPH-dependent enzymes in living cells, which turns the yellow tetrazolic salt into blue formazan (Mosmann, 1983; Berridge et al., 2005). Briefly, cells were seeded in a 96-well microtiter plate with a density of 1 x 10^4 cells per well and incubated at 37°C, 5% CO_2 and 95% rH for 24 h. The cells were washed twice with serum-free cell culture medium before the samples were added and the cells were incubated under previous conditions for the desired amount of time (4-24 h). After incubation, the samples were removed and replaced by 100 µL serum-free cell culture medium and 25 µL MTT solution (5 mg/mL in PBS). The cells were incubated under previous conditions for another 4 h before the medium was removed and 100 µL DMSO was added to each well in order to dissolve the formazan. After the well plates were incubated at 37°C for 30 min the absorbance was measured at λ = 570 nm in a microplate reader (EZ Read 400, Biochrom GmbH). Relative viability was calculated by dividing individual viabilities by the mean of the negative control (serum-free cell culture medium). 1% Triton® X-100 was used as positive control.

2.6.6 Mycoplasma test

A mycoplasma test was carried out regularly in order to rule out contamination of the cell lines. Mycoplasmas are the smallest self-replicating bacteria with a diameter of 0.3-0.8 µm, which makes a microscopic detection impossible. Contamination with these microorganisms can have various effects on cells such as altered levels of protein, DNA and

RNA synthesis, alteration of cell metabolism and proliferation characteristics or change of the cell membrane (Drexler and Uphoff, 2002).

Mycoplasma tests were conducted using the *Venor®GeM Advance Pre-aliquoted Mycoplasma Detection Kit for conventional PCR* (Minerva Biolabs, Berlin, D). Samples were taken from cell culture supernatant. The PCR was performed following the manufacturer's instructions. Subsequently, a DNA gel electrophoresis (1.5%) was performed to determine the outcome of the PCR using 5 µL of the PCR product. The gel was run at 100 V for approximately 30 min.

2.6.7 Determination of osmolality

Cell culture media and other solutions (e.g. ringer solution, PBS) should be isotonic in order to avoid shrinking or swelling of the cells. To ensure a healthy environment for the cells the osmolality of solutions was determined regularly. The osmolality is defined as the number of osmoles per kg of solvent (Osmol/kg). For cell culture, osmolality ranges from 230-340 mOsmol/kg (Waymouth, 1970).

Osmolality was determined with the cryoscopic osmometer *Osmomat® 030* (Gonotec Meß- und Regeltechnik GmbH, Berlin, D) by comparing the freezing points of water and solutions. Water has a freezing point of 0°C whereas a solution with an osmolality of 1 Osmol/kg has a freezing point of -1.86°C.

2.7 Transfection of cells

In case of wtCFTR-mRNA cell lines were transfected with 2.4 µg/cm^2 (Bangel-Ruland et al., 2013) and primary HNE cells were transfected with 0.6 µg/cm^2 (Fernández Fernández et al., 2016a). For experiments with ASO all cells were transfected with 0.45 µg/cm^2 (Sobczak et al., 2009).

2.7.1 Transfection with *Lipofectamine®2000*

Cationic lipids consist of a positively charged head group and a tail of one or two hydrocarbon chains. Their positive charge allows interaction with the negatively charged nucleic acid, which results in condensation of the latter. This liposomal structure has a

positive charge and allows interaction with the negatively charged cell membrane. The lipoplex is thought to enter the cell via endocytosis (Chesnoy and Huang, 2000).

For transfection with cationic lipids *Lipofectamine®2000 Reagent* (*Lipofectamine*; Invitrogen) was used and transfection was conducted according to the manufacturer's instructions using 2 µL per *Transwell®permeable* filter (Ø = 6.5 mm corresponding to 0.33 cm^2), 5 µL per 24-well and 10 µL per 6-well.

24 h before transfection the medium of the cells was replaced with fresh antibiotic-free medium in order to minimize cellular stress. The required amounts of nucleic acid and *Lipofectamine* were diluted in *Opti-MEM™* (Thermo Fisher Scientific), respectively (Table 34) and incubated at RT for 5 min. The solutions were then mixed and incubated at RT for another 20 min in order to give the lipoplexes time to form. Finally, the lipoplexes were added to the cells and they were incubated at 37°C, 5% CO2 and 95% rH for 4 h before replacing the medium with fresh cell culture medium. The cells were then incubated for another 20 h before experiments were conducted.

Table 34: Transfection with *Lipofectamine*. Required amounts of nucleic acid and *Lipofectamine* were diluted in *Opti-MEM™*.

Culture vessel	*Volume of dilution nucleic acid (µL)*	*Volume of dilution* Lipofectamine *(µL)*	*Final volume (µL)*
Filter (6.5 mm)	150	150	300
24-well	250	250	500
6-well	1000	1000	2000

2.7.2 Transfection with nanoformulations

Transfection with biopolymers such as chitosan works similar to transfection with cationic lipids. The positively charged chitosan is able to bind to the negatively charged nucleic acid. If the nanoformulations are formed at a certain N/P charge ratio, they have a positively charged surface potential. As the lipoplexes, the positive biopolymer-nucleic acid

complexes and capsules can interact with the negatively charged cell membrane and are assumed to be taken up by the cell via endocytosis (Ishii et al., 2001).

24 h before transfection the medium of the cells was replaced with fresh antibiotic-free medium. The chitosan-mRNA complexes were prepared with the desired amount of nucleic acid to reach an N/P charge ratio of 37 as described in 2.4.2. Chitosan-ASO complexes were prepared with the desired amount of nucleic acid in 85 mM NaCl to reach a N/P charge ratio of 90 as described in 2.4.3. The formulations were incubated at RT for 30 min to allow self-assembly of the complexes. After the incubation, the complexes were mixed with either *Opti-MEM™* (Thermo Fisher Scientific) or *Opti-MEM™* supplemented with HEPES (20 mM) and mannitol (270 mM) and incubated for another 5 min at RT (Table 35). Finally, the nanocomplexes were added to the cells and cells were incubated for 24 h at 37°C, 5% CO2 and 95% rH before experiments were conducted.

Table 35: Transfection with chitosan nanocomplexes. Chitosan complexes were diluted with *Opti-MEM™* or *Opti-MEM™* supplemented with HEPES (20 mM) and mannitol (270 mM).

	Culture vessel	*N/P charge ratio*	*Final volume of dilution (µL)*
CS-mRNA complexes	Filter (6.5 mm)	37	300
	24-well	37	500
	6-well	37	2000
CS-ASO complexes	Filter (6.5 mm)	90	300
	24-well	90	500
	6-well	90	2000

2.7.3 Transfection efficiency

Transfection efficiency was determined with a luciferase assay. This method is based on the enzymatic properties of the firefly luciferase. The *Photinus pyralis* enzyme catalyzes the oxidation of D-luciferin in the presence of ATP-Mg^{2+} and O_2 to generate oxyluciferin and light. The light emitted by the reaction has a wavelength of 562 nm and can be detected by a luminometer (Gould and Subramani, 1988).

Primary HNE cells were seeded on rat tail collagen (Gibco) in 24-well plates with a density of 5 x 10^4 cells per well and cultivated in antibiotic-free UG medium (Table 30) at 37°C, 5% CO_2 and 95% rH for 24 h. The growth medium was removed from the wells and the cells were washed carefully with PBS (Table 23; 37°C). Cells were then transfected with the plasmid pGL4.50[*luc2*/CMV/Hygro] (Figure 13; Promega GmbH, Mannheim, D) containing the luciferase reporter gene *luc2* from *P. pyralis* with a concentration of 500 ng/well.

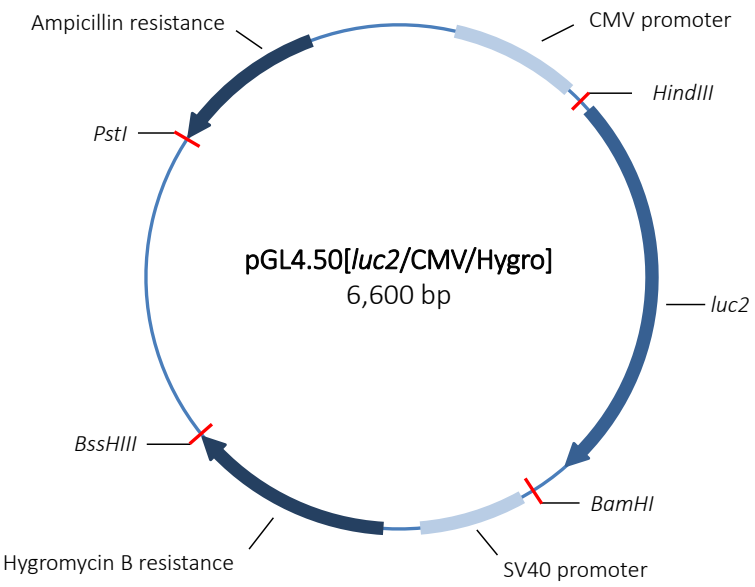

Figure 13: pGL4.50[*luc2*/CMV/Hygro]. The plasmid contains amongst others the *luc2* (*Photinus pyralis*) reporter gene for expression in mammalian cells, a cytomegalovirus (CMV) promoter for high translational expression, a synthetic hygromycin B resistance gene for mammalian cell selection of the plasmid and an ampicillin resistance gene for bacterial selection for vector amplification. Furthermore, the plasmid contains *HindIII*, *BamHI*, *BssHIII* and *PstI* restriction sites.

Cells were transfected using NC-CAP and NC-Blank. For this different amounts of NC were mixed with 500 ng DNA and incubated at RT for 30 min. The volume was then filled to 500 µL with either *Opti-MEM™* (Thermo Fisher Scientific) or *Opti-MEM™* supplemented with HEPES (20 mM) and mannitol (270 mM) and the formulation was given onto the cells. As positive control, cells were transfected using the commercially available transfection reagent *FuGENE® HD Transfection Reagent* (*FuGENE*; Promega GmbH). Transfection was conducted according to the manufacturer's instructions with a ratio of 3:1 (*FuGENE*:DNA) in 500 µL *Opti-MEM™*. As negative controls, cells were treated with *FuGENE* and NC

without DNA or only with *Opti-MEM™*. Cells were then incubated for 24 h at 37°C, 5% CO_2 and 95% rH.

Finally, the transfection efficiency was assessed using the *Luciferase Assay System* (Promega GmbH). The assay was performed according to the manufacturer's instructions using 200 µL 1 x *lysis buffer* per 24-well and the light intensity was measured in relative light units (RLU) with a *GloMax® 20/20 Luminometer* (Promega GmbH).

2.8 Fluorescence optical methods

2.8.1 Preparation of glass cover slips

Glass cover slips (Ø = 12 mm; Carl Roth GmbH & Co. KG, Karlsruhe, D) were incubated in acetone for 2-4 h following incubation in 2% sodium carbonate solution overnight. The glass cover slips were then washed three times with water and covered in ethanol (70%) until all the fluid was evaporated. All of the steps were performed on a shaker. Subsequently, the glass cover slips were autoclaved. Prior to seeding of the cells, the glass cover slips were coated with the respective coating solution (e.g. rat tail collagen for HNE cells). Finally, cells were seeded with a density of 1 x 10^5 one day before transfection and incubated in antibiotic-free medium.

2.8.2 Fixation of transfected cells on glass cover slips

In order to verify the success of transfection procedures cells were transfected with 5'Fam-ASOgreen containing the fluorescent 6-Fam tag (0.15 µg per glass cover slip) and incubated for 24 h at 37°C with 5% CO_2 and 95% rH. As control, cells were transfected with the non-fluorescent ASOgreen.

Transfected cells on glass cover slips were washed three times with PBS (Table 23; 37°C). Subsequently, cells were fixed with 500 µL 3.5% paraformaldehyde (PFA) in PBS (37°C) for 30 min. During this process, aldehyde groups cross-link proteins and thereby fix the cells. After two more washing steps with PBS, cells were incubated for 10 min in 500 µL glycine (100 mM in PBS) in order to quench the residual PFA. Cells were washed three more times with PBS and finally placed top down onto microscope slides on a drop of the mounting

medium *Fluoroshield™ with DAPI* (Sigma-Aldrich, St. Louis, USA). Fixed cells were analyzed using the confocal laser scanning microscope *LSM 510 META* (Carl Zeiss AG, Oberkochen, D) and the program *LSM 5* (Carl Zeiss AG). Analysis of total fluorescence intensities was carried out using the plug-in for RGB (red, green, blue) intensity measurement of the program *ImageJ 1.48v*.

2.9 Protein biochemical methods

2.9.1 Isolation of protein from cells

Proteins were isolated from cells using *RIPA Buffer* (Thermo Fisher Scientific). Before isolation, cells were washed twice with ice cold PBS (Table 23; pH 7.4). Cold *RIPA Buffer* supplemented with 1% protease inhibitor cocktail (PIC; Sigma-Aldrich) was added to the cells (6-well plate 100 µL; T25 flask 500 µL) followed by incubation for 5 min on ice, shaking the dish occasionally. The cells were then removed from the dish with a cell scraper and the lysate was sonicated twice for 2 s. The lysate was incubated on ice for 10 min and then centrifuged for 15 min at 4°C and 14,000 x *g*. The supernatant containing the proteins was blast-frozen with liquid nitrogen and stored at -20°C until further experiments were conducted.

2.9.2 BCA assay

In order to determine the concentration of isolated proteins a bicinchoninic acid (BCA) assay was performed. This assay is based on colorimetric detection of proteins and was first described by Smith *et al.* in 1985. After the reduction of Cu^{2+} to Cu^{+} by peptide bonds in proteins, two BCA molecules form a purple complex with one Cu^{+}, which absorbs light at λ = 562 nm (Smith et al., 1985).

For the experiment, the *Pierce® BCA Protein Assay Kit* (Thermo Fisher Scientific) was used. The isolated proteins were diluted 1:5 with H_2O and 50 µL of the sample were mixed with 1 mL of freshly prepared working reagent (50 parts reagent A : 1 part reagent B). The samples were then incubated in a water bath at 37°C in the dark for 30 min. Afterwards, samples were kept on ice for 2 min before measuring the absorbance at λ = 562 nm in a

photo spectrometer (WPA Biowave S2100, Biochrom GmbH). The calibration curve was created with serial dilution of the albumin standard in the range of concentration 0-2 mg/mL. The values of the protein concentration were extrapolated from the obtained equation.

2.9.3 SDS-PAGE

For separation of the isolated proteins, a sodium dodecyl sulfate polyacrylamide gel electrophoresis (SDS-PAGE) was conducted. This method was first described by Laemmli in 1970 (Laemmli, 1970) and is a biochemical method to separate proteins according to their molecular mass in an electric field. SDS denaturates proteins and covers their intrinsic charge enabling the proteins to be separated according to their Mw, as proteins with higher mass move slower than proteins with lower mass.

The resolving gel and stacking gel were prepared according to Table 36 and Table 37. Before addition of N,N,N',N'-tetramethylethylenediamine (TEMED) and ammonium persulfate (APS), the catalyst and radical initiator of the polymerization, the mixture was degassed for 10 min with a vacuum pump.

Table 36: Composition of stacking buffer and resolving buffer for SDS gels

Component	*Stacking buffer*	*Resolving buffer*
Tris	0.5 M	1.5 M
SDS	0.4% (w/v)	0.4% (w/v)
H_2O	ad 100 mL	ad 100 mL
	pH 6.8	pH 8.8

Table 37: Composition of stacking and resolving gel for SDS gels

Component	*Stacking gel (3.9%)*	*Resolving gel (7.5%)*
30% Acrylamide (w/v)	325 µL	1.25 mL
Buffer	625 µL	1.25 mL
H_2O	1.55 mL	2.5 mL
TEMED	2.5 µL	1.7 µL
10% APS (w/v)	25 µL	33.3 µL

For preparation of the samples, 40 µg of total protein were mixed with *4 x loading buffer* (*Roti®-Load,* Carl Roth GmbH & Co. KG). Samples were incubated at 95°C for 5 min in order to denaturate the proteins and then kept on ice for 1-5 min before application to the gel. As a marker, *PageRuler™ Prestained Protein Ladder* (Thermo Fisher Scientific; Appendix Figure 61) was used. The composition of the applied running buffer is shown in Table 38. The SDS-PAGE was run in a gel chamber at 30 mA and maximal voltage for 1-1.5 h.

Table 38: SDS-PAGE running buffer

Component	*Amount*
Tris	23 mM
Glycine	190 mM
SDS	0.2% (w/v)
H_2O	3 L
pH 8.3	

2.9.4 Semi-dry western blot

The western blot was first conducted in 1979 and is a common technique to detect specific proteins in an isolate (Towbin et al., 1979). Using a semi-dry blotting system (Biometra, Göttingen, D) the isolated and electrophoretic separated proteins were transferred onto a polyvinylidene fluoride (PVDF) membrane (0.45 µm; Carl Roth GmbH & Co. KG). For this 10 filter papers (190 g/cm²; Hartenstein, Würzburg, D) were soaked in transfer buffer (Table 39) and the PVDF membrane was activated in methanol for about 30 seconds before being washed with transfer buffer. Filter papers, SDS gel and PVDF membrane were stacked according to Figure 14. The blot was run for 32 min at 5 mA/cm^2. The applied voltage results in the proteins migrating to the anode onto the PVDF membrane. To determine a successful outcome of the semi-dry western blot the SDS gel as well as the PVDF membrane were stained with Coomassie staining solutions and bleached afterwards (Table 40-Table 43).

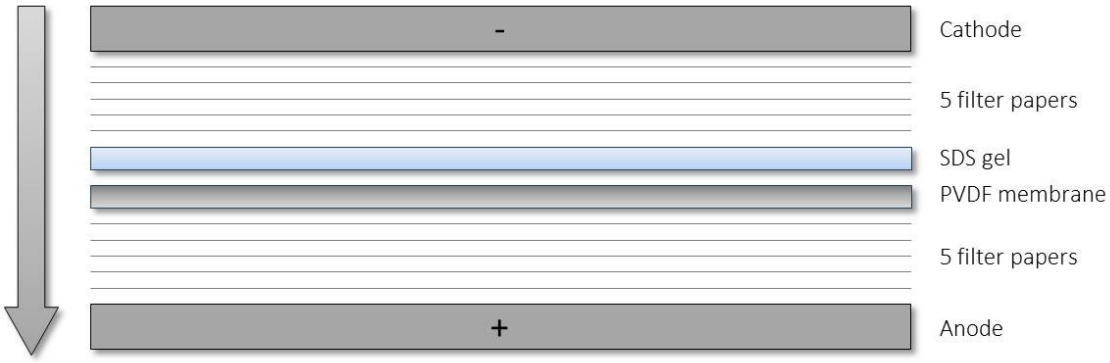

Figure 14: Schematic illustration of the semi-dry western blot set-up. The SDS gel is stacked on top of the PVDF membrane with 5 filter papers separating the gel and membrane from the cathode and the anode, respectively. The arrow indicates the direction of migration. When current is applied to the set-up the proteins in the gel migrate onto the PVDF membrane.

Table 39: Transfer buffer

Component	*Amount*
Tris	48 mM
Glycine	39 mM
SDS	0.037% (w/v)
Methanol	10% (v/v)
H_2O	
pH 8.3	

Table 40: Coomassie staining solution for PDVF membranes

Component	*Amount*
Coomassie-Brilliant-Blue R-250	0.075% (w/v)
Methanol	

Table 41: Bleaching solution for PVDF membranes

Component	*Amount*
Acetic acid	10% (v/v)
Ethanol	40% (v/v)
H_2O	

Table 42: Coomassie staining solution for SDS gels

Component	*Amount*
Coomassie-Brilliant-Blue R-250	0.2% (w/v)
Acetic acid	7.5% (v/v)
Methanol	10% (v/v)
H_2O	

Table 43: Bleaching solution for SDS gels

Component	*Amount*
Isopropanol	20% (v/v)
H_2O	

Table 44: Tris buffered saline (TBS)

Component	*Amount*
Tris	1 mM
NaCl	150 µM
pH 7.5	

After bleaching, the PVDF membrane was washed once with TBS-T (0.05% Tween-20 in TBS (Table 44)) in order to remove the acetic acid present in the bleaching solution. The PVDF membrane was then incubated with 5% dry-milk in TBS-T for 2 h at RT in order to block the unspecific binding sites on the membrane. Then the membrane was incubated with the primary antibodies diluted in 5% dry-milk in TBS-T at 4°C overnight under continuous shaking. In case of TRPV1, one sample was additionally incubated with a human TRPV1 peptide to specifically block TRPV1 as negative control. After washing the membrane three times with TBS-T for 10 min to remove the residual antibodies it was incubated for 1 h at RT with the secondary antibody diluted in 5% dry-milk in TBS-T, which was coupled to a horseradish peroxidase (HRP). Finally, the membrane was washed three times with TBS-T for 10 min and once with TBS for 2 min. Further information about the antibodies and their dilutions can be found in the appendix in Table 56.

2.9.5 Enhanced chemiluminescence detection

Enhanced chemiluminescence (ECL) detection is a sensitive and non-radioactive method for the detection of HRP. The detection was accomplished with the *SuperSignal™ West Pico Chemiluminescent Substrate Kit* (Pierce, Thermo Fisher Scientific) through oxidation of luminol in the presence of HRP and peroxide according to the manufacturer's instructions. Documentation of the blot was performed with a *Fusion SL Vilber Lourmat* (Peqlab Biotechnologie GmbH, Erlangen, D) using the software *FUSION FX7 Advance™* (Peqlab Biotechnologie GmbH). The exposure time was adjusted automatically.

2.10 Ussing chamber

The Ussing chamber is a technique to study ion transport and barrier functions of epithelial tissues. The technique was first introduced in 1951 by Hans H. Ussing to measure sodium transport in isolated frog skin (Ussing and Zerahn, 1951). Up to the present day it is being used to investigate epithelial cell monolayers or tissue e. g. of the skin, the gastrointestinal tract or the airways (Guo et al., 2019; Hahn et al., 2018; Heffell et al., 2018; Kmit et al., 2019; Makrane et al., 2019; Yang et al., 2019). In this study modified Ussing chambers by Professor Willy van Driessche (Figure 15; EP-Devices, Bertem, B) were used to measure ion transport in human airway epithelial cells with emphasis on the epithelial ion channels CFTR and ENaC.

The modified Ussing chamber consists of two halves, in between which a *Costar Transwell®permeable* filter (Ø = 6.5 mm) with a confluent cell monolayer can be inserted. Due to the barrier function of the epithelial cells the apical and basolateral side of the Ussing chamber are separated from each other when a filter is inserted. An inflow and an outflow on each side of the set up allow the application of different solutions to each side of the filter. Four Ag/AgCl electrodes are connected to the solutions in the chamber, two voltage electrodes and two current electrodes, one on the basolateral side and one on the apical side, respectively. The voltage electrodes measure the transepithelial potential (V_t), which is created by the flow of ions through the ion channels of the cell monolayer. The current electrodes balance V_t to 0 V by applying a short-circuit current (I_{sc}) using a low-noise voltage clamp. During measurements the program *ImpDsp 1.4* (KU Leuven, Leuven,

B) can record the short-circuit current (I_{sc}), the transepithelial conductance (G_t) and the transepithelial capacitance (C_t). For analysis of the data, all values are normalized to 1 cm^2.

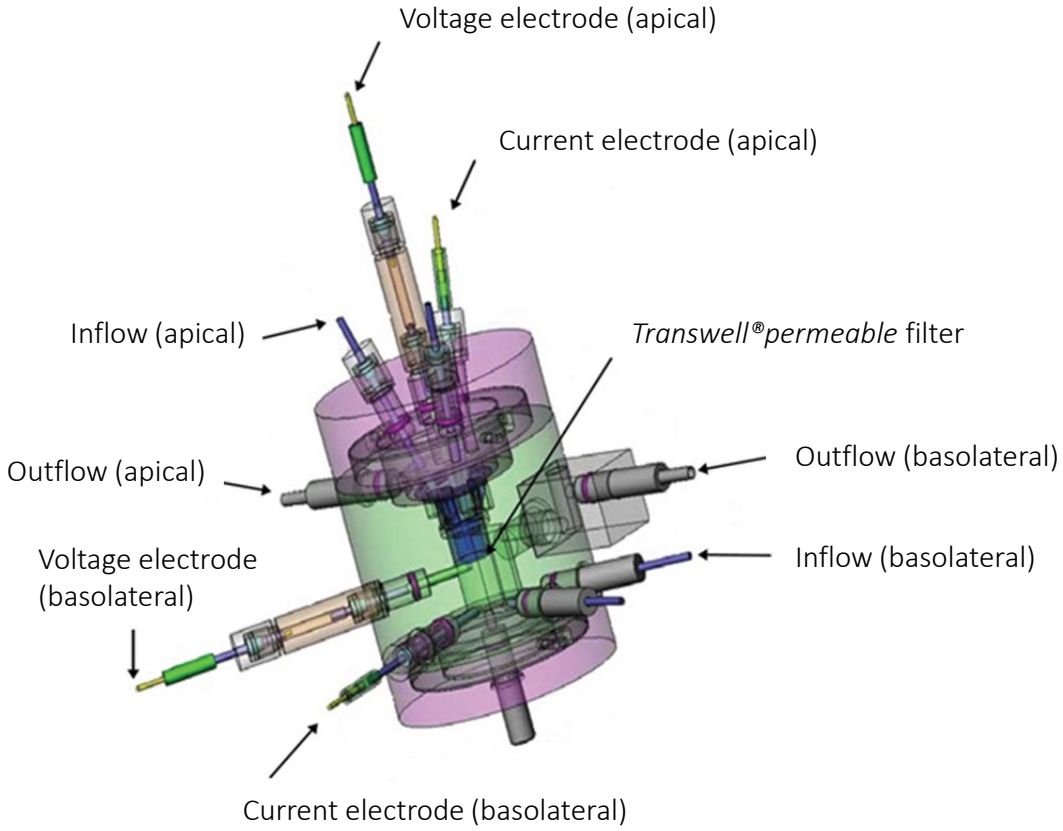

Figure 15: Modified Ussing Chamber. A *Costar Transwell®permeable* filter (blue) can be inserted into the Ussing chamber separating the two halves into apical and basolateral side. Several inflows and outflows allow the application of different solutions to each side of the cell monolayer grown on the filter. The Ag/AgCl voltage electrodes measure the transepithelial potential (V_t) while the Ag/AgCl current electrodes apply a short-circuit current to keep V_t at 0 V at all times. Adapted from EP-Devices, 2008.

2.10.1 Functional Ussing chamber measurements

Measurements in the modified Ussing chambers were conducted according to the protocol in Table 45. After inserting the filter into the Ussing chamber, ringer solution (Table 46) was applied to the apical as well as basolateral side. Solutions were changed after the stabilization of I_{sc}, G_t and C_t. The solutions amiloride (10 µM in ringer solution), sodium-free ringer solution (Table 47) and CFTR-Inhibitor 172 (10 µM in amiloride solution) were applied to the apical side of the filter. The 8-CPT-cAMP (cAMP)/3-isobutyl-1-methylxanthine (IBMX) cocktail (100 µM/1 mM in ringer solution) was applied to the basolateral side. Amiloride is a diuretic, which is known for its ability to block ENaC

specifically. In CF it is used to reduce sodium reabsorption (Rodgers and Knox, 2001). The thiazolidinone CFTR-Inhibitor 172 is a direct blocker of CFTR. Previous studies imply that it binds to the channel via Arg347 at an intracellular site (Caci et al., 2008; Kelly et al., 2010). The second messenger cAMP is used to activate CFTR. In the cocktail, it is protected from degradation by the phosphodiesterase inhibitor IBMX. Before measurements, all solutions as well as the Ussing chamber were heated to 37°C.

Table 45: Protocol for Ussing chamber measurements

Channel of interest	*Apical*	*Basolateral*
ENaC	Ringer	Ringer
	Amiloride	Ringer
	Na^+-free ringer	Ringer
CFTR	Ringer	Ringer
	Amiloride	Ringer
	Amiloride	cAMP/IBMX cocktail
	CFTR-Inhibitor 172	cAMP/IBMX cocktail
	Ringer	Ringer

Table 46: Ringer solution

Component	*Amount*
NaCl	130 mM
KCl	5 mM
$CaCl_2$	1 mM
$MgCl_2$	2 mM
Glucose	5 mM
HEPES	10 mM
pH 7.3	

Table 47: Sodium-free ringer solution

Component	*Amount*
Tetramethylammonium chloride	130 mM
KCl	5 mM
$CaCl_2$	1 mM
$MgCl_2$	2 mM
Glucose	5 mM
HEPES	10 mM
pH 7.3	

2.11 Statistical analysis

The statistical analysis was performed with *GraphPad Prism® Version 6.01* (GraphPad Software Inc., La Jolla, USA). For analysis of the data, the arithmetic mean values ± standard deviations (SD) of at least three independent experiments were determined, if not stated otherwise. Ussing chamber data are expressed as the arithmetic mean values ± standard error of the mean (SEM). In order to assess the significant differences of the results, the non-parametric Kruskal-Wallis test was performed. Differences were considered statistically significant when $p \leq 0.05$ (*), $p \leq 0.01$ (**), $p \leq 0.001$ (***), $p \leq 0.0001$ (****).

3 RESULTS

3.1 Chitosan-mRNA complexes

The chitosan-mRNA complexes were developed as part of the Master's Thesis "Evaluation of chitosan for CFTR-mRNA application in human airway epithelial cells" (Kolonko, 2016). For *in vitro* cell transfection experiments, CFBE41o- cells were incubated with the complexes for 4 h. 24 h after transfection functional Ussing chamber measurements were conducted, which confirmed successful transfection (Kolonko et al., 2016). In the course of this Thesis, the experiments with the chitosan-mRNA complexes were extended in order to optimize transfection of CFBE41o- as well as primary HNE cells.

3.1.1 Evaluation of wtCFTR-mRNA

After linearization of the plasmid pSTI-A120/hCFTR-cDNA containing the human CFTR gene, an IVT was performed to prepare wtCFTR-mRNA. In order to confirm a successful IVT reaction a 1% denaturing formaldehyde-agarose gel electrophoresis was carried out (Figure 16). The IVT reaction products in line 1 and 2 show a specific band in the range of 5,000 bases corresponding to the size of wtCFTR-mRNA (4,443 bases). The evaluation of the obtained wtCFTR-mRNA indicated optimal quality and size for transfection experiments.

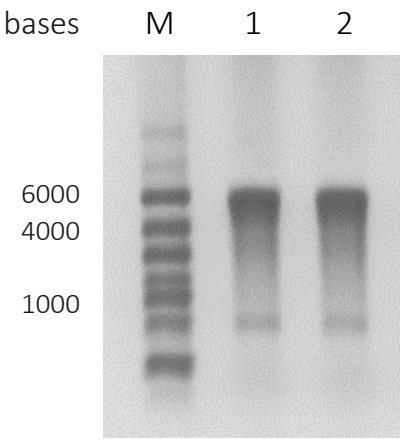

Figure 16: Representative wtCFTR-mRNA gel electrophoresis. The image shows a 1% denaturing formaldehyde-agarose gel electrophoresis to confirm a successful IVT reaction. Line 1 and 2 display the products of two independent IVT reactions and present a fragment in the range of 5,000 bases respectively, corresponding to wtCFTR-mRNA size. Marker (M): *RiboRuler™ High Range RNA Ladder* (Thermo Fisher Scientific).

3.1.2 Experiments with CFBE41o- cells

The natural polysaccharide chitosan is known for its non-cytotoxic characteristics (Cheung et al., 2015; Lim et al., 2001). Hence, it is possible to incubate cells with the chitosan-mRNA complexes for longer periods than 4 h. In order to optimize the transfection procedure CFBE41o- cells were transfected with 2.4 µg/cm^2 wtCFTR-mRNA and incubated either 4 h or 24 h with the chitosan-mRNA complexes. As control, cells were transfected using *Lipofectamine*. Since the commercially available transfection reagent displays cytotoxic features (Chernousova and Epple, 2017; Wang et al., 2018), cells were only incubated with *Lipofectamine* for 4 h. 24 h after transfection functional Ussing chamber measurements were carried out in order to evaluate the outcome of the transfection.

Already after 4 h of incubation with chitosan-mRNA complexes CFBE41o- cells displayed a slight increase in short-circuit current (I_{sc}) after application of cAMP (7.5 ± 2.0 µA/cm^2), while I_{sc} increased strongly after 24 h of incubation (25.5 ± 5.2 µA/cm^2) compared to non-transfected control cells as shown in the representative measurements in Figure 17. Statistical evaluation of the measurements revealed a highly significant increase in cAMP-mediated short-circuit current after transfection with chitosan and incubation for 24 h indicating successful transfection and CFTR expression (Figure 18a). The increase was also significant compared to short-circuit current in cells transfected with *Lipofectamine* (5.8 ± 2.2 µA/cm^2 vs. 25.5 ± 5.2 µA/cm^2). Furthermore, amiloride-sensitive current was evaluated in order to estimate a possible effect of wtCFTR-mRNA transfection on ENaC (Figure 18b). Compared to non-transfected control cells amiloride-sensitive short-circuit current decreased after transfection with *Lipofectamine* and decreased further after transfection with chitosan and incubation for 4 h (30.1 ± 8.1% vs. 18.9 ± 2.5% vs. 9.8 ± 3.0%). However, no effect on amiloride-sensitive current could be observed after transfection with chitosan and incubation for 24 h (25.4 ± 7.0%).

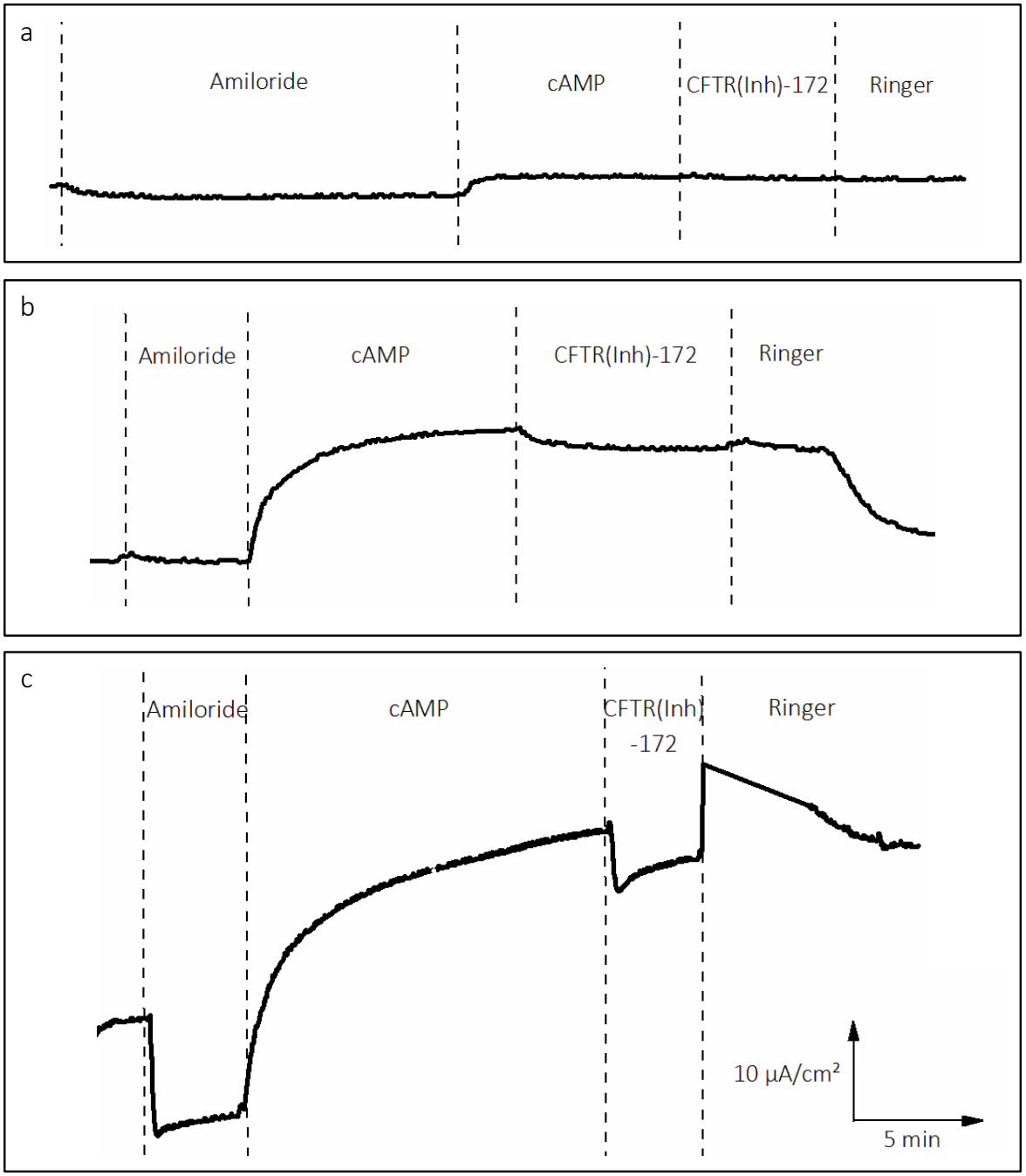

Figure 17: Representative time courses of transepithelial measurements of CFBE41o- cells. Shown is the short-circuit current (I_{sc}) of a typical Ussing chamber measurement. **(a)** Non-transfected cells showed a smooth increase of I_{sc} after cAMP addition. After inhibition of CFTR with CFTR Inhibitor-172 no decrease of I_{sc} was observed. **(b)** In cells transfected with chitosan (2.4 µg/cm² wtCFTR-mRNA) and incubation for 4 h, I_{sc} increased further after cAMP application and was slightly inhibited by CFTR Inhibitor-172. **(c)** The strongest increase of I_{sc} after cAMP application was observed in cells transfected with chitosan (2.4 µg/cm² wtCFTR-mRNA) and incubation for 24 h.

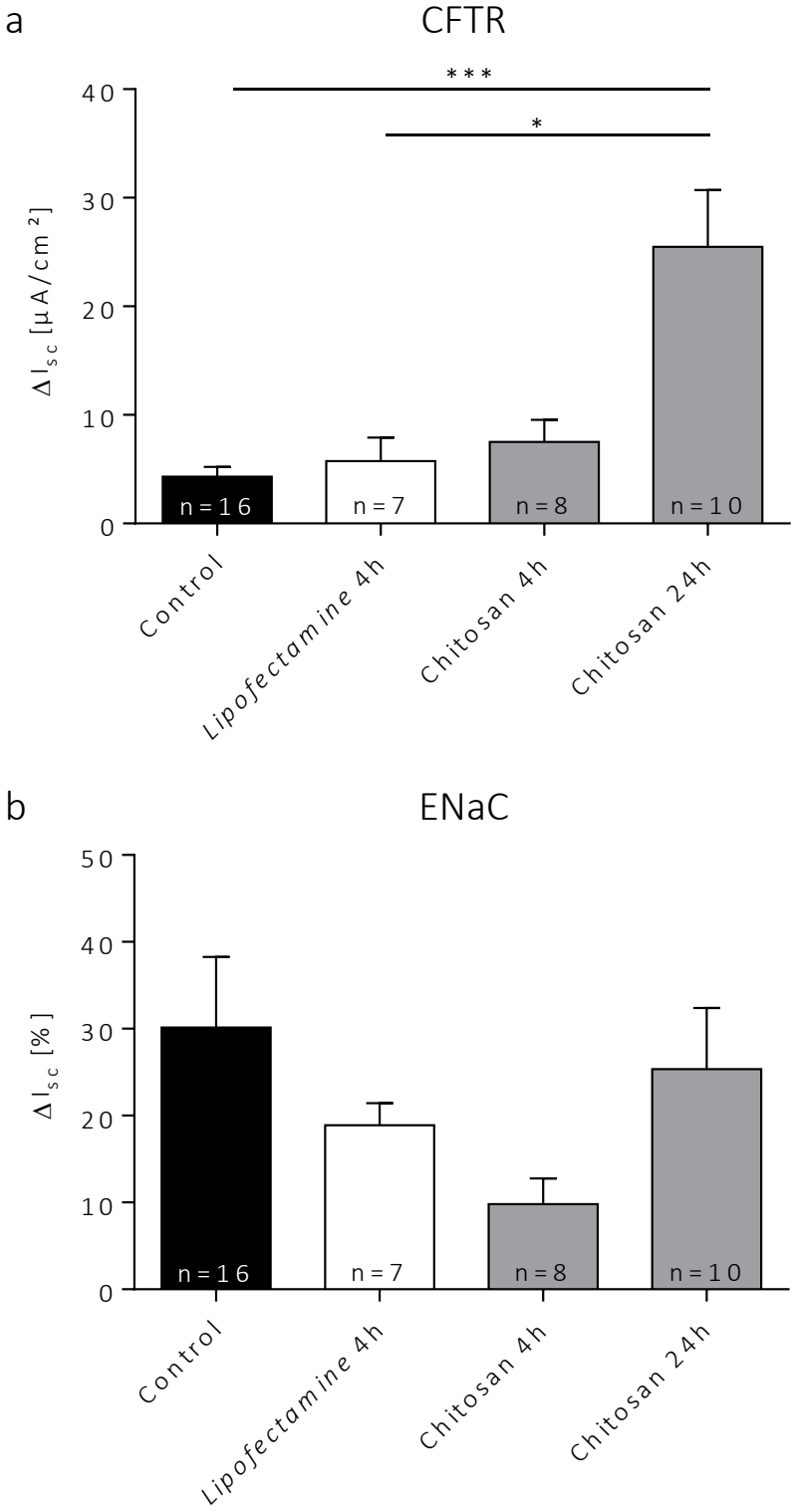

Figure 18: Statistical evaluation of short-circuit current (I_{sc}) in CFBE41o- cells after wtCFTR-mRNA transfection with *Lipofectamine* and chitosan. Cells were transfected with 2.4 µg/cm² wtCFTR-mRNA and incubated either 4 or 24 h with the transfection reagent, respectively; control cells were not transfected. Measurements were conducted 24 h after transfection. **(a)** Shown is the increase of I_{sc} after CFTR activation by application of cAMP. Strongest increase was observed in cells transfected with chitosan and incubation for 24 h (25.5 ± 5.2 µA/cm^2). **(b)** Evaluation of the amiloride-sensitive current revealed the strongest decrease in I_{sc} after transfection with chitosan and incubation for 4 h (9.8 ± 3.0%). After incubation with chitosan for 24 h amiloride-sensitive I_{sc} was similar to I_{sc} of control cells ($p \leq 0.05$ (*), $p \leq 0.001$ (***)).

3.1.3 Experiments with primary HNE cells

In order to test the effect of chitosan as well as *Lipofectamine* on the viability of cells an MTT assay was carried out. Primary HNE cells were incubated with the samples for 4 h. Figure 19 displays the result of the experiment. While chitosan alone and in combination with wtCFTR-mRNA only had a slight effect on the viability of cells (~80%) the commercially available transfection reagent caused a highly significant decrease of cell viability (~60%). After the evaluation of the cytotoxicity of the transfection reagents, transfection experiments were performed with primary HNE cells.

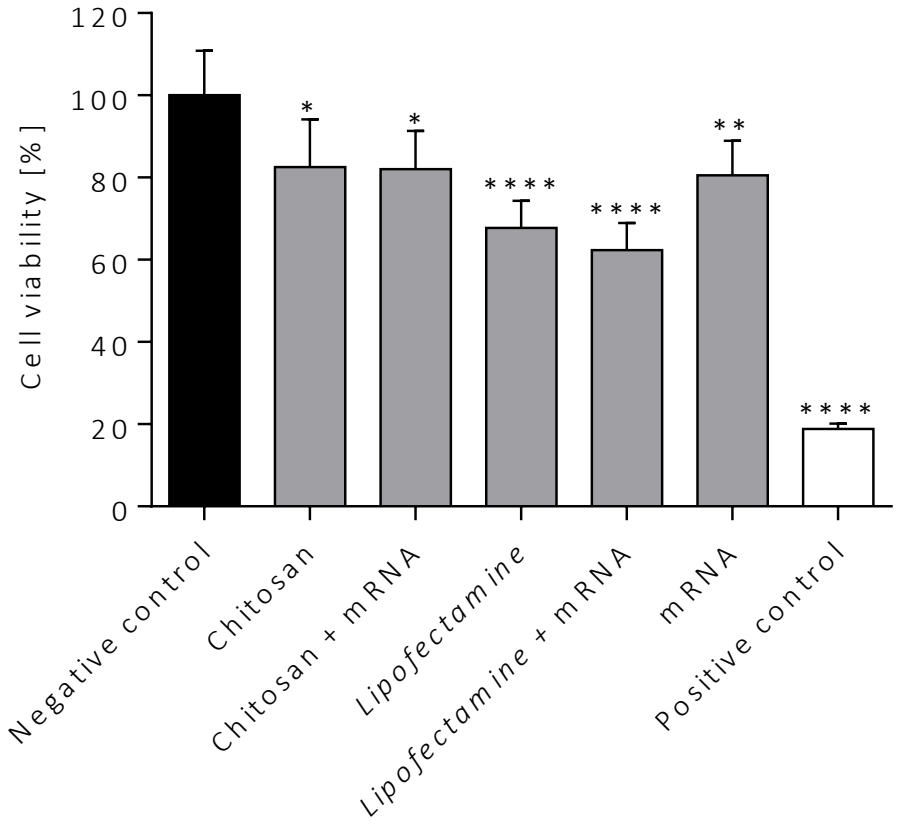

Figure 19: Effect of wtCFTR mRNA in combination with *Lipofectamine* and chitosan on the viability of primary HNE cells. Cells were incubated with the samples for 4 h before an MTT assay was conducted. Cell culture medium was used as negative control; Triton® X-100 was used as positive control. While chitosan in combination with mRNA only had a slight effect on the cell viability (82.1 ± 1.9%), the decrease in cell viability caused by *Lipofectamine* in combination with mRNA was highly significant (62.3 ± 1.4%; $p \leq 0.05$ (*), $p \leq 0.01$ (**), $p \leq 0.0001$ (****); n=3).

Cells were transfected with 0.6 µg/cm^2 wtCFTR-mRNA using chitosan and *Lipofectamine*. As in experiments with CFBE41o- cells, primary HNE cells were incubated with chitosan for either 4 h or 24 h, while incubation with *Lipofectamine* was only conducted for 4 h due to the cytotoxic effect of the commercially available transfection reagent. Transepithelial Ussing chamber measurements were conducted 24 h after transfection and revealed similar results as in transfection experiments with CFBE41o- cells.

Representative transepithelial measurements in Figure 20 show that a slight increase of cAMP-mediated short-circuit current was observed after transfection with chitosan and incubation for 4 h (10.9 ± 3.6 µA/cm^2) while the short-circuit current increased strongly after incubation for 24 h (20.1 ± 6.9 µA/cm^2). Statistical evaluation of Ussing chamber measurements showed similar trends as in CFBE41o- cells as well. Compared to non-transfected control cells cAMP-mediated short-circuit current increased after transfection with *Lipofectamine* and increased further after transfection with chitosan resulting in highest short-circuit current after transfection with chitosan and incubation for 24 h indicating successful transfection and wtCFTR expression (Figure 21a). Evaluation of amiloride-sensitive current revealed the strongest decrease of current after transfection with *Lipofectamine* (23.9 ± 7.1%; Figure 21b). Transfection with chitosan only led to a slight decrease of amiloride-sensitive current. However, no statistical difference was found.

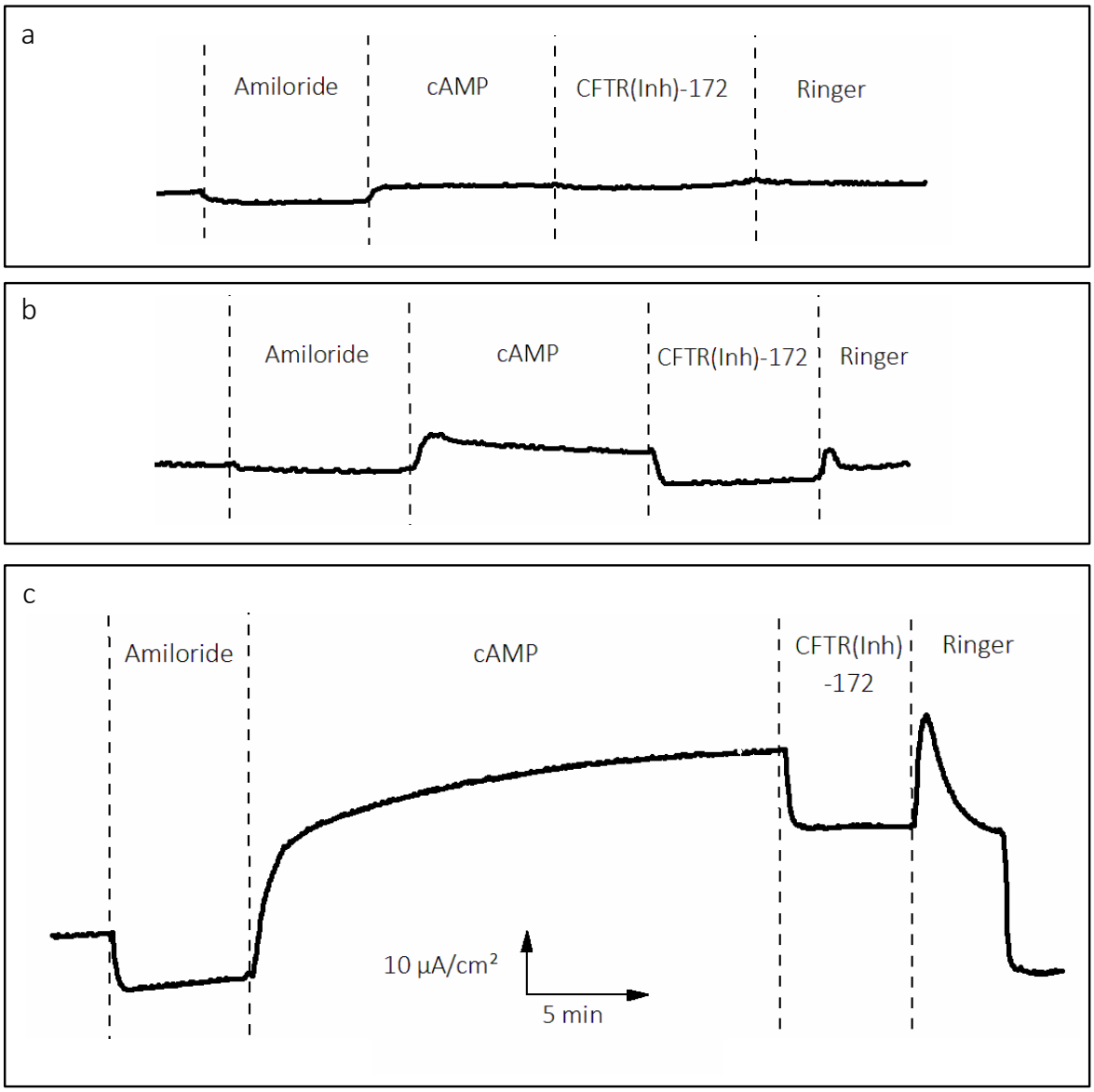

Figure 20: Representative time courses of transepithelial measurements of primary HNE cells. Shown is the short-circuit current (I_{sc}) of a typical Ussing chamber measurement. **(a)** Non-transfected cells showed a smooth increase of I_{sc} after cAMP addition. After inhibition of CFTR with CFTR Inhibitor-172 no decrease of I_{sc} was observed. **(b)** In cells transfected with chitosan (2.4 µg/cm² wtCFTR-mRNA) and incubation for 4 h, I_{sc} increased further after cAMP application and was slightly inhibited by CFTR Inhibitor-172. **(c)** The strongest increase of I_{sc} after cAMP application was observed in cells transfected with chitosan (2.4 µg/cm² wtCFTR-mRNA) and incubation for 24 h.

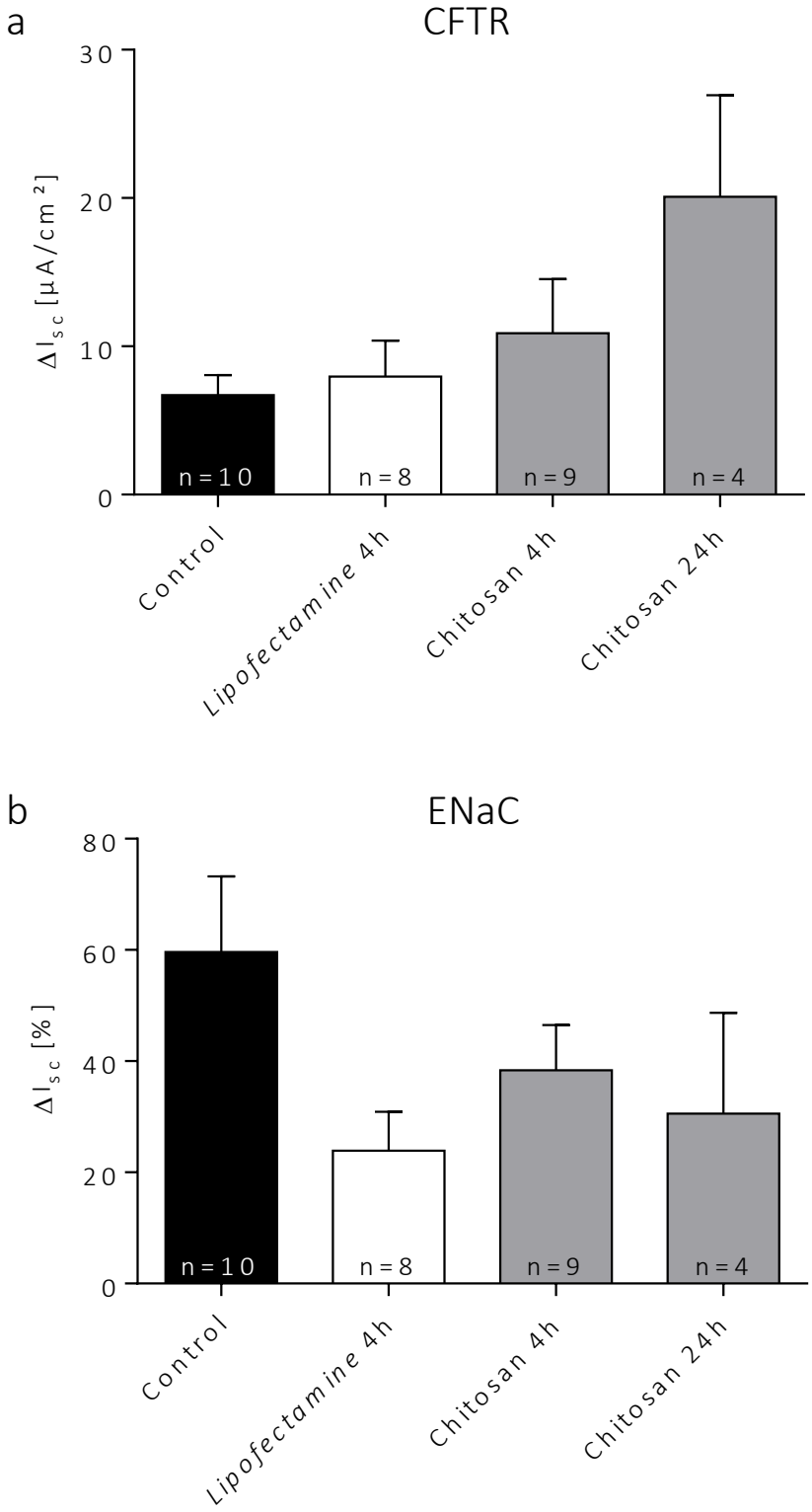

Figure 21: Evaluation of short-circuit current (I_{sc}) in primary HNE cells after wtCFTR-mRNA transfection with *Lipofectamine* and chitosan. Cells were transfected with 0.6 µg/cm² wtCFTR-mRNA and incubated either 4 or 24 h with the transfection reagent, respectively; control cells were not transfected. Measurements were conducted 24 h after transfection. **(a)** Shown is the increase of I_{sc} after CFTR activation by application of cAMP. Strongest increase was observed in cells transfected with chitosan and incubation for 24 h (20.1 ± 6.9 µA/cm^2). **(b)** Evaluation of amiloride-sensitive current revealed the strongest decrease in I_{sc} after transfection with *Lipofectamine* (23.9 ± 7.1%).

3.2 Chitosan-ASO complexes

Given that wtCFTR-mRNA transfection with chitosan did not have the awaited effect of decreasing the amiloride-sensitive current, a different approach to inhibit ENaC activity was adopted. To this end, chitosan-ASO complexes were designed for transfection purposes in order to downregulate ENaC expression. This project is based on previous studies by Sobczak *et al*. who transfected primary HNE cells with α-ENaC-ASO using the commercially available transfection reagent *Effectene®* (Qiagen; Sobczak et al., 2009).

3.2.1 Characterization of chitosan-ASO complexes

Chitosan-ASO complexes were formed by electrostatic self-assembly at different N/P charge ratios (30, 50, 70, 90, 100) using CS working solutions with or without 85 mM NaCl and three different ASO (0.3 µg/µL) against the α-subunit of ENaC. The complexes were then characterized in terms of their physicochemical properties such as size, PDI, zeta potential, as well as their binding efficiency.

The Z-average hydrodynamic diameter and the PDI of the complexes were determined by DLS-NIBS. Particle size of all complexes varied between 100 and 200 nm (Figure 22). PDI measurement revealed that on average complexes prepared in the presence of NaCl had a lower PDI than complexes prepared without the salt. Furthermore, a decrease of PDI with increasing N/P charge ratio could be observed, with lowest PDI in complexes at N/P charge ratio 90 (Figure 23). Overall, the PDI varied between 0.15 and 0.35 indicating that the complexes are in general monodisperse. These results coincide with the size distribution by intensity of the chitosan-ASO complexes exhibiting only one peak (Figure 24). Figure 25 displays the correlograms of the complexes. The decay of the lines of samples prepared with 85 mM NaCl (Figure 25d-f) appears to be steeper than in samples without NaCl. These findings suggest that the complexes prepared with NaCl are in general slightly more monodisperse than those prepared in water, in correspondence with the PDI measurements.

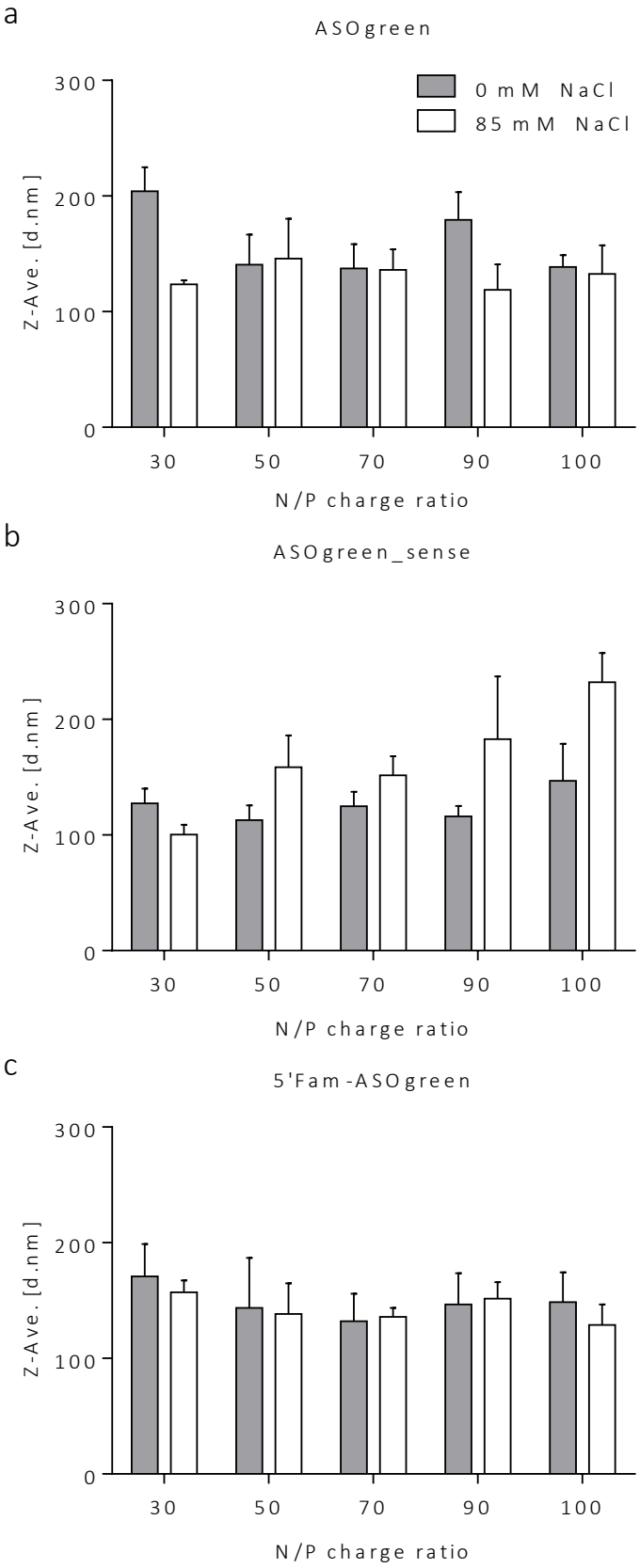

Figure 22: Z-average hydrodynamic diameter of CS-ASO complexes at varying N/P charge ratios. The size of CS-ASO complexes with **(a)** ASOgreen, **(b)** ASOgreen_sense and **(c)** 5'Fam-ASOgreen varied between 100 and 200 nm. On average, complexes prepared in the presence of 85 mM NaCl were smaller than complexes prepared without NaCl (n=3).

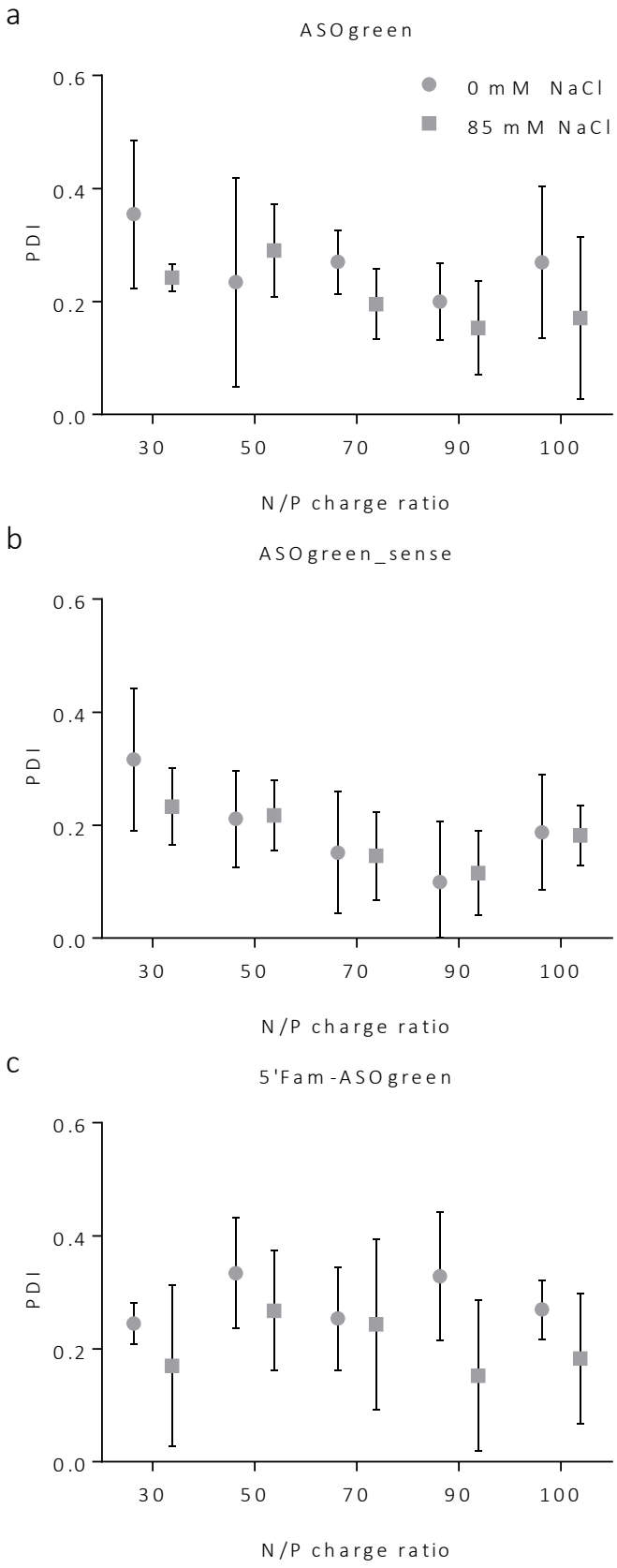

Figure 23: Polydispersity index (PDI) of CS-ASO complexes at varying N/P charge ratios. The PDI of CS-ASO complexes with **(a)** ASOgreen, **(b)** ASOgreen_sense and **(c)** 5'Fam-ASOgreen varied between 0.1 and 0.4. On average, complexes prepared in the presence of 85 mM NaCl had a lower PDI than complexes prepared without NaCl. Lowest PDI was observed in complexes at N/P charge ratio 90 (n=3).

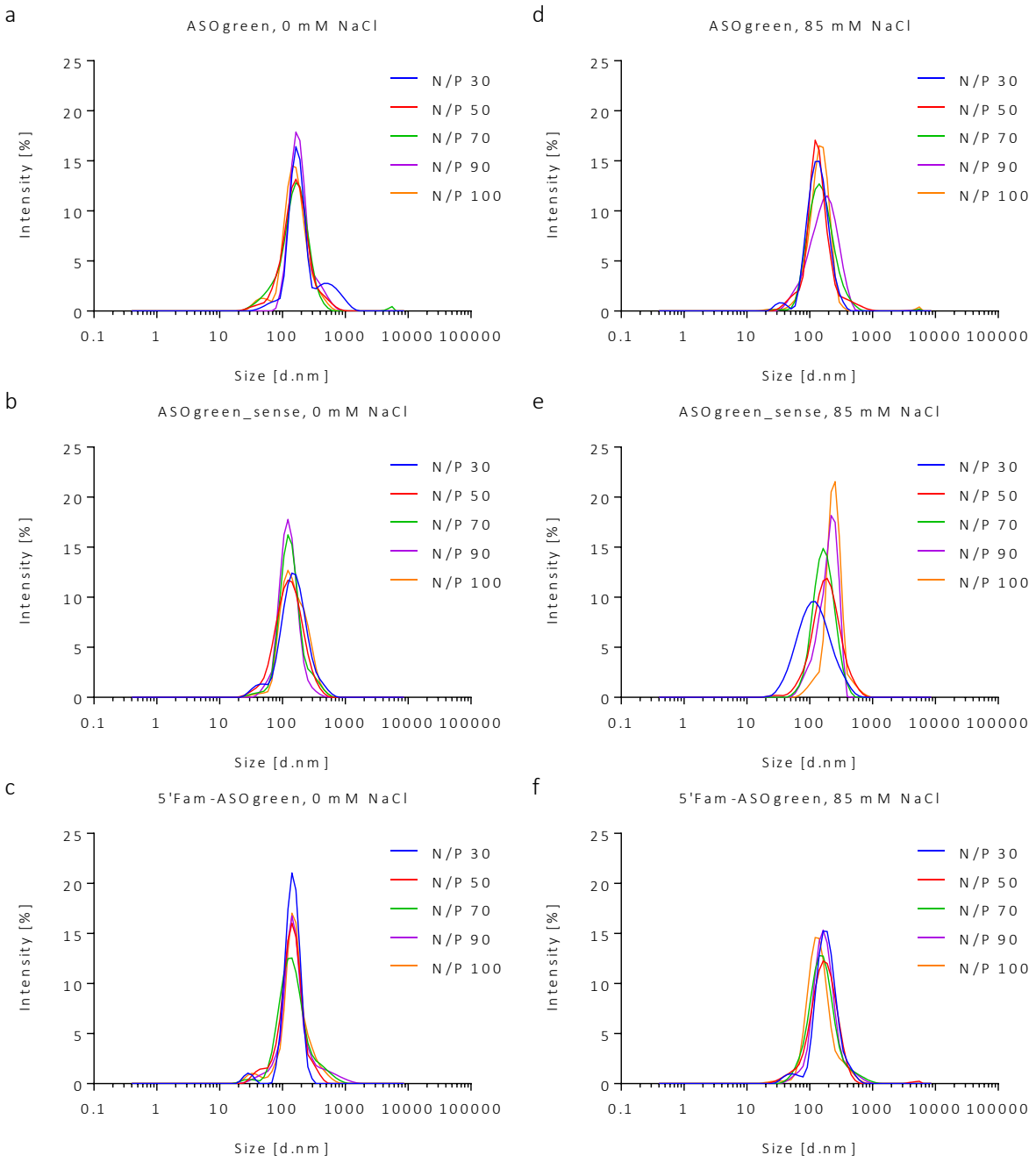

Figure 24: Size distribution of CS-ASO complexes at varying N/P charge ratios by intensity. Relative intensity of light scattered by CS-ASO complexes with **(a,d)** ASOgreen, **(b,e)** ASOgreen_sense and **(c,f)** 5'Fam-ASOgreen were prepared with **(d,e,f)** and without **(a,b,c)** 85 mM NaCl (n=3).

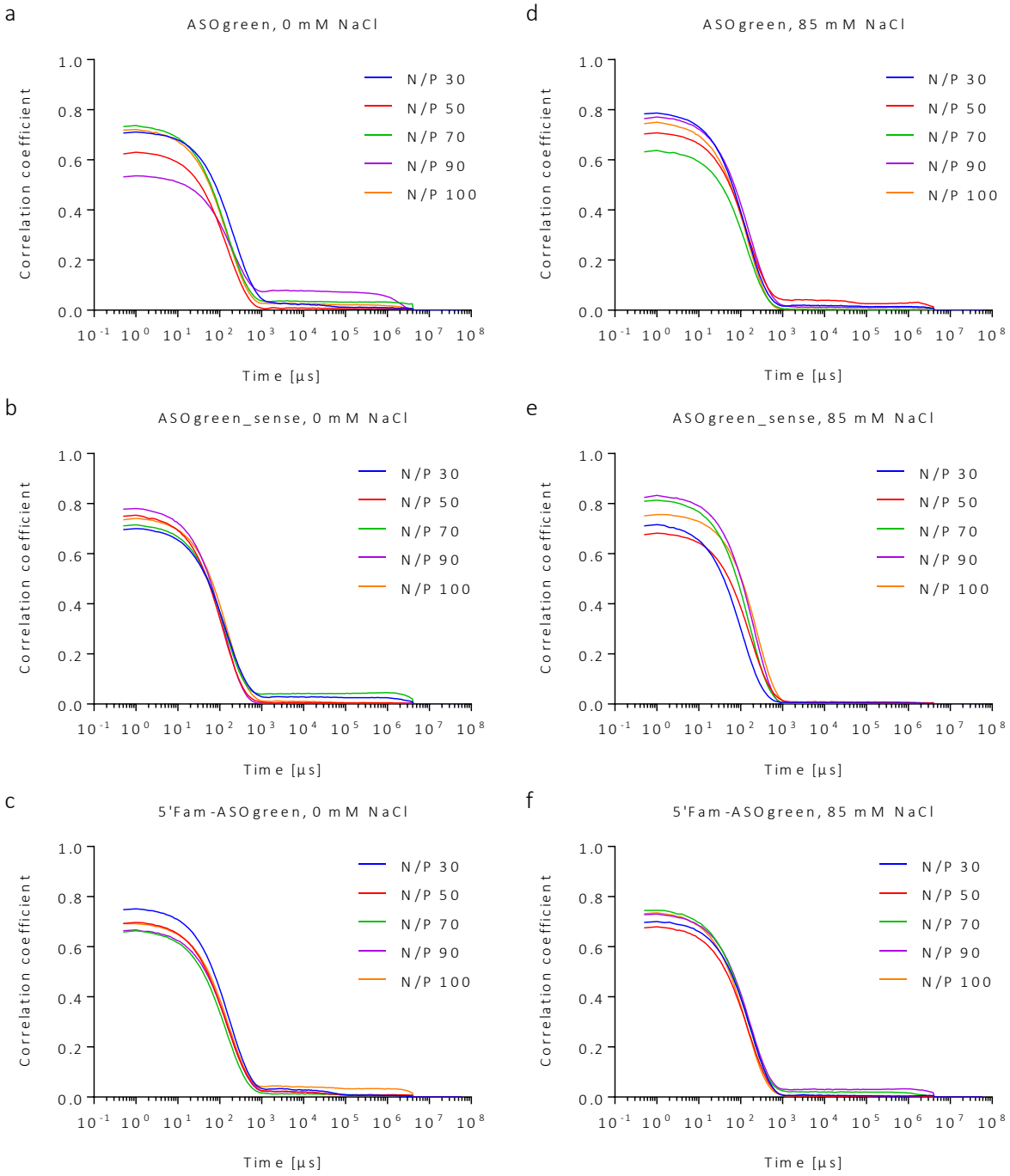

Figure 25: Correlograms of CS-ASO complexes at varying N/P charge ratios. CS-ASO complexes with **(a,d)** ASOgreen, **(b,e)** ASOgreen_sense and **(c,f)** 5'Fam-ASOgreen were prepared with **(d,e,f)** and without **(a,b,c)** 85 mM NaCl (n=3).

The zeta potential of the complexes was determined by their electrophoretic mobility and is displayed in Figure 26. The zeta potential increased with increasing N/P charge ratio from approximately +25 to +35 mV. On average complexes prepared in the presence of 85 mM NaCl had a lower zeta potential than complexes prepared without NaCl. Of note, the dependence of zeta potential with N/P ratio observed between the chitosan-ASOgreen and chitosan-ASOgreen _sense is different (Figure 26a and Figure 26b, respectively). In addition, the complexes formed with the fluorescently labelled ASO showed a linear dependence between zeta potential and N/P ratio by contrast with the other two systems that showed a non-linear profile.

In order to evaluate the binding efficiency of chitosan and ASO a gel retardation assay was performed (Figure 27). Due to its negative charge the naked ASO ran through the gel and showed a specific band below 100 bp corresponding to their size of 16 bp. Positively charged chitosan was retained in the pocket. Chitosan-ASO complexes at different N/P charge ratios did not show a specific band as the negatively charged nucleic acid was retained in the pocket by chitosan whereas the retained amount of ASO appeared to be proportional to the N/P charge ratio.

After careful consideration of the assessed physicochemical properties, complexes at N/P charge ratio 90 prepared in the presence of 85 mM NaCl were chosen for transfection experiments. Table 48 summarizes the Z-average hydrodynamic diameter, PDI and zeta potential of the chosen complexes.

Table 48: Physicochemical properties of CS-ASO complexes at N/P charge ratio 90 prepared with 85 mM NaCl

	ASOgreen	*ASOgreen_sense*	*5'Fam-ASOgreen*
Hydrodynamic diameter [d.nm]	119.0 ± 17.9	182.9 ± 44.3	151.7 ± 11.6
PDI	0.15 ± 0.07	0.12 ± 0.06	0.15 ± 0.11
Zeta potential [mV]	+28.9 ± 1.7	+31.6 ± 0.7	+29.6 ± 2.4

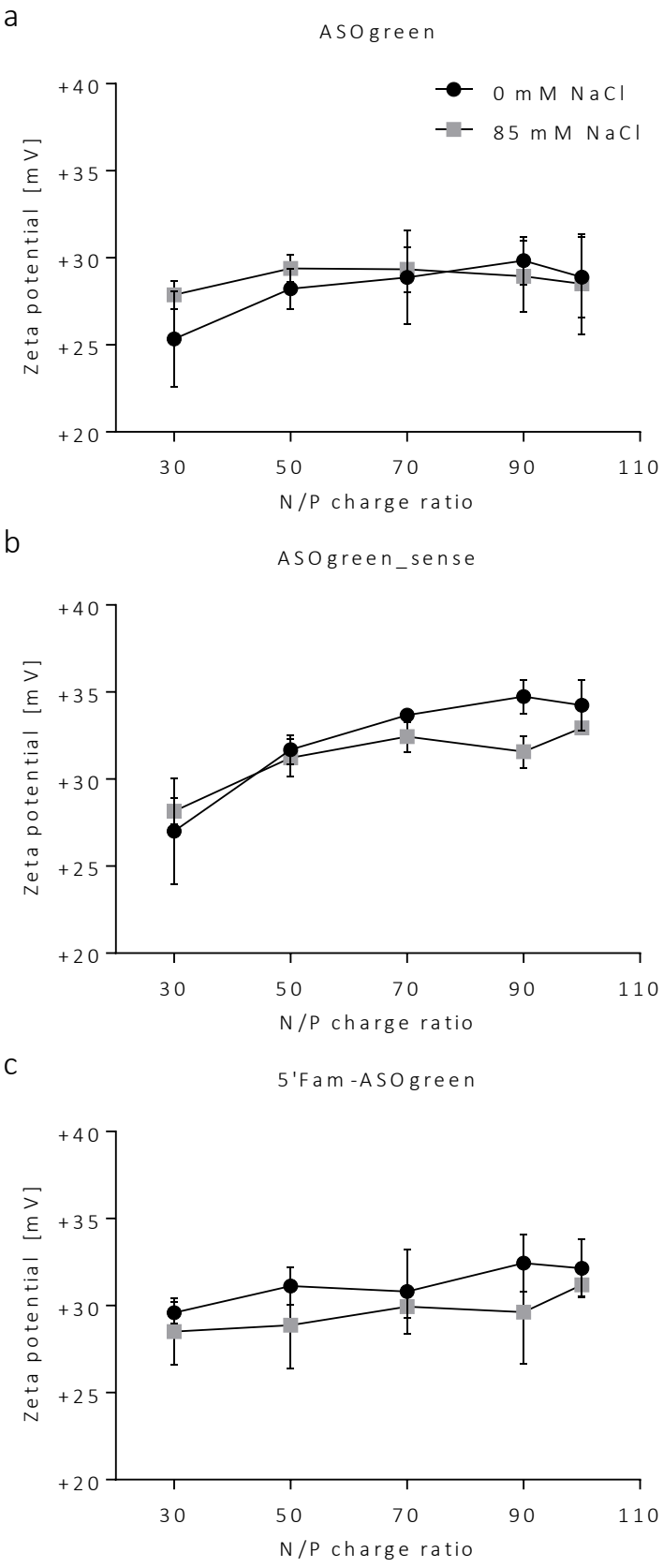

Figure 26: Zeta potential of CS-ASO complexes at varying N/P charge ratios. The zeta potential of CS-ASO complexes with **(a)** ASOgreen, **(b)** ASOgreen_sense and **(c)** 5'Fam-ASOgreen increased with increasing N/P charge ratio. On average, complexes prepared in the presence of 85 mM NaCl had a lower zeta potential than complexes prepared without NaCl (n=3).

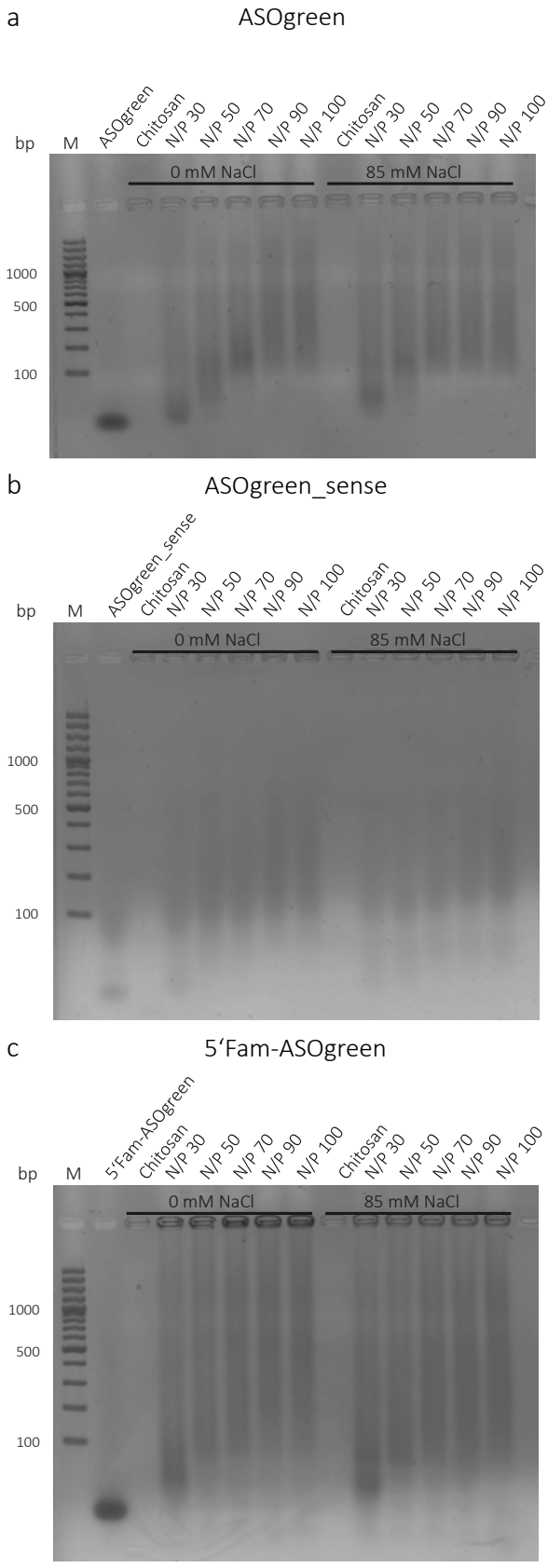

Figure 27: Gel retardation assay of CS-ASO complexes at varying N/P charge ratios. Shown is the result of a 1.5% agarose gel electrophoresis of CS-ASO complexes with **(a)** ASOgreen, **(b)** ASOgreen_sense and **(c)** 5'Fam-ASOgreen prepared with and without 85 mM NaCl. Naked ASO showed a band below 100 bp. Chitosan was retained in the pocket. The retained amount of ASO by chitosan was proportional to the charge ratio. Marker (M): *O'Gene Ruler 100 bp Plus* (Thermo Fisher Scientific).

3.2.2 Stability of chitosan-ASO complexes

The stability of the complexes in cell culture transfection medium was determined by measuring their size by DLS-NIBS during incubation. For this complexes were incubated in *Opti-MEM™* or *Opti-MEM™* supplemented with HEPES (20 mM) and mannitol (270 mM) at 37°C for 24 h. Figure 28 shows the Z-average hydrodynamic diameter of the complexes in the media. Chitosan-ASOgreen complexes in *Opti-MEM™* supplemented with HEPES and mannitol were stable for the first hours while complexes in *Opti-MEM™* without supplements aggregated immediately. After approximately 5 h though, the systems settled around 2,000 nm. The other two systems seemed to be less stable in supplemented *Opti-MEM™* during the first five hours. However, all these also settled at longer incubation periods. Overall, complexes appeared to be slightly more stable in *Opti-MEM™* supplemented with HEPES and mannitol. Visible aggregation was not observed in either medium at any time. Size distribution by intensity (Figure 29) and correlograms (Figure 30) of the complexes show similar results at 4 h and 24 h that confirm these observations.

When working with cell cultures it is crucial to maintain optimal conditions such as temperature or CO_2 concentration in order to minimize cell stress. Therefore, the osmolality of the transfection media was determined by a cryoscopic osmometer. Table 49 displays the osmolality of different cell culture media as well as the transfection media. While the osmolality of *Opti-MEM™* without supplements was similar to the osmolality of the cell culture media, the osmolality of *Opti-MEM™* supplemented with HEPES and mannitol was more than twice as high. This high osmolality could severely affect the health of cells and impair the transfection. Therefore, transfection experiments were conducted with *Opti-MEM™* without supplements, even though complexes were more stable in the medium supplemented with HEPES and mannitol.

Table 49: Osmolality of cell culture and transfection media

	Osmolality (mOsmol/kg)
CFBE41o- cell culture medium	288.7 ± 2.1
UG medium	307.0 ± 0.8
H441 cell culture medium	270.3 ± 1.7
Opti-MEM™	272.7 ± 2.6
Opti-MEM™ + HEPES (20 mM) + mannitol (270 mM)	582.7 ± 4.0

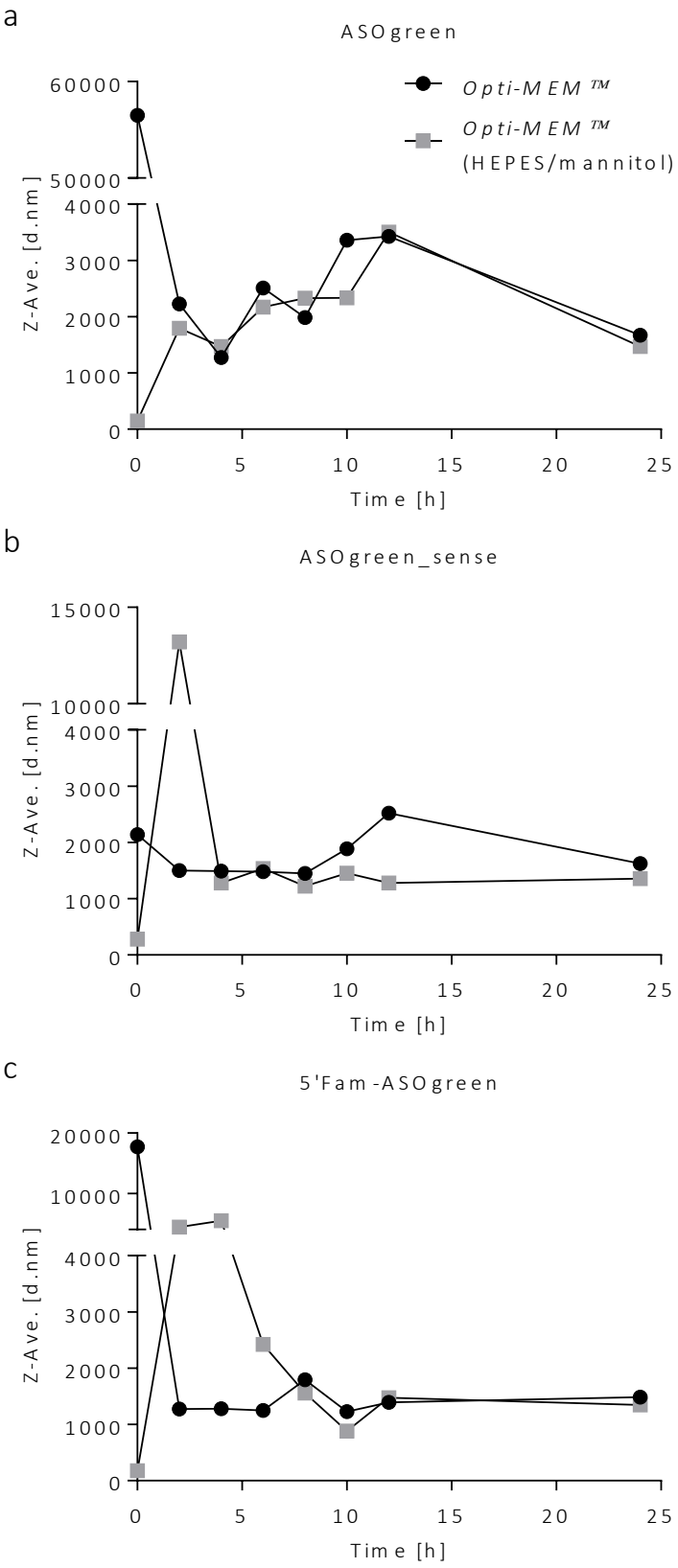

Figure 28: Stability of CS-ASO complexes in transfection medium. Shown is the stability of CS-ASO complexes with **(a)** ASOgreen, **(b)** ASOgreen_sense and **(c)** 5'Fam-ASOgreen at N/P charge ratio 90 with 85 mM NaCl. Complexes were incubated in *Opti-MEM™* or *Opti-MEM™* supplemented with HEPES (20 mM) and mannitol (270 mM) at 37°C. Complexes in *Opti-MEM™* supplemented with HEPES and mannitol appeared to be more stable than complexes in *Opti-MEM™* alone.

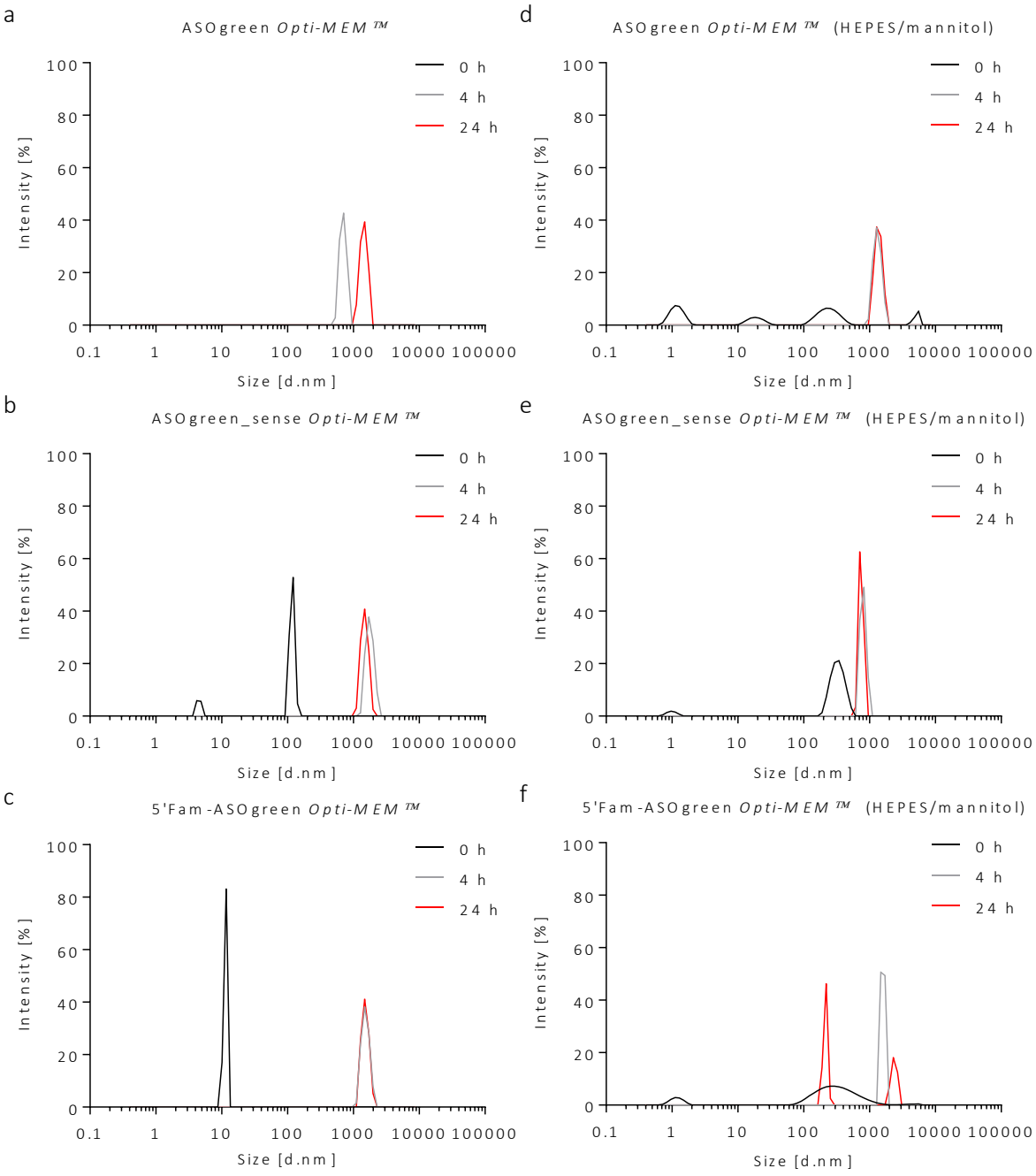

Figure 29: Size distribution by intensity of CS-ASO complexes in transfection medium. Relative intensity of light scattered by CS-ASO complexes with **(a,d)** ASOgreen, **(b,e)** ASOgreen_sense and **(c,f)** 5'Fam-ASOgreen at N/P charge ratio 90 with 85 mM NaCl in transfection media. Complexes were incubated in **(a,b,c)** *Opti-MEM™* or **(d,e,f,)** *Opti-MEM™* supplemented with HEPES (20 mM) and mannitol (270 mM) at 37°C. Complexes appear to stabilize after 4 h.

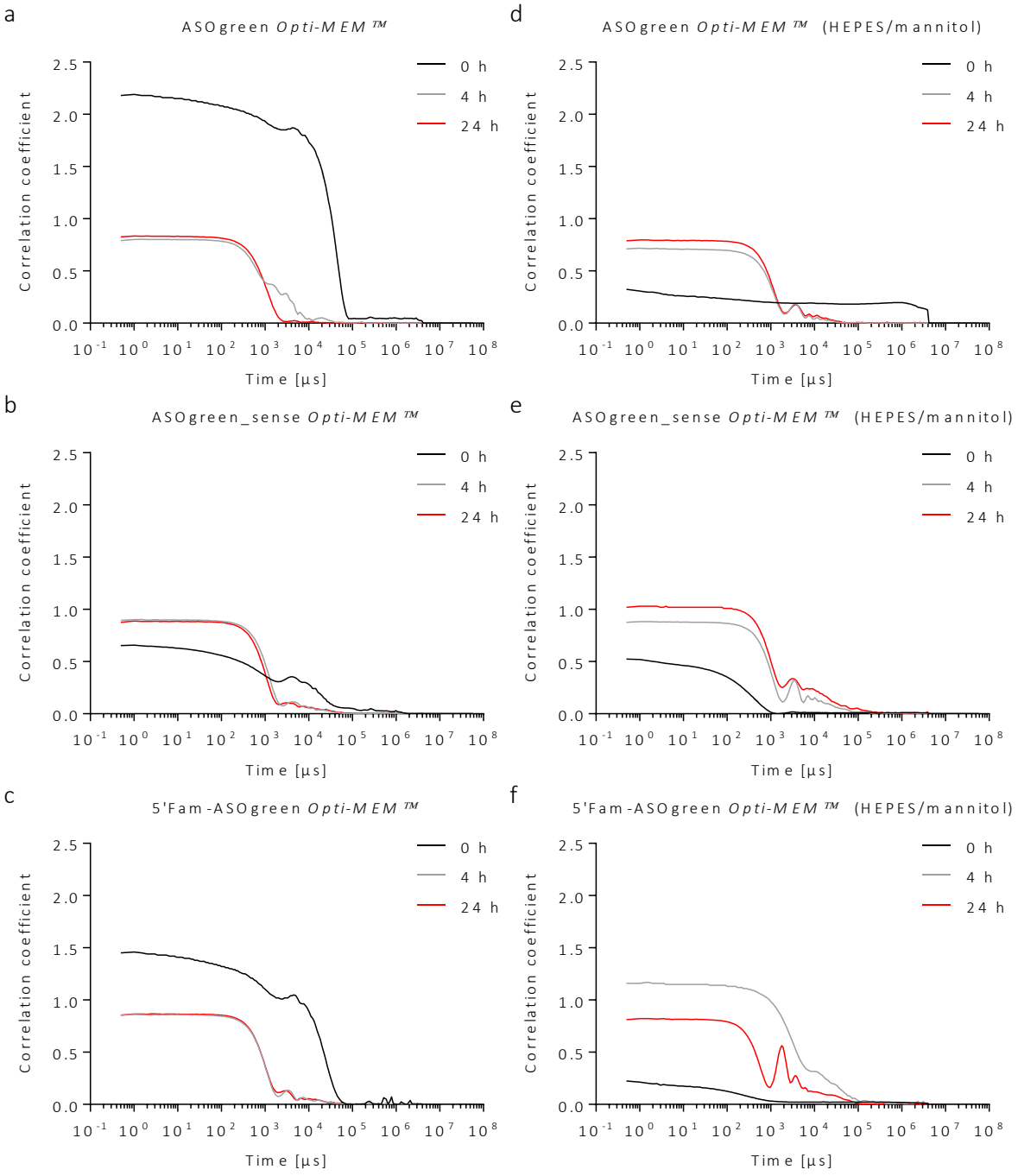

Figure 30: Correlograms of CS-ASO complexes in transfection medium. Shown is the stability of CS-ASO complexes with **(a,d)** ASOgreen, **(b,e)** ASOgreen_sense and **(c,f)** 5'Fam-ASOgreen at N/P charge ratio 90 with 85 mM NaCl. Complexes were incubated in **(a,b,c)** *Opti-MEM™* or **(d,e,f,)** *Opti-MEM™* supplemented with HEPES (20 mM) and mannitol (270 mM) at 37°C.

3.2.3 Cell culture experiments with chitosan-ASO complexes

Before conducting transfection experiments with chitosan-ASO complexes, the effect of the complexes on the viability of cells was determined. For this H441 and primary HNE cells were incubated with the complexes and the other treatments and controls for 24 h and subsequently an MTT assay was carried out. The MTT test of H441 cells showed that chitosan-ASO complexes did not have a significant effect on the viability of the cells while *Lipofectamine* displayed highly significant cytotoxicity (Figure 31a). Furthermore, the test confirmed the negative effect of the high osmolality of *Opti-MEM™* supplemented with HEPES and mannitol as the transfection medium displayed a highly significant impairment of the cell viability compared to *Opti-MEM™* without supplements. The MTT test of primary HNE cells showed the same result (Figure 31b). In contrast to H441 cells, cell viability of primary HNE cells was significantly impaired by chitosan-ASO complexes, though to levels not below ~75%. However, in this experiment, complexes were diluted in *Opti-MEM™* supplemented with HEPES and mannitol, which could be the reason for the cytotoxicity. After ruling out cytotoxicity of the complexes transfection experiments were performed.

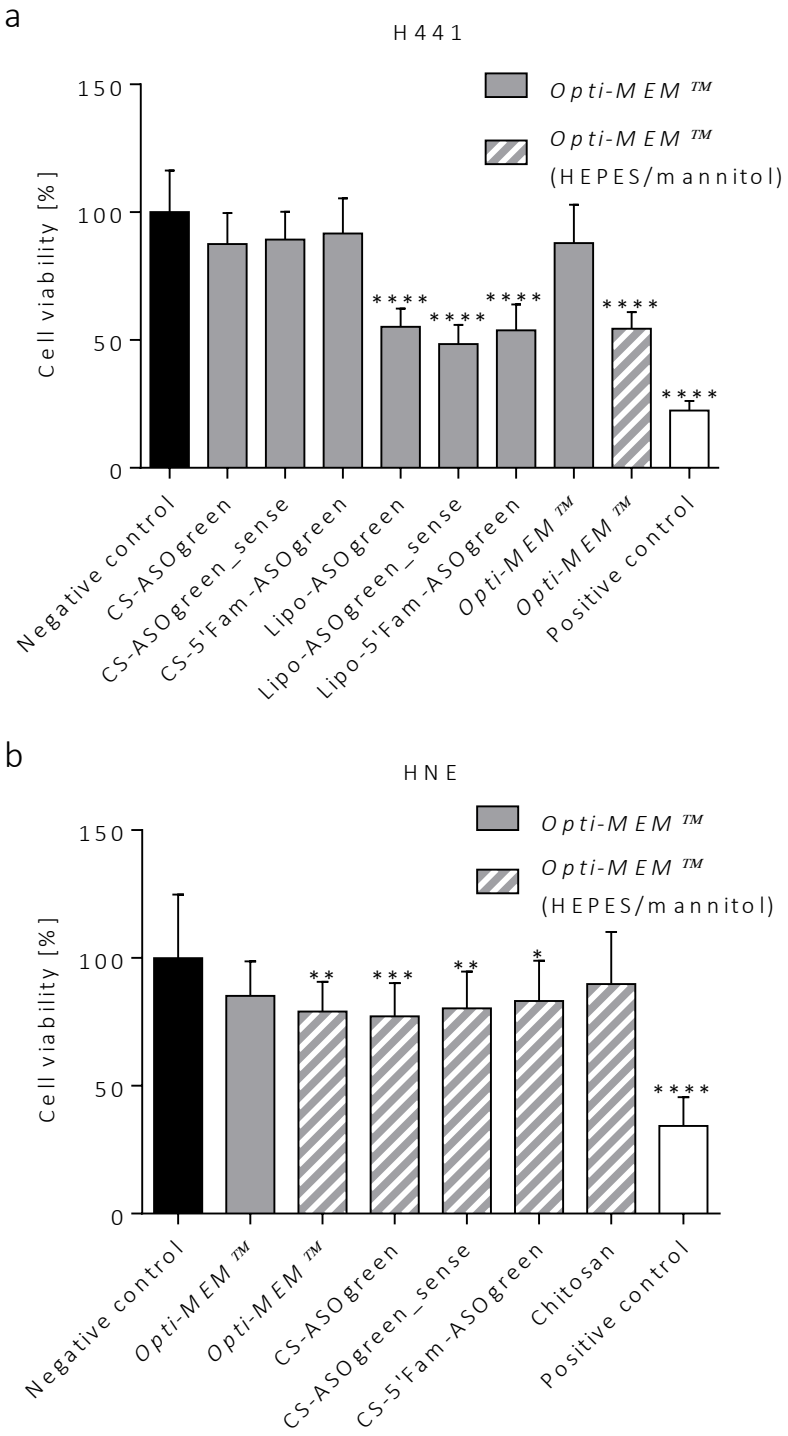

Figure 31: Effect of varying ASO in combination with *Lipofectamine* and chitosan on the viability of cells. (a) H441 cells and **(b)** primary HNE cells were incubated with the samples for 24 h before an MTT assay was conducted. Cell culture medium was used as negative control; Triton® X-100 was used as positive control. While chitosan in combination with ASO only had a slight effect on the cell viability (~80-90%), the decrease in cell viability caused by *Lipofectamine* in combination with ASO was highly significant (~50%; $p \leq 0.05$ (*), $p \leq 0.01$ (**), $p \leq 0.001$ (***), $p \leq 0.0001$ (****); n=3).

First, transfection experiments were performed with H441 cells and the fluorescently labeled ASO in order to verify successful cellular uptake. For this cells were seeded on glass cover slips and transfected with 5'Fam-ASOgreen using *Lipofectamine* or chitosan. As control, cells were transfected with the non-fluorescent ASOgreen. Comparison of total RGB fluorescent intensities revealed no significant difference between transfection with *Lipofectamine* and chitosan (Figure 32). In fact, the significant difference between control cells and cells transfected with the fluorescently labeled ASO was higher when using chitosan as transfection reagent than when using *Lipofectamine.* Figure 33 depicts representative images of the transfected cells. While the ASO transfected with *Lipofectamine* appear very bright and clear, the nucleotides transfected with chitosan seem more diffuse and dimmed. Having proven successful cellular uptake of chitosan-ASO complexes, further transfection experiments were conducted.

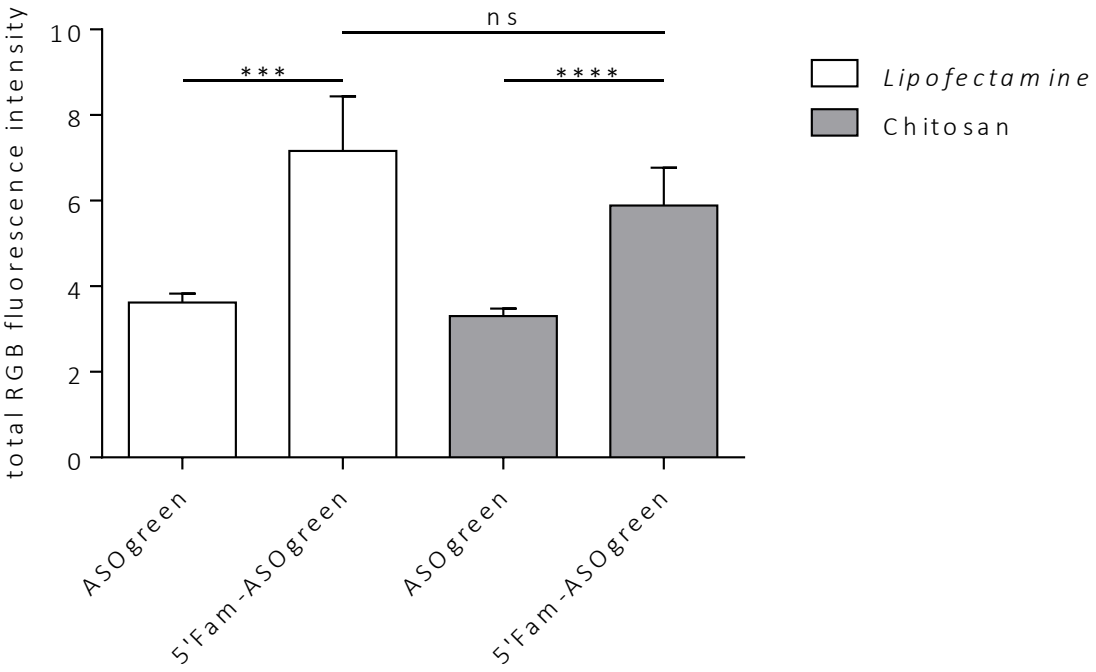

Figure 32: Fluorescence intensities of H441 cells transfected with ASOgreen and 5'Fam-ASOgreen. Cells were transfected with the fluorescent 5'Fam-ASOgreen as well as the non-fluorescent ASOgreen as controls. Lipofectamine and chitosan were used as transfection reagents. Total RGB fluorescence intensity was determined 24 h after transfection (non-significant (ns), $p \leq 0.001$ (***), $p \leq 0.0001$ (****); n=12).

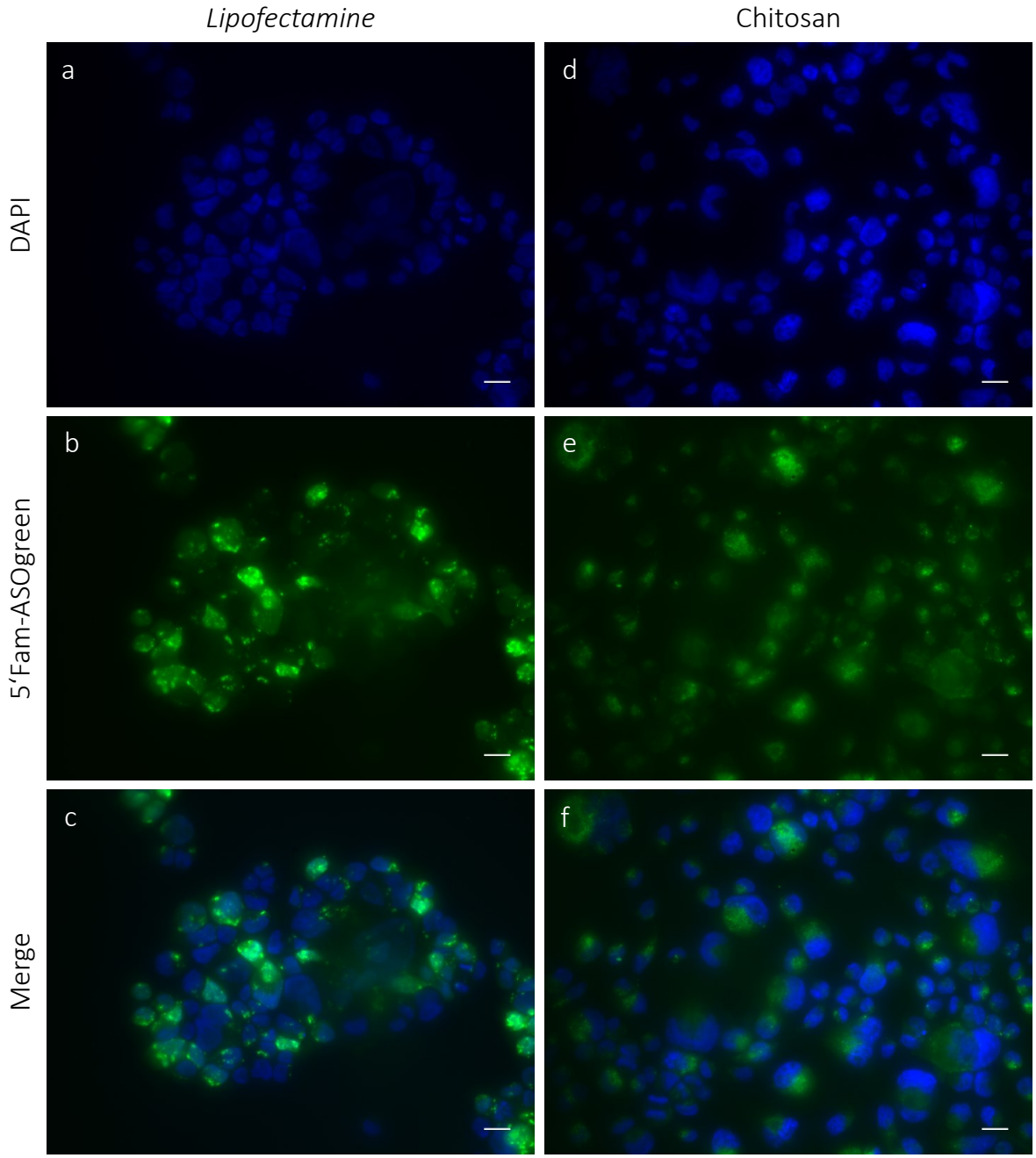

Figure 33: Representative fluorescence microscopy images of H441 cells transfected with 5'Fam-ASOgreen. Cells were transfected using **(a-c)** *Lipofectamine* and **(d-f)** chitosan. Images were taken 24 h after transfection. **(a,d)** DAPI; **(b,e)** 5'Fam-ASOgreen; **(c,f)** Merge (scale bar = 20 µm).

In order to test the ability of the ASO to functionally inhibit ENaC activity H441 cells were transfected with 0.45 µg/cm^2 ASOgreen and ASOgreen_sense using chitosan and *Lipofectamine*, respectively. 24 h after transfection functional Ussing chamber measurements were conducted. During the measurements, ENaC was blocked by the specific blocker amiloride followed by complete apical withdrawal of sodium with the purpose of determining the amount of amiloride-sensitive sodium current. In non-transfected control cells only a very slight decrease of short-circuit current was observed after removal of sodium (Figure 34a). This suggests that most of the sodium current is mediated by ENaC. On the contrary, in cells transfected with ASOgreen using chitosan the decrease of short-circuit current after application of sodium-free ringer solution was much greater indicating that only a very small amount of sodium current is mediated by ENaC (Figure 34b). Statistical evaluation of the short-circuit current confirmed these observations (Figure 35). After transfection with ASOgreen, the amiloride-sensitive current decreased notably compared to non-transfected control cells. Actually, in cells transfected using chitosan the decrease was significant (48.4 ± 8.5% vs. 8.9 ± 2.4%) demonstrating successful inhibition of ENaC by ASOgreen. Transfection with ASOgreen_sense led to a slight decrease of amiloride-sensitive current. However, no significant difference to control cells was identified indicating ASOgreen_sense having no effect on ENaC expression as expected.

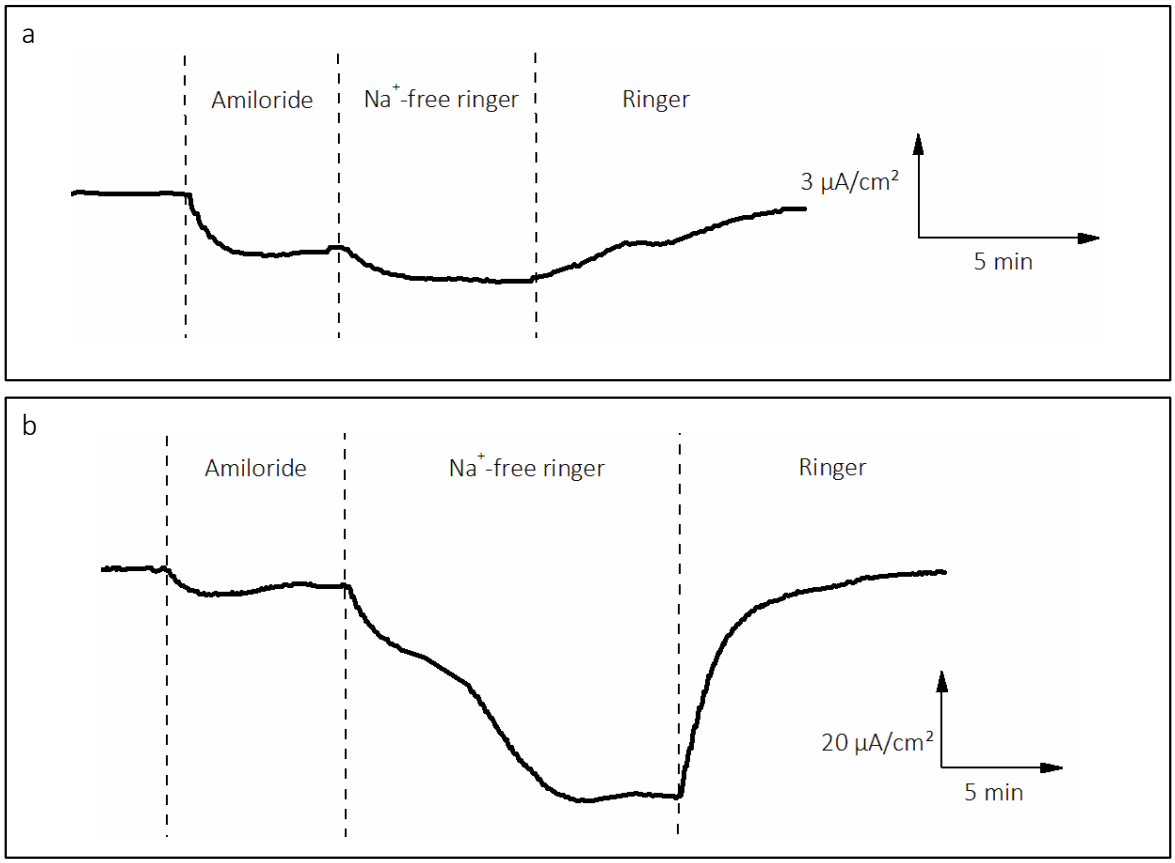

Figure 34: Representative time courses of transepithelial measurements of H441 cells. Shown is the short-circuit current (I_{sc}) of a typical Ussing chamber measurement. **(a)** Non-transfected cells showed a slight decrease of I_{sc} after application of Na^+-free ringer solution. **(b)** In cells transfected with ASOgreen using chitosan (0.45 µg/cm² ASOgreen), I_{sc} strongly decreased after withdrawal of Na^+.

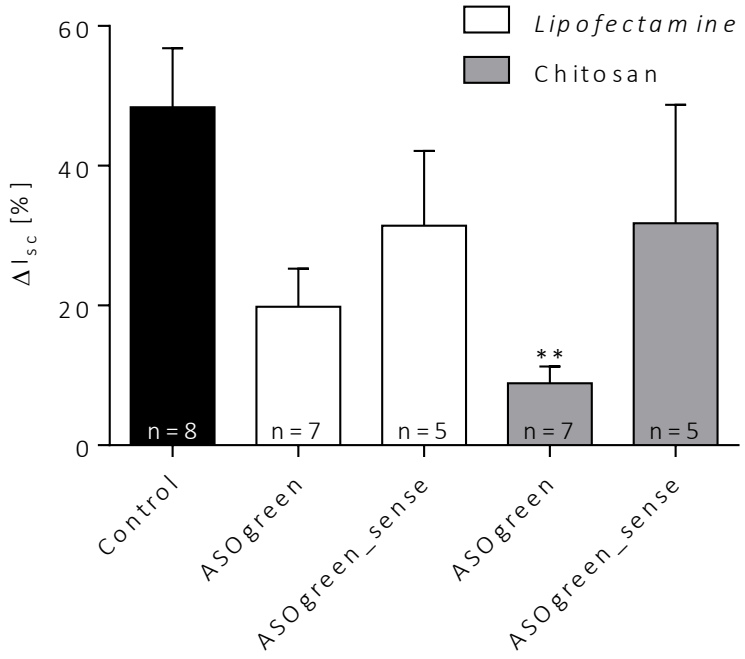

Figure 35: Statistical evaluation of amiloride-sensitive short-circuit current (I_{sc}) in H441 cells after ASO transfection with *Lipofectamine* and chitosan. Cells were transfected with 0.45 µg/cm² ASO, respectively; control cells were not transfected. Measurements were conducted 24 h after transfection. Amiloride-sensitive I_{sc} decreased after transfection with ASOgreen. Cells transfected with ASOgreen_sense only showed a slight decrease of amiloride-sensitive current ($p \leq 0.01$ (**)).

3.3 Chitosan-mRNA-ASO complexes

After successful transfection of wtCFTR-mRNA as well as α-ENaC-ASO using chitosan as a vector, an attempt was made to design chitosan complexes containing both nucleic acids in order to co-target both ion channels at the same time.

3.3.1 Characterization of chitosan-mRNA-ASO complexes

As described before the complexes were formed by electrostatic self-assembly at varying N/P charge ratios (10, 30, 50, 70, 90) using CS working solutions, wtCFTR-mRNA (0.53 µg/µL) and three different ASO (0.3 µg/µL) against the α-subunit of ENaC, respectively. Again the complexes were characterized in terms of their physicochemical properties (size, PDI and zeta potential).

The double complexes displayed a Z-average hydrodynamic diameter of averagely 150 nm varying between 100 and 200 nm (Figure 36) measured by DLS-NIBS. No obvious trend relating to the N/P charge ratio could be identified. Evaluation of the PDI showed similar results. The index varied between 0.4 and 0.5 for all N/P charge ratios (Figure 37) hinting at relatively polydisperse complexes. This theory is supported by the size distribution by intensity and correlograms of the complexes shown in Figure 38. The intensity size distribution plots (Figure 38a-c) reveal the presence of three populations of particles for all N/P charge ratios at approximately 100, 1,000 and 10,000 nm. The narrow decay of the correlograms and low plateau correlation coefficient at short correlation times (Figure 38d-f) are also diagnostic of a high size distribution.

The zeta potential of the complexes was determined by their electrophoretic mobility. Unlike in size and PDI measurements a trend regarding the N/P charge ratio was perceptible. Zeta potential of the three different complexes increased with increasing N/P charge ratio from approximately +20 to +30 mV hinting at successful complexation and condensation of the nucleic acids (Figure 39).

However, due to their relatively high PDI and multimodal size distributions, these complexes were regarded as not suitable for transfection purposes and were therefore not used for cell culture experiments.

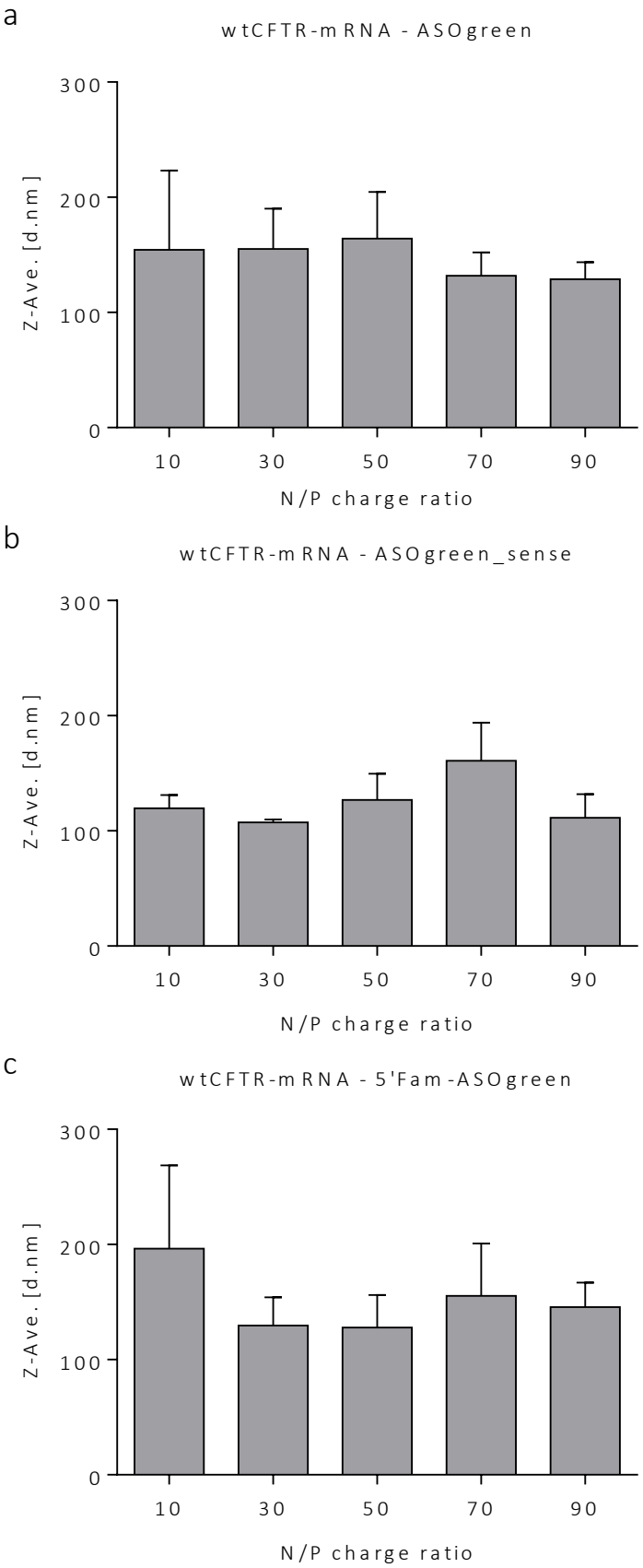

Figure 36: Z-average hydrodynamic diameter of CS-mRNA-ASO complexes at varying N/P charge ratios. The size of CS-mRNA-ASO complexes with **(a)** ASOgreen, **(b)** ASOgreen_sense and **(c)** 5'Fam-ASOgreen varied between 100 and 200 nm (n=3).

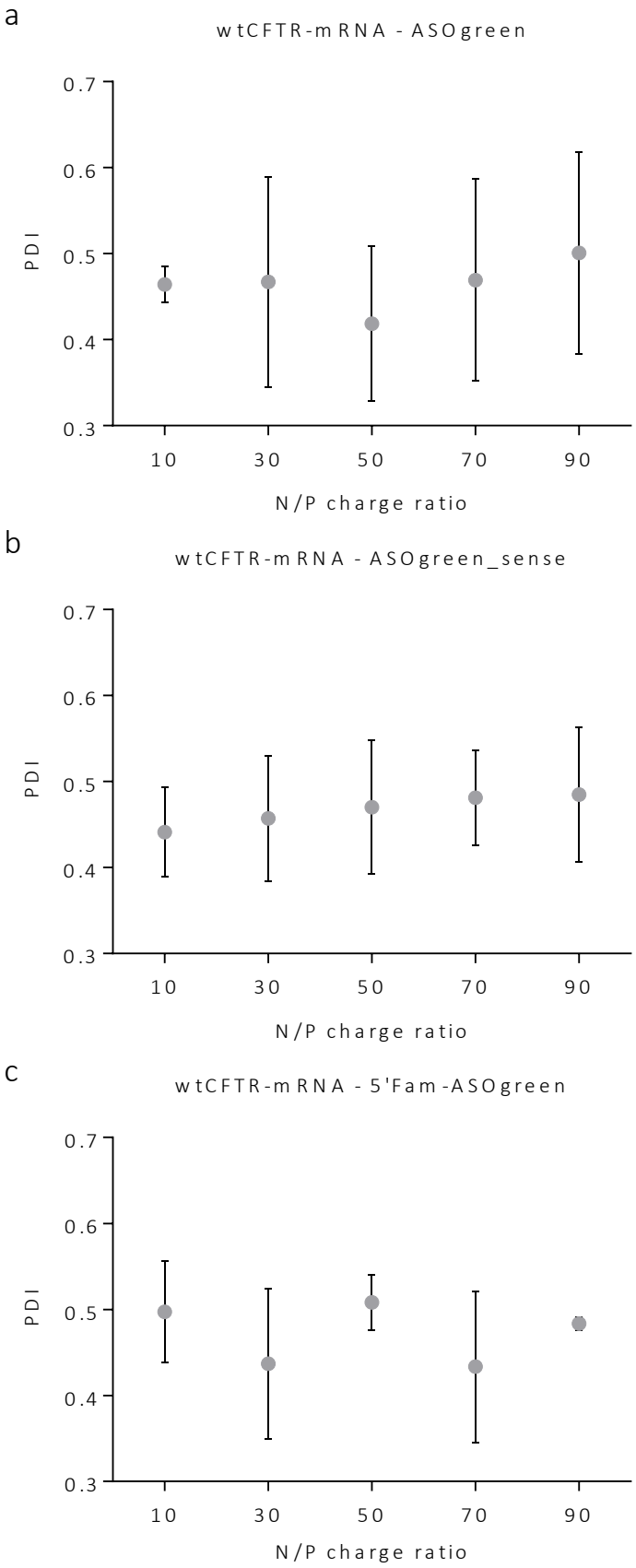

Figure 37: Polydispersity index (PDI) of CS-mRNA-ASO complexes at varying N/P charge ratios. The PDI of CS-mRNA-ASO complexes with **(a)** ASOgreen, **(b)** ASOgreen_sense and **(c)** 5'Fam-ASOgreen varied between 0.4 and 0.5 (n=3).

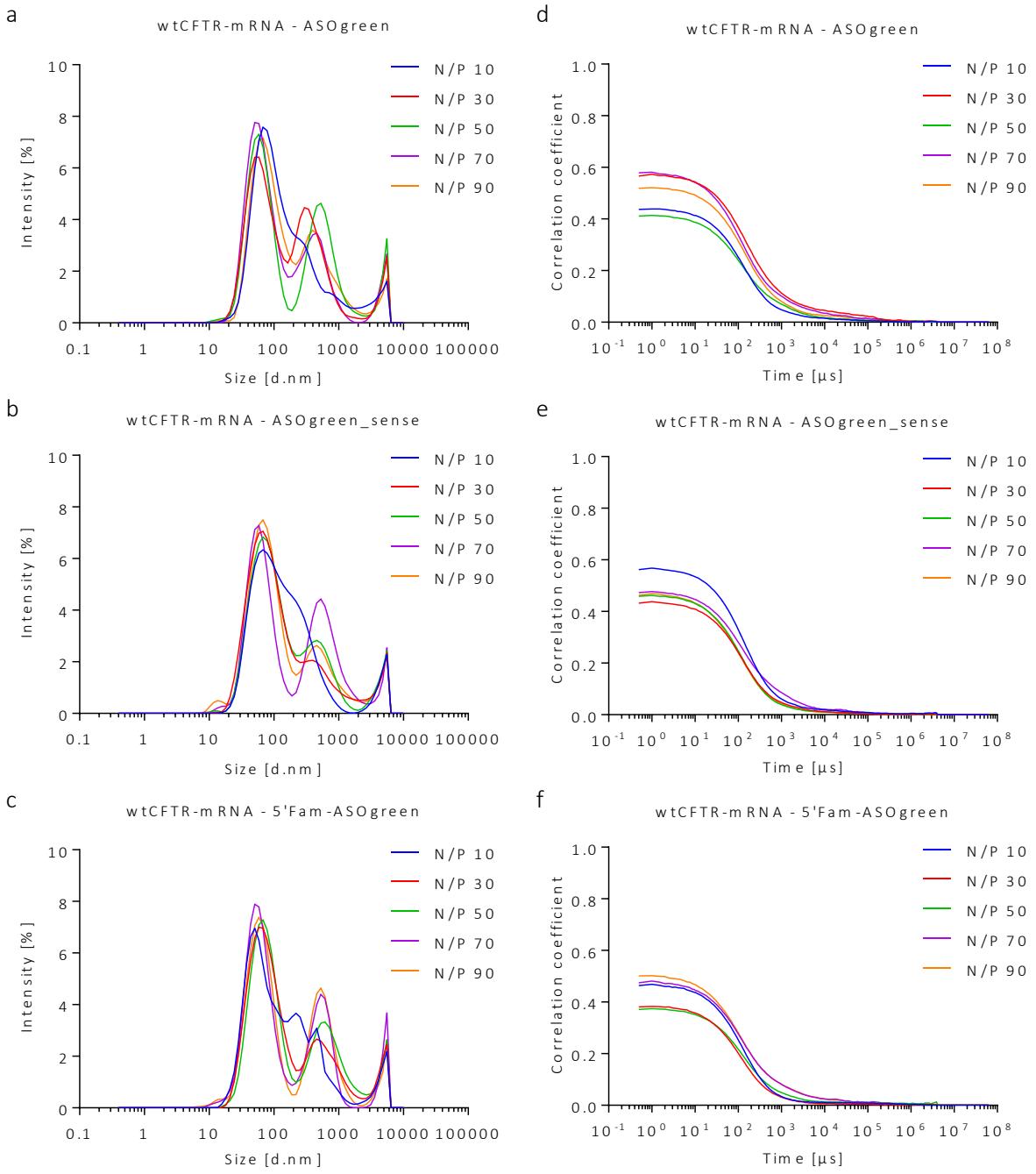

Figure 38: Size distribution by intensity and correlograms of CS-mRNA-ASO complexes at varying N/P charge ratios. Relative intensity of scattered light and correlograms of complexes prepared with **(a,d)** ASOgreen, **(b,e)** ASOgreen_sense and **(c,f)** 5'Fam-ASOgreen (n=3).

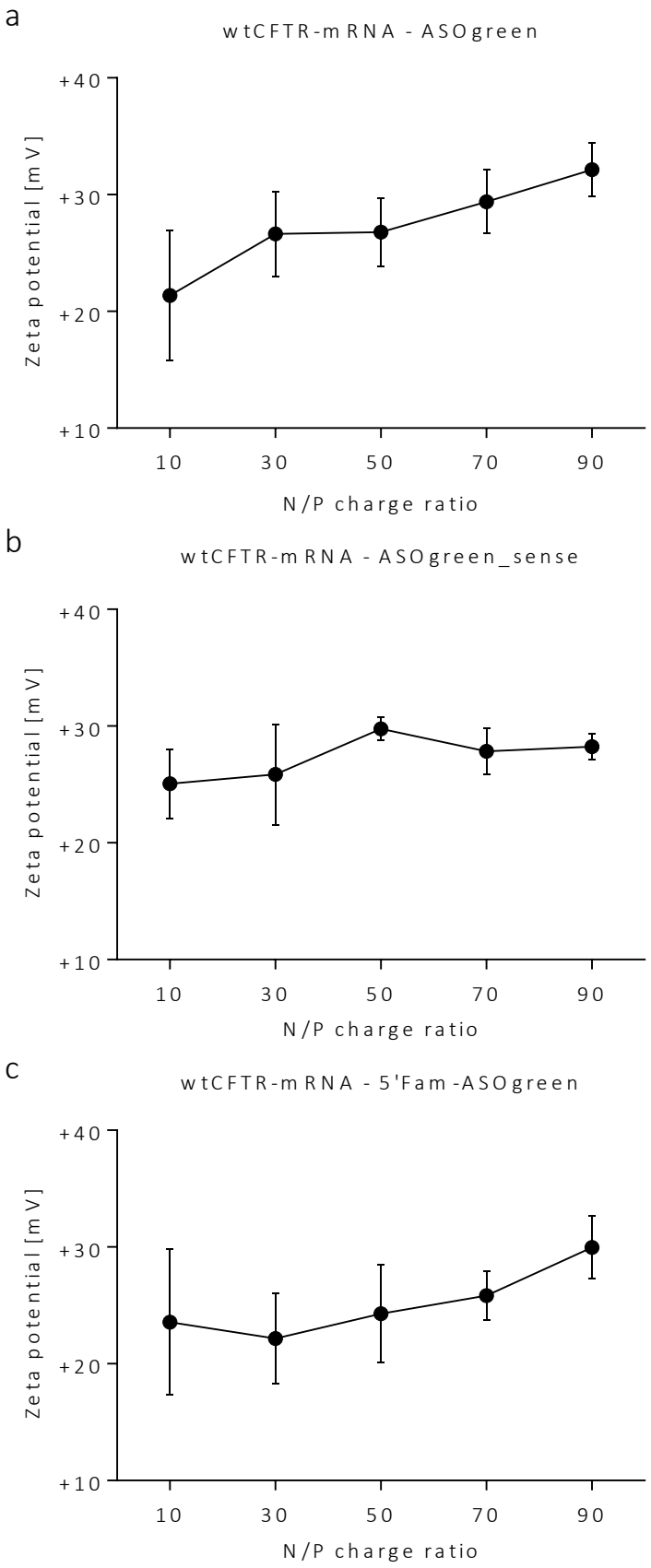

Figure 39: Zeta potential of CS-mRNA-ASO complexes at varying N/P charge ratios. The zeta potential of CS-mRNA-ASO complexes with **(a)** ASOgreen, **(b)** ASOgreen_sense and **(c)** 5'Fam-ASOgreen increased with increasing N/P charge ratio (n=3).

3.4 Chitosan-lecithin oil-core nanocapsules

As a second approach of a doubled tracked strategy to co-target both CFTR and ENaC simultaneously, chitosan-lecithin oil-core nanocapsules loaded with capsaicin were prepared. This this idea was born based on the study of Li *et al.* who showed that capsaicin inhibits the expression of the α-ENaC subunit by activation of TRPV1 in the kidney of mice (Li et al., 2014). The design of the capsules is based on studies by Kaiser *et al.* (Kaiser et al., 2015a, 2015b) and taken further by adsorbing wtCFTR-mRNA to the surface in line with previous studies that showed the feasibility to adsorb hepatitis B surface antigen at chitosan-coated nanocapsules (Vicente et al., 2013).

3.4.1 Detection of TRPV1 in primary HNE cells

Before the effect of capsaicin on cells was tested, TRPV1 was detected in primary HNE cells. For this the total RNA of cells was isolated and reverse transcribed into cDNA. Subsequently, a PCR was carried out using specific primers for TRPV1 and α-ENaC. GAPDH was amplified as reference gene. The outcome of the PCR was verified by an agarose gel electrophoresis. Both gels show specific bands for α-ENaC (Figure 40a) and TRPV1 (Figure 40b) below 100 bp corresponding to their amplicon lengths of 88 bp and 92 bp, respectively (Appendix Figure 57 and Figure 58). The reference gene GAPDH showed a specific band above 300 bp corresponding to its amplicon length of 325 bp (Appendix Table 55), thus validating the outcome of the PCR.

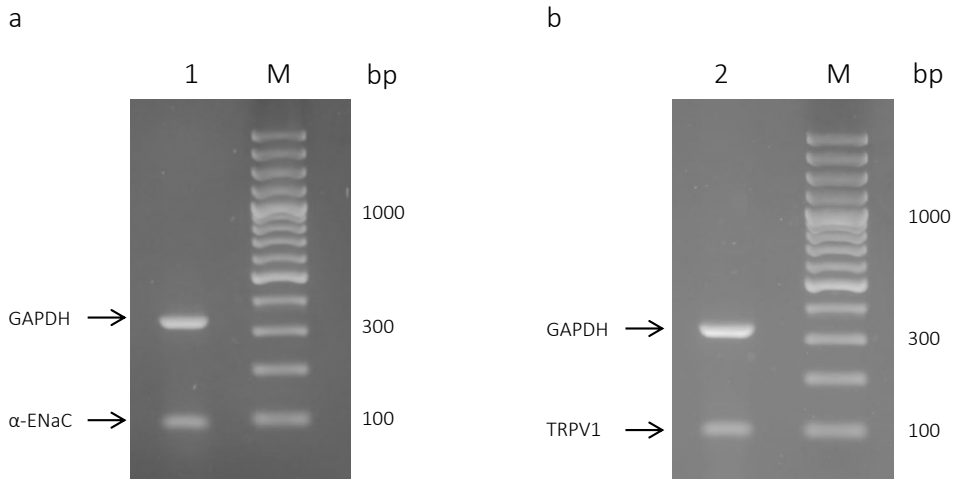

Figure 40: PCR of cDNA from primary HNE cells. The image shows 1.5% agarose gels after amplification of **(a)** α-ENaC and **(b)** TRPV1. Line 1 and 2 show specific bands for α-ENaC and TRPV1, respectively, corresponding to their amplicon lengths (88 bp and 92 bp). GAPDH was amplified as reference gene and shows specific bands above 300 bp. Marker (M): *O'GeneRuler™ 100 bp Plus DNA Ladder* (Thermo Fisher Scientific).

To confirm expression of TRPV1 in primary HNE cells the amplified TRPV1 fragment was sequenced. Figure 41 displays the alignment of the TRPV1 fragment and a sequence of human TRPV1 from the NCBI database (NM_080706.3; 4,443 bp). The 92 bases of the amplified TRPV1 fragment coincide perfectly with the sequence of the database proving evidence of the expression of the vanilloid receptor on mRNA level in primary HNE cells.

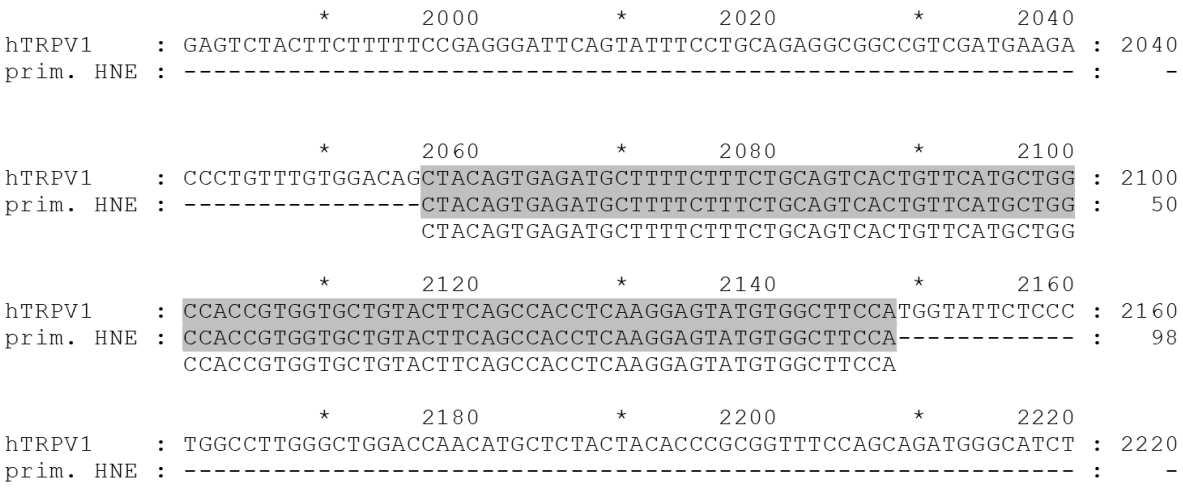

Figure 41: Alignment of human TRPV1 and amplified TRPV1 from primary HNE cells. The image shows the alignment of human TRPV1 from the NCBI database (NM_080706.3; 4443 bp; hTRPV1) and the amplified TRPV1 fragment from primary HNE cells (prim. HNE). The matching segments are highlighted in grey.

Furthermore, a western blot was performed in order to confirm expression of TRPV1 and α-ENaC in primary HNE cells on protein level. Proteins were isolated from cells and separated electrophoretically by SDS-PAGE. After blotting of the proteins on a PVDF membrane TRPV1 and α-ENaC were visualized by immunodetection. α-Tubulin was used as reference gene. A representative western blot is shown in Figure 42. TRPV1 shows a specific band around 100 kDa corresponding to the proteins Mw of about 95,000 Da (Caterina et al., 1997). Further weak bands were detected around 130 and 170 kDa. As negative control, TRPV1 was blocked with a human TRPV1 synthetic peptide. No bands were detected in this section of the membrane confirming specific binding of TRPV1 antibodies in the first membrane segment. α-ENaC was also successfully detected showing a specific band above 70 kDa corresponding to the subunit's Mw of approximately 85 kDa (Bhalla and Hallows, 2008). Additional faint bands were detected around 120 and 160 kDa. The reference gene α-Tubulin was detected at 55 kDa validating the outcome of the western blot.

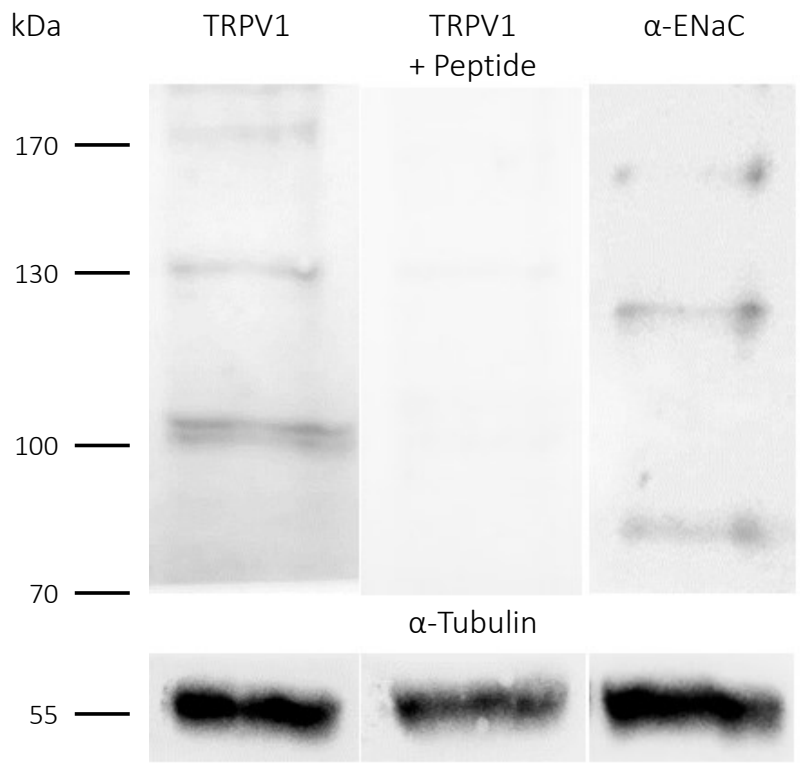

Figure 42: Detection of TRPV1 and α-ENaC in primary HNE cells on protein level by western blot. Total proteins were isolated from cells and separated in a 7.5% SDS-PAGE. Proteins were transferred to a PVDF membrane and visualized by immunodetection. Both TRPV1 and α-ENaC were successfully detected. TRPV1 blocked with a human TRPV1 synthetic peptide served as negative control. α-Tubulin was used as reference gene. Marker (kDa): *PageRuler™ Prestained Protein Ladder* (Thermo Fisher Scientific)

3.4.2 Effect of capsaicin on primary HNE cells

After successful detection of TRPV1 and α-ENaC in primary HNE cells, the effect of capsaicin on these cells was tested. First, an MTT assay was carried out in order to test the effect of capsaicin on the viability of primary HNE cells. Up until a concentration of 100 µM the vanilloid only caused a slight decrease of cell viability to approximately 80% as shown in Figure 43. Starting at a concentration of 150 µM, viability of the cells decreased significantly with increasing capsaicin concentration until finally at a concentration of 500 µM the viability was decreased to the level of the positive control (~15%). As the vanilloid was solved in ethanol, the effect of the alcohol on the viability of the cells was tested as well. Both 0.01% as well as 0.5% ethanol corresponding to the amount of ethanol in the lowest (10 µM) and highest (500 µM) capsaicin concentration did not have a negative effect on cell viability. This confirms that the negative effect on the viability of cells is caused primarily by capsaicin.

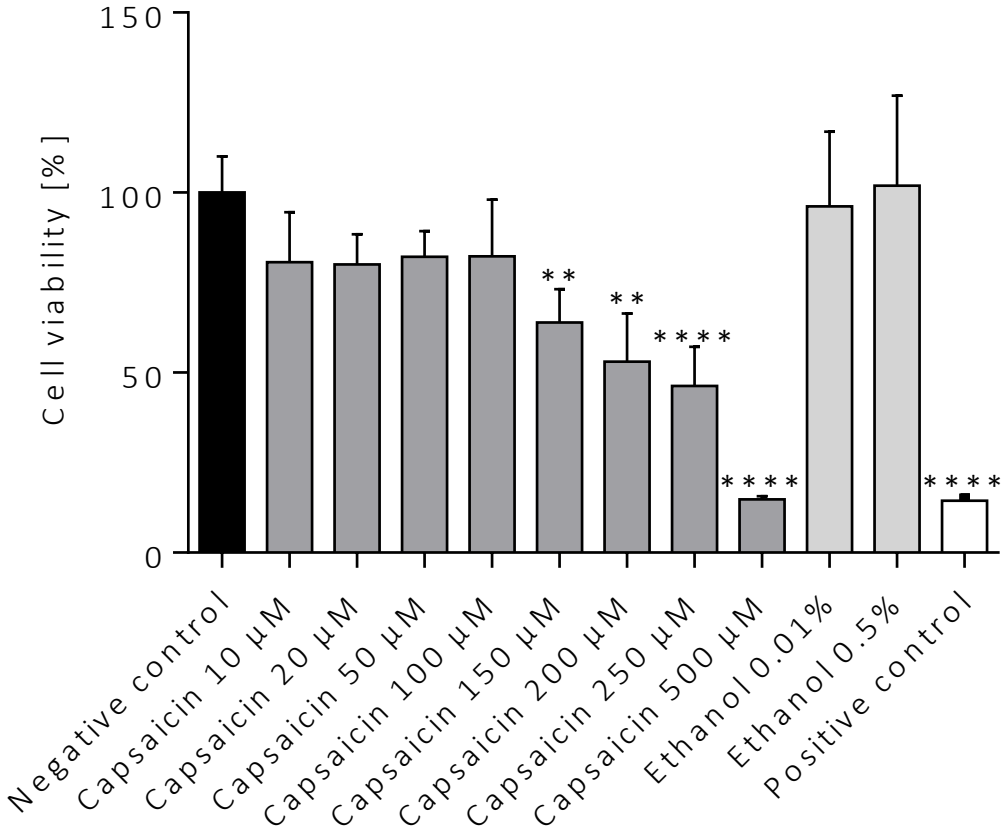

Figure 43: Effect of capsaicin and ethanol on the viability of cells. Primary HNE cells were incubated with capsaicin at different concentrations for 4 h before an MTT assay was conducted. Furthermore, cells were incubated with 0.01% and 0.5% ethanol corresponding to the amount of ethanol in the lowest and highest capsaicin concentration. Cell culture medium was used as negative control; Triton® X-100 was used as positive control ($p \leq 0.001$ (***), $p \leq 0.0001$ (****)).

After determination of the cytotoxic effects of capsaicin, primary HNE cells were incubated with 100 µM capsaicin for either 4 or 24 h. Subsequently, functional Ussing chamber measurements were conducted to evaluate the effect of the vanilloid on the amiloride-sensitive current. Figure 44 shows that after 4 h of incubation no effect was observed compared to non-treated control cells (62.8 ± 4.8% vs. 59.7 ± 10.5%). However, after 24 h of incubation a slight decrease of amiloride-sensitive current could be detected indicating successful inhibition of ENaC by capsaicin (42.8 ± 9.8%).

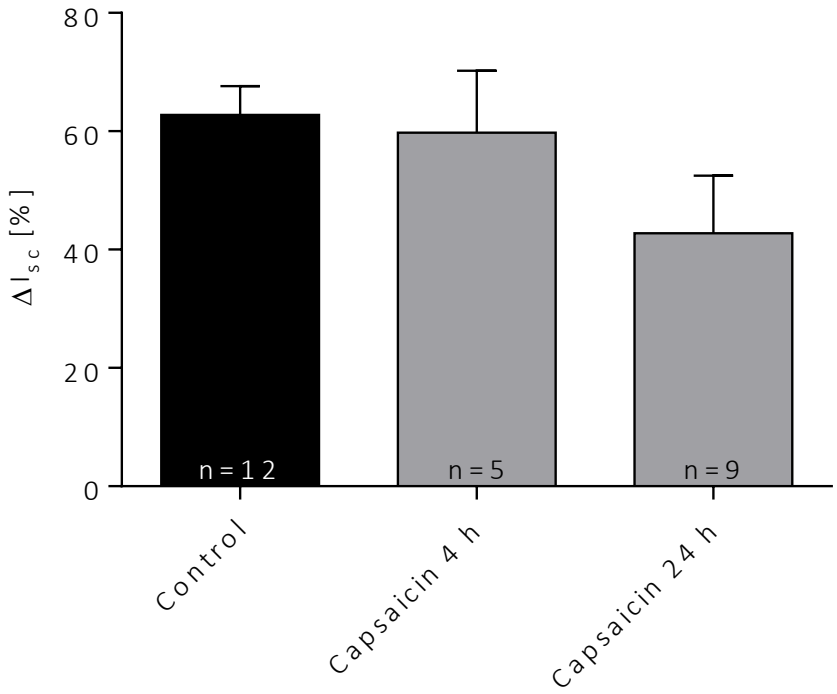

Figure 44: Statistical evaluation of amiloride-sensitive short-circuit current (I_{sc}) in primary HNE cells after incubation with capsaicin. Cells were incubated with 100 µM capsaicin for either 4 h or 24 h. Control cells were not incubated. Measurements were conducted immediately after incubation. The amiloride-sensitive current was not affected after 4 h of incubation with capsaicin. However, after 24 h of incubation a slight decrease of amiloride-sensitive current could be detected indicating successful inhibition of ENaC by capsaicin.

3.4.3 Characterization of chitosan-lecithin oil-core nanocapsules

Blank nanocapsules as well as nanocapsules loaded with capsaicin both naked and coated with wtCFTR-mRNA at N/P charge ratio 75 were characterized regarding their physicochemical properties. As described before size and PDI were determined by DLS-NIBS while zeta potential was determined by the capsules' electrophoretic mobility. Physicochemical properties of the capsules are presented in Figure 45. Z-average hydrodynamic diameter of blank nanocapsules was around 150 nm and increased significantly to 200 nm when loaded with capsaicin while the PDI of blank nanocapsules was significantly higher than PDI of capsules loaded with capsaicin (0.18 ± 0.03 vs. 0.11 ± 0.02). However, the low PDI values of both capsules hint at very monodisperse samples, which is also shown in the size distribution by intensity and the correlograms of the capsules (Figure 46). The intensity plot shows only one monomodal population of capsules and the correlograms display a steep and smooth decay. The difference in size of the capsules is also visible in the two graphs as the peaks for capsaicin loaded capsules shift slightly to the right and the correlograms of capsaicin loaded capsules start to decay slightly later than the correlograms of blank nanocapsules. Measurements of zeta potential show a non-significant increase after loading capsaicin to the capsules (+58.3 ± 4.6 mV vs. +61.3 ± 3.1 mV; Figure 45c).

Coating of the capsules with wtCFTR-mRNA did not have a recognizable effect on the physicochemical properties of the capsules. All of the capsules' characteristics are summarized in Table 50.

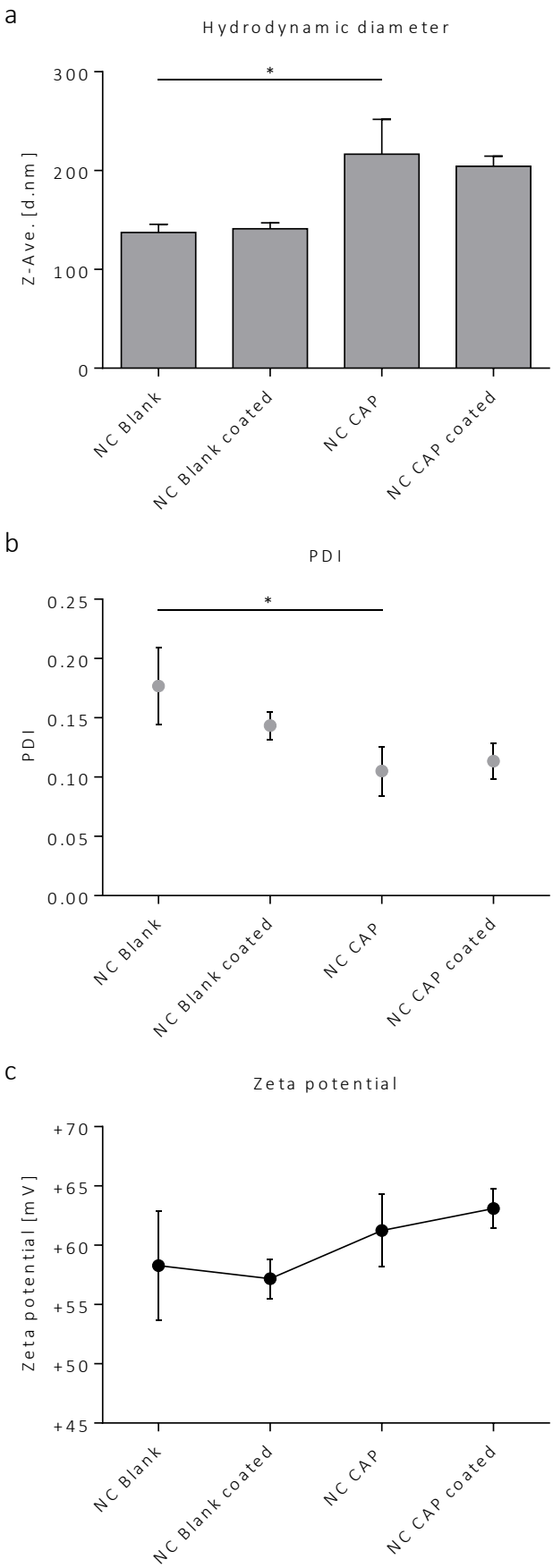

Figure 45: Physicochemical properties of CS nanocapsules. Shown is **(a)** the Z-average hydrodynamic diameter, **(b)** polydispersity index (PDI) and **(c)** zeta potential of blank (NC Blank) and capsaicin loaded (NC CAP) nanocapsules either naked or coated with wtCFTR-mRNA at N/P charge ratio 75 ($p \leq 0.05$ (*); n=3).

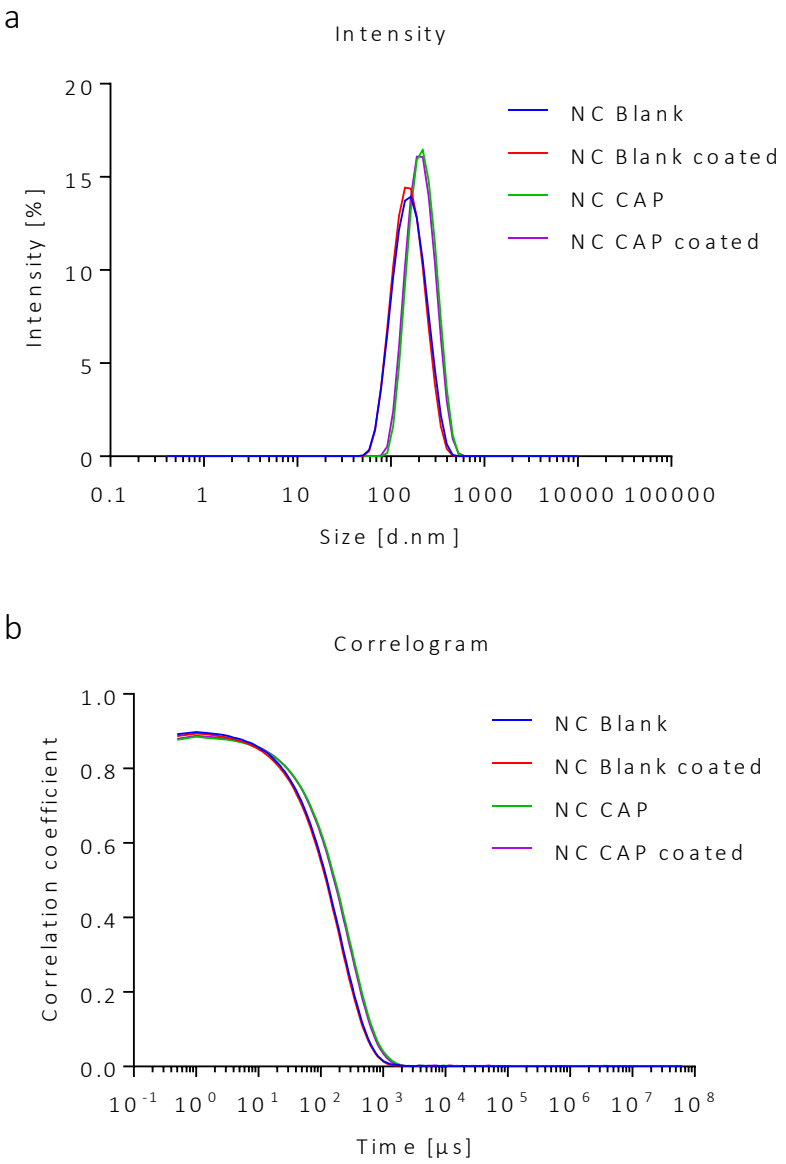

Figure 46: Size distribution by intensity and correlogram of CS nanocapsules. Shown is **(a)** the relative intensity of scattered light and **(b)** the correlogram of blank (NC Blank) and capsaicin loaded (NC CAP) nanocapsules either naked or coated with wtCFTR-mRNA at N/P charge ratio 75 (n=3).

Table 50: Physicochemical properties of CS nanocapsules and CS nanocapsules coated with wtCFTR-mRNA at N/P charge ratio 75. (NC Blank) Blank nanocapsules; **(NC CAP)** nanocapsules loaded with capsaicin (n=3).

	NC Blank	*NC Blank coated*	*NC CAP*	*NC CAP coated*
Hydrodynamic diameter [d.nm]	137.5 ± 8.2	141.2 ± 5.9	216.6 ± 35.3	204.3 ± 10.2
PDI	0.18 ± 0.03	0.14 ± 0.01	0.11 ± 0.02	0.11 ± 0.02
Zeta potential [mV]	+58.3 ± 4.6	+57.2 ± 1.7	+61.3 ± 3.1	+63.1 ± 1.6

Blank and capsaicin loaded particles were also successfully characterised by AF4 shown by an increasing hydrodynamic radius (R_h) with increasing elution time in the elugrams shown in Figure 47. Capsaicin loaded capsules eluted slightly later than did blank capsules, consistent with a greater size of the loaded capsules as evidenced by DLS-NIBS measurements. The shift in elution is also observed in the comparison of the R_g/R_h ratios depicted in Figure 48. Even though the ratios of both capsules seem to be comparable capsaicin loaded capsules eluted later than blank capsules. The size distribution parameters measured by AF4 are reported in Table 51. As seen in Figure 48 the the R_g/R_h ratios of both capsules are similar indicating identical shapes of both blank and loaded capsules.

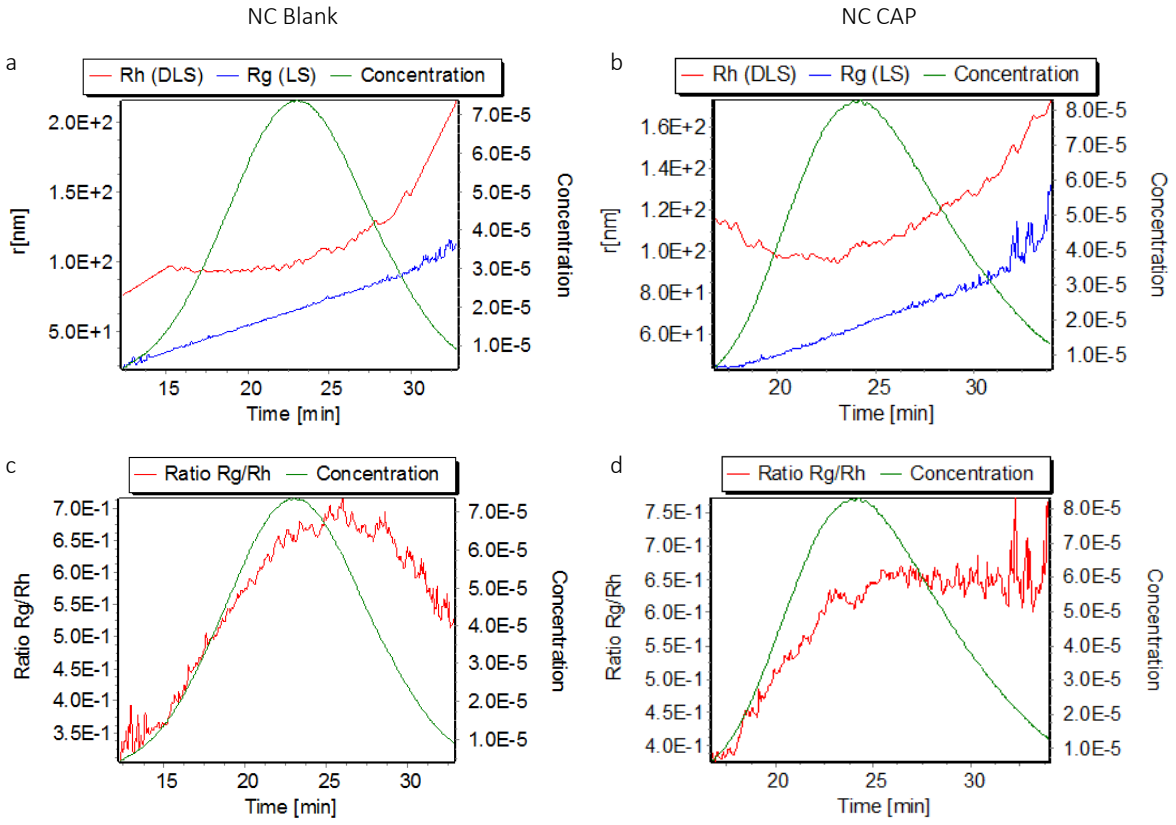

Figure 47: Asymmetric flow field-flow fractionation of blank and capsaicin loaded CS nanocapsules. (a,b) Hydrodynamic radii (R_h) determined by DLS-NIBS (red line), gyration radii (R_g) determined by MALS (blue line) and concentration (green line) over elution time. **(c,d)** R_g/R_h ratio (red line) and concentration (green line) over elution time.

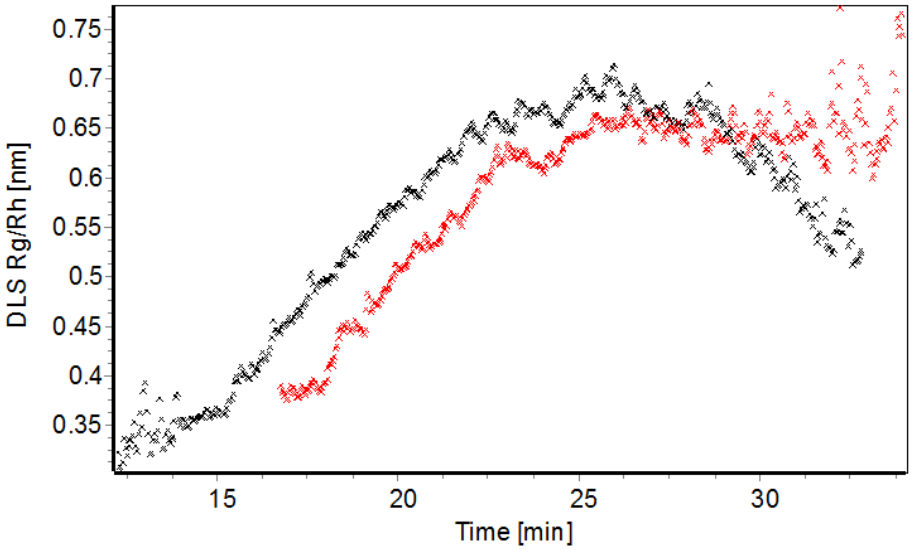

Figure 48: R_g/R_h ratio of CS nanocapsules determined by asymmetric flow field-flow fractionation. Shown is the R_g/R_h ratio of blank (black) and capsaicin loaded (red) nanocapsules over elution time.

Table 51: Size distribution of CS nanocapsules determined by asymmetric flow field-flow fractionation. Average gyration radii (R_g) determined by MALS, hydrodynamic radii (R_h) determined by DLS-NIBS and R_g/R_h ratio of blank (NC Blank) and capsaicin loaded (NC CAP) nanocapsules (n=3).

	R_g [nm]	R_h [nm]	R_g/R_h
NC Blank	72.70 ± 1.34	103.33 ± 3.12	0.70 ± 0.01
NC CAP	71.03 ± 0.05	102.50 ± 6.38	0.69 ± 0.05

TEM images of the capsules were taken in order to visualize and further analyze the nanosystems. Figure 49 shows representative images of both blank and capsaicin loaded nanocapsules. As reported before by DLS-NIBS and AF4, capsaicin loaded capsules are larger than blank capsules. According to the images taken, blank capsules have diameter of around 100 to 150 nm, whereas capsules loaded with the vanilloid appear to have a diameter of around 200 to 250 nm. Furthermore, TEM images show that the shape of the capsules is not completely spherical nor homogeneous, but some of the imaged particles appear as slightly elliptical objects.

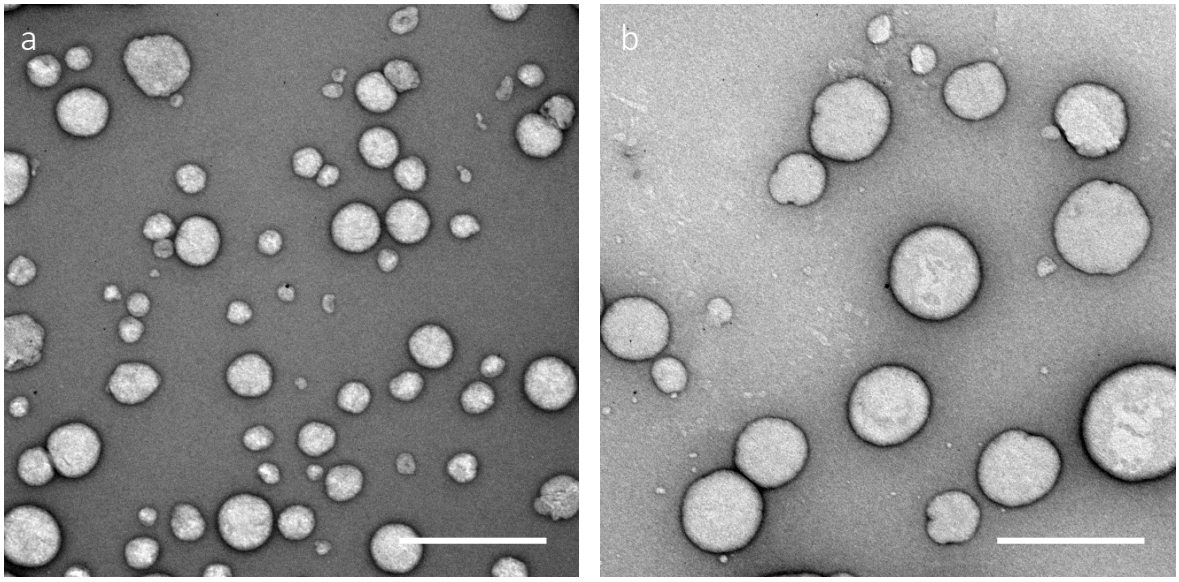

Figure 49: Representative transmission electron microscopy images of CS nanocapsules. (a) Blank nanocapsules; **(b)** capsaicin loaded nanocapsules (uranyl acetate staining; scale bar = 500 nm).

In a further step capaicin loaded nanocapsules were coated with wtCFTR-mRNA at a broad range of N/P charge ratios (5, 10, 50, 75, 100) in order to analyze the effect of different amounts of nucleic acids adsorbing to the surface of the capsules. Again capsules were investigated regarding their physicochemical properties. Results are displayed in Figure 50. Adsorbtion of different amounts of nucleic acids to the surface of the capsules did not have any effect on their size and PDI. The Z-average hydrodynamic diameter of the capsules remained unchanged around 200 nm and a PDI of 0.1 was measured for all N/P charge ratios. Size distribution by intensity and correlograms displayed in Figure 51 exibit the same results. No change in the graphs is visible for any of the N/P charge ratios.

By contrast, a change in zeta potential was observed (Figure 50c). Zeta potential of the coated capsules increased with increasing N/P charge ratio from approximately +59 to +63 mV indicating that the adsorption of the nucleic acid to the surface of the capsules results in the modification of the electrophoretic mobility.

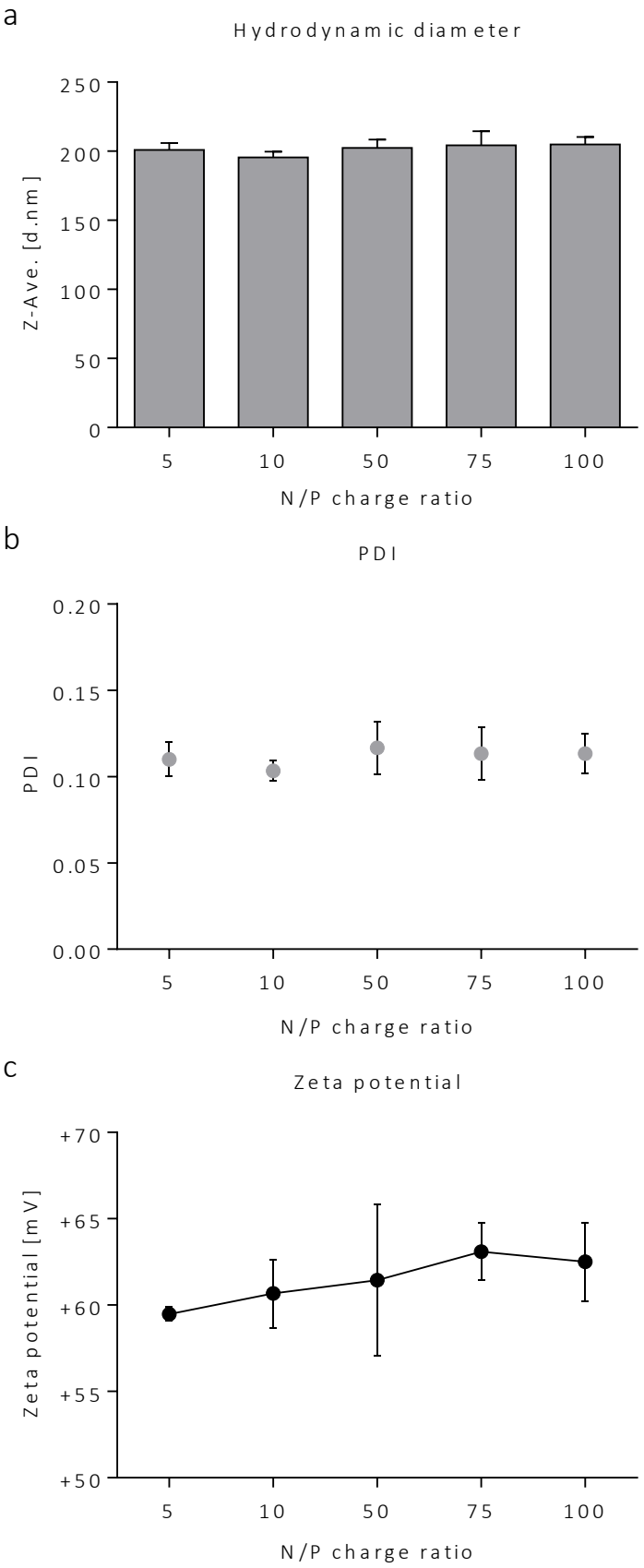

Figure 50: Physicochemical properties of CS nanocapsules coated with mRNA at varying N/P charge ratios. Shown is **(a)** the Z-average hydrodynamic diameter, **(b)** polydispersity index (PDI) and **(c)** zeta potential of capsaicin loaded nanocapsules coated with wtCFTR-mRNA (n=3).

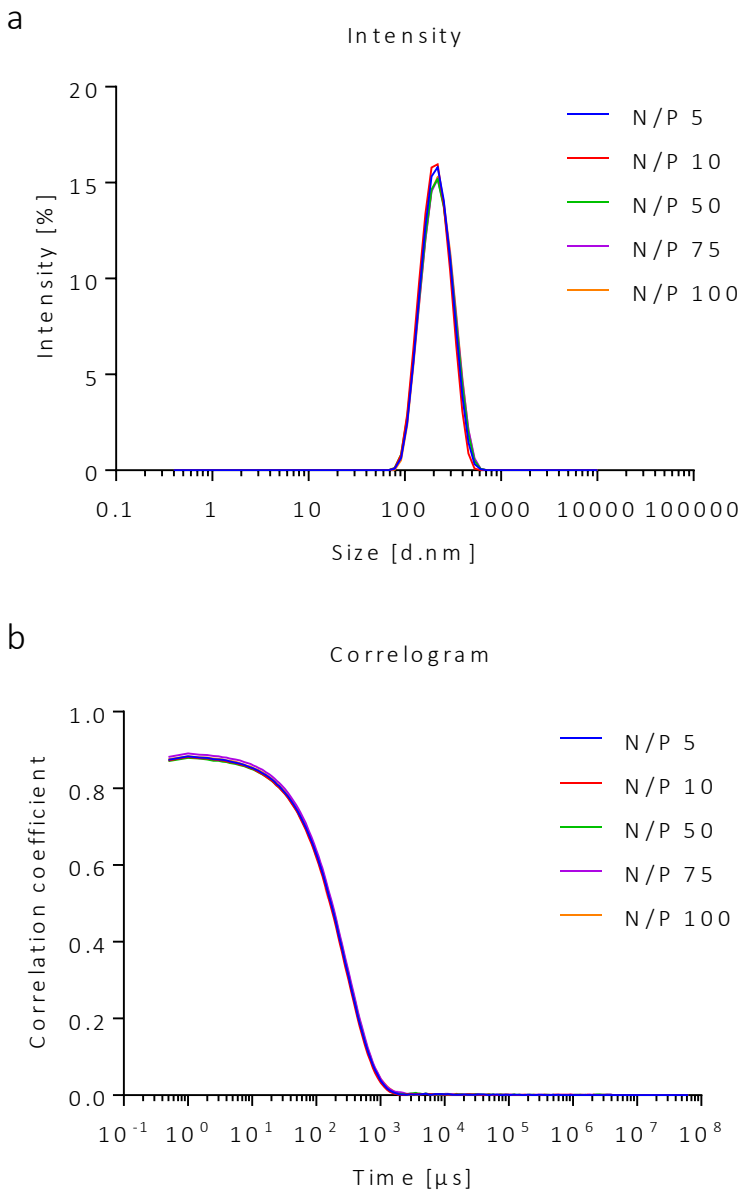

Figure 51: Size distribution by intensity and correlogram of CS nanocapsules coated with mRNA at varying N/P charge ratios. Shown is **(a)** the relative intensity of scattered light and **(b)** the correlogram of capsaicin loaded nanocapsules coated with wtCFTR-mRNA (n=3).

In order to investigate whether the wtCFTR-mRNA actualy adorbed to the surface of the capsules a gel retardation assay was carried out (Figure 52). Negatively charged wtCFTR-mRNA ran through the gel and showed a specific band aroud 5,000 bases corresponding to its size of 4,443 bases. Due to their positive charge both blank and capsaicin loaded nanocapsules were retained in the pockets of the gel. Capsules coated with wtCFTR-mRNA did not show a specific band either suggesting successful adsorbtion and strong binding efficiency of the nucleic acid to the chitosan-covered capsules.

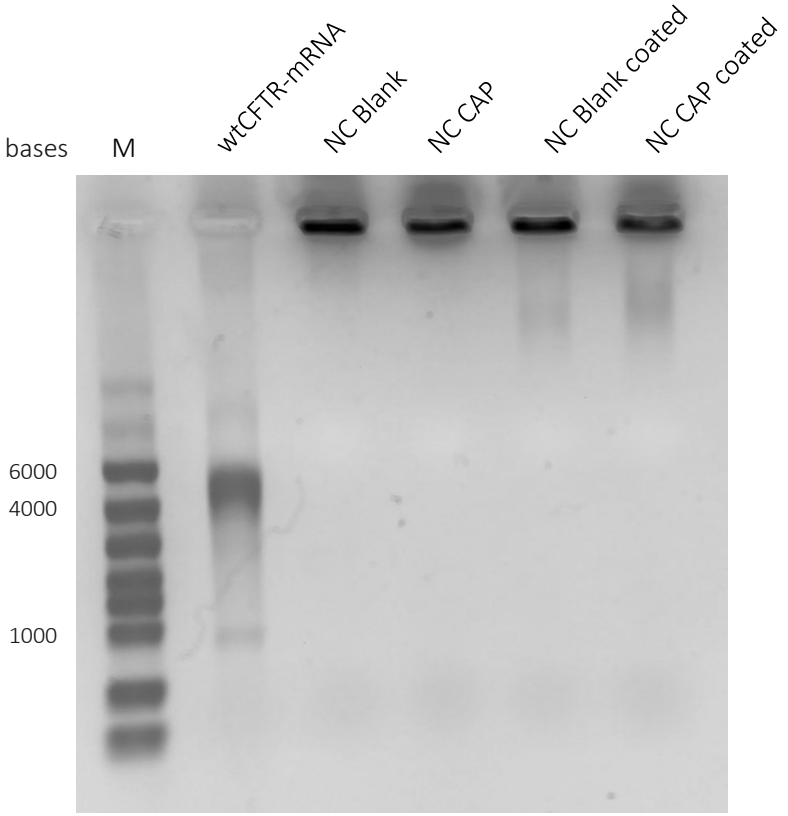

Figure 52: Gel retardation assay of CS nanocapsules coated with mRNA. Shown is the result of a 1% agarose-formaldehyde gel electrophoresis of blank (NC Blank) and capsaicin loaded (NC CAP) nanocapsules either naked or coated with wtCFTR-mRNA at N/P charge ratio 75. Naked wtCFTR-mRNA showed a band at 5,000 bases. Nanocapsules, both naked and coated, were retained in the pocket. Marker (M): *RiboRuler™ High Range RNA Ladder* (Thermo Fisher Scientific).

3.4.4 Stability of chitosan-lecithin oil-core nanocapsules

Before cell culture experiments with the nanocapsules were conducted, their stability in transfection medium was examined. For this both naked capsules and capsules coated with wtCFTR-mRNA at N/P charge ratio 75 were incubated in *Opti-MEM™* supplemented with HEPES and mannitol at 37°C for 24 h. After 0, 4 and 24 h, the size of the capsule was determined by DLS-NIBS. Both naked and coated capsules remained stable over time as shown in Figure 53. The Z-average hydrodynamic diameter of the capsules remained around 210 nm throughout 24 h. Size distribution by intensity and correlograms of capsules in transfection medium support the results, as both graphs did not show any change during measurements (Figure 54).

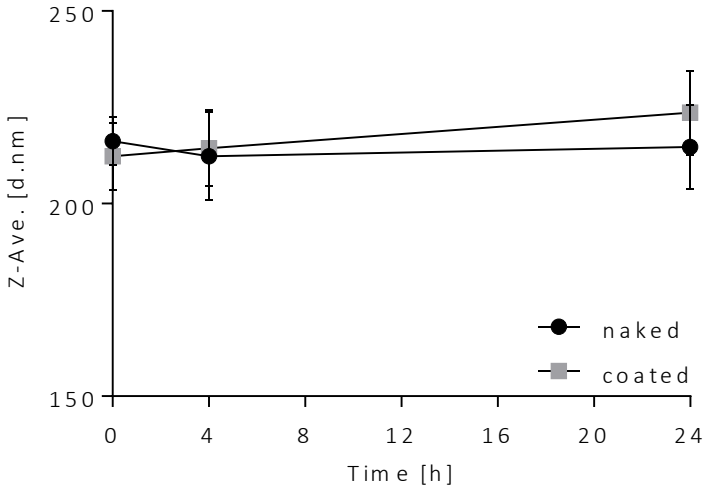

Figure 53: Stability of CS nanocapsules in transfection medium. Shown is the stability of capsaicin loaded nanocapsules either naked or coated with wtCFTR-mRNA at N/P charge ratio 75. Capsules were incubated in *Opti-MEM™* supplemented with HEPES (20 mM) and mannitol (270 mM) at 37°C. Both naked and coated nanocapsules remained stable over time (n=3).

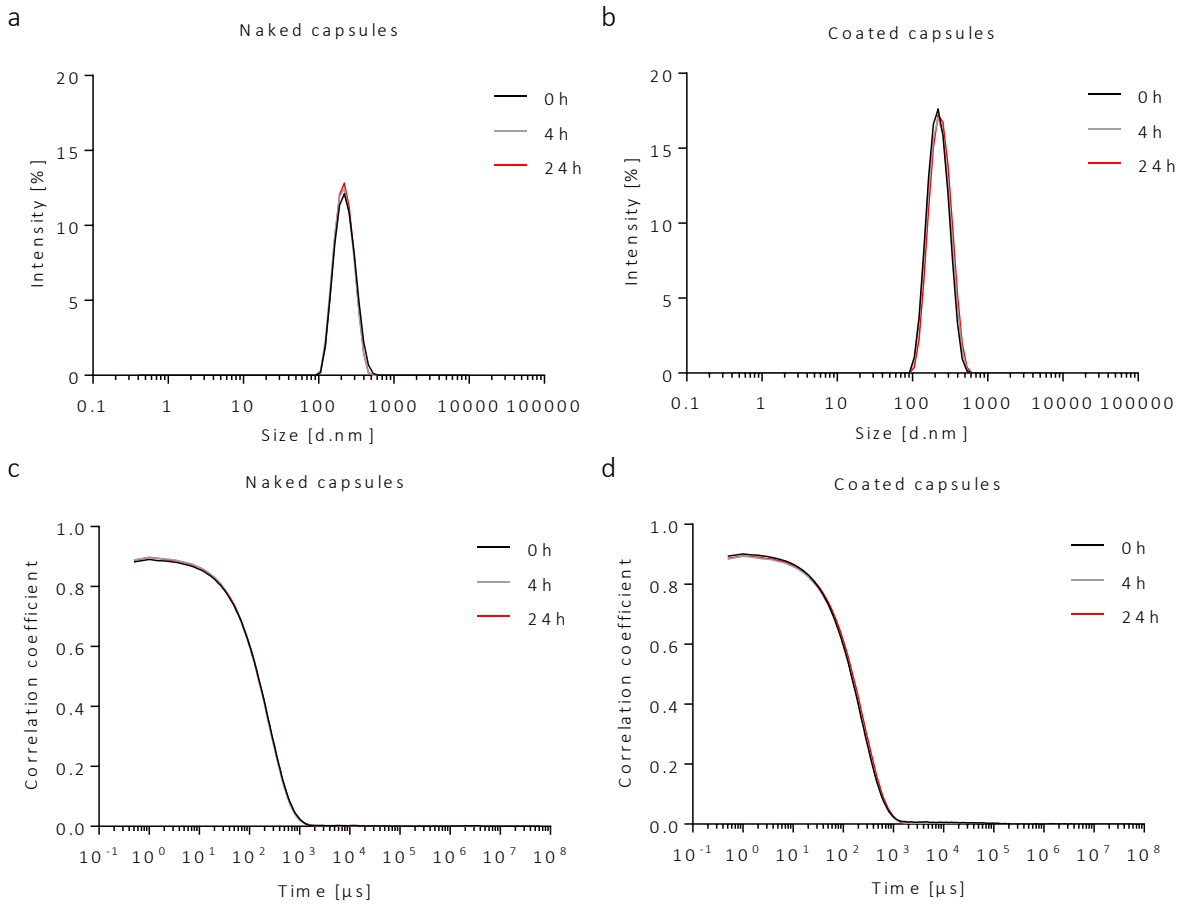

Figure 54: Size distribution by intensity and correlograms of CS nanocapsules in transfection medium. Shown is the stability of capsaicin loaded nanocapsules either **(a,c)** naked or **(b,d)** coated with wtCFTR-mRNA at N/P charge ratio 75 as relative intensity of scattered light and correlogram. Nanocapsules were incubated in *Opti-MEM™* supplemented with HEPES (20 mM) and mannitol (270 mM) at 37°C. Both naked and coated nanocapsules remained stable over time (n=3).

3.4.5 Cell culture experiments with chitosan-lecithin oil-core nanocapsules

The viability of primary HNE cells incubated with nanocapsules under varying conditions was evaluated by an MTT assay. First, cells were incubated with capsaicin loaded capsules at different concentrations of the vanilloid in *Opti-MEM™* or *Opti-MEM™* supplemented with HEPES and mannitol (Figure 55a). While *Opti-MEM™* alone did not have an effect on the viability of cells (107.6 ± 9.0%) *Opti-MEM™* with supplements decreased the viability to 65.7 ± 5.9%. This supports the theory that the high osmolality of the supplemented medium affects the negatively the cell viability (Table 49). Capsaicin up to 100 µM did not affect the viability of the cells in *Opti-MEM™* while it decreased it to 73.4 ± 13.0% at a concentration of 250 µM. At a concentration of 500 µM of capsaicin the cell viability was significantly decreased to the level of the positive control. In *Opti-MEM™* supplemented with HEPES and mannitol, the significant decrease to the level of the positive control already occurred at 250 µM capsaicin.

Since *Opti-MEM™* supplemented with HEPES and mannitol highly affected the viability of cells a second MTT assay was carried out incubating primary HNE cells with blank and capsaicin loaded capsules at different concentrations in *Opti-MEM™* alone (Figure 55b). Blank nanocapsules at low concentrations from 0.5% to 2.5% significantly decreased cell viability while a high concentration of the blank capsules (5%) only decreased the viability non-significantly to 77.3 ± 14.2%. Capsaicin loaded complexes on the other hand showed no cytotoxic effect at the same volumes until a capsaicin concentration of 100 µM. Capsaicin concentrations of 250 µM and higher significantly decreased cell viability to levels of the positive control.

The outcome of the MTT assays suggested that the gene transfection experiments to be done with capsaicin loaded capsules at concentrations of 50 or 100 µM of the vanilloid.

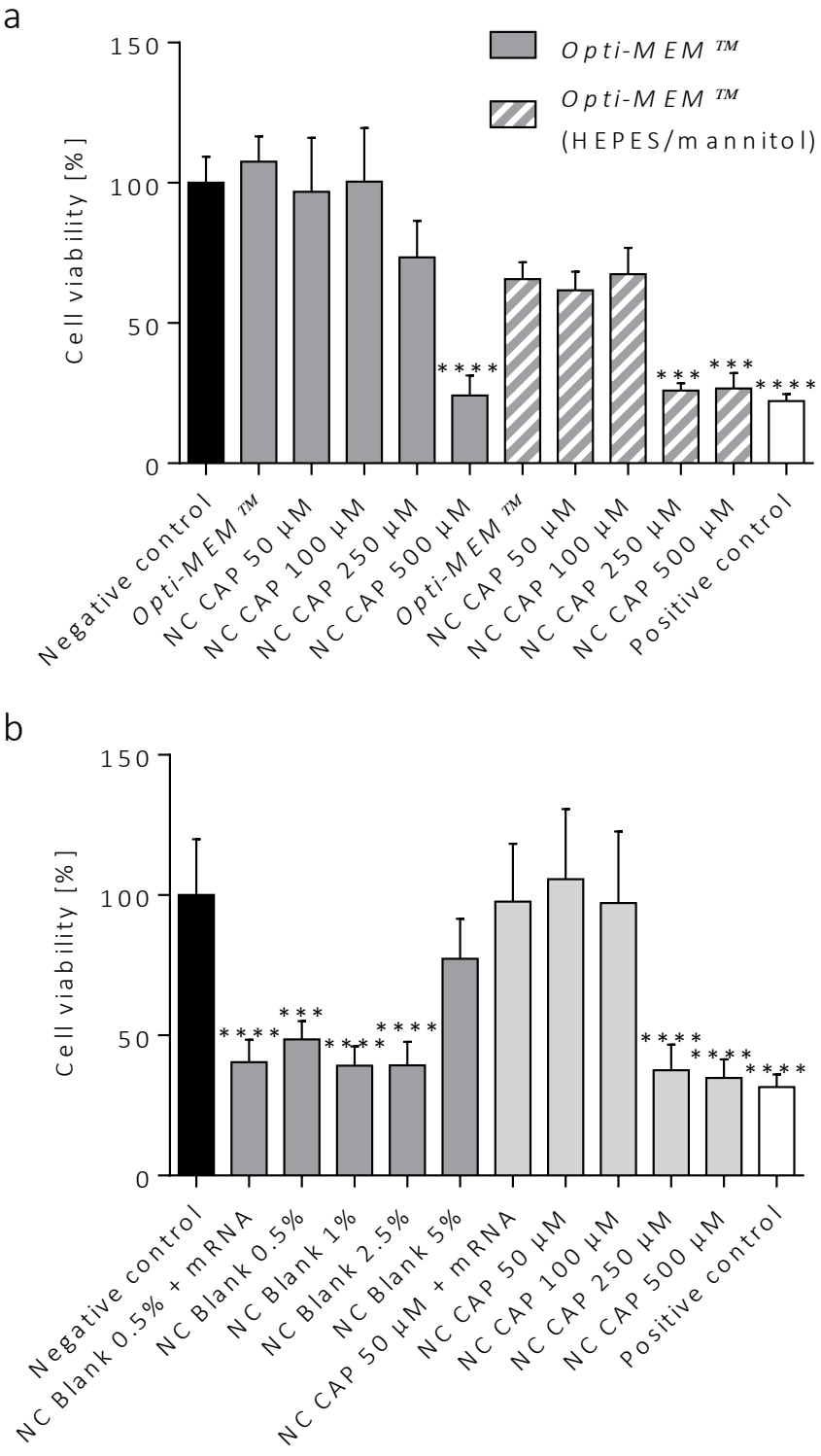

Figure 55: Effect of chitosan nanocapsules and transfection media on the viability of primary HNE cells. Cells were incubated with **(a)** nanocapsules loaded with capsaicin at different concentrations in *Opti-MEM™* or *Opti-MEM™* supplemented with HEPES (20 mM) and mannitol (270 mM) and with **(b)** blank nanocapsules and nanocapsules loaded with capsaicin at varying concentrations in *Opti-MEM™* for 24 h before an MTT assay was conducted. Cell culture medium was used as negative control; Triton® X-100 was used as positive control ($p \leq 0.001$ (***), $p \leq 0.0001$ (****); n=3).

In order to determine the transfection efficiency of blank and capsaicin loaded nanocapsules a luciferase assay was conducted as a model gene to provide a first indication of the validity of the pursued approach. As previous experiments showed that covering the capsules with any amount of nucleic acid did not have an effect on the physicochemical properties of the nanosystems, the capsules were coated with the plasmid pGL4.50 containing the luciferase reporter gene *luc2*. Transfection experiments were carried out with either *Opti-MEM™* or *Opti-MEM™* supplemented with HEPES and mannitol. Results of the luciferase assay are presented in Figure 56. As positive control, primary HNE cells were transfected with the plasmid using the commercially available transfection reagent *FuGENE*. The positive control showed a significant increase in transfection efficiency compared to non-transfected cells (125,042 ± 82,345 RLU vs. 259 ± 15 RLU). Transfection of the cells with *FuGENE* in *Opti-MEM™* supplemented with HEPES and mannitol only led to a lower transfection efficiency (14,775 ± 18,872 RLU) supporting the theory of the supplemented transfection reagent negatively affecting cells. However, transfection of the cells using the nanocapsules was not successful. The only slight elevation of RLU was detected in cells transfected with capsaicin loaded nanocapsules at a concentration of 50 µM capsaicin in *Opti-MEM™* supplemented with HEPES and mannitol (443 ± 152 RLU) supporting the results of the MTT assays, which showed that transfection experiments should be conducted with capsaicin loaded capsules at capsaicin concentrations of 50 µM or 100 µM.

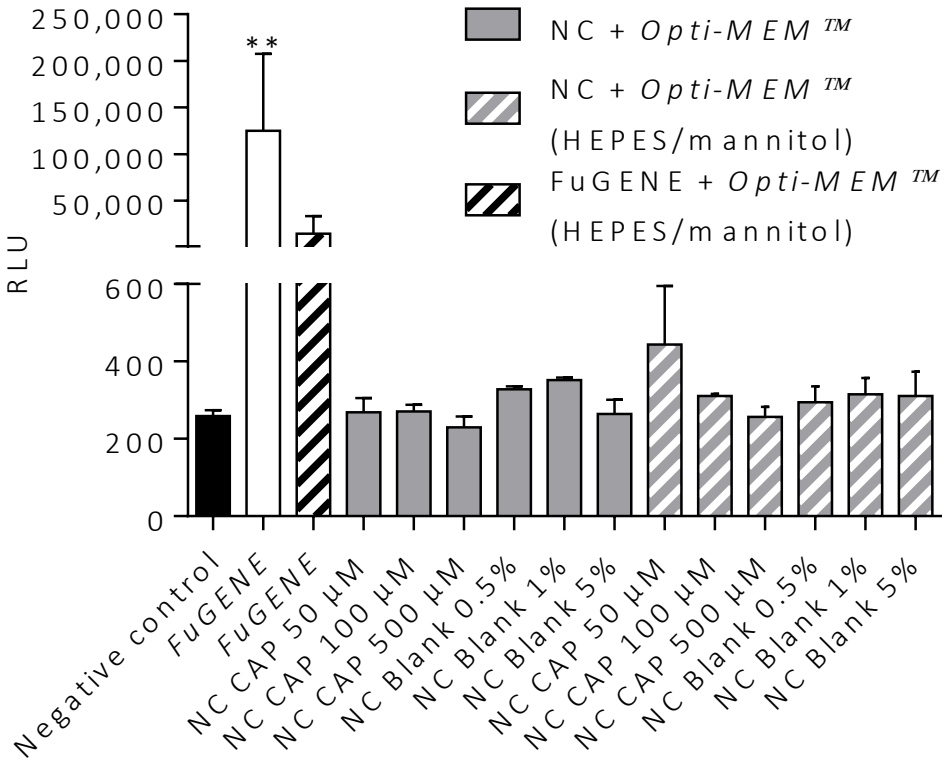

Figure 56: Transfection efficiency of CS nanocapsules in primary HNE cells. Cells were transfected with the plasmid pGL4.50 containing the luciferase reporter gene *luc2* using *FuGENE* and blank as well as capsaicin loaded nanocapsules at varying concentrations in *Opti-MEM™* or *Opti-MEM™* supplemented with HEPES (20 mM) and mannitol (270 mM). 24 h after transfection, a luciferase assay was conducted. Non-transfected cells served as negative control ($p \leq 0.01$ (**); n=3).

4 DISCUSSION

Nanobiotechnology, especially nanoscale drug delivery systems, underwent tremendous developments in recent years (Patra et al., 2018). Nanosystems in general exhibit a broad range of application and promising treatment of various medical conditions targeting amongst others the skin, central nervous system, cardiovascular apparatus, immune system, liver or diabetes (Alvarez-Figueroa et al., 2019; Biscaglia et al., 2019; Ferreira et al., 2017; Ganugula et al., 2017; Lozić et al., 2016; Marcianes et al., 2017; Xu et al., 2019; Zolnik et al., 2010). In recent years CF has also been the target of nano-based drug delivery systems strengthening the relevance of the research discussed in this Thesis (Haque et al., 2018; Kolte et al., 2017; Robinson et al., 2018).

Being a monogenic hereditary disease CF is a promising target for gene therapy treating the disease on a cellular level. Already four years after the discovery of the gene in 1989 (Riordan et al., 1989) the first patients were treated with an adenoviral vector carrying a CFTR expression cassette (Zabner et al., 1993). One or three days after application of the vector to nasal turbinates, a restored nasal potential difference response to a cAMP agonist was reported. However, neither CFTR-mRNA nor protein could be detected. Since then many efforts have been made to develop a suitable gene therapy to treat CF leading to over 25 clinical trials (Cooney et al., 2018; Donnelley and Parsons, 2018; Griesenbach et al., 2015). However, until today no clinical benefit could be achieved. One of the obstacles of gene therapy is the delivery of DNA to the nucleus as it brings amongst others the risk of insertional mutagenesis (Davé et al., 2004). Furthermore, the often used viral vectors raise many safety concerns such as high immunogenicity and potential reversion of the virus to pathogenicity (Lundstrom and Boulikas, 2003). To circumvent these problems it is crucial to find a suitable non-viral vector to deliver genes to their target successfully. An alternative for viral gene delivery is represented by cationic lipids (Martin et al., 2005). Features such as non-immunogenicity and non-oncogenicity as well as the fact that they are easy to produce on a large scale with acceptable costs make them very attractive for the field of gene therapy (Lv et al., 2006). However, DNA/lipid complexes or liposomes often display reduced transfection efficiency *in vivo* and increased cellular toxicity (Li et al., 1998). A solution to the stated problems might be the natural polysaccharide chitosan. Its positive characteristics such as low cytotoxicity and biodegradability make it a promising

vector for gene delivery purposes as shown by the latest research (Santos-Carballal et al., 2018).

In the present study several chitosan-based nanosystems targeting CF were harnessed. Since the physical and chemicals properties as well as the biological performance, hence transfection efficiency, of chitosan are strongly dependent on its DA or Mw it is essential to characterize the polysaccharide in order to design the most optimal formulation for a specific purpose (Mao et al., 2010). Santos-Carballal *et al.* performed a screening of various chitosans in order to find the most suitable polymer to deliver miRNA to a breast cancer cell line (Santos-Carballal et al., 2015). Following this study Fernández Fernández *et al.* successfully transfected CFBE41o- cells with plasmid DNA and siRNA using one of the chitosans from that screening (Fernández Fernández et al., 2016b). Furthermore, it was reported that this chitosan polymer is able to bind to mucin and reduce the viscosity of the mucus (Menchicchi et al., 2015, 2014), which could be very advantageous in the CF lung. Consideration of these preceding studies led to the choice of chitosan used in this study with a DA of 17% and a Mw of 29.3 kDa.

As the underlying problem of CF is an impaired chloride secretion through defect CFTR and associated sodium hyperabsorption via ENaC this Thesis aimed at establishing a double tracked strategy targeting both proteins to correct abnormal ion transports. For this chitosan nanoparticles complexing wtCFTR-mRNA and α-ENaC ASO were designed and characterized for their physicochemical properties. The complexes were then tested for their ability to successfully transfect human respiratory epithelial cells and evoke CFTR function and reduced ENaC activity. Furthermore, the pungent vanilloid capsaicin was tested for its ability to reduce ENaC activity as a novel approach to treat sodium hyperabsorption with a natural compound. Subsequently, chitosan-lecithin oil-core nanocapsules encapsulating capsaicin were prepared and physicochemically characterized and the influence of the nanocapsules on primary human nasal epithelial cells was tested. The results obtained from the characterization of the various nanosystems as well as from subsequent *in vitro* an *ex vivo* cell studies are being discussed in detail below.

4.1 Chitosan-mRNA complexes

4.1.1 wtCFTR-mRNA transfection leads to increased CFTR activity in human respiratory epithelial cells

The concept of *transcript therapy* using mRNA to correct gene expression in cells has been gaining ground in recent years (Bangel-Ruland et al., 2013; Sahin et al., 2014). This model of treatment is very promising for a potential CF therapy. In fact, an ongoing clinical trial is currently testing the inhalation of lipid nanoparticles carrying wtCFTR-mRNA (Kowalski et al., 2019). Some advantages of mRNA over DNA are decreased immunogenicity, higher translation efficacy and safety as mRNA is not incorporated into the genome (Kuhn et al., 2012). Therefore, we used wtCFTR-mRNA to transfect CF airway epithelial cells in order to correct CFTR function and hence abnormal chloride secretion (Kolonko et al., 2016). In this study CFBE41o- as well as primary HNE cells were transfected with wtCFTR-mRNA using chitosan and the commercially available transfection reagent *Lipofectamine*. Functional Ussing chamber measurements were conducted 24 h after transfection and revealed increased cAMP-dependent short-circuit current in both cell models indicating successful transfection and hence increased CFTR function (Figure 18a and Figure 21a). Highest increase in short-circuit current could be detected in cells transfected using chitosan and incubation with the complexes for 24 h. In CFBE41o- cells this increase was highly significant. Even after 4 h of incubation with the chitosan complexes cAMP-dependent short-circuit current was higher than in cells transfected with *Lipofectamine*. The difference in transfection efficiency might be explained by the cytotoxic effect of the commercially available transfection reagent, which was revealed by an MTT assay (Figure 19) and shown before in other studies (Chernousova and Epple, 2017; Wang et al., 2018). Chitosan on the other hand is known to be non-toxic and shows penetration-enhancing effects on cells increasing its transfection efficiency (Florea et al., 2006; Lim et al., 2001). Fernández Fernández *et al.* reported a transfection efficiency of > 50% using chitosan in CFBE41o- cells (Fernández Fernández et al., 2016b). It has been shown that the airway epithelium requires approximately 6-10% epithelial cells with functional CFTR for a correct chloride secretion (Johnson et al., 1992) and about 25% so as to guarantee mucociliary clearance (Zhang et al., 2009). Ramalho *et al.* reported that approximately 5% of the

normal level of wtCFTR-mRNA is sufficient to avoid the severe complications of CF (Ramalho et al., 2002). Therefore, it can be assumed that in this study enough cells were transfected and hence express functional CFTR for a sufficient chloride secretion.

Recently, two other studies used nanomedicine in order to transfect chemically modified CFTR-mRNA *in vivo*. Haque *et al.* used chitosan-coated poly-(lactic-*co*-glycolic acid) nanoparticles assembled with CFTR-mRNA. They observed significant improvement of lung function after intratracheal spraying and intravenous injection in *CFTR*$^{-/-}$ (CFTR^{tm1Unc}) mice (Haque et al., 2018). Robinson *et al.* formulated lipid-based nanoparticles for nasal application in the same mouse line. They were able to restore CFTR-mediated chloride secretion in CFTR knockout mice for at least 14 days and recovered up to 55% of the net chloride efflux (Robinson et al., 2018). These studies demonstrate the relevance of nanotechnology for mRNA *transcript therapy* in CF. Moreover, they support the outcome of the Ussing chamber experiments in this Thesis also showing increased CFTR function after CFTR-mRNA transfection. However, the pertinence of these studies should be considered with care as the murine model of CF often fails to reflect human pulmonary pathology (Cohen and Prince, 2012; Semaniakou et al., 2018).

In CF decreased chloride secretion due to defect CFTR is associated with sodium hyperabsorption through ENaC resulting in mucus dehydration and failure to clear mucus via the mucociliary escalator (Hobbs et al., 2013). Therefore, the amiloride-sensitive current of CFBE41o- and primary HNE cells transfected with wtCFTR-mRNA was also assessed in this Thesis. Amiloride is a specific blocker of ENaC making it a suitable substance to investigate sodium transport in human respiratory epithelial cells with Ussing chamber experiments (Blank et al., 1995). In both cell types amiloride-sensitive current was decreased after transfection with wtCFTR-mRNA using *Lipofectamine* as well as chitosan after incubation for 4 h. These results indicate decreased ENaC activity due to increased CFTR function. However, after 24 h of incubation with the chitosan-wtCFTR-mRNA complexes only a very slight decrease of amiloride-sensitive current was observed in CFBE41o- cells (Figure 18b). In primary HNE cells amiloride-sensitive current further decreased even though the high standard error leaves room for speculation (Figure 21b). Faulty wtCFTR-mRNA can be excluded as a reason for this phenomenon as the reactivity and size of the nucleic acid was tested regularly (Figure 16). Chitosan has been reported to

have various effects on proteins of the cell. For example Yang *et al.* revealed an upregulation of eight proteins associated with cell growth, differentiation, division and cycle regulation in liver cells after incubation with chitosan-sodium tripolyphosphate (TPP) particles (Yang et al., 2014). Furthermore, Smith *et al.* reported an effect of chitosan on the tight junctions by translocation of tight junction proteins from the membrane to the cytoskeleton (Smith et al., 2004). Therefore, an effect of chitosan on ENaC cannot be excluded as the unexpected amiloride-sensitive current only occurred in cells after 24 h of incubation with the polysaccharide. It would be interesting to further elucidate the impact of chitosan on proteins of respiratory epithelia.

The results obtained from transfection experiments with CFBE41o- cells should be regarded cautiously in respect to ENaC activity as these cells do not represent the typical CF disease pattern including sodium hyperabsorption. CFBE41o- cells lack significant functional ENaC expression and thus may not be a suitable model system for the study of CF airway pathophysiology (Myerburg et al., 2010). In fact, CFBE41o- cells exhibit reduced expression of α- and γ-ENaC (Rubenstein et al., 2011). Moreover, it was reported that CFBE41o- cells do not display amiloride-sensitive current even after treatment with dexamethasone suggesting that ENaC stays absent from the cell surface (Rubenstein et al., 2011). Also 16HBE14o- cells, which are often used to reflect the wt situation of the respiratory tract, display a lack of amiloride-sensitive current (Cozens et al., 1994). Similar to the results gained with CFBE41o- cells the outcomes of the experiments with primary HNE cells do not completely represent the CF *in vivo* situation as the cells were obtained from healthy volunteers. Primary HNE cells acquired from CF patients would give more physiological meaning to the transfection experiments. The lack of an appropriate cell culture system hinders satisfactory evaluation of the presented data. Therefore, it is possible that mRNA transfection alone as *transcript therapy* would be sufficient to restore both chloride secretion and sodium hyperabsorption simultaneously *in vivo*.

Nevertheless, since primary cell culture displays a high donor-to-donor variability (Cho et al., 2010) immortalized cell culture systems are very helpful to standardize transfection experiments. Hence, we built on the results obtained from the *in vitro* and *ex vivo* cell culture experiments performed in this study to carry on the project. Even though transfection with wtCFTR-mRNA led to a significantly increased cAMP-dependent short

circuit current indicating increased CFTR function, no definite evidence on the intrinsic downregulation of ENaC could be found. Therefore, we aimed at developing a second chitosan nanoparticle complexing ASO against the α-subunit of ENaC in order to decrease ENaC activity extrinsically *in vitro*.

4.2 Chitosan-ASO complexes

4.2.1 Salt benefits the formation of chitosan-ASO complexes

In order to optimize the function of nanocomplexes as a transfection reagent it is crucial to characterize them for their physicochemical properties and understand them on a molecular level. Chitosan-ASO complexes were formed at varying N/P charge ratios (30, 50, 70, 90, 100) in either water or in 85 mM NaCl according to the principle of electrostatic self-assembly by spontaneously mixing the components in aqueous solution. Electrostatic self-assembly is defined as assembly of molecules that are connected by non-covalent interactions and form via association of small building blocks (Gröhn, 2008; Willerich and Gröhn, 2011). Three different complexes were designed incorporating an ASO directed against the α-subunit of ENaC, respectively. Finally, physicochemical properties of the particles were determined by DLS-NIBS and zeta potential measurements.

The hydrodynamic diameter of the complexes varied between approximately 100 and 200 nm (Figure 22). No trend regarding the N/P charge ratio was observed. However, on average complexes formed in the presence of NaCl appeared to be of smaller size. Higher ionic strength has been shown to be beneficial for chitosan particle formation decreasing the particles' size with increasing NaCl concentrations (Jonassen et al., 2012; Sreekumar et al., 2018). NaCl screens out the charges of chitosan and thereby lowers repulsive electrostatic forces potentially reducing aggregation. Furthermore, it reduces stiffness of chitosan chains leading to the formation of more compact particles. This is reflected in the measurements of the complexes' PDI as complexes formed in the presence of NaCl displayed a lower PDI than complexes formed without salt (Figure 23). Similar results have been reported by Sawtarie *et al.* who observed narrower size distribution of chitosan-TPP particles with increasing NaCl concentration reinforcing the theory (Sawtarie et al., 2017).

Measurements of the complexes' electrophoretic mobility revealed increasing zeta potential from approximately +25 to +35 mV (Figure 26). The increase of zeta potential with increasing N/P charge ratio shows that complexes were successfully formed as the positive charge arises from the protonated amino groups that were not neutralized by the negatively charged phosphate groups of the ASO. With increasing N/P charge ratio the amount of chitosan is increased and therefore an increasing excess of positively charged amino groups leads to an increasing zeta potential as shown in previous studies (Fernández Fernández et al., 2016b; Mansouri et al., 2006; Puras et al., 2013; Santos-Carballal et al., 2015). Furthermore, it was observed that complexes prepared with NaCl had a slightly lower zeta potential. This can be explained by the salts' ability to screen charges and coincides with the findings of other studies (Huang and Lapitsky, 2011; Jonassen et al., 2012). All in all, the positive zeta potential of approximately +30 mV is an indication for a stable formulation of nanoparticles as a minimum of +30 mV is required to stabilize complexes solely by electrostatic repulsion (Singare et al., 2010). Yet another unexpected result was to observe differences in the zeta potential dependence on N/P ratio between chitosan-ASOgreen and chitosan-ASOgreen_sense complexes. This result hints to differences in the actual molecular architecture of the formed complexes. So far, chitosan-gene complexes are assumed to be formed by non-specific electrostatic self-assembly, however, it is possible that specific sequences of chitosan given by the pattern of acetylation display high specific binding affinity for given nucleotide sequences. This is still poorly understood and calls for new studies using both computational chemistry and experimental studies.

The protection of ASO and binding efficiency of ASO and chitosan was evaluated with a gel retardation assay. Results revealed that the nucleic acid was retained in the gel pocket by chitosan with advanced efficiency in higher N/P charge ratios (Figure 27). The findings of strong binding efficiency of nucleic acids and chitosan correspond to previous reports (Fernández Fernández et al., 2016b; Lee et al., 2001; Yhee et al., 2015). Deng *et al.* even demonstrated protection of plasmid DNA from DNases by complexation with chitosan and hyaluronic acid (Deng et al., 2018). Overall, chitosan proves to be a suitable carrier for nucleic acids in general.

Finally, complexes at N/P charge ratio 90 prepared in the presence of 85 mM NaCl were chosen for transfection experiments (Table 48). One barrier the complexes need to overcome in the lung are the respiratory secretions (Sanders et al., 2009). Atomic force microscopy revealed that the sputum of CF patients displays pores with sizes varying from 300 to 700 nm (Broughton-Head et al., 2007). Another study reported pore sizes of 100-400 nm discovered by TEM (Sanders et al., 2000). The same group also evaluated the transport of nanospheres and cationic lipoplexes through a 220 µm thick layer of CF sputum (Sanders et al., 2000). They report that particles with a size of 120 nm moved through the mucus only with a 1.3-fold retardation compared to an equally sized buffer layer. Particles with a diameter of 270 nm still moved with a 6.8-fold retardation while the mucus almost completely sterically blocked 560 nm particles. Therefore, with a diameter of 150 nm the complexes of the present study are likely to pass through the thick CF mucus. Furthermore, their size makes them promising for transfection purposes as complexes smaller than 500 nm are suitable for endocytotic uptake by the cell (Kou et al., 2013). The positive zeta potential of around +30 mV makes the complexes not only stable but also able to intertact with the negatively charged cell membrane further facilitating endocytosis (Huang et al., 2005). After endocytotic uptake of the complexes, they are believed to be released from the endosome due to the proton sponge effect hypothesis. In the acidified milieu of the endosome, the NH_2 groups at the D-glucosamine of chitosan promote influx of protons into the vesicle. The transport of counter ions into the endosome to balance the accumulated protons leads to swelling and finally bursting of the vesicle, thus releasing its content (Freeman et al., 2013; Richard et al., 2013). The nucleic acid is then likely released by enzymatic degradation of its carrier. In vertebrates chitosan is thought to be primarily degraded by lysozyme or bacterial enzymes in the colon (Kean and Thanou, 2010). Moreover, three enzymatically active forms of human chitinases, also known to cleave the chitin derivate, have been identified (Funkhouser and Aronson, 2007). One of them, namely the human mammalian chitinase AMCase, was recognized in the lung (Boot et al., 2001). These hypotheses demonstrate that a safe and successful transfection as well as degradation of chitosan complexes in human respiratory epithelia is possible.

4.2.2 Supplemented transfection medium stabilizes complexes but harms human respiratory epithelial cells

In order to guarantee appropriate biological performance and a successful transfection with the complexes it is crucial to evaluate their colloidal stability in transfection medium. In this study we used *Opti-MEM™* as it is commonly used for transfection purposes in various cell lines (Liang et al., 2015; Lisakowski et al., 2018; Pezzoli et al., 2017). Furthermore, we supplemented the medium with HEPES and mannitol based on a recommendation for transfection with the commercially available chitosan-based transfection reagent *Novafect* from *NovaMatrix®* (Sandvika, N). Interestingly, HEPES has been reported to be beneficial for transfection purposes before (Chen et al., 2019; Riedl et al., 2018). As expected complexes were relatively stable in *Opti-MEM™* with supplements in contrast to complexes in the pure medium even though the size of the complexes increased slightly (Figure 28, Figure 29 and Figure 30). This increase can be explained by interaction of the complexes with electrolytes and proteins in the medium also observed by Fernández Fernández *et al.* (Fernández Fernández et al., 2018). The supplements in the medium likely accumulate in proximity to the hydrophilic surface of the complexes producing short-range repulsive hydration forces and thereby stabilizing the complexes (Fernández Fernández et al., 2018, 2016b). Based on the results of the stability measurements transfection experiments should be performed with the supplemented medium. However, in order to assure a successful transfection not only the stability of the complexes should be taken into consideration but also the well-being of the cells in general. Therefore, osmolality of the different cell culture media was assessed ranging from approximately 270 to 310 mOsmol/kg (Table 49). These findings conform with the osmolality of varying cell culture media ranging from 230 to 340 mOsmol/kg (Waymouth, 1970). Conversely, osmolality of *Opti-MEM™* supplemented with HEPES and mannitol displayed an osmolality of roughly 580 mOsmol/kg making the medium highly hypertonic. This elevated concentration can strongly affect cells as reported by Kastl *et al.* who showed that an osmolality of 500 mOsmol/kg lead to significant shrinking of pancreatic tumor cells (Kastl et al., 2017). The negative effect of the supplemented medium was also demonstrated by an MTT assay. Cell viability of H441 and primary HNE cells was significantly decreased by *Opti-MEM™* supplemented with HEPES and mannitol in contrast

to the medium without supplements (Figure 31). The increase in cytotoxicity might also be enforced by mannitol as it has been reported to negatively affect cells (Grenha et al., 2010).

Even though results of the stability measurements suggest the experiments to be conducted with the supplemented medium the osmolality of the medium as well as the result of the MTT assay advise otherwise. Hence, transfection experiments were conducted with *Opti-MEM™* without supplements.

4.2.3 ASO transfection successfully inhibits ENaC activity in human respiratory epithelial cells

For *in vitro* transfection experiments using chitosan-ASO complexes the cell line H441 was chosen as these distal lung epithelial cells express sufficient α-ENaC for knockdown purposes (Sayegh et al., 1999). In an approach to show a proof-of-principle that successful cellular uptake with ASO using chitosan can be achieved, H441 cells were transfected with the fluorescently labeled 5'Fam-ASOgreen. Figure 33 displays representative confocal laser scanning microscopy images of transfected cells showing strong fluorescence after transfection with *Lipofectamine* as well as chitosan. These outcomes corroborate the results from Sobczak *et al.* proofing the functionality of the fluorescent 6-fam tag (Sobczak et al., 2009). An approach of transfection similar to the one in this study was made by Nafee *et al.* using chitosan and poly(lactid-*co*-glycolid) (PLGA) to transfect 2'-*O*-methyl-RNA ASO coupled with a 5'Fam tag into A549 cells, a human lung cancer cell line. Confocal laser scanning microscopy images clearly show the green fluorescence from the 5'Fam inside the cell (Nafee et al., 2007). These findings prove that chitosan-ASO complexes successfully enter human airway epithelial cells.

Evaluation of total RGB fluorescence intensities showed a highly significant increase of fluorescence after transfection using both *Lipofectamine* and chitosan (Figure 32). Even though the transfection efficiency of chitosan appears to be slightly lower, no significant difference between the two transfection reagents was determined proving chitosan to be as effective as the commercially available transfection reagent. The same observations were made by Fernández Fernández *et al.* who used chitosan to transfect CFBE41o- cells

with plasmid DNA encoding enhanced green fluorescent protein (pEGFP). They also showed slightly higher transfection efficiency when using *Lipofectamine* but no significant difference between *Lipofectamine* and chitosan (Fernández Fernández et al., 2016b) reinforcing the hypothesis of chitosan being an effective transfection reagent.

In order to test whether the α-ENaC ASO effectively decrease ENaC activity H441 cells were transfected with ASOgreen. 24 h after transfection functional Ussing chamber measurements were conducted and the amiloride-sensitive current was evaluated. While transfection with *Lipofectamine* only led to an insignificant decrease of amiloride-sensitive short-circuit current, the decrease observed after transfection with chitosan was highly significant (Figure 35). As already discussed in the context of the chitosan-mRNA complexes the difference in transfection efficiencies might be caused by the cytotoxicity of the commercially available transfection reagent. The MTT test assessing the cell viability of H441 cells after incubation with the different transfection reagents showed a significant decrease in cell viability after being exposed to *Lipofectamine* (Figure 31a). Chitosan on the other hand did not have an effect on the viability of cells enforcing its non-cytotoxicity and potential as transfection reagent. The findings of decreased ENaC activity after transfection of ASO directed against the α-subunit of the sodium channel are conform with previous studies (Jain et al., 1999; Segal et al., 2002; Sobczak et al., 2009). Jain *et al*. even reported that only inhibition of α-ENaC led to a significant decrease of density of non-selective cation channels. Knock-down of β- and γ-ENaC did not have such an effect (Jain et al., 1999) showing that α-ENaC is relevant for the formation of the channel pore (Loffing and Schild, 2005).

The use of ASO to reduce ENaC activity and thereby evoking rehydration of the airway surface has already been of interest in CF research. Griesenbach *et al.* could not observe a decrease in ENaC activity after transfection using Genzyme lipid 67 in mice (Griesenbach et al., 2006) showing that lipid-based transfection is not always suitable. Crosby *et al.* on the other hand could successfully decrease ENaC expression and ameliorate inflammation and airway hyper-responsiveness after ENaC ASO inhalation in mice with CF lung disease (Crosby et al., 2017). Even though CF animal models fail to mirror the pathology of human CF lung disease (Cohen and Prince, 2012; Semaniakou et al., 2018) these studies

demonstrate the importance of targeting ENaC for a successful restoration of ion transports and hence airway surface rehydration in CF.

After successfully transfecting human respiratory epithelial cells with wtCFTR-mRNA as well as α-ENaC ASO using chitosan and effectively increasing CFTR function as well as decreasing ENaC activity, respectively, an attempt was made at developing a co-transfection system. We designed chitosan-mRNA-ASO complexes as a double-tracked strategy to co-target both proteins at the same time.

4.3 Chitosan-mRNA-ASO complexes

4.3.1 Complexation of two nucleic acids by chitosan forms moderately monodisperse nanoparticles

Chitosan-mRNA-ASO complexes were developed at varying N/P charge rations (10, 30, 50, 70, 90) by harnessing the principle of electrostatic self-assembly as described before (4.2.1). Due to the good results achieved at forming chitosan-ASO complexes in the presence of 85 mM NaCl, the co-transfection system was prepared under the same conditions. As before, three different complexes were designed incorporating one of the three ASO directed against the α-subunit of ENaC, respectively, and wtCFTR-mRNA. Physicochemical characterization of the complexes was carried out using DLS-NIBS.

All complexes displayed an average size around 150 nm and a PDI of approximately 0.5 without any correlation regarding the N/P charge ratio (Figure 36 and Figure 37). Even though complexes having a size distribution with a PDI of < 0.7 is still regarded as relatively monodisperse (Nidhin et al., 2008) complexes with a narrower size distribution would be preferable for appropriate biological performance and transfection efficiency. Measurements of the zeta potential revealed increasing values with increasing N/P charge ratio confirming successful formation of complexes as described in other studies (Figure 39; Fernández Fernández et al., 2016b; Mansouri et al., 2006; Puras et al., 2013; Santos-Carballal et al., 2015).

To the best of our knowledge until today, there are only two studies about chitosan as a co-delivery system for genes. Lee *et al.* used glycol chitosan to co-transfect two siRNAs *in*

vivo in a tumor mouse model for cancer therapy. However, they randomly co-polymerized the nucleic acids into a single backbone of siRNA polymer (Lee et al., 2015) making comparison with the co-transfection system in this study difficult. In the other study, conducted in our research group, Fernández Fernández *et al.* made a more comparable approach. The chitosan complexes containing pEGFP as well as siRNA and were able to successfully transfect CFBE41o- cells. In their study they used the same chitosan applied in this work, developing suitable complexes with a size of 300 nm and a narrow size distribution (PDI 0.2) at N/P charge ratio 12 (Fernández Fernández et al., 2016b). At nearly the same N/P charge ratio (10) our attempt led to complexes with a broader size distribution. The plasmid DNA as well was the siRNA used in the study of Fernández Fernández *et al.* are both double stranded nucleic acids. In contrast to that, the mRNA as well as the ASO in this study are both single stranded. Double stranded nucleic acids display a higher charge density providing more negative charges to interact with the positively charged chitosan in the same area than single stranded nucleic acids. This likely leads to more densely packed complexes displaying a narrower size distribution. Furthermore, the ratio of pEGFP and siRNA was nearly 10-fold higher than the ratio of wtCFTR-mRNA and ENaC-ASO (55.5:1 vs. 5.4:1) probably also leading to different behavior of complex formation. It would be interesting to increase the ratio of the wtCFTR-mRNA to ENaC-ASO and elucidate whether the proportion of the nucleic acids may lead to the formation of more densely packed complexes.

In order to use the complexes for transfection purposes they need to be relatively stable in transfection medium. However, the presumably loosely packed double-complexes would likely aggregate in the presence of the proteins and electrolytes abundant in the medium. Therefore, the approach of co-delivering wtCFTR-mRNA and ENaC-ASO using chitosan was dismissed and is deemed to require further optimization in future studies. Nevertheless, a new attempt was made to target both proteins at the same time. For this chitosan-lecithin oil-core nanocapsules loaded with capsaicin and covered with wtCFTR-mRNA were designed.

4.4 Chitosan-lecithin oil-core nanocapsules

4.4.1 Capsaicin might decrease ENaC activity by activation of TRPV1 in primary human nasal epithelial cells

Capsaicin, the main pungent ingredient in chili peppers, is the agonist to TRPV1, a non-selective cation channel mainly expressed in cells of the nervous system (Ross, 2003). Activation of TRPV1 usually leads to acute and persistent pain (Basbaum et al., 2009). However, in 2014 Li and colleagues reported that activation of TRPV1 via capsaicin reduced α-ENaC expression and ENaC activity in the kidney of mice (Li et al., 2014). They argue that activation of the vanilloid receptor activates amongst others protein kinase C, which in turn inhibits ENaC activity (Li et al., 2014). This theory is corroborated by Soukup *et al.* who report that activation of protein kinase C inhibits ENaC currents in the lung of rats (Soukup et al., 2012). This discovery is very interesting regarding the work of the present study. Reducing ENaC activity with a natural compound would circumvent the need to co-deliver two nucleic acids to the cell simultaneously. Before designing a new nanosystem targeting the respiratory epithelium, we determined expression of TRPV1 in primary HNE cells on mRNA and protein level and assessed the effect of capsaicin on the cells.

PCR of cDNA from primary HNE cells could successfully amplify α-ENaC as well as TRPV1 (Figure 40). While expression of α-ENaC in primary HNE cells was already established by our group (Bangel et al., 2008) actual expression of TRPV1 in the used cells still needed to be confirmed. Sequencing of the amplified TRPV1 fragment and alignment with a human TRPV1 gene undoubtedly validated the expression of the cation channel in primary HNE cells (Figure 41). These findings are conforming with previous studies detecting TRPV1 in nasal epithelial cells (Seki et al., 2006; Van Gerven et al., 2014). In a further step, TRPV1 and α-ENaC were also successfully detected in primary HNE cells on protein level by western blot (Figure 42). Detection of α-ENaC with a main band at 85 kDa confirmed expression of the subunit in primary HNE cells as published before (Prulière-Escabasse et al., 2007). Expression of TRPV1 was confirmed with a specific band at 95 kDa conforming with a previous publication, which reported the detection of the receptor in primary bronchial epithelia cells (McGarvey et al., 2014). For both proteins, faint signals above the

main bands were detected as well. These might be explained by posttranslational modifications such as glycosylations or splicing variants of the proteins. Nevertheless, expression of both TRPV1 as well as the α-ENaC subunit in primary HNE cells was unquestionably confirmed on mRNA and protein level.

After successfully determining the expression of TRPV1 in primary HNE cells, the effect of its antagonist capsaicin on the cells was evaluated. An MTT assay showed that the vanilloid had a cytotoxic effect on the cells at a concentration of 150 µM and higher (Figure 43). The same observations were made by Kaiser *et al.* in a murine endothelial capillary brain cell line (Kaiser et al., 2019). Reilly *et al.* reported similar results for A549 cells with a lethal concentration of 110 µM (Reilly et al., 2003). A probable cause for cytotoxicity in higher doses might be the increased influx of calcium into the cell through TRPV1 and following swelling of the cell (Caterina et al., 1997). However, another study reported lethal capsaicin concentrations in nasal epithelial cells starting at 500 µM (Van Gerven et al., 2014). They conducted *in vivo* studies with patients suffering from idiopathic rhinitis applying 100 µM capsaicin to the nasal mucosa resulting in decreased nasal hyperreactivity and reduced nasal obstruction (Van Gerven et al., 2014). These findings are converse to studies suggesting that capsaicin through activation of TRPV1 leads to the production of pro-inflammatory cytokines to protect against potentially harmful inhaled cytotoxic substances, which in turn leads to cell death (Lee and Gu, 2009; Reilly et al., 2005, 2003). Given the converse findings, no definitive statement about the cytotoxicity (nor the toxicity *in vivo* indeed) of capsaicin can be made at this stage. After careful consideration of these data, a concentration of 100 µM capsaicin was applied to the cells before assessing the amiloride-sensitive current in order to evaluate the influence of the vanilloid in human respiratory epithelial cells.

While incubation with capsaicin for only 4 h did not have an effect on primary HNE cells incubation for 24 h led to a decrease of amiloride-sensitive current of 32% (Figure 44). These findings indicate that capsaicin indeed decreased ENaC activity in human respiratory epithelial cells supporting the findings of Li and colleagues (Li et al., 2014). However, since the results are not significant treatment of the cells with capsaicin should be optimized. Li *et al*. fed the mice a constant diet high in capsaicin for 10 months before assessing the effect of the vanilloid on ENaC expression (Li et al., 2014). Van Gerven *et al.* observed the

outcome of capsaicin treatment of the nasal epithelium after 12 weeks (Van Gerven et al., 2014). Therefore, longer and constant incubation with capsaicin should be considered to increase the effect of the vanilloid on ENaC activity.

Nevertheless, the results of these data are very promising regarding the treatment of sodium hyperabsorption with capsaicin as a complete inactivation of ENaC is not desirable for the treatment of CF. In combination with wtCFTR-mRNA transfection a slight decrease of ENaC activity might be enough to correct abnormal ion transports in CF. Therefore, we designed a novel nanosystem by incorporating capsaicin and wtCFTR-mRNA in the same formulation to co-target ENaC and CFTR simultaneously.

4.4.2 Highly monodisperse and positively charged nanocapsules successfully adsorb wtCFTR-mRNA

Chitosan-based nanocapsules have been of interest for transmucosal delivery of drugs because of their increased stability and interaction with mucosal surfaces (Goycoolea et al., 2012; Prego et al., 2006, 2005). We therefore aimed at developing such a nanosystem to enhance transfection efficiency in the hostile environment of the CF lung.

Chitosan covered nanocapsules were obtained by harnessing the well-known phenomenon of spontaneous emulsification also known as solvent displacement (López-Montilla et al., 2002). Characterization regarding the capsules' physicochemical properties ensued by various methods. DLS-NIBS measurements revealed a 1.5-fold increase in Z-average hydrodynamic diameter after loading the capsules with capsaicin indicating encapsulation of the drug (Figure 45). These findings are in concordance with previous studies (Goycoolea et al., 2012; Kaiser et al., 2015b). Furthermore, it was reported that the nanocapsules display a strong capsaicin-association efficiency of 92% (Kaiser et al., 2015b) validating successful encapsulation. Zeta potential also increased after capsaicin encapsulation. This can be explained by the enlarged surface of the nanocapsules having more chitosan attached to it and therefore displaying more positive charges. Overall, the nanocapsules exhibited promising characteristics like their small size, low PDI and high zeta potential (Table 50). To gain further information about the capsules' size and shape they were characterized upon fractionation by AF4 with multidetection. Elution profiles of the

blank and loaded nanocapsules showed that the loaded capsules are of bigger size as already shown by DLS-NIBS measurements (Figure 47 and Figure 48). The R_g/R_h ratio was calculated from the radii obtained from MALS and DLS-NIBS measurements and revealed a value of approximately 0.7 for both systems (Table 51). It has been reported that the theoretical value of a homogeneous hard sphere is 0.778 while for a soft and hollow sphere like a vesicle the theoretical value is 0.977 (Brewer and Striegel, 2009). This indicates that the nanocapsules in this study having a vesicle-like structure are probably not completely spherical. This hypothesis was confirmed by TEM imaging. The images exhibit the shape of the nanocapsules showing that the systems display round shapes but are partially elliptical (Figure 49).

In a further step, the nanocapsules were coated with wtCFTR-mRNA at varying N/P charge ratios (5, 10, 50, 75, 100) and again characterized for their physicochemical properties. DLS-NIBS measurements revealed that attachment of nucleic acid to the surface of the capsules did not have any effect on the size and PDI of the systems (Figure 50). However, zeta potential of the capsules slightly increased with increasing N/P charge ratio, thus indicating successful adsorption of wtCFTR-mRNA. The increasing positive charge arises from the positively charged amine groups not being neutralized by a negatively charged phosphate group. Therefore, with decreasing amount of nucleic acid, hence an increasing N/P charge ratio, less phosphate groups take part in the neutralization and the zeta potential increases as described before in this study and by others (Fernández Fernández et al., 2016b; Mansouri et al., 2006; Puras et al., 2013; Santos-Carballal et al., 2015). The successful attachment of wtCFTR-mRNA to the surface of the complexes was validated by a gel retardation assay (Figure 52). As already shown for the chitosan-ASO complexes chitosan was able to retain the nucleic acid in the gel pocket. This enforces the findings of previous studies proving strong binding efficiency of chitosan and nucleic acids in general (Fernández Fernández et al., 2016b; Lee et al., 2001; Yhee et al., 2015).

As elucidated for the chitosan-ASO complexes (4.2.1), the small size, low PDI and highly positive zeta potential as well as the successful adsorption of wtCFTR-mRNA to the surface of the chitosan-covered nanocapsules makes the system very promising for transfection purposes.

4.4.3 Nanocapsules are highly stable in transfection medium but did not transfect primary human nasal epithelial cells

Before cell culture experiments were done with the nanocapsules, their stability in transfection medium was evaluated. For this naked and coated nanocapsules were incubated in *Opti-MEM™* supplemented with HEPES and mannitol for 24 h at 37°C. Both systems remained stable over time (Figure 53 and Figure 54) as reported by previous studies (Kaiser et al., 2015b, 2015a). However, as discussed before the transfection medium supplemented with HEPES and mannitol displays a very high osmolality around 580 mOsmol/kg having a shrinking effect on the cells. An MTT assay conducted with capsaicin loaded nanocapsules in *Opti-MEM™* with and without supplements supports these findings (Figure 55a). While capsules in the supplemented medium decreased viability of the cells to approximately 60% the capsules in pure medium did not show such an effect. Based on this data, transfection experiments should be conducted in medium without supplements. Kaiser and colleagues showed that nanocapsules also remained stable in unsupplemented medium, which can be applied to our systems as well (Kaiser et al., 2015b, 2015a). Additionally, in a second MTT test the effect on blank nanocapsules on primary HNE cells was assessed. Blank nanocapsules in low concentrations displayed a highly toxic influence on the cells while in higher concentrations only a non-significant decrease of cell viability was observed (Figure 55b). Interestingly, capsaicin loaded nanocapsules had the opposite effect on the cells. These result suggest that capsaicin has a beneficial influence on nasal epithelial cells as reported before (Van Gerven et al., 2014). Kaiser *et al.* reported a similar result in a canine kidney epithelial cell line (MDCK-C7). While loaded nanocapsules hat no significant effect on cell viability unloaded capsules significantly decreased cell viability (Kaiser et al., 2015b). Nevertheless, the negative effect of blank nanocapsules in low concentrations remains questionable.

Like free capsaicin, encapsulated capsaicin displayed cytotoxic effects on cell viability at concentrations higher than 100 µM. This is in contradiction to previous studies. Kaiser and colleagues reported that 500 µM of encapsulated capsaicin did not have an effect on the viability of MDCK-C7 cells (Kaiser et al., 2015b). However, the effect of capsaicin on the viability differs between cell lines. For example Reilly *et al.* showed that the vanilloid has a

stronger effect on cell viability of cells of the respiratory epithelium compared to liver cells (Reilly et al., 2003). This might be explained by the varying expression levels of TRPV1 in different human tissues (Vos et al., 2006). After careful consideration of the results transfection experiments should likely be carried out with loaded nanocapsules at capsaicin concentrations of 50 or 100 µM.

Finally, the transfection efficiency of blank and capsaicin loaded nanocapsules was assessed with a luciferase assay. For this a plasmid containing a model luciferase reporter gene was absorbed to the surface of the capsules. Transfection of the plasmid using the commercially available transfection reagent *FuGENE* led to a significant increase in RLU proving successful transfection of primary HNE cells with the plasmid (Figure 56). In transfection medium supplemented with HEPES and mannitol the increase was not significant supporting the preceding MTT assays and the hypothesis that the supplemented medium is harmful for the cells. However, transfection with the nanocapsules either blank or loaded with capsaicin did not show an increase in RLU. Merely a slight increase of RLU was observed after transfection with loaded nanocapsules at a capsaicin concentration of 50 µM supporting the evaluation of the MTT assay. Luciferase assays using chitosan in general have been reported to be successful (Jiang et al., 2007; Sang Yoo et al., 2005; Thibault et al., 2016). The low transfection efficiency of the nanocapsules might be explained by the fact that the systems were not evaluated regarding their physicochemical properties after adsorption of the relatively large plasmid. The systems were not characterized as adsorption of wtCFTR-mRNA at any concentration did not have an effect on the constitution of the capsules (Figure 50). However, the plasmid is larger than the wtCFTR-mRNA and double-stranded. As explained before, double-stranded nucleic acids have a higher charge density and therefore might interact with chitosan differently than single-stranded nucleic acids. Evaluation of the systems with the adsorbed plasmid should be conducted to elucidate the poor transfection efficiency. Another reason for the low RLU values might be that not enough of the plasmid actually entered the cell. Kaiser *et al.* showed with structural illumination fluorescence microscopy that some of the capsaicin loaded nanocapsules were internalized by MDCK-C7 cells but that others accumulated at the cell surface releasing the vanilloid outside of the cell (4% in 12 h; Kaiser et al., 2015b). Therefore, concentration of the plasmid containing the luciferase reporter gene should be

increased to possibly increase transfection efficiency of the nanocapsules. In general, while there are a lot of studies reporting about chitosan-based nanocapsules to deliver amongst others drugs, peptides or antigens (Bussio et al., 2018; Chanphai et al., 2019; Natrajan et al., 2015; Prego et al., 2006; Wu et al., 2017) only very few studies can be found about chitosan nanocapsules delivering nucleic acids (Gaspar et al., 2011; Ramesh kumar et al., 2016). Furthermore, these capsules are loaded with the genetic material and do not adsorb it to the surface making the approach in this study very unique. This shows that more research in this field needs to be done in order to optimize gene delivery using chitosan-based nanocapsules.

Even though successful transfection with the nanocapsules could not be achieved until now, the auspicious results of the nanocapsules' physicochemical characterization and stability measurements make the nanosystems very promising for future transfection purposes. Furthermore, the effect of capsaicin on the cells reported here and in other studies gives hope for a successful translation into the treatment of CF lung disease.

4.5 Conclusion and outlook

Until today, CF remains the most common life-threatening hereditary disease in the Caucasian population. Even though treatment has come a long way at alleviating the symptoms of the disease and prolonging the life expectancy of patients a causative treatment to cure the illness on a cellular level has yet to be developed. A promising concept of treatment is gene therapy aiming at the therapeutic delivery of DNA to the cell. However, many limitations prevented the successful development of such a treatment to the present day including the risk of insertional mutagenesis associated with DNA or unwanted host immune responses towards viral vectors. Nanobiotechnology and nanomedicine continue offering promising possibilities to circumvent these difficulties with systems constituted of natural non-toxic non-viral nanocarriers for potential drugs such as mRNA for *transcript therapy*.

The results presented in this Thesis corroborate the aspiring opportunities of nanobiotechnology for a possible CF treatment. Chitosan-based nanosystems were designed and characterized demonstrating the ability of the polymer to successfully form

small and monodisperse complexes for transfection purposes with wtCFTR-mRNA and α-ENaC ASO, respectively. Functional Ussing chamber measurements showed significantly increased CFTR function as well as significantly decreased ENaC activity in human respiratory epithelial cells after successful transfection with chitosan nanoparticles complexing wtCFTR-mRNA and α-ENaC ASO, respectively. Furthermore, a new approach to reduce ENaC activity using a natural compound was tested. The pungent ingredient of the chili pepper, namely capsaicin, displayed a slightly decreasing effect on the amiloride-sensitive current demonstrating its great value for a possible CF treatment. Finally, chitosan nanocapsules incorporating capsaicin and adsorbing wtCFTR-mRNA to the surface were harnessed and characterized. The capsules displayed many advantages over the complexes such as an increased stability making them more promising for transfection purposes.

However, a simultaneous treatment of CFTR and ENaC on functional level could not yet be achieved and is substance for future research. As chitosan complexes displayed a high transfection efficiency the co-transfection system constituted of wtCFTR-mRNA and ENaC ASO should be improved. This might be achieved by changing the ratio of mRNA towards ASO or increasing or decreasing the N/P charge ratio.

As the chitosan nanocapsules exhibited more promising physicochemical properties than the complexes, their transfection efficiency should be improved. Firstly, characterization of capsules with the plasmid containing the luciferase reporter gene should clarify whether the complexes are suitable as a carrier for such large cargo. Subsequently, incubation time of the capsules with the cells or concentration of the nucleic acid should be increased to facilitate the transfection. If the transfection efficiency of these nanocapsules can be improved, they might represent a very promising carrier for gene therapy in general as theoretically any type of nucleic acid could adsorb to their surface. This could also be an alternative for simultaneous delivery of wtCFTR-mRNA and α-ENaC ASO, if complexation of the two nucleic acids by chitosan should remain unsuccessful.

As the reports regarding the cytotoxicity of capsaicin are converse, the effect of the vanilloid on respiratory epithelial cells concerning the immune response and cell viability should be elucidated further. Cytokine arrays or cell viability assays besides MTT assays might help to bring light to this matter.

As discussed before (4.1.1) the ion transport in the cell culture systems used in the present study does not represent a proper *in vivo* situation. A more suitable model to perform transfection experiments with wtCFTR-mRNA and investigate subsequent ion transport via CFTR and ENaC might be the cell lines NuLi (normal lung, University of Iowa) and CuFi (cystic fibrosis, University of Iowa) (Zabner et al., 2003). The cells were derived from healthy and CF bronchial epithelium of human donor lungs and transformed using the reverse transcriptase component of telomerase and human papillomavirus type 16 E6 and E7 genes. Both cell lines are capable of forming polarized differentiated epithelia, maintaining the ion channel physiology expected for their genotypes and exhibit transepithelial resistance. Furthermore, they display the predicted cAMP-dependent as well as amiloride-sensitive currents associated with their genotypes (Zabner et al., 2003). In recent years, the work with these cell lines as an alternative to CFBE41o- and 14HBE16o-cells has been gaining ground opening more possibilities in the field of CF research (Molina et al., 2015; Mroz and Harvey, 2019; Santoro et al., 2018).

Finally, *in vivo* studies should be conducted in order to estimate the efficacy of the nanosystems on a model animal organism like the CF pig as they are susceptible to lung disease like humans (Meyerholz, 2016).

There are still a lot of steps ahead until a translation of the chitosan-based nanosystems into clinical application will be possible and successful therapy can actually be applied. Nevertheless, the results presented and discussed herein demonstrate that a promising start for the development of a double-tracked strategy to treat abnormal ion transports in CF has been made.

5 REFERENCES

Ahmad, A., Ahmed, A., Patrizio, P., 2013. "Cystic fibrosis and fertility". *Curr. Opin. Obstet. Gynecol.* 25, 167–172.

Akabas, M.H., 2000. "Cystic fibrosis transmembrane conductance regulator. Structure and function of an epithelial chloride channel.". *J. Biol. Chem.* 275, 3729–32.

Alton, E.W.F.W., Armstrong, D.K., Ashby, D., Bayfield, K.J., Bilton, D., Bloomfield, E. V, Boyd, A.C., Brand, J., Buchan, R., Calcedo, R., Carvelli, P., Chan, M., Cheng, S.H., Collie, D.D.S., Cunningham, S., Davidson, H.E., Davies, G., Davies, J.C., Davies, L.A., Dewar, M.H., Doherty, A., Donovan, J., Dwyer, N.S., Elgmati, H.I., Featherstone, R.F., Gavino, J., Gea-Sorli, S., Geddes, D.M., Gibson, J.S.R., Gill, D.R., Greening, A.P., Griesenbach, U., Hansell, D.M., Harman, K., Higgins, T.E., Hodges, S.L., Hyde, S.C., Hyndman, L., Innes, J.A., Jacob, J., Jones, N., Keogh, B.F., Limberis, M.P., Lloyd-Evans, P., Maclean, A.W., Manvell, M.C., McCormick, D., McGovern, M., McLachlan, G., Meng, C., Montero, M.A., Milligan, H., Moyce, L.J., Murray, G.D., Nicholson, A.G., Osadolor, T., Parra-Leiton, J., Porteous, D.J., Pringle, I.A., Punch, E.K., Pytel, K.M., Quittner, A.L., Rivellini, G., Saunders, C.J., Scheule, R.K., Sheard, S., Simmonds, N.J., Smith, K., Smith, S.N., Soussi, N., Soussi, S., Spearing, E.J., Stevenson, B.J., Sumner-Jones, S.G., Turkkila, M., Ureta, R.P., Waller, M.D., Wasowicz, M.Y., Wilson, J.M., Wolstenholme-Hogg, P., UK Cystic Fibrosis Gene Therapy Consortium, 2015. "Repeated nebulisation of non-viral CFTR gene therapy in patients with cystic fibrosis: a randomised, double-blind, placebo-controlled, phase 2b trial". *Lancet Respir. Med.* 3, 684–691.

Alvarez-Figueroa, M.J., Abarca-Riquelme, J.M., González-Aramundiz, J.V., 2019. "Influence of protamine shell on nanoemulsions as a carrier for cyclosporine - a skin delivery". *Pharm. Dev. Technol.* 24, 630–638.

Alvarez de la Rosa, D., Canessa, C.M., Fyfe, G.K., Zhang, P., 2000. "Structure and regulation of amiloride-sensitive sodium channels.". *Annu. Rev. Physiol.* 62, 573–94.

Andersen, D.H., 1938. "Cystic fibrosis of the pancreas and its relation to celiac disease". *Am. J. Dis. Child.* 56, 344.

Ansari, S.H., Islam, F., Sameem, M., 2012. "Influence of nanotechnology on herbal drugs: a review". *J. Adv. Pharm. Technol. Res.* 3, 142.

Baker, B.F., Lot, S.S., Condon, T.P., Cheng-Flournoy, S., Lesnik, E.A., Sasmor, H.M., Bennett, C.F., 1997. "2'-O-(2-Methoxy)ethyl-modified anti-intercellular adhesion molecule 1 (ICAM-1) oligonucleotides selectively increase the ICAM-1 mRNA level and inhibit formation of the ICAM-1 translation initiation complex in human umbilical vein endothelial cells.". *J. Biol. Chem.* 272, 11994–2000.

Bals, R., Hiemstra, P.S., 2004. "Innate immunity in the lung: how epithelial cells fight against respiratory pathogens". *Eur. Respir. J.* 23, 327–333.

Bangel-Ruland, N., Sobczak, K., Christmann, T., Kentrup, D., Langhorst, H., Kusche-Vihrog, K., Weber, W.-M., 2010. "Characterization of the epithelial sodium channel δ-subunit in human nasal epithelium". *Am. J. Respir. Cell Mol. Biol.* 42, 498–505.

Bangel-Ruland, N., Tomczak, K., Fernández Fernández, E., Leier, G., Leciejewski, B., Rudolph, C., Rosenecker, J., Weber, W.-M., 2013. "Cystic fibrosis transmembrane conductance regulator-mRNA delivery: a novel alternative for cystic fibrosis gene therapy.". *J. Gene Med.* 15, 414–26.

Bangel, N., Dahlhoff, C., Sobczak, K., Weber, W.-M., Kusche-Vihrog, K., 2008. "Upregulated expression of ENaC in human CF nasal epithelium". *J. Cyst. Fibros.* 7, 197–205.

Basbaum, A.I., Bautista, D.M., Scherrer, G., Julius, D., 2009. "Cellular and molecular mechanisms of pain". *Cell* 139, 267–284.

Bennett, C.F., 2019. "Therapeutic antisense oligonucleotides are coming of age". *Annu. Rev. Med.* 70, 307–321.

Berdiev, B.K., Qadri, Y.J., Benos, D.J., 2009. "Assessment of the CFTR and ENaC association.". *Mol. Biosyst.* 5, 123–7.

Berridge, M. V, Herst, P.M., Tan, A.S., 2005. "Tetrazolium dyes as tools in cell biology: new insights into their cellular reduction.". *Biotechnol. Annu. Rev.* 11, 127–52.

Bhalla, V., Hallows, K.R., 2008. "Mechanisms of ENaC regulation and clinical implications.". *J. Am. Soc. Nephrol.* 19, 1845–54.

Bhattacharjee, S., 2016. "DLS and zeta potential – what they are and what they are not?". *J. Control. Release* 235, 337–351.

Biscaglia, F., Quarta, S., Villano, G., Turato, C., Biasiolo, A., Litti, L., Ruzzene, M., Meneghetti, M., Pontisso, P., Gobbo, M., 2019. "PreS1 peptide-functionalized gold nanostructures with SERRS tags for efficient liver cancer cell targeting". *Mater. Sci. Eng. C* 103, 109762.

Blair, H.A., 2018. "Capsaicin 8% dermal patch: a review in peripheral neuropathic pain". *Drugs* 78, 1489–1500.

Blank, U., Clauss, W., Weber, W.-M., 1995. "Effects of benzamil in human cystic fibrosis airway epithelium". *Cell. Physiol. Biochem.* 5, 385–390.

Blouquit-Laye, S., Chinet, T., 2007. "Ion and liquid transport across the bronchiolar epithelium". *Respir. Physiol. Neurobiol.* 159, 278–282.

Boot, R.G., Blommaart, E.F.C., Swart, E., Vlugt, K.G. der, Bijl, N., Moe, C., Place, A., Aerts, J.M.F.G., 2001. "Identification of a novel acidic mammalian chitinase distinct from chitotriosidase". *J. Biol. Chem.* 276, 6770–6778.

Borchard, G., 2001. "Chitosans for gene delivery.". *Adv. Drug Deliv. Rev.* 52, 145–50.

Boucher, R.., 2002. "An overview of the pathogenesis of cystic fibrosis lung disease". *Adv. Drug Deliv. Rev.* 54, 1359–1371.

Boyle, M.P., De Boeck, K., 2013. "A new era in the treatment of cystic fibrosis: correction of the underlying CFTR defect". *Lancet Respir. Med.* 1, 158–163.

Bradley, J.M., Moran, F.M., Elborn, J.S., 2006. "Evidence for physical therapies (airway clearance and physical training) in cystic fibrosis: an overview of five Cochrane systematic reviews.". *Respir. Med.* 100, 191–201.

Brewer, A.K., Striegel, A.M., 2009. "Particle size characterization by quadruple-detector hydrodynamic chromatography". *Anal. Bioanal. Chem.* 393, 295–302.

Broughton-Head, V.J., Smith, J.R., Shur, J., Shute, J.K., 2007. "Actin limits enhancement of nanoparticle diffusion through cystic fibrosis sputum by mucolytics". *Pulm. Pharmacol. Ther.* 20, 708–717.

Brower, M., Carney, D.N., Oie, H.K., Gazdar, A.F., Minna3, J.D., 1986. "Growth of cell lines and clinical specimens of human non-small cell lung cancer in a serum-free defined medium". *Cancer Res.* 46, 798–806.

Bubien, J.K., 2010. "Epithelial Na^+ channel (ENaC), hormones, and hypertension.". *J. Biol. Chem.* 285, 23527–31.

Buschmann, M.D., Merzouki, A., Lavertu, M., Thibault, M., Jean, M., Darras, V., 2013. "Chitosans for delivery of nucleic acids". *Adv. Drug Deliv. Rev.* 65, 1234–1270.

Bussio, J., Molina-Perea, C., González-Aramundiz, J., 2018. "Lower-sized chitosan nanocapsules for transcutaneous antigen delivery". *Nanomaterials* 8, 659.

Butterworth, M.B., 2010. "Regulation of the epithelial sodium channel (ENaC) by membrane trafficking.". *Biochim. Biophys. Acta* 1802, 1166–77.

Button, B., Boucher, R.C., 2008. "Role of mechanical stress in regulating airway surface hydration and mucus clearance rates". *Respir. Physiol. Neurobiol.* 163, 189–201.

Caci, E., Caputo, A., Hinzpeter, A., Arous, N., Fanen, P., Sonawane, N., Verkman, A.S., Ravazzolo, R., Zegarra-Moran, O., Galietta, L.J. V, 2008. "Evidence for direct CFTR inhibition by CFTR(inh)-172 based on Arg347 mutagenesis.". *Biochem. J.* 413, 135–42.

Canessa, C.M., Schild, L., Buell, G., Thorens, B., Gautschi, I., Horisberger, J.-D., Rossier, B.C., 1994. "Amiloride-sensitive epithelial Na^+ channel is made of three homologous subunits". *Nature* 367, 463–467.

Castellani, C., Assael, B.M., 2017. "Cystic fibrosis: a clinical view". *Cell. Mol. Life Sci.* 74, 129–140.

Castellani, C., Cuppens, H., Macek, M., Cassiman, J.J., Kerem, E., Durie, P., Tullis, E., Assael, B.M., Bombieri, C., Brown, A., Casals, T., Claustres, M., Cutting, G.R., Dequeker, E., Dodge, J., Doull, I., Farrell, P., Ferec, C., Girodon, E., Johannesson, M., Kerem, B., Knowles, M., Munck, A., Pignatti, P.F., Radojkovic, D., Rizzotti, P., Schwarz, M., Stuhrmann, M., Tzetis, M., Zielenski, J., Elborn, J.S., 2008. "Consensus on the use and interpretation of cystic fibrosis mutation analysis in clinical practice.". *J. Cyst. Fibros.* 7, 179–96.

Castellani, S., Trapani, A., Spagnoletta, A., di Toma, L., Magrone, T., Di Gioia, S., Mandracchia, D., Trapani, G., Jirillo, E., Conese, M., 2018. "Nanoparticle delivery of grape seed-derived proanthocyanidins to airway epithelial cells dampens oxidative stress and inflammation". *J. Transl. Med.* 16, 140.

Caterina, M.J., Schumacher, M.A., Tominaga, M., Rosen, T.A., Levine, J.D., Julius, D., 1997. "The capsaicin receptor: a heat-activated ion channel in the pain pathway". *Nature* 389, 816–824.

Chang, K.L.B., Tsai, G., Lee, J., Fu, W.-R., 1997. "Heterogeneous N-deacetylation of chitin in alkaline solution". *Carbohydr. Res.* 303, 327–332.

Chanphai, P., Thomas, T.J., Tajmir-Riahi, H.A., 2019. "Design of functionalized folic acid–chitosan nanoparticles for delivery of tetracycline, doxorubicin, and tamoxifen". *J. Biomol. Struct. Dyn.* 37, 1000–1006.

Chen, J.-M., Scotet, V., Ferec, C., 2000. "Definition of a “functional R domain” of the cystic fibrosis transmembrane conductance regulator". *Mol. Genet. Metab.* 71, 245–249.

Chen, S.-H., Chao, A., Tsai, C.-L., Sue, S.-C., Lin, C.-Y., Lee, Y.-Z., Hung, Y.-L., Chao, A.-S., Cheng, A.-J., Wang, H.-S., Wang, T.-H., 2019. "Utilization of HEPES for enhancing protein transfection into mammalian cells". *Mol. Ther. - Methods Clin. Dev.* 13, 99–111.

Chernousova, S., Epple, M., 2017. "Live-cell imaging to compare the transfection and gene silencing efficiency of calcium phosphate nanoparticles and a liposomal transfection agent". *Gene Ther.* 24, 282–289.

Chesnoy, S., Huang, L., 2000. "Structure and function of lipid-DNA complexes for gene delivery.". *Annu. Rev. Biophys. Biomol. Struct.* 29, 27–47.

Cheung, R., Ng, T., Wong, J., Chan, W., 2015. "Chitosan: an update on potential biomedical and pharmaceutical applications". *Mar. Drugs* 13, 5156–5186.

Cho, H.-J., Termsarasab, U., Kim, J.S., Kim, D.-D., 2010. "*In vitro* nasal cell culture systems for drug transport studies". *J. Pharm. Investig.* 40, 321–332.

Cholon, D.M., Quinney, N.L., Fulcher, M.L., Esther, C.R., Das, J., Dokholyan, N. V., Randell, S.H., Boucher, R.C., Gentzsch, M., 2014. "Cystic fibrosis: potentiator ivacaftor abrogates pharmacological correction of ΔF508 CFTR in cystic fibrosis". *Sci. Transl. Med.* 6, 246ra96.

Clancy, J.P., 2014. "CFTR potentiators: not an open and shut case.". *Sci. Transl. Med.* 6, 246fs27.

Clancy, J.P., Cotton, C.U., Donaldson, S.H., Solomon, G.M., VanDevanter, D.R., Boyle, M.P., Gentzsch, M., Nick, J.A., Illek, B., Wallenburg, J.C., Sorscher, E.J., Amaral, M.D., Beekman, J.M., Naren, A.P., Bridges, R.J., Thomas, P.J., Cutting, G., Rowe, S., Durmowicz, A.G., Mense, M., Boeck, K.D., Skach, W., Penland, C., Joseloff, E., Bihler, H., Mahoney, J., Borowitz, D., Tuggle, K.L., 2019. "CFTR modulator theratyping: current status, gaps and future directions". *J. Cyst. Fibros.* 18, 22–34.

Clark, R., Lee, S.-H., 2016. "Anticancer properties of capsaicin against human cancer.". *Anticancer Res.* 36, 837–43.

Cohen, T.S., Prince, A., 2012. "Cystic fibrosis: a mucosal immunodeficiency syndrome". *Nat. Med.* 18, 509–519.

Colombo, C., 2007. "Liver disease in cystic fibrosis". *Curr. Opin. Pulm. Med.* 13, 529–536.

Conese, M., Ascenzioni, F., Boyd, A.C., Coutelle, C., De Fino, I., De Smedt, S., Rejman, J., Rosenecker, J., Schindelhauer, D., Scholte, B.J., 2011. "Gene and cell therapy for cystic fibrosis: from bench to bedside.". *J. Cyst. Fibros.* 10 Suppl 2, S114-28.

Connett, G.J., 2019. "Lumacaftor-ivacaftor in the treatment of cystic fibrosis: design, development and place in therapy.". *Drug Des. Devel. Ther.* 13, 2405–2412.

Cooney, A.L., McCray, P.B., Sinn, P.L., 2018. "Cystic fibrosis gene therapy: looking back, looking forward". *Genes (Basel).* 9, 538.

Cozens, A.L., Yezzi, M.J., Kunzelmann, K., Ohrui, T., Chin, L., Eng, K., Finkbeiner, W.E., Widdicombe, J.H., Gruenert, D.C., 1994. "CFTR expression and chloride secretion in polarized immortal human bronchial epithelial cells.". *Am. J. Respir. Cell Mol. Biol.* 10, 38–47.

Crosby, J.R., Zhao, C., Jiang, C., Bai, D., Katz, M., Greenlee, S., Kawabe, H., McCaleb, M., Rotin, D., Guo, S., Monia, B.P., 2017. "Inhaled ENaC antisense oligonucleotide ameliorates cystic fibrosis-like lung disease in mice". *J. Cyst. Fibros.* 16, 671–680.

Csanády, L., Vergani, P., Gadsby, D.C., 2019. "Structure, gating, and regulation of the CFTR anion channel". *Physiol. Rev.* 99, 707–738.

Cutting, G.R., 2015. "Cystic fibrosis genetics: from molecular understanding to clinical application". *Nat. Rev. Genet.* 16, 45–56.

Cutz, E., Yeger, H., Pan, J., 2007. "Pulmonary neuroendocrine cell system in pediatric lung disease—recent advances". *Pediatr. Dev. Pathol.* 10, 419–435.

Danielsen, S., Vårum, K.M., Stokke, B.T., 2004. "Structural analysis of chitosan mediated DNA condensation by AFM: influence of chitosan molecular parameters". *Biomacromolecules* 5, 928–936.

Davé, U.P., Jenkins, N.A., Copeland, N.G., 2004. "Gene therapy insertional mutagenesis insights.". *Science* 303, 333.

Davies, J.W., Hainsworth, A.H., Guerin, C.J., Lambert, D.G., 2010. "Pharmacology of capsaicin-, anandamide-, and N-arachidonoyl-dopamine-evoked cell death in a homogeneous transient receptor potential vanilloid subtype 1 receptor population". *Br. J. Anaesth.* 104, 596–602.

Davis, P.B., 2006. "Cystic fibrosis since 1938". *Am. J. Respir. Crit. Care Med.* 173, 475–482.

De Boeck, K., Amaral, M.D., 2016. "Progress in therapies for cystic fibrosis". *Lancet Respir. Med.* 4, 662–674.

De Leo, V., Ruscigno, S., Trapani, A., Di Gioia, S., Milano, F., Mandracchia, D., Comparelli, R., Castellani, S., Agostiano, A., Trapani, G., Catucci, L., Conese, M., 2018. "Preparation of drug-loaded small unilamellar liposomes and evaluation of their potential for the treatment of chronic respiratory diseases". *Int. J. Pharm.* 545, 378–388.

De Rose, V., Molloy, K., Gohy, S., Pilette, C., Greene, C.M., 2018. "Airway epithelium dysfunction in cystic fibrosis and COPD". *Mediators Inflamm.* 2018, 1–20.

De Water, R., Willems, L.N., Van Muijen, G.N., Franken, C., Fransen, J.A., Dijkman, J.H., Kramps, J.A., 1986. "Ultrastructural localization of bronchial antileukoprotease in central and peripheral human airways by a gold-labeling technique using monoclonal antibodies.". *Am. Rev. Respir. Dis.* 133, 882–90.

Deeks, E.D., 2016. "Lumacaftor/ivacaftor: a review in cystic fibrosis". *Drugs* 76, 1191–1201.

Delgado, A. V, González-Caballero, F., Hunter, R.J., Koopal, L.K., Lyklema, J., 2007. "Measurement and interpretation of electrokinetic phenomena.". *J. Colloid Interface Sci.* 309, 194–224.

Demetzos, C., Pippa, N., 2014. "Advanced drug delivery nanosystems (aDDnSs): a mini-review". *Drug Deliv.* 21, 250–257.

Deng, R.-H., Qiu, B., Zhou, P.-H., 2018. "Chitosan/hyaluronic acid/plasmid-DNA nanoparticles encoding interleukin-1 receptor antagonist attenuate inflammation in synoviocytes induced by interleukin-1 beta". *J. Mater. Sci. Mater. Med.* 29, 155.

Donnelley, M., Parsons, D.W., 2018. "Gene therapy for cystic fibrosis lung disease: overcoming the barriers to translation to the clinic". *Front. Pharmacol.* 9, 1381.

Döring, G., Flume, P., Heijerman, H., Elborn, J.S., 2012. "Treatment of lung infection in patients with cystic fibrosis: current and future strategies.". *J. Cyst. Fibros.* 11, 461–79.

Drexler, H.G., Uphoff, C.C., 2002. "Mycoplasma contamination of cell cultures: Incidence, sources, effects, detection, elimination, prevention.". *Cytotechnology* 39, 75–90.

Duijvestijn, Y., Brand, P., 2007. "Systematic review of N-acetylcysteine in cystic fibrosis". *Acta Paediatr.* 88, 38–41.

Dupuis, A., Keenan, K., Ooi, C.Y., Dorfman, R., Sontag, M.K., Naehrlich, L., Castellani, C., Strug, L.J., Rommens, J.M., Gonska, T., 2016. "Prevalence of meconium ileus marks the severity of mutations of the cystic fibrosis transmembrane conductance regulator (CFTR) gene". *Genet. Med.* 18, 333–340.

Ecelbarger, C.A., Kim, G.-H., Wade, J.B., Knepper, M.A., 2001. "Regulation of the abundance of renal sodium transporters and channels by vasopressin". *Exp. Neurol.* 171, 227–234.

Edmondson, C., Davies, J.C., 2016. "Current and future treatment options for cystic fibrosis lung disease: latest evidence and clinical implications.". *Ther. Adv. Chronic Dis.* 7, 170–83.

Effros, R.M., 2006. "Anatomy, development, and physiology of the lungs". *GI Motil. online* 1.

Ehrhardt, C., Collnot, E.-M., Baldes, C., Becker, U., Laue, M., Kim, K.-J., Lehr, C.-M., 2006. "Towards an *in vitro* model of cystic fibrosis small airway epithelium: characterisation of the human bronchial epithelial cell line CFBE41o-". *Cell Tissue Res.* 323, 405–415.

EP-Devices, 2008. Ussing chamber for Costar filters, http://users.telenet.be/ep-devices/EPD Ussing chamber - Costar filters.pdf ; date accessed 2019-10-09.

Faraj, J., Bodas, M., Pehote, G., Swanson, D., Sharma, A., Vij, N., 2019. "Novel cystamine-core dendrimer-formulation rescues ΔF508-CFTR and inhibits *Pseudomonas aeruginosa* infection by augmenting autophagy". *Expert Opin. Drug Deliv.* 16, 177–186.

Fattori, V., Hohmann, M., Rossaneis, A., Pinho-Ribeiro, F., Verri, W., 2016. "Capsaicin: current understanding of its mechanisms and therapy of pain and other pre-clinical and clinical uses". *Molecules* 21, 844.

Ferizi, M., Leonhardt, C., Meggle, C., Aneja, M.K., Rudolph, C., Plank, C., Rädler, J.O., 2015. "Stability analysis of chemically modified mRNA using micropattern-based single-cell arrays". *Lab Chip* 15, 3561–3571.

Fernández Fernández, E., Bangel-Ruland, N., Tomczak, K., Weber, W.-M., 2016a. "Optimization of CFTR-mRNA transfection in human nasal epithelial cells". *Transl. Med. Commun.* 1, 5.

Fernández Fernández, E., Santos-Carballal, B., de Santi, C., Ramsey, J., MacLoughlin, R., Cryan, S.-A., Greene, C., 2018. "Biopolymer-based nanoparticles for cystic fibrosis lung gene therapy studies". *Materials (Basel).* 11, 122.

Fernández Fernández, E., Santos-Carballal, B., Weber, W.-M., Goycoolea, F.M., 2016b. "Chitosan as a non-viral co-transfection system in a cystic fibrosis cell line.". *Int. J. Pharm.* 502, 1–9.

Ferreira, M.P.A., Ranjan, S., Kinnunen, S., Correia, A., Talman, V., Mäkilä, E., Barrios-Lopez, B., Kemell, M., Balasubramanian, V., Salonen, J., Hirvonen, J., Ruskoaho, H., Airaksinen, A.J., Santos, H.A., 2017. "Drug-loaded multifunctional nanoparticles targeted to the endocardial layer of the injured heart modulate hypertrophic signaling". *Small* 13, 1701276.

Feynman, R.P., 1960. "There's plenty of room at the bottom". *Eng. Sci.* 23, 22–36.

Florea, B.I., Thanou, M., Junginger, H.E., Borchard, G., 2006. "Enhancement of bronchial octreotide absorption by chitosan and N-trimethyl chitosan shows linear *in vitro/in vivo* correlation". *J. Control. Release* 110, 353–361.

Foldvari, M., Chen, D.W., Nafissi, N., Calderon, D., Narsineni, L., Rafiee, A., 2016. "Non-viral gene therapy: Gains and challenges of non-invasive administration methods". *J. Control. Release* 240, 165–190.

Foster, H.E., Lake, A.G., 2014. "Use of vanilloids in urologic disorders.". *Prog. drug Res.* 68, 307–17.

Freeman, E.C., Weiland, L.M., Meng, W.S., 2013. "Modeling the proton sponge hypothesis: examining proton sponge effectiveness for enhancing intracellular gene delivery through multiscale modeling". *J. Biomater. Sci. Polym. Ed.* 24, 398–416.

Fuchs, W., Larsen, E.H., Lindemann, B., 1977. "Current-voltage curve of sodium channels and concentration dependence of sodium permeability in frog skin". *J. Physiol.* 267, 137–166.

Funkhouser, J.D., Aronson, N.N., 2007. "Chitinase family GH18: evolutionary insights from the genomic history of a diverse protein family". *BMC Evol. Biol.* 7, 96.

G. de la Torre, B., Albericio, F., 2019. "The pharmaceutical industry in 2018. An analysis of FDA drug approvals from the perspective of molecules". *Molecules* 24, 809.

Gadsby, D.C., Vergani, P., Csanády, L., 2006. "The ABC protein turned chloride channel whose failure causes cystic fibrosis.". *Nature* 440, 477–83.

Ganta, S., Singh, A., Coleman, T.P., Williams, D., Amiji, M., 2014. "Pharmaceutical nanotechnology: overcoming drug delivery challenges in contemporary medicine", in: Nanomedicine. pp. 191–236.

Ganugula, R., Arora, M., Jaisamut, P., Wiwattanapatapee, R., Jørgensen, H.G., Venkatpurwar, V.P., Zhou, B., Rodrigues Hoffmann, A., Basu, R., Guo, S., Majeti, N.V.R.K., 2017. "Nano-curcumin safely prevents streptozotocin-induced inflammation and apoptosis in pancreatic beta cells for effective management of Type 1 diabetes mellitus". *Br. J. Pharmacol.* 174, 2074–2084.

Garibyan, L., Avashia, N., 2013. "Research techniques made simple: polymerase chain reaction (PCR)". *J Invest Dermatol* 133, e6.

Garland, A.L., Walton, W.G., Coakley, R.D., Tan, C.D., Gilmore, R.C., Hobbs, C.A., Tripathy, A., Clunes, L.A., Bencharit, S., Stutts, M.J., Betts, L., Redinbo, M.R., Tarran, R., 2013. "Molecular basis for pH-dependent mucosal dehydration in cystic fibrosis airways". *Proc. Natl. Acad. Sci.* 110, 15973–15978.

Garty, H., Palmer, L.G., 1997. "Epithelial sodium channels: function, structure, and regulation.". *Physiol. Rev.* 77, 359–96.

Gaspar, V.M., Sousa, F., Queiroz, J.A., Correia, I.J., 2011. "Formulation of chitosan–TPP–pDNA nanocapsules for gene therapy applications". *Nanotechnology* 22, 015101.

Gentzsch, M., Dang, H., Dang, Y., Garcia-Caballero, A., Suchindran, H., Boucher, R.C., Stutts, M.J., 2010. "The cystic fibrosis transmembrane conductance regulator impedes proteolytic stimulation of the epithelial Na^+ channel.". *J. Biol. Chem.* 285, 32227–32.

Gilmore, E.S., Stutts, M.J., Milgram, S.L., 2001. "Src family kinases mediate epithelial Na^+ channel inhibition by endothelin". *J. Biol. Chem.* 276, 42610–42617.

Ginn, S.L., Amaya, A.K., Alexander, I.E., Edelstein, M., Abedi, M.R., 2018. "Gene therapy clinical trials worldwide to 2017: An update". *J. Gene Med.* 20, e3015.

Gohil, K., 2015. "Pharmaceutical approval update.". *P T* 40, 567–568.

González-Espinosa, Y., Sabagh, B., Moldenhauer, E., Clarke, P., Goycoolea, F.M., 2019. "Characterisation of chitosan molecular weight distribution by multi-detection asymmetric flow-field flow fractionation (AF4) and SEC". *Int. J. Biol. Macromol.* 136, 911–919.

Gould, S.J., Subramani, S., 1988. "Firefly luciferase as a tool in molecular and cell biology". *Anal. Biochem.* 175, 5–13.

Goycoolea, F.M., Valle-Gallego, A., Stefani, R., Menchicchi, B., David, L., Rochas, C., Santander-Ortega, M.J., Alonso, M.J., 2012. "Chitosan-based nanocapsules: physical characterization, stability in biological media and capsaicin encapsulation". *Colloid Polym. Sci.* 290, 1423–1434.

Grenha, A., Al-Qadi, S., Seijo, B., Remuñán-López, C., 2010. "The potential of chitosan for pulmonary drug delivery". *J. Drug Deliv. Sci. Technol.* 20, 33–43.

Griesenbach, U., Kitson, C., Garcia, E.S., Farley, R., Singh, C., Somerton, L., Painter, H., Smith, R.L., Gill, D.R., Hyde, S.C., Chow, Y.-H., Hu, J., Gray, M., Edbrooke, M., Ogilvie, V., MacGregor, G., Scheule, R.K., Cheng, S.H., Caplen, N.J., Alton, E.W., 2006. "Inefficient cationic lipid-mediated siRNA and antisense oligonucleotide transfer to airway epithelial cells in vivo". *Respir. Res.* 7, 26.

Griesenbach, U., Pytel, K.M., Alton, E.W.F.W., 2015. "Cystic fibrosis gene therapy in the UK and elsewhere.". *Hum. Gene Ther.* 26, 266–75.

Gröhn, F., 2008. "Electrostatic self-assembly as route to supramolecular structures". *Macromol. Chem. Phys.* 209, 2295–2301.

Gruenert, D.C., Basbaum, C.B., Welsh, M.J., Li, M., Finkbeiner, W.E., Nadel, J.A., 1988. "Characterization of human tracheal epithelial cells transformed by an origin-defective simian virus 40.". *Proc. Natl. Acad. Sci. U. S. A.* 85, 5951–5.

Gruenert, D.C., Willems, M., Cassiman, J.J., Frizzell, R. a., 2004. "Established cell lines used in cystic fibrosis research". *J. Cyst. Fibros.* 3, 191–196.

Guggino, W.B., Stanton, B.A., 2006. "New insights into cystic fibrosis: molecular switches that regulate CFTR". *Nat. Rev. Mol. Cell Biol.* 7, 426–436.

Guo, P., Li, N., Fan, L., Lu, J., Liu, B., Zhang, B., Wu, Y., Liu, Z., Li, J., Pi, J., Qi, D., 2019. "Study of penetration mechanism of labrasol on rabbit cornea by Ussing chamber, RT-PCR assay, Western blot and immunohistochemistry". *Asian J. Pharm. Sci.* 14, 329–339.

Hahn, A., Salomon, J.J., Leitz, D., Feigenbutz, D., Korsch, L., Lisewski, I., Schrimpf, K., Millar-Büchner, P., Mall, M.A., Frings, S., Möhrlen, F., 2018. "Expression and function of Anoctamin 1/TMEM16A calcium-activated chloride channels in airways of *in vivo* mouse models for cystic fibrosis research". *Pflügers Arch. - Eur. J. Physiol.* 470, 1335–1348.

Hanukoglu, I., Hanukoglu, A., 2016. "Epithelial sodium channel (ENaC) family: phylogeny, structure–function, tissue distribution, and associated inherited diseases". *Gene* 579, 95–132.

Haq, I.J., Parameswaran, M.C., Abidin, N.Z., Socas, A., Gonzalez-Ciscar, A., Gardner, A.I., Brodlie, M., 2019. "Modulator therapies for cystic fibrosis". *Paediatr. Child Health (Oxford).* 29, 151–157.

Haque, A.K.M.A., Dewerth, A., Antony, J.S., Riethmüller, J., Schweizer, G.R., Weinmann, P., Latifi, N., Yasar, H., Pedemonte, N., Sondo, E., Weidensee, B., Ralhan, A., Laval, J., Schlegel, P., Seitz, C., Loretz, B., Lehr, C.-M., Handgretinger, R., Kormann, M.S.D., 2018. "Chemically modified hCFTR mRNAs recuperate lung function in a mouse model of cystic fibrosis". *Sci. Rep.* 8, 16776.

Harrison, F., 2007. "Microbial ecology of the cystic fibrosis lung". *Microbiology* 153, 917–923.

Heffell, Q., Turko, A.J., Wright, P.A., 2018. "Plasticity of skin water permeability and skin thickness in the amphibious mangrove rivulus *Kryptolebias marmoratus*". *J. Comp. Physiol. B* 188, 305–314.

Hobbs, C.A., Da Tan, C., Tarran, R., 2013. "Does epithelial sodium channel hyperactivity contribute to cystic fibrosis lung disease?". *J. Physiol.* 591, 4377–87.

Hollenhorst, M.I., Richter, K., Fronius, M., 2011. "Ion transport by pulmonary epithelia". *J. Biomed. Biotechnol.* 2011, 174306.

Holzer, P., Lippe, I.T., 1988. "Stimulation of afferent nerve endings by intragastric capsaicin protects against ethanol-induced damage of gastric mucosa". *Neuroscience* 27, 981–987.

Hong, K.U., Reynolds, S.D., Watkins, S., Fuchs, E., Stripp, B.R., 2004. "*In vivo* differentiation potential of tracheal basal cells: evidence for multipotent and unipotent subpopulations". *Am. J. Physiol. Cell. Mol. Physiol.* 286, L643–L649.

Huang, M., Fong, C.W., Khor, E., Lim, L.Y., 2005. "Transfection efficiency of chitosan vectors: effect of polymer molecular weight and degree of deacetylation". *J. Control. Release* 106, 391–406.

Huang, Y., Lapitsky, Y., 2011. "Monovalent salt enhances colloidal stability during the formation of chitosan/tripolyphosphate microgels". *Langmuir* 27, 10392–10399.

Hurley, M.N., McKeever, T.M., Prayle, A.P., Fogarty, A.W., Smyth, A.R., 2014. "Rate of improvement of CF life expectancy exceeds that of general population—observational death registration study". *J. Cyst. Fibros.* 13, 410–415.

Hwang, T.-C., Kirk, K.L., 2013. "The CFTR ion channel: gating, regulation, and anion permeation.". *Cold Spring Harb. Perspect. Med.* 3, a009498.

Ikpa, P.T., Bijvelds, M.J.C., de Jonge, H.R., 2014. "Cystic fibrosis: toward personalized therapies.". *Int. J. Biochem. Cell Biol.* 52, 192–200.

Immke, D.C., Gavva, N.R., 2006. "The TRPV1 receptor and nociception". *Semin. Cell Dev. Biol.* 17, 582–591.

Ishii, T., Okahata, Y., Sato, T., 2001. "Mechanism of cell transfection with plasmid/chitosan complexes.". *Biochim. Biophys. Acta* 1514, 51–64.

Jain, L., Chen, X.-J., Malik, B., Al-Khalili, O., Eaton, D.C., 1999. "Antisense oligonucleotides against the α-subunit of ENaC decrease lung epithelial cation-channel activity". *Am. J. Physiol. Cell. Mol. Physiol.* 276, L1046–L1051.

Jatzkewitz, H., 1955. "An ein kolloidales Blutplasma-Ersatzmittel (Polyvinylpyrrolidon) gebundenes Peptamin (Glycyl-L-leucyl-mezcalin) als neuartige Depotform für biologisch aktive primäre Amine (Mezcalin)". *Zeitschrift für Naturforsch. B* 10, 27–31.

Jeffery, P.K., 1983. "Morphologic features of airway surface epithelial cells and glands.". *Am. Rev. Respir. Dis.* 128, S14-20.

Ji, H.-L., Su, X.-F., Kedar, S., Li, J., Barbry, P., Smith, P.R., Matalon, S., Benos, D.J., 2006. "Delta-subunit confers novel biophysical features to alpha beta gamma-human epithelial sodium channel (ENaC) via a physical interaction.". *J. Biol. Chem.* 281, 8233–41.

Ji, H.L., Chalfant, M.L., Jovov, B., Lockhart, J.P., Parker, S.B., Fuller, C.M., Stanton, B.A., Benos, D.J., 2000. "The cytosolic termini of the beta- and gamma-ENaC subunits are involved in the functional interactions between cystic fibrosis transmembrane conductance regulator and epithelial sodium channel.". *J. Biol. Chem.* 275, 27947–56.

Jiang, H.-L., Kim, Y.-K., Arote, R., Nah, J.-W., Cho, M.-H., Choi, Y.-J., Akaike, T., Cho, C.-S., 2007. "Chitosan-graft-polyethylenimine as a gene carrier". *J. Control. Release* 117, 273–280.

Johnson, L.G., Olsen, J.C., Sarkadi, B., Moore, K.L., Swanstrom, R., Boucher, R.C., 1992. "Efficiency of gene transfer for restoration of normal airway epithelial function in cystic fibrosis.". *Nat. Genet.* 2, 21–25.

Jonassen, H., Kjøniksen, A.L., Hiorth, M., 2012. "Effects of ionic strength on the size and compactness of chitosan nanoparticles". *Colloid Polym. Sci.* 290, 919–929.

Kaiser, M., Burek, M., Britz, S., Lankamp, F., Ketelhut, S., Kemper, B., Förster, C., Gorzelanny, C., Goycoolea, F.M., 2019. "The influence of capsaicin on the integrity of microvascular endothelial cell monolayers". *Int. J. Mol. Sci.* 20, 122.

Kaiser, M., Kirsch, B., Hauser, H., Schneider, D., Seuß-Baum, I., Goycoolea, F.M., 2015a. "*In vitro* and sensory evaluation of capsaicin-loaded nanoformulations". *PLoS One* 10, e0141017.

Kaiser, M., Pereira, S., Pohl, L., Ketelhut, S., Kemper, B., Gorzelanny, C., Galla, H.J., Moerschbacher, B.M., Goycoolea, F.M., 2015b. "Chitosan encapsulation modulates the effect of capsaicin on the tight junctions of MDCK cells". *Sci. Rep.* 5, 10048.

Kamei, S., Maruta, K., Fujikawa, H., Nohara, H., Ueno-Shuto, K., Tasaki, Y., Nakashima, R., Kawakami, T., Eto, Y., Suico, M.A., Suzuki, S., Gruenert, D.C., Li, J.-D., Kai, H., Shuto, T., 2019. "Integrative expression analysis identifies a novel interplay between CFTR and linc-SUMF1-2 that involves CF-associated gene dysregulation". *Biochem. Biophys. Res. Commun.* 509, 521–528.

Karagozlu, M.Z., 2014. "Anticancer effects of chitin and chitosan derivatives". *Adv. Food Nutr. Res.* 72, 215–225.

Kashlan, O.B., Kleyman, T.R., 2011. "ENaC structure and function in the wake of a resolved structure of a family member.". *Am. J. Physiol. Renal Physiol.* 301, F684-96.

Kastl, L., Isbach, M., Dirksen, D., Schnekenburger, J., Kemper, B., 2017. "Quantitative phase imaging for cell culture quality control". *Cytom. Part A* 91, 470–481.

Kawami, M., Honda, N., Miyamoto, M., Yumoto, R., Takano, M., 2019. "Reduced folate carrier-mediated methotrexate transport in human distal lung epithelial NCl-H441 cells". *J. Pharm. Pharmacol.* 71, 167–175.

Kean, T., Thanou, M., 2010. "Biodegradation, biodistribution and toxicity of chitosan.". *Adv. Drug Deliv. Rev.* 62, 3–11.

Kellenberger, S., Gautschi, I., Schild, L., 2002. "An external site controls closing of the epithelial Na^+ channel ENaC". *J. Physiol.* 543, 413–424.

Kelly, M., Trudel, S., Brouillard, F., Bouillaud, F., Colas, J., Nguyen-Khoa, T., Ollero, M., Edelman, A., Fritsch, J., 2010. "Cystic fibrosis transmembrane regulator inhibitors CFTR(inh)-172 and GlyH-101 target mitochondrial functions, independently of chloride channel inhibition.". *J. Pharmacol. Exp. Ther.* 333, 60–9.

Keogh, R.H., Szczesniak, R., Taylor-Robinson, D., Bilton, D., 2018. "Up-to-date and projected estimates of survival for people with cystic fibrosis using baseline characteristics: a longitudinal study using UK patient registry data". *J. Cyst. Fibros.* 17, 218–227.

Kerem, B.S., Rommens, J.M., Buchanan, J.A., Markiewicz, D., Cox, T.K., Chakravarti, A., Buchwald, M., Tsui, L.C., 1989. "Identification of the cystic fibrosis gene: genetic analysis". *Science* 245, 1073–80.

Kim, C.-S., Kawada, T., Kim, B.-S., Han, I.-S., Choe, S.-Y., Kurata, T., Yu, R., 2003. "Capsaicin exhibits anti-inflammatory property by inhibiting IkB-a degradation in LPS-stimulated peritoneal macrophages". *Cell. Signal.* 15, 299–306.

Kleyman, T.R., Carattino, M.D., Hughey, R.P., 2009. "ENaC at the cutting edge: regulation of epithelial sodium channels by proteases.". *J. Biol. Chem.* 284, 20447–51.

Klimova, B., Kuca, K., Novotny, M., Maresova, P., 2017. "Cystic fibrosis revisited – a review study". *Med. Chem. (Los. Angeles).* 13, 102–109.

Kmit, A., Marson, F.A.L., Pereira, S.V.-N., Vinagre, A.M., Leite, G.S., Servidoni, M.F., Ribeiro, J.D., Ribeiro, A.F., Bertuzzo, C.S., Amaral, M.D., 2019. "Extent of rescue of F508del-CFTR function by VX-809 and VX-770 in human nasal epithelial cells correlates with SNP rs7512462 in SLC26A9 gene in F508del/F508del cystic fibrosis patients". *Biochim. Biophys. Acta - Mol. Basis Dis.* 1865, 1323–1331.

Kolonko, A.K., 2016. "Evaluation of chitosan for CFTR-mRNA application in human airway epithelial cells". *Master's thesis;* University of Münster.

Kolonko, A.K., Fernández Fernández, E., Santos-Carballal, B., Goycoolea, F.M., Weber, W.-M., 2016. "Functional restoring of defect CFTR by transfection of CFTR- mRNA using chitosan". *JSM Genet Genomics* 3, 1016.

Kolte, A., Patil, S., Lesimple, P., Hanrahan, J.W., Misra, A., 2017. "PEGylated composite nanoparticles of PLGA and polyethylenimine for safe and efficient delivery of pDNA to lungs". *Int. J. Pharm.* 524, 382–396.

König, J., Schreiber, R., Voelcker, T., Mall, M., Kunzelmann, K., 2001. "The cystic fibrosis transmembrane conductance regulator (CFTR) inhibits ENaC through an increase in the intracellular Cl^- concentration". *EMBO Rep.* 2, 1047–1051.

Kou, L., Sun, J., Zhai, Y., He, Z., 2013. "The endocytosis and intracellular fate of nanomedicines: implication for rational design". *Asian J. Pharm. Sci.* 8, 1–10.

Kowalski, P.S., Rudra, A., Miao, L., Anderson, D.G., 2019. "Delivering the messenger: advances in technologies for therapeutic mRNA delivery". *Mol. Ther.* 27, 710–728.

Kuhn, A., Beißert, T., Simon, P., Vallazza, B., Buck, J., P. Davies, B., Tureci, O., Sahin, U., 2012. "mRNA as a versatile tool for exogenous protein expression". *Curr. Gene Ther.* 12, 347–361.

Kunzelmann, K., 2003. "ENaC is inhibited by an increase in the intracellular Cl^- concentration mediated through activation of Cl^- channels". *Pflugers Arch. Eur. J. Physiol.* 445, 504.

Kunzelmann, K., Kiser, G.., Schreiber, R., Riordan, J.., 1997. "Inhibition of epithelial Na^+ currents by intracellular domains of the cystic fibrosis transmembrane conductance regulator". *FEBS Lett.* 400, 341–344.

Kurreck, J., 2003. "Antisense technologies. Improvement through novel chemical modifications". *Eur. J. Biochem.* 270, 1628–1644.

Laemmli, U.K., 1970. "Cleavage of structural proteins during the assembly of the head of bacteriophage T4.". *Nature* 227, 680–685.

Lee, L.-Y., Gu, Q., 2009. "Role of TRPV1 in inflammation-induced airway hypersensitivity". *Curr. Opin. Pharmacol.* 9, 243–249.

Lee, M., Nah, J.-W., Kwon, Y., Koh, J.J., Ko, K.S., Kim, S.W., 2001. "Water-soluble and low molecular weight chitosan-based plasmid DNA delivery". *Pharm. Res.* 18, 427–431.

Lee, R.J., Foskett, J.K., 2014. "Ca^{2+} signaling and fluid secretion by secretory cells of the airway epithelium.". *Cell Calcium* 55, 325–36.

Lee, S.J., Yook, S., Yhee, J.Y., Yoon, H.Y., Kim, M.-G., Ku, S.H., Kim, S.H., Park, J.H., Jeong, J.H., Kwon, I.C., Lee, S., Lee, H., Kim, K., 2015. "Co-delivery of VEGF and Bcl-2 dual-targeted siRNA polymer using a single nanoparticle for synergistic anti-cancer effects *in vivo*". *J. Control. Release* 220, 631–641.

Letchford, K., 2007. "A review of the formation and classification of amphiphilic block copolymer nanoparticulate structures: micelles, nanospheres, nanocapsules and polymersomes". *Eur. J. Pharm. Biopharm.* 65, 259–269.

Leung, F.W., 2014. "Capsaicin as an anti-obesity drug", in: Capsaicin as a Therapeutic Molecule. Springer Basel, Basel, pp. 171–179.

Lewinski, N., Colvin, V., Drezek, R., 2008. "Cytotoxicity of nanoparticles". *Small* 4, 26–49.

Li, L., Wang, F., Wei, X., Liang, Y., Cui, Y., Gao, F., Zhong, J., Pu, Y., Zhao, Y., Yan, Z., Arendshorst, W.J., Nilius, B., Chen, J., Liu, D., Zhu, Z., 2014. "Transient receptor potential vanilloid 1 activation by dietary capsaicin promotes urinary sodium excretion by inhibiting epithelial sodium channel α subunit–mediated sodium reabsorption". *Hypertension* 64, 397–404.

Li, S., Rizzo, M., Bhattacharya, S., Huang, L., 1998. "Characterization of cationic lipid-protamine–DNA (LPD) complexes for intravenous gene delivery". *Gene Ther.* 5, 930–937.

Liang, X., Potter, J., Kumar, S., Zou, Y., Quintanilla, R., Sridharan, M., Carte, J., Chen, W., Roark, N., Ranganathan, S., Ravinder, N., Chesnut, J.D., 2015. "Rapid and highly efficient mammalian cell engineering via Cas9 protein transfection". *J. Biotechnol.* 208, 44–53.

Lim, S., Forbes, B., Martin, G., Brown, M., 2001. "*In vivo* and *in vitro* characterization of novel microparticulates based on hyaluronan and chitosan hydroglutamate". *AAPS PharmSciTech* 2, 1–12.

Lisakowski, V.B., Füchtbauer, A.C., Füchtbauer, E.-M., 2018. "Optimized co-transfection of murine embryonic stem cells". *Transgenic Res.* 27, 131–133.

Liu, Y., Miyoshi, H., Nakamura, M., 2007. "Nanomedicine for drug delivery and imaging: a promising avenue for cancer therapy and diagnosis using targeted functional nanoparticles". *Int. J. Cancer* 120, 2527–2537.

Loffing, J., Schild, L., 2005. "Functional domains of the epithelial sodium channel.". *J. Am. Soc. Nephrol.* 16, 3175–81.

López-Montilla, J.C., Herrera-Morales, P.E., Pandey, S., Shah, D.O., 2002. "Spontaneous emulsification: mechanisms, physicochemical aspects, modeling, and applications". *J. Dispers. Sci. Technol.* 23, 219–268.

Lozić, I., Hartz, R.V., Bartlett, C.A., Shaw, J.A., Archer, M., Naidu, P.S.R., Smith, N.M., Dunlop, S.A., Iyer, K.S., Kilburn, M.R., Fitzgerald, M., 2016. "Enabling dual cellular destinations of polymeric nanoparticles for treatment following partial injury to the central nervous system". *Biomaterials* 74, 200–216.

Lu, C., Jiang, C., Pribanic, S., Rotin, D., 2007. "CFTR stabilizes ENaC at the plasma membrane". *J. Cyst. Fibros.* 6, 419–422.

Lundstrom, K., Boulikas, T., 2003. "Viral and non-viral vectors in gene therapy: technology development and clinical trials". *Technol. Cancer Res. Treat.* 2, 471–485.

Lv, H., Zhang, S., Wang, B., Cui, S., Yan, J., 2006. "Toxicity of cationic lipids and cationic polymers in gene delivery". *J. Control. Release* 114, 100–109.

MacRobbie, E.A.C., Ussing, H.H., 1961. "Osmotic behaviour of the epithelial cells of frog skin". *Acta Physiol. Scand.* 53, 348–365.

Maji, A.K., Banerji, P., 2016. "Phytochemistry and gastrointestinal benefits of the medicinal spice, *Capsicum annuum L.* (chilli): a review". *J. Complement. Integr. Med.* 13, 97–122.

Makrane, H., Aziz, M., Mekhfi, H., Ziyyat, A., Legssyer, A., Melhaoui, A., Berrabah, M., Bnouham, M., Alem, C., Elombo, F.K., Gressier, B., Desjeux, J.-F., Eto, B., 2019. "Origanum majorana L. extract exhibit positive cooperative effects on the main mechanisms involved in acute infectious diarrhea". *J. Ethnopharmacol.* 239, 111503.

Manjunatha, H., Srinivasan, K., 2007. "Hypolipidemic and antioxidant effects of dietary curcumin and capsaicin in induced hypercholesterolemic rats". *Lipids* 42, 1133–1142.

Mansouri, S., Cuie, Y., Winnik, F., Shi, Q., Lavigne, P., Benderdour, M., Beaumont, E., Fernandes, J.C., 2006. "Characterization of folate-chitosan-DNA nanoparticles for gene therapy". *Biomaterials* 27, 2060–2065.

Mao, H.Q., Roy, K., Troung-Le, V.L., Janes, K.A., Lin, K.Y., Wang, Y., August, J.T., Leong, K.W., 2001. "Chitosan-DNA nanoparticles as gene carriers: synthesis, characterization and transfection efficiency.". *J. Control. Release* 70, 399–421.

Mao, S., Sun, W., Kissel, T., 2010. "Chitosan-based formulations for delivery of DNA and siRNA.". *Adv. Drug Deliv. Rev.* 62, 12–27.

Marcianes, P., Negro, S., García-García, L., Montejo, C., Barcia, E., Fernández-Carballido, A., 2017. "Surface-modified gatifloxacin nanoparticles with potential for treating central nervous system tuberculosis.". *Int. J. Nanomedicine* 12, 1959–1968.

Marshall, B.C., Butler, S.M., Stoddard, M., Moran, A.M., Liou, T.G., Morgan, W.J., 2005. "Epidemiology of cystic fibrosis-related diabetes". *J. Pediatr.* 146, 681–687.

Marson, F.A.L., Bertuzzo, C.S., Ribeiro, J.D., 2016. "Classification of CFTR mutation classes.". *Lancet. Respir. Med.* 4, e37–e38.

Martin, B., Sainlos, M., Aissaoui, A., Oudrhiri, N., Hauchecorne, M., Vigneron, J.-, Lehn, J.-, Lehn, P., 2005. "The design of cationic lipids for gene delivery". *Curr. Pharm. Des.* 11, 375–394.

Martin, T.R., 2005. "Innate immunity in the lungs". *Proc. Am. Thorac. Soc.* 2, 403–411.

Martins, A., Facchi, S., Follmann, H., Pereira, A., Rubira, A., Muniz, E., 2014. "Antimicrobial activity of chitosan derivatives containing N-quaternized moieties in its backbone: a review". *Int. J. Mol. Sci.* 15, 20800–20832.

McClements, D.J., 2015. "Nanoscale nutrient delivery systems for food applications: improving bioactive dispersibility, stability, and bioavailability". *J. Food Sci.* 80, N1602–N1611.

McGarvey, L.P., Butler, C.A., Stokesberry, S., Polley, L., McQuaid, S., Abdullah, H., Ashraf, S., McGahon, M.K., Curtis, T.M., Arron, J., Choy, D., Warke, T.J., Bradding, P., Ennis, M., Zholos, A., Costello, R.W., Heaney, L.G., 2014. "Increased expression of bronchial epithelial transient receptor potential vanilloid 1 channels in patients with severe asthma". *J. Allergy Clin. Immunol.* 133, 704-712.e4.

Menchicchi, B., Fuenzalida, J.P., Bobbili, K.B., Hensel, A., Swamy, M.J., Goycoolea, F.M., 2014. "Structure of chitosan determines its interactions with mucin". *Biomacromolecules* 15, 3550–3558.

Menchicchi, B., Fuenzalida, J.P., Hensel, A., Swamy, M.J., David, L., Rochas, C., Goycoolea, F.M., 2015. "Biophysical analysis of the molecular interactions between polysaccharides and mucin.". *Biomacromolecules* 16, 924–35.

Meyerholz, D.K., 2016. "Lessons learned from the cystic fibrosis pig.". *Theriogenology* 86, 427–32.

Mies, F., Virreira, M., Goolaerts, A., Djerbib, S., Beauwens, R., Shlyonsky, V., Boom, A., 2019. "DUOX1-mediated hydrogen peroxide release regulates sodium transport in H441 bronchiolar epithelial cells". *Acta Physiol.* 225, e13166.

Mir, M., Ishtiaq, S., Rabia, S., Khatoon, M., Zeb, A., Khan, G.M., ur Rehman, A., ud Din, F., 2017. "Nanotechnology: from *in vivo* imaging system to controlled drug delivery". *Nanoscale Res. Lett.* 12, 500.

Mirtajani, S., Farnia, Poopak, Hassanzad, M., Ghanavi, J., Farnia, Parissa, Velayati, A., 2017. "Geographical distribution of cystic fibrosis; the past 70 years of data analyzis". *Biomed. Biotechnol. Res. J.* 1, 105.

Molina, S.A., Stauffer, B., Moriarty, H.K., Kim, A.H., McCarty, N.A., Koval, M., 2015. "Junctional abnormalities in human airway epithelial cells expressing F508del CFTR". *Am. J. Physiol. Cell. Mol. Physiol.* 309, L475–L487.

Montesanto, S., Smithers, N.P., Bucchieri, F., Brucato, V., La Carrubba, V., Davies, D.E., Conforti, F., 2019. "Establishment of a pulmonary epithelial barrier on biodegradable poly-L-lactic-acid membranes". *PLoS One* 14, e0210830.

Montoro, D.T., Haber, A.L., Biton, M., Vinarsky, V., Lin, B., Birket, S.E., Yuan, F., Chen, S., Leung, H.M., Villoria, J., Rogel, N., Burgin, G., Tsankov, A.M., Waghray, A., Slyper, M., Waldman, J., Nguyen, L., Dionne, D., Rozenblatt-Rosen, O., Tata, P.R., Mou, H., Shivaraju, M., Bihler, H., Mense, M., Tearney, G.J., Rowe, S.M., Engelhardt, J.F., Regev, A., Rajagopal, J., 2018. "A revised airway epithelial hierarchy includes CFTR-expressing ionocytes". *Nature* 560, 319–324.

Moore, P.J., Tarran, R., 2018. "The epithelial sodium channel (ENaC) as a therapeutic target for cystic fibrosis lung disease". *Expert Opin. Ther. Targets* 22, 687–701.

Mora-Huertas, C.E., Fessi, H., Elaissari, A., 2010. "Polymer-based nanocapsules for drug delivery". *Int. J. Pharm.* 385, 113–142.

Moran, O., 2017. "The gating of the CFTR channel". *Cell. Mol. Life Sci.* 74, 85–92.

Mosmann, T., 1983. "Rapid colorimetric assay for cellular growth and survival: application to proliferation and cytotoxicity assays". *J. Immunol. Methods* 65, 55–63.

Mroz, M.S., Harvey, B.J., 2019. "Ursodeoxycholic acid inhibits ENaC and Na/K pump activity to restore airway surface liquid height in cystic fibrosis bronchial epithelial cells". *Steroids* 151, 108461.

Mullis, K.B., 1990. "The unusual origin of the polymerase chain reaction". *Sci. Am.* 262, 56–65.

Mumper, R.J., Wang, J., Claspell, J.M., Rolland, A.P., 1995. "Novel polymeric condensing carriers for gene delivery". *Proc. Control. Release Soc.* 22, 178.

Murgia, X., Yasar, H., Carvalho-Wodarz, C., Gordon, S., Schwarzkopf, K., 2017. "Modelling the bronchial barrier in pulmonary drug delivery: a human bronchial epithelial cell line supplemented with human tracheal mucus". *Eur. J. Pharm. Biopharm.* 118, 79–88.

Myerburg, M.M., King, J.D., Oyster, N.M., Fitch, A.C., Magill, A., Baty, C.J., Watkins, S.C., Kolls, J.K., Pilewski, J.M., Hallows, K.R., 2010. "AMPK agonists ameliorate sodium and fluid transport and inflammation in cystic fibrosis airway epithelial cells". *Am. J. Respir. Cell Mol. Biol.* 42, 676–684.

Naehrig, S., Chao, C.-M., Naehrlich, L., 2017. "Cystic fibrosis.". *Dtsch. Arztebl. Int.* 114, 564–574.

Nafee, N., Taetz, S., Schneider, M., Schaefer, U.F., Lehr, C.-M., 2007. "Chitosan-coated PLGA nanoparticles for DNA/RNA delivery: effect of the formulation parameters on complexation and transfection of antisense oligonucleotides". *Nanomedicine* 3, 173–183.

Nagel, G., Barbry, P., Chabot, H., Brochiero, E., Hartung, K., Grygorczyk, R., 2005. "CFTR fails to inhibit the epithelial sodium channel ENaC expressed in *Xenopus laevis* oocytes". *J. Physiol.* 564, 671–682.

Natrajan, D., Srinivasan, S., Sundar, K., Ravindran, A., 2015. "Formulation of essential oil-loaded chitosan–alginate nanocapsules". *J. Food Drug Anal.* 23, 560–568.

Nevitt, S.J., Thornton, J., Murray, C.S., Dwyer, T., 2018. "Inhaled mannitol for cystic fibrosis". *Cochrane Database Syst. Rev.* 2, CD008649.

Ngo, D.-H., 2014. "Antioxidant effects of chitin, chitosan, and their derivatives". *Adv. Food Nutr. Res.* 73, 15–31.

Nidhin, M., Indumathy, R., Sreeram, K.J., Nair, B.U., 2008. "Synthesis of iron oxide nanoparticles of narrow size distribution on polysaccharide templates". *Bull. Mater. Sci.* 31, 93–96.

O'Sullivan, B.P., Freedman, S.D., 2009. "Cystic fibrosis.". *Lancet* 373, 1891–904.

Olivença, D. V., Fonseca, L.L., Voit, E.O., Pinto, F.R., 2019. "Thickness of the airway surface liquid layer in the lung is affected in cystic fibrosis by compromised synergistic regulation of the ENaC ion channel". *J. R. Soc. Interface* 16, 20190187.

Patra, J.K., Das, G., Fernandes Fraceto, L., Vangelie, E., Campos, R., Del Pilar Rodriguez-Torres, M., Acosta-Torres, L.S., Armando Diaz-Torres, L., Grillo, R., Kumara Swamy, M., Sharma, S., Habtemariam, S., Shin, H.-S., 2018. "Nano based drug delivery systems: recent developments and future prospects". *J. Nanobiotechnology* 16, 71.

Pecora, R., 2000. "Dynamic light scattering measurement of nanometer particles in liquids". *J. Nanoparticle Res.* 2, 123–131.

Pedemonte, N., Lukacs, G.L., Du, K., Caci, E., Zegarra-Moran, O., Galietta, L.J. V, Verkman, A.S., 2005. "Small-molecule correctors of defective DeltaF508-CFTR cellular processing identified by high-throughput screening.". *J. Clin. Invest.* 115, 2564–71.

Pezzoli, D., Giupponi, E., Mantovani, D., Candiani, G., 2017. "Size matters for *in vitro* gene delivery: investigating the relationships among complexation protocol, transfection medium, size and sedimentation". *Sci. Rep.* 7, 44134.

Pittman, J.E., Ferkol, T.W., 2015. "The evolution of cystic fibrosis care.". *Chest* 148, 533–42.

Plasschaert, L.W., Žilionis, R., Choo-Wing, R., Savova, V., Knehr, J., Roma, G., Klein, A.M., Jaffe, A.B., 2018. "A single-cell atlas of the airway epithelium reveals the CFTR-rich pulmonary ionocyte". *Nature* 560, 377–381.

Pranke, I., Golec, A., Hinzpeter, A., Edelman, A., Sermet-Gaudelus, I., 2019. "Emerging therapeutic approaches for cystic fibrosis. From gene editing to personalized medicine". *Front. Pharmacol.* 10, 121.

Prego, C., García, M., Torres, D., Alonso, M.J., 2005. "Transmucosal macromolecular drug delivery". *J. Control. Release* 101, 151–162.

Prego, C., Torres, D., Alonso, M.J., 2006. "Chitosan nanocapsules: a new carrier for nasal peptide delivery". *J. Drug Deliv. Sci. Technol.* 16, 331–337.

Prulière-Escabasse, V., Planès, C., Escudier, E., Fanen, P., Coste, A., Clerici, C., 2007. "Modulation of epithelial sodium channel trafficking and function by sodium 4-phenylbutyrate in human nasal epithelial cells.". *J. Biol. Chem.* 282, 34048–57.

Puglia, M., Landi, C., Gagliardi, A., Breslin, L., Armini, A., Brunetti, J., Pini, A., Bianchi, L., Bini, L., 2018. "The proteome speciation of an immortalized cystic fibrosis cell line: new perspectives on the pathophysiology of the disease". *J. Proteomics* 170, 28–42.

Puras, G., Zarate, J., Aceves, M., Murua, A., Díaz, A.R., Avilés-Triguero, M., Fernández, E., Pedraz, J.L., 2013. "Low molecular weight oligochitosans for non-viral retinal gene therapy". *Eur. J. Pharm. Biopharm.* 83, 131–140.

Rackley, C.R., Stripp, B.R., 2012. "Building and maintaining the epithelium of the lung". *J. Clin. Invest.* 122, 2724–2730.

Ramalho, A.S., Beck, S., Meyer, M., Penque, D., Cutting, G.R., Amaral, M.D., 2002. "Five percent of normal cystic fibrosis transmembrane conductance regulator mRNA ameliorates the severity of pulmonary disease in cystic fibrosis". *Am. J. Respir. Cell Mol. Biol.* 27, 619–627.

Ramesh kumar, D., Elumalai, R., Raichur, A.M., Sanjuktha, M., Rajan, J.J., Alavandi, S.V., Vijayan, K.K., Poornima, M., Santiago, T.C., 2016. "Development of antiviral gene therapy for Monodon baculovirus using dsRNA loaded chitosan-dextran sulfate nanocapsule delivery system in *Penaeus monodon* post-larvae". *Antiviral Res.* 131, 124–130.

Ramminger, S.J., Richard, K., Inglis, S.K., Land, S.C., Olver, R.E., Wilson, S.M., 2004. "A regulated apical Na^+ conductance in dexamethasone-treated H441 airway epithelial cells". *Am. J. Physiol. Cell. Mol. Physiol.* 287, L411–L419.

Randell, S.H., Boucher, R.C., 2006. "Effective mucus clearance is essential for respiratory health". *Am. J. Respir. Cell Mol. Biol.* 35, 20–28.

Ranjbar, B., Gill, P., 2009. "Circular dichroism techniques: biomolecular and nanostructural analyses - a review". *Chem. Biol. Drug Des.* 74, 101–120.

Ratjen, F., Döring, G., 2003. "Cystic fibrosis". *Lancet* 361, 681–689.

Ratjen, F., Durham, T., Navratil, T., Schaberg, A., Accurso, F.J., Wainwright, C., Barnes, M., Moss, R.B., TIGER-2 Study Investigator Group, 2012. "Long term effects of denufosol tetrasodium in patients with cystic fibrosis". *J. Cyst. Fibros.* 11, 539–549.

Ravi Kumar, M.N.., 2000. "A review of chitin and chitosan applications". *React. Funct. Polym.* 46, 1–27.

Reece, E., Doyle, S., Greally, P., Renwick, J., McClean, S., 2018. "*Aspergillus fumigatus* inhibits *Pseudomonas aeruginosa* in co-culture: implications of a mutually antagonistic relationship on virulence and inflammation in the CF airway". *Front. Microbiol.* 9, 1205.

Reilly, C.A., Johansen, M.E., Lanza, D.L., Lee, J., Lim, J.-O., Yost, G.S., 2005. "Calcium-dependent and independent mechanisms of capsaicin receptor (TRPV1)-mediated cytokine production and cell death in human bronchial epithelial cells". *J. Biochem. Mol. Toxicol.* 19, 266–275.

Reilly, C.A., Taylor, J.L., Lanza, D.L., Carr, B.A., Crouch, D.J., Yost, G.S., 2003. "Capsaicinoids cause inflammation and epithelial cell death through activation of vanilloid receptors". *Toxicol. Sci.* 73, 170–181.

Reis, C.P., Damgé, C., 2012. "Nanotechnology as a promising strategy for alternative routes of insulin delivery". *Methods Enzymol.* 508, 271–294.

Ren, C.L., Morgan, R.L., Oermann, C., Resnick, H.E., Brady, C., Campbell, A., DeNagel, R., Guill, M., Hoag, J., Lipton, A., Newton, T., Peters, S., Willey-Courand, D.B., Naureckas, E.T., 2018. "Cystic fibrosis foundation pulmonary guidelines. Use of cystic fibrosis transmembrane conductance regulator modulator therapy in patients with cystic fibrosis". *Ann. Am. Thorac. Soc.* 15, 271–280.

Rezaee, F., Georas, S.N., 2014. "Breaking barriers: new insights into airway epithelial barrier function in health and disease". *Am. J. Respir. Cell Mol. Biol.* 50, 857–869.

Richard, I., Thibault, M., De Crescenzo, G., Buschmann, M.D., Lavertu, M., 2013. "Ionization behavior of chitosan and chitosan–DNA polyplexes indicate that chitosan has a similar capability to induce a proton-dponge effect as PEI". *Biomacromolecules* 14, 1732–1740.

Riedl, S., Kaiser, P., Raup, A., Synatschke, C., Jérôme, V., Freitag, R., 2018. "Non-viral transfection of human T lymphocytes". *Processes* 6, 188.

Rinaldi, C., Wood, M.J.A., 2018. "Antisense oligonucleotides: the next frontier for treatment of neurological disorders". *Nat. Rev. Neurol.* 14, 9–21.

Rinaudo, M., 2006. "Chitin and chitosan: properties and applications". *Prog. Polym. Sci.* 31, 603–632.

Riordan, J.R., Rommens, J.M., Kerem, B., Alon, N., Rozmahel, R., Grzelczak, Z., Zielenski, J., Lok, S., Plavsic, N., Chou, J.L., 1989. "Identification of the cystic fibrosis gene: cloning and characterization of complementary DNA.". *Science* 245, 1066–73.

Robinson, E., MacDonald, K.D., Slaughter, K., McKinney, M., Patel, S., Sun, C., Sahay, G., 2018. "Lipid nanoparticle-delivered chemically modified mRNA restores chloride secretion in cystic fibrosis". *Mol. Ther.* 26, 2034–2046.

Rodgers, H.C., Knox, A.J., 2001. "Pharmacological treatment of the biochemical defect in cystic fibrosis airways.". *Eur. Respir. J.* 17, 1314–21.

Roesch, E.A., Nichols, D.P., Chmiel, J.F., 2018. "Inflammation in cystic fibrosis: an update". *Pediatr. Pulmonol.* 53, S30–S50.

Rommens, J., Iannuzzi, M., Kerem, B., Drumm, M., Melmer, G., Dean, M., Rozmahel, R., Cole, J., Kennedy, D., Hidaka, N., Et, A., 1989. "Identification of the cystic fibrosis gene: chromosome walking and jumping". *Science* 245, 1059–1065.

Ross, R.A., 2003. "Anandamide and vanilloid TRPV1 receptors". *Br. J. Pharmacol.* 140, 790–801.

Rossier, B.C., 2014. "Epithelial sodium channel (ENaC) and the control of blood pressure". *Curr. Opin. Pharmacol.* 15, 33–46.

Rowe, S.M., Miller, S., Sorscher, E.J., 2005. "Cystic fibrosis". *N. Engl. J. Med.* 352, 1992–2001.

Rubenstein, R.C., Lockwood, S.R., Lide, E., Bauer, R., Suaud, L., Grumbach, Y., 2011. "Regulation of endogenous ENaC functional expression by CFTR and ΔF508-CFTR in airway epithelial cells". *Am. J. Physiol. Cell. Mol. Physiol.* 300, L88–L101.

Sagel, S.D., Chmiel, J.F., Konstan, M.W., 2007. "Sputum biomarkers of inflammation in cystic fibrosis lung disease". *Proc. Am. Thorac. Soc.* 4, 406–417.

Sahin, U., Karikó, K., Türeci, Ö., 2014. "mRNA-based therapeutics — developing a new class of drugs". *Nat. Rev. Drug Discov.* 13, 759–780.

Salomon, J.J., Muchitsch, V.E., Gausterer, J.C., Schwagerus, E., Huwer, H., Daum, N., Lehr, C.M., Ehrhardt, C., 2014. "The cell line NCl-H441 is a useful *in vitro* model for transport studies of human distal lung epithelial barrier". *Mol. Pharm.* 11, 995–1006.

Sanders, N., Rudolph, C., Braeckmans, K., De Smedt, S.C., Demeester, J., 2009. "Extracellular barriers in respiratory gene therapy". *Adv. Drug Deliv. Rev.* 61, 115–127.

Sanders, N.N., De Smedt, S.C., Van Rompaey, E., Simoens, P., De Baets, F., Demeester, J., 2000. "Cystic fibrosis sputum". *Am. J. Respir. Crit. Care Med.* 162, 1905–1911.

Sang Yoo, H., Eun Lee, J., Chung, H., Chan Kwon, I., Young Jeong, S., 2005. "Self-assembled nanoparticles containing hydrophobically modified glycol chitosan for gene delivery". *J. Control. Release* 103, 235–243.

Santoro, A., Ciaglia, E., Nicolin, V., Pescatore, A., Prota, L., Capunzo, M., Ursini, M. V., Nori, S.L., Bifulco, M., 2018. "The isoprenoid end product N6-isopentenyladenosine reduces inflammatory response through the inhibition of the NFκB and STAT3 pathways in cystic fibrosis cells". *Inflamm. Res.* 67, 315–326.

Santos-Carballal, B., Aaldering, L.J., Ritzefeld, M., Pereira, S., Sewald, N., Moerschbacher, B.M., Götte, M., Goycoolea, F.M., 2015. "Physicochemical and biological characterization of chitosan-microRNA nanocomplexes for gene delivery to MCF-7 breast cancer cells.". *Sci. Rep.* 5, 13567.

Santos-Carballal, B., Fernández, E.F., Goycoolea, F.M., 2018. "Chitosan in non-viral gene delivery: role of structure, characterization methods, and insights in cancer and rare diseases therapies". *Polymers (Basel).* 10, 1–51.

Sato, T., Ishii, T., Okahata, Y., 2001. "*In vitro* gene delivery mediated by chitosan. Effect of pH, serum, and molecular mass of chitosan on the transfection efficiency". *Biomaterials* 22, 2075–80.

Sawtarie, N., Cai, Y., Lapitsky, Y., 2017. "Preparation of chitosan/tripolyphosphate nanoparticles with highly tunable size and low polydispersity". *Colloids Surfaces B Biointerfaces* 157, 110–117.

Sayegh, R., Auerbach, S.D., Li, X., Loftus, R.W., Husted, R.F., Stokes, J.B., Thomas, C.P., 1999. "Glucocorticoid induction of epithelial sodium channel expression in lung and renal epithelia occurs via trans-activation of a hormone response element in the 5'-flanking region of the human epithelial sodium channel alpha subunit gene.". *J. Biol. Chem.* 274, 12431–7.

Schild, L., 2010. "The epithelial sodium channel and the control of sodium balance". *Biochim. Biophys. Acta - Mol. Basis Dis.* 1802, 1159–1165.

Schmidt, M.C., Peter, H., Lang, S.R., Ditzinger, G., Merkle, H.P., 1998. "*In vitro* cell models to study nasal mucosal permeability and metabolism". *Adv. Drug Deliv. Rev.* 29, 51–79.

Schmitz, C., Auza, L.G., Koberidze, D., Rasche, S., Fischer, R., Bortesi, L., 2019. "Conversion of chitin to defined chitosan oligomers: current status and future prospects". *Mar. Drugs* 17, 452.

Schuster, B.S., Kim, A.J., Kays, J.C., Kanzawa, M.M., Guggino, W.B., Boyle, M.P., Rowe, S.M., Muzyczka, N., Suk, J.S., Hanes, J., 2014. "Overcoming the cystic fibrosis sputum barrier to leading adeno-associated virus gene therapy vectors". *Mol. Ther.* 22, 1484–1493.

Schwiebert, E.M., Egan, M.E., Hwang, T.-H., Fulmer, S.B., Allen, S.S., Cutting, G.R., Guggino, W.B., 1995. "CFTR regulates outwardly rectifying chloride channels through an autocrine mechanism involving ATP". *Cell* 81, 1063–1073.

Scott, V., Clark, A.R., Docherty, K., 1994. "The gel retardation assay", in: Protocols for Gene Analysis. Humana Press, New Jersey, pp. 339–348.

Segal, A., Van Driessche, W., Weber, W.-M., 2002. "Specific effects of antisense oligonucleotides on ENaC expressed in *Xenopus laevis* oocytes". *Pflugers Arch.* 443, 228.

Seki, N., Shirasaki, H., Kikuchi, M., Sakamoto, T., Watanabe, N., Himi, T., 2006. "Expression and localization of TRPV1 in human nasal mucosa". *Rhinology* 44, 128–34.

Semaniakou, A., Croll, R.P., Chappe, V., 2018. "Animal models in the pathophysiology of cystic fibrosis.". *Front. Pharmacol.* 9, 1475.

Sharma, N., Evans, T.A., Pellicore, M.J., Davis, E., Aksit, M.A., McCague, A.F., Joynt, A.T., Lu, Z., Han, S.T., Anzmann, A.F., Lam, A.-T.N., Thaxton, A., West, N., Merlo, C., Gottschalk, L.B., Raraigh, K.S., Sosnay, P.R., Cotton, C.U., Cutting, G.R., 2018. "Capitalizing on the heterogeneous effects of CFTR nonsense and frameshift variants to inform therapeutic strategy for cystic fibrosis". *PLOS Genet.* 14, e1007723.

Sheng, S., McNulty, K.A., Harvey, J.M., Kleyman, T.R., 2001. "Second transmembrane domains of ENaC subunits contribute to ion permeation and selectivity.". *J. Biol. Chem.* 276, 44091–8.

Sheppard, D.N., Welsh, M.J., 1999. "Structure and function of the CFTR chloride channel.". *Physiol. Rev.* 79, S23–S45.

Shiobara, T., Usui, T., Han, J., Isoda, H., Nagumo, Y., 2013. "The reversible increase in tight junction permeability induced by capsaicin is mediated via cofilin-actin cytoskeletal dynamics and decreased level of occludin". *PLoS One* 8, e79954.

Singare, D.S., Marella, S., Gowthamrajan, K., Kulkarni, G.T., Vooturi, R., Rao, P.S., 2010. "Optimization of formulation and process variable of nanosuspension: an industrial perspective". *Int. J. Pharm.* 402, 213–220.

Smith, J., Wood, E., Dornish, M., 2004. "Effect of chitosan on epithelial cell tight junctions.". *Pharm. Res.* 21, 43–9.

Smith, P.K., Krohn, R.I., Hermanson, G.T., Mallia, A.K., Gartner, F.H., Provenzano, M.D., Fujimoto, E.K., Goeke, N.M., Olson, B.J., Klenk, D.C., 1985. "Measurement of protein using bicinchoninic acid". *Anal. Biochem.* 150, 76–85.

Sobczak, K., Segal, A., Bangel-Ruland, N., Semmler, J., Van Driessche, W., Lindemann, H., Heermann, R., Weber, W.-M., 2009. "Specific inhibition of epithelial Na^+ channels by antisense oligonucleotides for the treatment of Na^+ hyperabsorption in cystic fibrosis". *J. Gene Med.* 11, 813–823.

Solomon, G.M., Marshall, S.G., Ramsey, B.W., Rowe, S.M., 2015. "Breakthrough therapies: cystic fibrosis (CF) potentiators and correctors". *Pediatr. Pulmonol.* 50, 3–13.

Soukup, B., Benjamin, A., Orogo-Wenn, M., Walters, D., 2012. "Physiological effect of protein kinase C on ENaC-mediated lung liquid regulation in the adult rat lung". *Am. J. Physiol. Cell. Mol. Physiol.* 302, L133–L139.

Sreekumar, S., Goycoolea, F.M., Moerschbacher, B.M., Rivera-Rodriguez, G.R., 2018. "Parameters influencing the size of chitosan-TPP nano-and microparticles". *Sci. Rep.* 8, 4695.

Stephenson, M.L., Zamecnik, P.C., 1978. "Inhibition of Rous sarcoma viral RNA translation by a specific oligodeoxyribonucleotide.". *Proc. Natl. Acad. Sci. U. S. A.* 75, 285–8.

Stoltz, D.A., Meyerholz, D.K., Welsh, M.J., 2015. "Origins of cystic fibrosis lung disease". *N. Engl. J. Med.* 372, 351–362.

Strandvik, B., 2010. "Fatty acid metabolism in cystic fibrosis". *Prostaglandins Leukot. Essent. Fat. Acids* 83, 121–9.

Stutts, M.J., Rossier, B.C., Boucher, R.C., 1997. "Cystic fibrosis transmembrane conductance regulator inverts protein kinase A-mediated regulation of epithelial sodium channel single channel kinetics.". *J. Biol. Chem.* 272, 14037–40.

Suffredini, G., East, J.E., Levy, L.M., 2014. "New applications of nanotechnology for neuroimaging". *Am. J. Neuroradiol.* 35, 1246–1253.

Sumi, T., Hirai, S., Yamaguchi, M., Tanaka, Y., Tada, M., Niki, T., Takahashi, H., Sakuma, Y., 2018. "Trametinib downregulates survivin expression in RB1-positive KRAS -mutant lung adenocarcinoma cells". *Biochem. Biophys. Res. Commun.* 501, 253–258.

Tam, A., Wadsworth, S., Dorscheid, D., Man, S.F.P., Sin, D.D., 2011. "The airway epithelium: more than just a structural barrier". *Ther. Adv. Respir. Dis.* 5, 255–273.

Tarran, R., 2004. "Regulation of airway surface liquid volume and mucus transport by active ion transport.". *Proc. Am. Thorac. Soc.* 1, 42–46.

Thibault, M., Lavertu, M., Astolfi, M., Buschmann, M.D., 2016. "Structure dependence of lysosomal transit of chitosan-based polyplexes for gene delivery". *Mol. Biotechnol.* 58, 648–656.

Thornton, D.J., Rousseau, K., McGuckin, M.A., 2008. "Structure and function of the polymeric mucins in airways mucus". *Annu. Rev. Physiol.* 70, 459–486.

Towbin, H., Staehelin, T., Gordon, J., 1979. "Electrophoretic transfer of proteins from polyacrylamide gels to nitrocellulose sheets: procedure and some applications.". *Proc. Natl. Acad. Sci. U. S. A.* 76, 4350–4.

Tsigos, I., Martinou, A., Kafetzopoulos, D., Bouriotis, V., 2000. "Chitin deacetylases: new, versatile tools in biotechnology". *Trends Biotechnol.* 18, 305–312.

Uhlmann, E., Peyman, A., 1990. "Antisense oligonucleotides: a new therapeutic principle". *Chem. Rev.* 90, 543–584.

Ussing, H.H., Zerahn, K., 1951. "Active transport of sodium as the source of electric current in the short-circuited isolated frog skin.". *Acta Physiol. Scand.* 23, 110–27.

Van Gerven, L., Alpizar, Y.A., Wouters, M.M., Hox, V., Hauben, E., Jorissen, M., Boeckxstaens, G., Talavera, K., Hellings, P.W., 2014. "Capsaicin treatment reduces nasal hyperreactivity and transient receptor potential cation channel subfamily V, receptor 1 (TRPV1) overexpression in patients with idiopathic rhinitis". *J. Allergy Clin. Immunol.* 133, 1332-1339.e3.

Vankeerberghen, A., Cuppens, H., Cassiman, J.-J., 2002. "The cystic fibrosis transmembrane conductance regulator: an intriguing protein with pleiotropic functions". *J. Cyst. Fibros.* 1, 13–29.

Venerando, A., Franchin, C., Cant, N., Cozza, G., Pagano, M.A., Tosoni, K., Al-Zahrani, A., Arrigoni, G., Ford, R.C., Mehta, A., Pinna, L.A., 2013. "Detection of phospho-sites generated by protein kinase CK2 in CFTR: mechanistic aspects of Thr1471 phosphorylation". *PLoS.One.* 8, e74232--.

Vicente, S., Diaz-Freitas, B., Peleteiro, M., Sanchez, A., Pascual, D.W., Gonzalez-Fernandez, A., Alonso, M.J., 2013. "A polymer/oil based nanovaccine as a single-dose immunization approach". *PLoS One* 8, e62500.

Villate-Beitia, I., Zarate, J., Puras, G., Pedraz, J.L., 2017. "Gene delivery to the lungs: pulmonary gene therapy for cystic fibrosis". *Drug Dev. Ind. Pharm.* 43, 1071–1081.

Vos, M.H., Neelands, T.R., McDonald, H.A., Choi, W., Kroeger, P.E., Puttfarcken, P.S., Faltynek, C.R., Moreland, R.B., Han, P., 2006. "TRPV1b overexpression negatively regulates TRPV1 responsiveness to capsaicin, heat and low pH in HEK293 cells". *J. Neurochem.* 99, 1088–1102.

Wagner, M., Holzschuh, S., Traeger, A., Fahr, A., Schubert, U.S., 2014. "Asymmetric flow field-flow fractionation in the field of nanomedicine". *Anal. Chem.* 86, 5201–5210.

Wahlund, K.G., Giddings, J.C., 1987. "Properties of an asymmetrical flow field-flow fractionation channel having one permeable wall.". *Anal. Chem.* 59, 1332–9.

Wainwright, C.E., Elborn, J.S., Ramsey, B.W., 2015. "Lumacaftor-ivacaftor in patients with cystic fibrosis homozygous for Phe508del CFTR.". *N. Engl. J. Med.* 373, 1783–4.

Wang, T., Larcher, L., Ma, L., Veedu, R., 2018. "Systematic screening of commonly used commercial transfection reagents towards efficient transfection of single-stranded oligonucleotides". *Molecules* 23, 2564.

Wark, P., McDonald, V.M., 2018. "Nebulised hypertonic saline for cystic fibrosis". *Cochrane Database Syst. Rev.* 9, CD001506.

Waymouth, C., 1970. "Osmolality of mammalian blood and of media for culture of mammalian cells". *In Vitro* 6, 109–127.

Weissman, D., 2015. "mRNA transcript therapy". *Expert Rev. Vaccines* 14, 265–281.

Whelan, J., 2001. "Nanocapsules for controlled drug delivery". *Drug Discov. Today* 6, 1183–1184.

Willerich, I., Gröhn, F., 2011. "Molecular structure encodes nanoscale assemblies: understanding driving forces in electrostatic self-assembly.". *J. Am. Chem. Soc.* 133, 20341–56.

Winey, M., Meehl, J.B., O'Toole, E.T., Giddings, T.H., Jr., 2014. "Conventional transmission electron microscopy.". *Mol. Biol. Cell* 25, 319–23.

Wu, D.-Y., Ma, Y., Hou, X.-S., Zhang, W.-J., Wang, P., Chen, H., Li, B., Zhang, C., Ding, Y., 2017. "Co-delivery of antineoplastic and protein drugs by chitosan nanocapsules for a collaborative tumor treatment". *Carbohydr. Polym.* 157, 1470–1478.

Wu, H., Lima, W.F., Zhang, H., Fan, A., Sun, H., Crooke, S.T., 2004. "Determination of the role of the human RNase H1 in the pharmacology of DNA-like antisense drugs.". *J. Biol. Chem.* 279, 17181–9.

Xu, C., Zhang, Y., Xu, K., Nie, J.-J., Yu, B., Li, S., Cheng, G., Li, Y., Du, J., Xu, F.-J., 2019. "Multifunctional cationic nanosystems for nucleic acid therapy of thoracic aortic dissection". *Nat. Commun.* 10, 3184.

Yamamoto, A., Kormann, M., Rosenecker, J., Rudolph, C., 2009. "Current prospects for mRNA gene delivery". *Eur. J. Pharm. Biopharm.* 71, 484–489.

Yang, C., Chilvers, M., Montgomery, M., Nolan, S.J., 2016. "Dornase alfa for cystic fibrosis". *Cochrane Database Syst. Rev.* 4, CD001127.

Yang, M.-H., Yuan, S.-S., Huang, Y.-F., Lin, P.-C., Lu, C.-Y., Chung, T.-W., Tyan, Y.-C., 2014. "A proteomic view to characterize the effect of chitosan nanoparticle to hepatic cells: is chitosan nanoparticle an enhancer of PI3K/AKT1/mTOR pathway?". *Biomed Res. Int.* 2014, 789591.

Yang, T., Magee, K.L., Colon-Perez, L.M., Larkin, R., Liao, Y.-S., Balazic, E., Cowart, J.R., Arocha, R., Redler, T., Febo, M., Vickroy, T., Martyniuk, C.J., Reznikov, L.R., Zubcevic, J., 2019. "Impaired butyrate absorption in the proximal colon, low serum butyrate and diminished central effects of butyrate on blood pressure in spontaneously hypertensive rats". *Acta Physiol.* 226, e13256.

Yhee, J.Y., Song, S., Lee, S.J., Park, S.-G., Kim, K.-S., Kim, M.G., Son, S., Koo, H., Kwon, I.C., Jeong, J.H., Jeong, S.Y., Kim, S.H., Kim, K., 2015. "Cancer-targeted MDR-1 siRNA delivery using self-cross-linked glycol chitosan nanoparticles to overcome drug resistance". *J. Control. Release* 198, 1–9.

Younes, I., Sellimi, S., Rinaudo, M., Jellouli, K., Nasri, M., 2014. "Influence of acetylation degree and molecular weight of homogeneous chitosans on antibacterial and antifungal activities". *Int. J. Food Microbiol.* 185, 57–63.

Zabner, J., Couture, L.A., Gregory, R.J., Graham, S.M., Smith, A.E., Welsh, M.J., 1993. "Adenovirus-mediated gene transfer transiently corrects the chloride transport defect in nasal epithelia of patients with cystic fibrosis". *Cell* 75, 207–216.

Zabner, J., Karp, P., Seiler, M., Phillips, S.L., Mitchell, C.J., Saavedra, M., Welsh, M., Klingelhutz, A.J., 2003. "Development of cystic fibrosis and noncystic fibrosis airway cell lines". *Am. J. Physiol. Cell. Mol. Physiol.* 284, L844–L854.

Zhang, L., Button, B., Gabriel, S.E., Burkett, S., Yan, Y., Skiadopoulos, M.H., Dang, Y.L., Vogel, L.N., McKay, T., Mengos, A., Boucher, R.C., Collins, P.L., Pickles, R.J., 2009. "CFTR delivery to 25% of surface epithelial cells restores normal rates of mucus transport to human cystic fibrosis airway epithelium". *PLoS Biol.* 7, e1000155.

Zolnik, B.S., González-Fernández, Á., Sadrieh, N., Dobrovolskaia, M.A., 2010. "Minireview: nanoparticles and the immune system". *Endocrinology* 151, 458–465.

6 APPENDIX

6.1 List of chemicals

Table 52: List of chemicals

Chemical	*Manufacturer*
2-Mercaptoethanol (99%, p.a.)	Carl Roth GmbH & Co. KG, Karlsruhe, D
2-Propanol (≥99.5%)	Carl Roth GmbH & Co. KG, Karlsruhe, D
3-(4,5-Dimethylthiazol-2-yl)-2,5-diphenyltetrazolium bromide (MTT)	Invitrogen, Carlsbad, USA
3-(N-morpholino) propanesulfonic acid (MOPS)	Carl Roth GmbH & Co. KG, Karlsruhe, D
3-Isobutyl-1-methylxanthin (IBMX)	Sigma-Aldrich, St. Louis, USA
4-(2-Hydroxyethyl)-1-piperazineethanesulfonic acid (HEPES)	Carl Roth GmbH & Co. KG, Karlsruhe, D
5-Bromo-4-chloro-3-indolyl-β-D-galactopyranoside (X-Gal)	Carl Roth GmbH & Co. KG, Karlsruhe, D
8-CPT-cAMP	Biolog, Bremen, D
Acetic acid	Carl Roth GmbH & Co. KG, Karlsruhe, D
Agarose Multi-Purpose LE	Segenetic, Borken, D
Amiloride	Sigma-Aldrich, St. Louis, USA
Ammonium acetate	Ambion, Texas, USA
Ammonium persulfate (APS)	Carl Roth GmbH & Co. KG, Karlsruhe, D
Boric acid (≥ 98%, p.a.)	Carl Roth GmbH & Co. KG, Karlsruhe, D
Calcium chloride dihydrate ($CaCl_2$)	Carl Roth GmbH & Co. KG, Karlsruhe, D
CFTR-Inhibitor 172	Tocris Cookson, Ellisville, USA
Chitosan Heppe 70/5 (Batch-No. 212-170614-01)	HMC+, Halle/Saale, D
Chloroform	Carl Roth GmbH & Co. KG, Karlsruhe, D
D-glucose	Merck, Darmstadt, D
Diethylpyrocarbonate (DEPC)	Carl Roth GmbH & Co. KG, Karlsruhe, D
Dimethyl sulfoxide (DMSO)	Carl Roth GmbH & Co. KG, Karlsruhe, D
Dimethylformamide (DMF)	Carl Roth GmbH & Co. KG, Karlsruhe, D
Disodium hydrogen phosphate (Na_2HPO_4)	Merck, Darmstadt, D
Dithiothreitol (DTT)	Carl Roth GmbH & Co. KG, Karlsruhe, D
Ethanol (≥ 99.5%, p.a.)	Carl Roth GmbH & Co. KG, Karlsruhe, D
Ethylenediaminetetraacetic acid (EDTA)	Carl Roth GmbH & Co. KG, Karlsruhe, D
Formaldehyde	Carl Roth GmbH & Co. KG, Karlsruhe, D
Hydrochloric acid (HCl)	Carl Roth GmbH & Co. KG, Karlsruhe, D
Magnesium chloride hexahydrate ($MgCl_2$)	Merck, Darmstadt, D
Mannitol	Carl Roth GmbH & Co. KG, Karlsruhe, D

Miglyol® 812 N	Sasol GmbH, Witten, D
Monopotassium phosphate (KH_2PO_4)	Carl Roth GmbH & Co. KG, Karlsruhe, D
N,N,N',N'-Tetramethylethylenediamine (TEMED)	Carl Roth GmbH & Co. KG, Karlsruhe, D
Potassium chloride (KCl)	Carl Roth GmbH & Co. KG, Karlsruhe, D
RNAse AWAY® surface decontaminant	Carl Roth GmbH & Co. KG, Karlsruhe, D
Roti®-Phenol/Chloroform/Isoamylalkohol	Carl Roth GmbH & Co. KG, Karlsruhe, D
Sodium acetate	Sigma-Aldrich, St. Louis, USA
Sodium acetate (3 M)	Fermentas, St. Leon-Rot, D
Sodium chloride (NaCl)	Carl Roth GmbH & Co. KG, Karlsruhe, D
Sodium hydrogen phosphate (Na_2HPO_4)	Merck, Darmstadt, D
Sodium hydroxide (NaOH)	Carl Roth GmbH & Co. KG, Karlsruhe, D
Sodium pyruvate solution	Sigma-Aldrich, St. Louis, USA
Soy lecithin (Epikuron 145 V)	Cargill Texturizing Solutions Deutschland GmbH & Co. KG, Hamburg, D
Tetramethylammonium chloride (TMA)	Carl Roth GmbH & Co. KG, Karlsruhe, D
Tris	Carl Roth GmbH & Co. KG, Karlsruhe, D
Triton® X-100	Carl Roth GmbH & Co. KG, Karlsruhe, D
Tryptone medium	Fluka, München, D
Yeast extract	Carl Roth GmbH & Co. KG, Karlsruhe, D

6.2 List of reagents and kits

Table 53: List of reagents and kits

Type	*Name*	*Manufacturer*
Amino acid	100x L-Glutamine (200 mM)	Gibco, Karlsruhe, D
Antibiotic	Gentamycin	Biochrom GmbH, Berlin, D
Antibiotic	Penicillin (10.000 U/mL)/Streptomycin (10.000 µg/mL)	PAA Laboratories GmbH, Pasching, AT
Antibiotic	Kanamycin	Carl Roth GmbH & Co. KG, Karlsruhe, D
Buffer	Buffer Tango (10x)	Thermo Fisher Scientific, Waltham, USA
Buffer	FD Green Buffer (10x)	Thermo Fisher Scientific, Waltham, USA
DNA loading dye	6x loading dye solution	Fermentas, St. Leon-Rot, D
DNA marker	O'GeneRuler™ 1 kb Plus DNA Ladder	Thermo Fisher Scientific, Waltham, USA
DNA marker	O'GeneRuler™ 100 bp Plus DNA Ladder	Thermo Fisher Scientific, Waltham, USA
DNA stain	Midori Green Advance	Nippon Genetics Europe GmbH, Dueren, D

Enzyme	LgUI	Thermo Fisher Scientific, Waltham, USA
Enzyme	Protease Type XIV	Sigma-Aldrich, St. Louis, USA
Enzyme	Trypsin/EDTA Solution 0.25%/0.02% (w/v)	Biochrom GmbH, Berlin, D
Enzyme	XhoI FD	Thermo Fisher Scientific, Waltham, USA
Enzyme	SpeI FD	Thermo Fisher Scientific, Waltham, USA
Enzyme	SuperScript® III Reverse Transcriptase	Invitrogen, Carlsbad, USA
Hormone	Hydrocortisone	Sigma-Aldrich, St. Louis, USA
Hormone	Insulin	Invitrogen, Carlsbad, USA
Hormone	Triido-Thyronin	Sigma-Aldrich, St. Louis, USA
Hormone	Dexamethasone	Sigma-Aldrich, St. Louis, USA
In vitro transcription	mMessage mMachine® T7 Kit	Invitrogen, Carlsbad, USA
Inhibitor	RiboLock RNase Inhibitor	Thermo Fisher Scientific, Waltham, USA
Inhibitor	Protease Inhibitor Cocktail	Sigma-Aldrich, St. Louis, USA
Media supplement	ITS media supplement	Sigma-Aldrich, St. Louis, USA
Media supplement	Ultroser G	Cytogen, Wetzlar, D
Medium	Ham's F12 Nutrient Mixture	Sigma-Aldrich, St. Louis, USA
Medium	LHC Basal Medium	Gibco, Karlsruhe, D
Medium	MEM Jokliks Modification Medium	Sigma-Aldrich, St. Louis, USA
Medium	MEM Earle's Medium	PAA Laboratories GmbH, Pasching, AT
Medium	Opti-MEM™	Invitrogen, Carlsbad, USA
Medium	RPMI 1640 Medium	Sigma-Aldrich, St. Louis, USA
Medium	DMEM/Ham's F12 (1:1)	Biochrom GmbH, Berlin, D
Mounting medium	Fluoroshield™ with DAPI	Sigma-Aldrich, St. Louis, USA
Mycoplasma test	Venor®GeM Advance Pre-aliquoted Mycoplasma Detection Kit for conventional PCR	Minerva Biolabs, Berlin, D
Nucleotide	dNTP mix (10 mM each)	Thermo Fisher Scientific, Waltham, USA
PCR	TopTaq™ DNA Polymerase Kit	Qiagen, Hilden, D
Peptide	Human TRPV1 (aa 7-21) Synthetic Peptide	Invitrogen, Karlsruhe, D
Plasmid preparation	QIA®prep Spin Miniprep Kit	Qiagen, Hilden, D
Plasmid preparation	mi-Plasmid Maxiprep Kit	Metabion international AG, Planegg, D
Primer	Oligo$(dT)_{18}$ primer	Thermo Fisher Scientific, Waltham, USA
Protein	Bovine collagen A	Biochrom GmbH, Berlin, D

Protein	Endothelial cell growth factor	Biochrom GmbH, Berlin, D
Protein	Epidermal growth factor	Sigma-Aldrich, St. Louis, USA
Protein	Human Fibronectin	Biochrom GmbH, Berlin, D
Protein	Transferrin	Gibco, Karlsruhe, D
Protein	Collagen I Rat Protein, Tail	Thermo Fisher Scientific, Waltham, USA
Protein assay	SuperSignal™ West Pico Chemiluminescent Substrate Kit	Thermo Fisher Scientific, Waltham, USA
Protein assay	Pierce® BCA Protein Assay Kit	Thermo Fisher Scientific, Waltham, USA
Protein isolation	RIPA Buffer	Thermo Fisher Scientific, Waltham, USA
Protein loading buffer	Roti®-Load 4x loading buffer	Carl Roth GmbH & Co. KG, Karlsruhe, D
Protein marker	PageRuler™ Prestained Protein Ladder	Thermo Fisher Scientific, Waltham, USA
Protein quantification	Pierce® BCA Protein Assay Kit	Thermo Fisher Scientific, Waltham, USA
RNA isolation	RNeasy® Plus Mini Kit	Qiagen, Hilden, D
RNA loading dye	2x RNA loading dye	Thermo Fisher Scientific, Waltham, USA
RNA marker	RiboRuler™ High Range RNA Ladder	Thermo Fisher Scientific, Waltham, USA
Serum	BSA	Gibco, Karlsruhe, D
Serum	FBS superior	Biochrom GmbH, Berlin, D
Transfection	Lipofectamine™2000 Reagent	Invitrogen, Carlsbad, USA
Transfection	FuGENE® HD Transfection Reagent	Promega GmbH, Mannheim, D
Transfection efficiency	Luciferase Assay System	Promega GmbH, Mannheim, D
Water	nuclease free water	Fermentas, St. Leon-Rot, D

6.3 List of devices

Table 54: List of devices

Type	*Name*	*Manufacturer*
AF4 System	AF2000 Multiflow system	Postnova Analytics GmbH, Landsberg am Lech, D
Autoclave	3850 EL	Systec GmbH, Wettenberg, D
Balance	CP4202S	Sartorius AG, Göttingen, D
Balance (fine scale)	CP124S	Sartorius AG, Göttingen, D

Camera	PowerShot G2	Canon, Krefeld, D
Centrifuge	Eppendorf 5702	Eppendorf AG, Hamburg, D
Centrifuge	Eppendorf 5415D	Eppendorf AG, Hamburg, D
Centrifuge	Eppendorf mini spin	Eppendorf AG, Hamburg, D
Centrifuge (cooling)	Eppendorf 5417R	Eppendorf AG, Hamburg, D
Gel documentation	BioDocAnalyze System	Analytik Jena, Jena, D
Heating block	Blockthermostat BT200	Kleinfeld Labortechnik GmbH, Gehrden, D
Incubator	Heraeus BBD 6220	Kendro, Hanau, D
Incubator (Shaking)	Innova 4000	New Brunswick Scientific, Edison, USA
Laminar airflow cabinet	Heraeus HERAsafe HS15	Kendro, Hanau, D
Luminometer	GloMax® 20/20 Luminometer	Promega GmbH, Mannheim, D
Magnetic stirrer	RCT basic	IKA® Werke GmbH & Co. KG, Staufen, D
Microplate reader	EZ Read 400	Biochrom GmbH, Berlin, D
Microscope	LSM 510 META	Carl Zeiss AG, Oberkochen, D
Oscilloscope	HM 507 analog	HAMEG Instrument, Frankfurt, D
Osmometer	Osmomat 030	Gonotec Meß- und Regeltechnik GmbH, Berlin, D
pH meter	inoLab pH Level 2	WTW GmbH & Co. KG, Weilheim, D
Photometer	NanoDrop 1000	Peqlab Biotechnologie GmbH, Erlangen, D
Photometer	WPA Biowave S2100	Biochrom GmbH, Berlin, D
Pipette	Eppendorf Research	Eppendorf, Hamburg, D
Pipettor	ErgoOne FAST Pipette Controller	Scientific USA, Ocala, USA
Power supply	Standard Power Pack P25	Biometra, Göttingen, D

Pump	Laborport	KNF Neuberger GmbH, Freiburg, D
Real-time PCR cycler	Rotor-Gene Q	Qiagen, Hilden, D
Roll mixer	RM5	Karl Hecht KG, Sondheim, D
Safety gas burner	Schütt Flammy S	Schuett-biotech GmbH, Göttingen, D
Shaker	Type 3005	GFL, Burgwedel, D
Sonifier	Sonifier B-12	Branson Sonic Power Company, Danbury, USA
SpeedVac	Eppendorf Concentrator 5301	Eppendorf, Hamburg, D
Thermocycler	T personal	Biometra, Göttingen, D
Thermocycler	T gradient	Biometra, Göttingen, D
Ultrasonic bath	Bandelin Sonorex	Bandelin Electronic, Berlin D
Ussing Chamber	UC-65-CP	Prof. W. van Driessche, KU Leuven, B
Vacuum pump	PC101	Vacuubrand GmbH & Co. KG, Wertheim, D
Vortex	MS1 Mini Shaker	IKA® Werke GmbH & Co. KG, Staufen, D
Water bath	Isotemp 210	Fischer Scientific, Schwerte, D
Water bath	Thermo Haake DC10/P5	Thermo Electron, Karlsruhe, D
Water bath	Type 1003	GFL®, Burgwedel, D
Water treatment	Milli-Q-Water Biocel	Millipore, Bedford, USA
Zetasizer	Zetasizer Nano ZS	Malvern Panalytical Ltd, Worcestershire, UK

6.4 Primers

Table 55: List of primers

Primer	*Gene*	*Sequence (5'-3')*	*Amplicon length*	*Manufacturer*
GAPDH Exon 1/2 sense	GAPDH	GGTCGGAGTCAACGGATTTGGTCG	325 bp	metabion international AG, Planegg, D
GAPDH Exon 3/4 antisense	GAPDH	CTGCAAATGAGCCCCAGCCTTC		

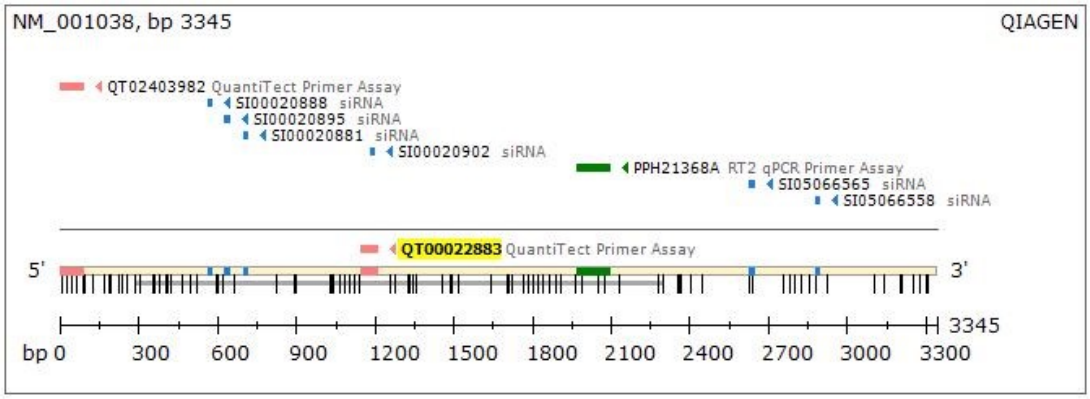

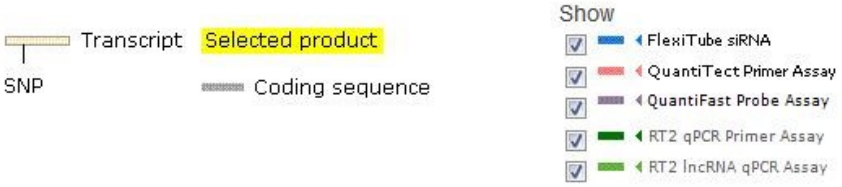

Name	Hs_SCNN1A_1_SG QuantiTect Primer Assay (QT00022883)
Official symbol	SCNN1A [Human]
Official name	sodium channel, non-voltage-gated 1 alpha subunit
Species	Human (Homo sapiens)
Entrez Gene ID	6337
Detected transcript(s)	NM_001038 (3345 bp) NM_001159575 (3216 bp) NM_001159576 (3497 bp)
Ensembl Transcript ID	ENST00000228916
Amplified exons*	4/5
Amplicon Length	88 (NM_001038) 88 (NM_001159575) 88 (NM_001159576)

Figure 57: α-ENaC primer. Hs_SCNN1A_1_SG QuantiTect® Primer Assay (Qiagen, Hilden, D.)

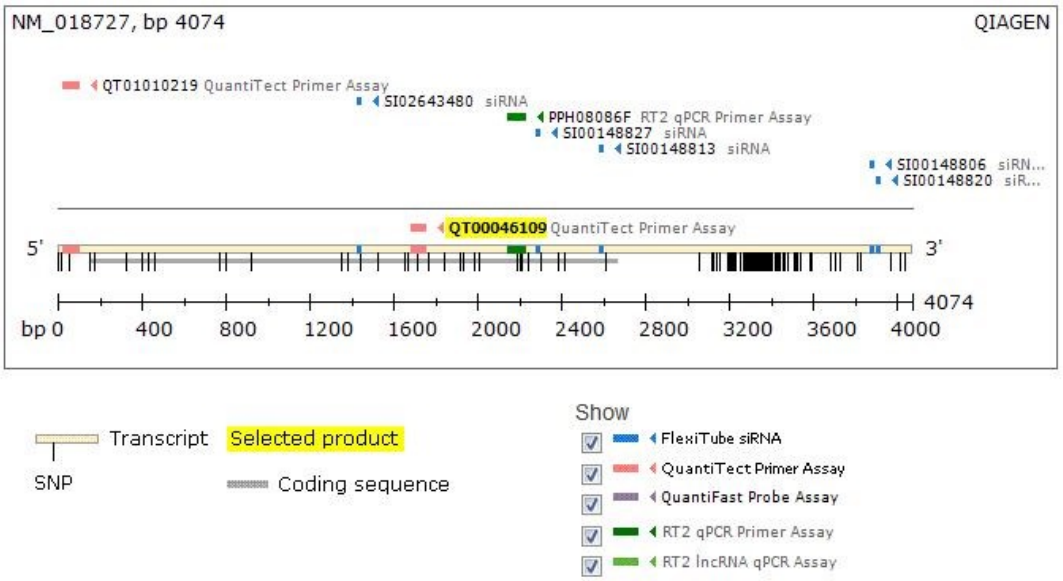

Name	Hs_TRPV1_1_SG QuantiTect Primer Assay (QT00046109)
Official symbol	TRPV1 [Human]
Official name	transient receptor potential cation channel subfamily V member 1
Species	Human (Homo sapiens)
Entrez Gene ID	7442
Detected transcript(s)	NM_018727 (4074 bp) NM_080704 (4191 bp) NM_080705 (4117 bp) NM_080706 (4443 bp)
Ensembl Transcript ID	ENST00000174621
Amplified exons*	10/11
Amplicon Length	92 (NM_018727) 92 (NM_080704) 92 (NM_080705) 92 (NM_080706)

Figure 58: TRPV1 primer. Hs_TRPV1_1_SG QuantiTect® Primer Assay (Qiagen, Hilden, D.)

6.5 Nucleic acid markers

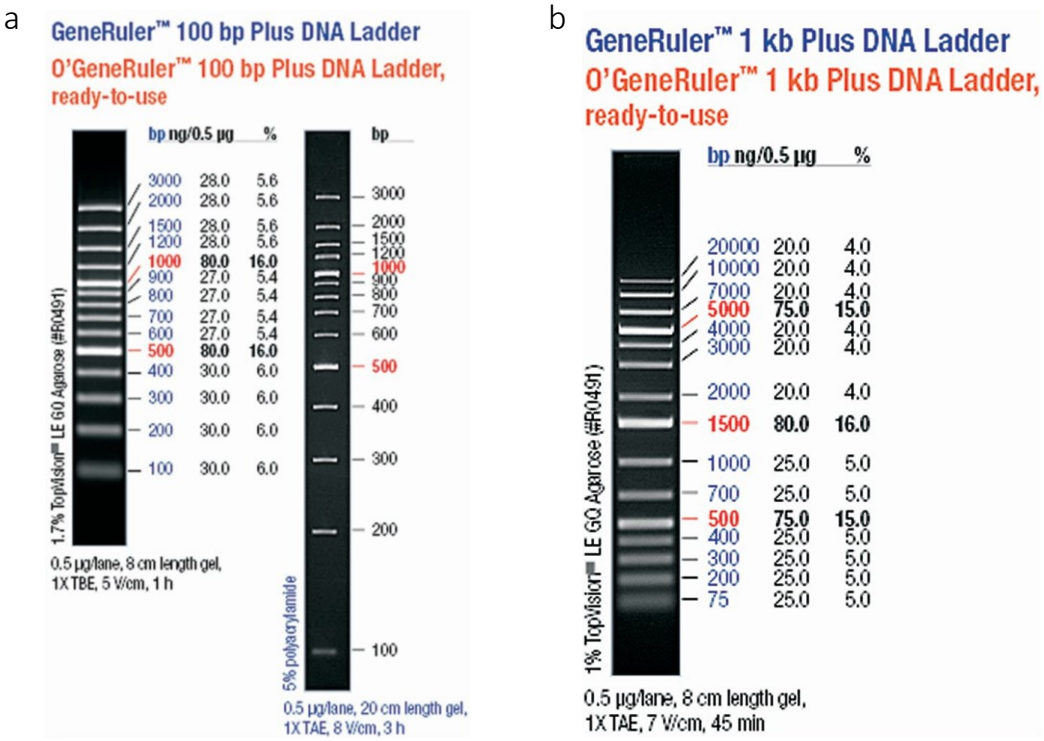

Figure 59: DNA markers. (a) *O'GeneRuler™ 1 kb Plus DNA Ladder* (Thermo Fisher Scientific, Waltham, USA); **(b)** *O'GeneRuler™ 100 bp Plus DNA Ladder* (Thermo Fisher Scientific, Waltham, USA)

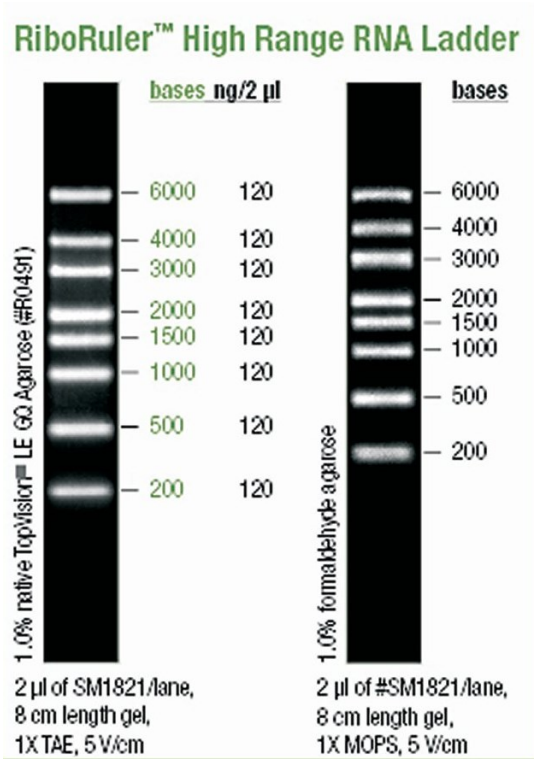

Figure 60: RNA marker. *RiboRuler™ High Range RNA Ladder* (Thermo Fisher Scientific, Waltham, USA)

6.6 Antibodies

Table 56: List of antibodies

Antibody	*Dilution*	*Cat. No.*	*Manufacturer*
alpha ENaC Rabbit Polyclonal Antibody	1:1,250	PA1-920A	Dianova, Hamburg, D
TRPV1 Rabbit Polyclonal Antibody	1:200	PA1-748	Invitrogen, Karlsruhe, D
Tubulin-α Mouse Monoclonal Antibody	1:1,000	DLN-09994	Dianova, Hamburg, D
Peroxidase-conjugated AffiniPure Goat-Anti-Mouse IgG	1:10,000	115-035-062	Dianova, Hamburg, D
Peroxidase-conjugated AffiniPure Goat-Anti-Rabbit IgG	1:10,000	111-035-144	Dianova, Hamburg, D

6.7 Protein markers

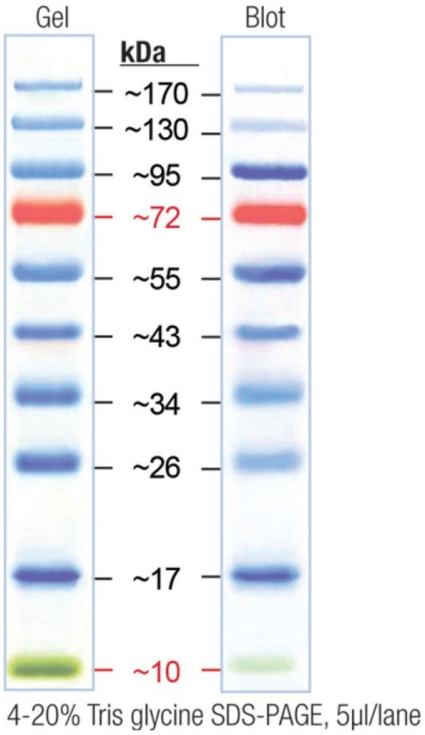

Figure 61: Protein marker. *PageRuler™ Prestained Protein Ladder* (Thermo Fisher Scientific, Waltham, USA)

SCIENTIFIC CONTRIBUTIONS

Publications

Kolonko, A.K., Fernández Fernández, E., Santos-Carballal, B., Goycoolea, F.M., Weber, W.-M., 2016. "Functional Restoring of Defect CFTR by Transfection of CFTR- mRNA Using Chitosan". *JSM Genet Genomics* 3(2): 1016.

Conferences

30 Sep – 02 Oct 2019 **98th Annual Meeting of the German Physiological Society – Ulm, Germany**
K. Kolonko, N. Bangel-Ruland, F.M. Goycoolea and W.-M. Weber
"Analyzing capsaicin-loaded chitosan nanocapsules coated with wtCFTR-mRNA as a potential treatment of abnormal ion transports in cystic fibrosis" (Talk)

10 Sep – 13 Sep 2019 **112th Annual Meeting of the German Zoological Society – Jena, Germany**
K. Kolonko, N. Bangel-Ruland, F.M. Goycoolea and W.-M. Weber
"Capsaicin-loaded chitosan nanocapsules coated with wtCFTR-mRNA as a potential treatment of abnormal ion transports in cystic fibrosis" (Poster)

27 Feb – 01 Mar 2019 **13th European CF Young Investigator Meeting – Paris, France**
K. Kolonko, N. Bangel-Ruland, F.M. Goycoolea and W.-M. Weber
"Analyzing chitosan for delivery of α-ENaC antisense oligonucleotides to reduce Na^+-hyperabsorption in cystic fibrosis" (Talk and Poster)

13 Sep – 16 Sep 2018 **Europhysiology 2018 – London, United Kingdom**
K. Kolonko, N. Bangel-Ruland, F.M. Goycoolea and W.-M. Weber
"Delivery of epithelial sodium channel antisense oligonucleotides to primary human airway epithelial cells via chitosan as a non-toxic transfection reagent" (Poster)

10 Sep – 15 Sep 2018 **111th Annual Meeting of the German Zoological Society – Greifswald, Germany**
K. Kolonko, N. Bangel-Ruland, F.M. Goycoolea and W.-M. Weber
"Chitosan as a non-toxic transfection reagent for ENaC antisense oligonucleotide delivery in human airway epithelial cells" (Poster)

28 Sep – 29 Sep 2017 **6th Symposium of the Young Physiologists – Jena, Germany**
K. Kolonko, E. Fernández Fernández, B. Santos-Carballal, N. Bangel-Ruland, F.M. Goycoolea and W.-M. Weber
"Chitosan-wtCFTR-mRNA complexes as a promising non-viral delivery system for Cystic fibrosis therapy" (Poster)

13 Sep – 15 Sep 2017 **110th Annual Meeting of the German Zoological Society – Bielefeld, Germany**
K. Kolonko, E. Fernández Fernández, B. Santos-Carballal, N. Bangel-Ruland, F.M. Goycoolea and W.-M. Weber
"Transfection of human airway epithelial cells using chitosan as a non-viral delivery system" (Poster)

16 Mar – 18 Mar 2017 **96th Annual Meeting of the German Physiological Society – Greifswald, Germany**
K. Kolonko, E. Fernández Fernández, B. Santos-Carballal, N. Bangel-Ruland, F.M. Goycoolea and W.-M. Weber
"Chitosan as a promising non-viral delivery system for wtCFTR-mRNA to human airway epithelial cells" (Poster)

15 Feb – 17 Feb 2017 **11th European CF Young Investigator Meeting – Paris, France**
K. Kolonko, E. Fernández Fernández, B. Santos-Carballal, F.M. Goycoolea and W.-M. Weber
"Alternative gene therapy in Cystic Fibrosis: Chitosan-wtCFTR-mRNA complexes as a promising non-viral delivery system" (Talk and Poster)

22 Sep – 23 Sep 2016 **5th Symposium of the Young Physiologists – Jülich, Germany**
K. Kolonko, E. Fernández Fernández, B. Santos-Carballal, F.M. Goycoolea and W.-M. Weber
"Chitosan-based mRNA transfection of human airway epithelial cells for cystic fibrosis therapy" (Talk)

14 Sep – 17 Sep 2016 **109th Annual Meeting of the German Zoological Society – Kiel, Germany**
K. Kolonko, E. Fernández Fernández, B. Santos-Carballal, F.M. Goycoolea and W.-M. Weber
"Chitosan-based delivery of mRNA to human airway epithelial cells for cystic fibrosis therapy" (Poster)

18 Jul – 22 Jul 2016 **Hands-on Workshop Epithelial Systems: Physiology and Pathophysiology – Lisbon, Portugal**

03 Mar – 05 Mar 2016 **95th Annual Meeting of the German Physiological Society – Lübeck, Germany**
K. Kolonko, E. Fernández Fernández, B. Santos-Carballal, F.M. Goycoolea and W.-M. Weber
"Chitosan-based delivery of mRNA for cystic fibrosis therapy" (Poster)

10 Feb – 12 Feb 2016 **10th European CF Young Investigator Meeting – Paris, France**
K. Kolonko, E. Fernández Fernández, B. Santos-Carballal, F.M. Goycoolea and W.-M. Weber
"Chitosan as a novel transfection reagent for wtCFTR-mRNA transfection in human airway epithelial cells" (Talk and Poster)

CURRICULUM VITAE

ACKNOWLEDGEMENTS